

APPLICATION OF TDHF METHODS TO NUCLEAR PHYSICS

Thesis by

Bradley A. Flanders

In Partial Fulfillment of the Requirements

for the Degree of

Doctor of Philosophy

California Institute of Technology

Pasadena, California

1981

(Submitted May 29, 1981)

## ACKNOWLEDGMENTS

Many thanks to my advisors, Steve Koonin and Tom Tombrello, for their help, inspiration, and encouragement throughout my study at Caltech, and, in particular, Steve, for his guidance with my thesis project. Their example has shown me the fruits of intelligence, creativity, dedication, and hard work. I am also grateful to my collaborators, especially Mort Weiss and Paul Bonche, for the ideas and knowledge they have shared with me throughout our association.

My parents, Ted and Jeanne, and my sister, Karen, deserve special thanks for the love and encouragement they gave me while I was growing up and which they continue to give me.

Special thanks also go to Pauline Hayashigawa for her love and understanding, for taking care of the mundane details of my life while I wrote my thesis, and for her help in typing it up.

I'd like to thank my many friends, too, for making the pleasant times pleasant and the unpleasant times bearable. I can't include all their names here, but I'm especially grateful to Barb Keenan, Steve Slutz, Ken Iverson, and Steve Trentalange. And "domo arigato" to Mr. Ohshima and the Caltech Karate Club for what I have learned about the human spirit.

I would also like to express my appreciation to Caltech for its financial support. This included both teaching and research assistantships and the following grants: PHY76-83685, PHY77-21602, ERDA #W-7405-Eng.-48 and 26, and NSF 77-12879.

## ABSTRACT

Part I presents results for TDHF calculations of realistic heavy-ion reactions. Results for a separable approximation, neglecting motion normal to the scattering plane, agree very well with the results of the full 3-D calculation. Results for the fusion cross section of two systems leading to the compound nucleus  $^{56}\text{Ni}$  are compared with experimental data. The  $^{16}\text{O} + ^{40}\text{Ca}$  results agree quite well with the experimental data, and the  $^{28}\text{Si} + ^{28}\text{Si}$  results agree quite well with experimental data for the similar  $^{32}\text{S} + ^{27}\text{Al}$  system. Results of calculations with the separable approximation for  $^{86}\text{Kr} + ^{139}\text{La}$  are compared with both axially symmetric calculations and experimental results. All three show substantial agreement.

Part II presents a stability criterion for the validity of TDHF solutions based on a time-dependent generalization of RPA theory. Results are tested in an exactly soluble model, the  $\text{SU}(3)$  generalization of the Lipkin model. Unfortunately, the exact solution could not be computed for a large enough number of particles to permit quantitative testing of this criterion. However, it does seem to correctly indicate the stability or instability of the TDHF path.

## TABLE OF CONTENTS

ACKNOWLEDGMENTS	ii
ABSTRACT	iii
PART I: TIME-DEPENDENT HARTREE-FOCK CALCULATIONS OF NUCLEAR COLLISIONS	1
Section 1: Time-Dependent Hartree-Fock Theory	2
Section 2: The Effective Interaction	9
Section 3: Brief Review of Heavy-Ion Reactions	19
Section 4: Application of TDHF to Heavy-Ion Reactions	24
Section 5: Brief Review of Earlier Calculations	33
Section 6: The Separable Approximation	37
"A Separable Approximation to Time-Dependent Hartree-Fock Calculations" Phys. Lett. <u>77B</u> , 13 (1978)	41
Section 7: The Filling Approximation	56
"TDHF Calculations of Fusion Cross Sections For $^{16}\text{O} + ^{40}\text{Ca}$ and $^{28}\text{Si} + ^{28}\text{Si}$ " Phys. Rev. C <u>20</u> , 641 (1979)	60
Section 8: Results for $^{86}\text{Kr} + ^{139}\text{La}$	88
Section 9: Summary	95
PART II: A STABILITY CRITERION FOR TDHF CALCULATIONS	96
Section 1: Introduction	97
Section 2: RPA Theory	99
Section 3: Time-Dependent Generalization of the RPA Theory	101
Section 4: TDHF for the SU(3) Model	107
Section 5: TDRPA for the SU(3) Model	112
Section 6: The Exact Solution for the SU(3) Model	117

Section 7: How to Compare Exact and TDHF Calculations	123
Section 8: TDRPA Results	127
Section 9: Summary	132
APPENDICES	133
A1. Derivation of the TDHF Equations	134
I. Variational Derivation	134
II. Derivation by Truncation	137
III. Hartree Potential and Fock Potential	139
IV. Conservation Laws	140
A2. $\langle H \rangle$ for the Skyrme Potential	143
I. Introduction and Kinetic Energy Term	143
II. Two-Body Terms	145
III. The Three-Body Term and Density-Dependent Two-Body Term	149
A3. Spatial Discretization of the Energy Functional	151
I. Introduction and Zero-Range Terms	151
II. Kinetic Energy Term	152
III. Nonlocal Terms	153
IV. Coulomb and Yukawa Terms	157
A4. Finite Difference Form for the TDHF Equations in Space	158
I. Introduction and Zero-Range Terms	158
II. Kinetic Energy Term	159
III. Nonlocal Terms	159
IV. Coulomb and Yukawa Terms	162

A5.	Implementation of the Separable Approximation	163
	I. General Features	163
	II. Incorporation into the Energy Functional	164
	III. Incorporation into the TDHF Hamiltonian	167
A6.	Discretization of the TDHF Equations in Time	172
	I. Introduction and Statement of the Problem	172
	II. Comparison of Taylor Expansions for the Exact and Discrete Solutions	174
	III. Derivation of the Discrete Evolution Operator from Energy Conservation	175
	IV. Evolution Algorithm	178
A7.	Binary Partition of the Nuclear Density	181
B1.	Expectation Values Needed for TDRPA	186
B2.	Invariance of the TDRPA Eigenvalues	190
B3.	Expectation Values for the SU(3) Model	193
B4.	Energy and Evolution Equation as Functions of the Four Rotation Angles	196
	REFERENCES	199
	FIGURE CAPTIONS	203
	FIGURES	207

PART I

TIME DEPENDENT HARTREE-FOCK CALCULATIONS

OF

NUCLEAR COLLISIONS

## Section 1: Time-Dependent Hartree-Fock Theory

A recent major effort in theoretical nuclear physics has been the development of microscopic dynamical theories to complement the phenomenological, macroscopic treatments. These macroscopic treatments, comprising virtually the entire history of nuclear physics, have been very valuable as a framework in which to visualize various phenomena; showing what degrees of freedom are needed and what laws govern the motion of these degrees of freedom. However, because these models are constructed to fit experiments on a particular phenomenon, they cannot give any underlying, unified explanation for diverse phenomena, nor show fully the relationships between these phenomena. Macroscopic theories also have a limited power for predicting new phenomena. To resolve these questions, we must turn to a microscopic many-body theory. The ultimate theory of nuclear physics, involving nucleons, pions, etc. is, of course, not feasible; but approximations can be made which should be valid for certain types of problems.

Time-Dependent Hartree-Fock theory (TDHF) (DI 30) is one such approximation. It consists of independent particles, in this case nucleons, moving in a self-consistent mean field generated from the internucleon interaction. This independent particle picture may seem unreasonable, since nucleons at normal nuclear densities are strongly interacting. However, since they are fermions, the Pauli principle is very effective at blocking their interaction at low energies.

A simple estimate of the mean free path of a particle  $p$ , with energy  $E/A + e_F$ , (where  $e_F$  is the fermi energy) may be obtained by considering binary collisions,  $(p)+(q) \rightarrow (p')+(q')$ , in infinite nuclear matter. The collision rate including Pauli blocking is (KO 79b,PI 66)

$$\Gamma_p = \sum_{qq'} v_p \left( \frac{\delta\sigma}{\delta\Omega} \right)_{pq \rightarrow p'q'} \delta(p+q-p'-q') f_q (1-f_{p'}) (1-f_{q'}) \quad (1.1)$$

where  $v_p$  is the velocity  $\frac{p}{m}$ ,  $\frac{\delta\sigma}{\delta\Omega}$  is the free-nucleon cross section, and  $f$  is the

phase-space occupation. These can be calculated assuming an isotropic differential cross section ( $\frac{\delta\sigma}{\delta\Omega} = \frac{\sigma_0}{4\pi}$ ), a Fermi-Dirac distribution at low temperature for the phase-space occupation, and a free-nucleon spectrum  $e_p = \frac{p^2}{2m}$ . For high energies,  $E/A \gg e_F$ , the Pauli blocking is ineffective and the collision rate,  $\Gamma_p$  has its classical value  $\rho v_p \sigma_0$  where  $\rho$  is the density of nuclear matter. With typical numbers  $\rho = .17 \text{fm}^{-3}$  and  $\sigma_0 = 250 \text{mb}$ , this leads to a short mean free path  $\lambda_p = \frac{v_p}{\Gamma_p} = .23 \text{fm}$ . However, for low energies,  $E/A \ll e_F$ , Pauli blocking severely limits the number of accessible final states<sup>+</sup> (KO 79b) so that

$$\Gamma_p = \rho v_p \sigma_0 \frac{3}{4} \left( \frac{E/A}{e_F} \right)^2 \quad (1.2)$$

and

$$\lambda_p = \frac{1}{\rho \sigma_0} \frac{4}{3} \left( \frac{e_F}{E/A} \right)^2 \quad (1.3)$$

With  $e_F = 41 \text{ MeV}$  this leads to a mean free path

$$\lambda_p = \frac{520}{(E/A)^2} \text{ fm} \quad (1.4)$$

and a lifetime,

$$\frac{1}{\Gamma_p} = \frac{5.9 \times 10^{-21}}{(E/A)^2} \text{ sec}, \quad (1.5)$$

where  $E/A$  is measured in MeV. For energies up to a few MeV per particle, the

<sup>+</sup> There is a simple way to show that this blocking factor,  $\frac{3}{4} \left( \frac{E/A}{e_F} \right)^2$  is reasonable. For a Fermi

gas, the number of states per unit volume with energies less than  $E$  is proportional to  $E^{\frac{3}{2}}$ . The density of states near the Fermi surface  $\frac{dn}{dE}$  is proportional to  $\frac{3}{2} e^{\frac{1}{2}}$ . The Pauli principle will require  $p'$  and  $q'$  to have energies above  $e_F$  and conservation of energy will require that all three particles  $q, p', q'$  have energies within  $E/A$  of the Fermi surface for  $E/A \ll e_F$ . For  $E/A$  small, the density of states will be approximately constant throughout this energy range. Since conservation of energy will specify the energy of one of these particles, the number of accessible states will be limited to approximately  $(\frac{3}{2} e^{\frac{1}{2}} E/A)^2$ . Since the number of states

without Pauli blocking would have been  $(\frac{3}{2} e^{\frac{1}{2}})^2$ , Pauli blocking will cause a factor approximately  $\frac{3}{4} \left( \frac{E/A}{e_F} \right)^2$ . Since conservation of energy actually requires all three particles to share this deviation  $E/A$  from the Fermi surface rather than merely being bound to within  $E/A$  of the surface, it isn't surprising that the actual blocking factor is three times smaller than above.

mean free path is much larger than the nuclear size ( $\approx 10$  fm) and the lifetime is comparable to the collision time (several  $10^{-21}$  sec.). Therefore, in nuclear collisions, this picture is expected to work for energies up to a few MeV per nucleon above the Coulomb barrier.

Indeed, this independent particle picture has been quite successful in explaining static properties of nuclei, from the early days of the shell model to the recent sophisticated, self-consistent, mean-field calculations, such as Density-Dependent Hartree-Fock (NE 70). The first extension of these ideas to time-dependent problems was the use of the RPA approximation (TH 61), a small amplitude approximation to TDHF, to calculate the near-equilibrium dynamics of low-lying vibrational states in nuclei (BER 75). This success prompted the investigation of TDHF in situations far from equilibrium, though still at relatively low excitation energies. Thus, although the derivation of the TDHF method dates back to Dirac in 1930, the application of these calculations to the collision of heavy ions was not attempted until the mid 1970's (BO 76a).

These TDHF calculations have several attractive features. First, they are the natural extensions of successful, near-equilibrium descriptions. Since they use the same internucleon interaction (see Section 2), they have no free parameters. This unified approach links these different problems and completely specifies the behavior of the TDHF solutions. Second, TDHF calculations treat implicitly both single-particle and collective degrees of freedom. By not imposing collective degrees of freedom, they provide a flexible treatment of the nuclear shape and surface. The mean field is the most obvious way of communicating collective information. Third, TDHF is the microscopic one-body theory to compare with macroscopic treatments of the long mean free path regime (KO 79b).

To discuss in more detail the nature of the approximation and the type of

results we will obtain, we begin with a derivation of the TDHF formula. Details can be found in Appendix A1. The exact Schroedinger equation can be derived by applying a variational principle to the action (KE 76),

$$I = \int dt \langle \Psi(t) | i\hbar \frac{\partial}{\partial t} - H | \Psi(t) \rangle \quad (1.6)$$

where  $H$  is the Hamiltonian. Looking for stationary points of  $I$  with respect to variation of the conjugate wavefunction,  $\Psi^*$ , gives  $i\hbar \frac{\partial}{\partial t} \Psi = H \Psi$ . The transition to a derivation of TDHF is straightforward (KE 76). Since the total wavefunction is assumed to be composed of independent particles, it can be written as a product of single-particle wavefunctions,  $\psi_j$ ; or in the case of identical fermions, where  $\Psi$  must be antisymmetrized, as a Slater determinant of the  $\psi_j$ . We then derive the TDHF formulas by looking for stationary action with respect to variation of a particular single-particle conjugate wavefunction,  $\psi_j^*$ . This leads to an evolution formula for each  $\psi_j$ ,

$$i\hbar \frac{\partial}{\partial t} \psi_j = \frac{\delta}{\delta \psi_j^*} \langle \Psi | H | \Psi \rangle \quad (1.7)$$

Although it isn't obvious that this leads to a mean field formulation,

$$i\hbar \frac{\partial}{\partial t} \psi_j = h \psi_j \quad (1.8)$$

with  $h$  a one-body operator; this is shown in Appendix A1, Part I. Thus, we see that the TDHF wavefunction is the best independent-particle approximation to the exact Schroedinger wavefunction. However, the independent-particle assumption greatly limits the usable information we can obtain from the TDHF wavefunction, since any quantity strongly dependent on correlations between two or more particles (other than antisymmetry) will not be correct. Therefore, the theory only attempts to approximate one-body operators and will give useful results for at most few-body operators.

This can be seen explicitly in an alternative derivation of the TDHF formulas detailed in Appendix A1, Part II. In this derivation, the exact equation for the

one-body density matrix,

$$\rho_{\alpha\beta}(t) = \langle \Psi(t) | a_{\beta}^{\dagger} a_{\alpha} | \Psi(t) \rangle \quad (1.9)$$

in terms of the two-body density matrix,

$$\rho_{\alpha\beta\gamma\delta}^{(2)}(t) = \langle \Psi(t) | a_{\gamma}^{\dagger} a_{\delta}^{\dagger} a_{\alpha} a_{\beta} | \Psi(t) \rangle \quad (1.10)$$

and higher-body density matrices is truncated by retaining only many-body correlations required by the Pauli principle and expressing these higher-body densities in terms of one-body density matrices (KO 79a).

The form of the TDHF equations is important for several reasons. First, they lead directly to several conservation laws which are not only desirable for a physically plausible theory, but will serve as checks for numerical computations. Since TDHF is a mean-field theory with each single-particle wavefunction evolving in time through the same hermitian Hamiltonian,  $h$ ; the overlap matrix of the  $\psi_j$ 's,  $\langle \psi_j | \psi_i \rangle$ , is time independent (normally  $\delta_{ij}$ ).

$$i\hbar \frac{\partial}{\partial t} \langle \psi_j | \psi_i \rangle = \langle \psi_j | -h | \psi_i \rangle + \langle \psi_j | h | \psi_i \rangle = 0 \quad (1.11)$$

Therefore, the norm of the TDHF wavefunction and the expectation value of the number operator are also time independent.

The variational formulation of TDHF is useful for demonstrating other conservation laws. For any operator,  $O$ , with no intrinsic time dependence, the time evolution of its expectation value in the TDHF wavefunction,  $\Psi$ , may be written as

$$i\hbar \frac{\partial}{\partial t} \langle \Psi | O | \Psi \rangle = \sum_{j\alpha} \left[ \frac{\delta \langle O \rangle}{\delta \psi_j(\alpha)} \left[ i\hbar \frac{\partial}{\partial t} \psi_j(\alpha) \right] + \frac{\delta \langle O \rangle}{\delta \psi_j^*(\alpha)} \left[ i\hbar \frac{\partial}{\partial t} \psi_j^*(\alpha) \right] \right] \quad (1.12)$$

where  $\langle O \rangle$  is viewed as a functional of  $\{\psi_j\}$  and  $\{\psi_j^*\}$ . Use of the evolution equation, (1.8), results in

$$i\hbar \frac{\partial}{\partial t} \langle O \rangle = \sum_{j\alpha} \left[ \frac{\delta \langle O \rangle}{\delta \psi_j(\alpha)} \frac{\delta \langle H \rangle}{\delta \psi_j^*(\alpha)} - \frac{\delta \langle O \rangle}{\delta \psi_j^*(\alpha)} \frac{\delta \langle H \rangle}{\delta \psi_j(\alpha)} \right] \quad (1.13)$$

the analogue of the Poisson bracket. Using  $O = H$  immediately results in conservation of energy. It can also be shown that  $i\hbar \frac{\partial}{\partial t} \langle O \rangle = 0$  for any one-body

operator, if the commutator,  $[H, C] = 0$  (see Appendix A1, Part IV). Thus, for any reasonable choice of  $H$ , that is a Galilean-invariant interaction, the total momentum and angular momentum will be conserved by the TDHF solution.

The form of the TDHF equations will also cause problems in the interpretation of the TDHF results (BO 76a). Since the mean field depends on the complete set of single-particle wavefunctions,  $\{\psi_j\}$ ; the TDHF equations will be coupled, nonlinear equations. Thus, if we tried to imagine two outgoing channels, they would be coupled even asymptotically. This arises because of the demand that the wavefunction be a single Slater determinant and not a sum over various possibilities. Thus, projecting the final state onto any final eigenstates of the system gives amplitudes which are time dependent (indicating transitions) even asymptotically. These "spurious cross-channel correlations" are the result of trying to extract information from the wavefunction which was already assumed not to be in the wavefunction. Since we can't calculate amplitudes for various final states, but merely some "average" final state, TDHF is a semiclassical theory.

An alternative way of arriving at the same conclusion is to notice that a Slater determinant is a wavepacket (FL 78). Thus, for example, a static Hartree-Fock (HF) solution with its localized center of mass represents a wavepacket of momentum eigenstates. When one of these Slater determinants is evolved with the TDHF equations, the coupling between the different eigenstates doesn't allow the wavepacket to spread. Thus, for the example above, the TDHF evolution of the static HF solution will merely involve multiplication of these solutions by a phase  $\exp(-i\sum_j e_j t / \hbar)$ . The wavepacket of momentum eigenstates can't spread because we aren't free to arbitrarily change the center of mass wavefunction. The TDHF (or HF) equations will simultaneously give the wavefunctions for the internal degrees of freedom and for the center of mass. This non-spreading of the initial wavepacket is a sure signal that TDHF is a semiclassical theory.

The moral of this discussion is that TDHF theory is a deterministic theory, calculating some kind of average evolution of our initial wavepacket; and that this wavepacket is only useful for calculating expectation values of few-body operators. Thus, our primary information will be simply the density as a function of time, and our principal results will be the number of fragments and their sizes, masses, charges, and motion. As we shall see later, the rich collision phenomenology exhibited by real nuclei will make the comparison of such gross, inclusive measurements with the theoretical results quite interesting.

## Section 2: The Effective Interaction

For the internucleon nuclear interaction we use a phenomenological force familiar from static Hartree-Fock and RPA calculations, the Skyrme potential (SK 56), with a slight modification described later. Although in principle we might like to use a potential or G matrix more directly connected to nucleon-nucleon scattering (DAV 74), the computations would be far too cumbersome. In fact, even the most direct methods require some minor phenomenological adjustment to agree with the data (NE 72). This isn't too surprising since the choice of a potential to fit the scattering data is ambiguous; the calculation of the many-body effects in a finite nucleus to determine the mean field is very difficult for even a two-body potential, requiring some approximations; and the effect of higher-body correlations is completely undetermined. It was found that an effective two- and three-body interaction could give very accurate results for both binding energies and densities of nuclei (BEI 75).

The Skyrme force is used because it is particularly simple to calculate. The potential energy is taken to be (VAU 72, EN 75)

$$\frac{1}{2} \sum_{ij} V_{ij}^{(2)} + \frac{1}{6} \sum_{ijk} V_{ijk}^{(3)} \quad (2.1)$$

This three-body force gives a density dependence, which aids saturation of the nuclear force. The Skyrme form parametrizes the potential by an expansion in momentum space.

$$\langle \vec{k} | V^{(2)} | \vec{k}' \rangle = t_0(1 + \chi_0 P_\sigma) + \frac{1}{2} t_1 (k^2 + k'^2) + t_2 \vec{k} \cdot \vec{k}' + i W_0 (\vec{\sigma}_1 + \vec{\sigma}_2) \cdot \vec{k} \times \vec{k}' \quad (2.2)$$

where  $t_0, t_1, t_2, W_0$  and  $\chi_0$  are constants, the Skyrme parameters;  $P_\sigma$  is the spin-exchange operator,  $P_\sigma = \frac{1}{2}(1 + \vec{\sigma}_1 \cdot \vec{\sigma}_2)$ ;  $\vec{\sigma}_1$  and  $\vec{\sigma}_2$  are the spin operators; and  $\vec{k}$  and  $\vec{k}'$  are the relative momenta of the two particles. Notice that in general  $\langle \vec{k} | V^{(2)} | \vec{k}' \rangle \neq v(k - k')$ , so the transformation to coordinate space does not give a local potential,  $\langle \vec{r} | V^{(2)} | \vec{r}' \rangle = \delta(\vec{r} - \vec{r}') v(\vec{r})$ . The transformation to coordinate space,

$$\langle \vec{r} | V^{(2)} | \vec{r}' \rangle = \frac{1}{(2\pi)^6} \int d\vec{k} d\vec{k}' e^{-i\vec{k}\cdot\vec{r}} \langle \vec{k} | V^{(2)} | \vec{k}' \rangle e^{i\vec{k}'\cdot\vec{r}'} \quad , \quad (2.3)$$

gives

$$\begin{aligned} \langle \vec{r} | V^{(2)} | \vec{r}' \rangle = & t_0(1+\chi_0 P_\sigma) \delta(\vec{r}) \delta(\vec{r}') - \frac{1}{2} t_1 \{ [\nabla^2 \delta(\vec{r})] \delta(\vec{r}') + [\nabla^2 \delta(\vec{r}')] \delta(\vec{r}) \} \\ & + t_2 [ \vec{\nabla} \delta(\vec{r}) ] \cdot [ \vec{\nabla} \delta(\vec{r}') ] + i W_0 (\vec{\sigma}_1 + \vec{\sigma}_2) \cdot [ \vec{\nabla} \delta(\vec{r}) ] \times [ \vec{\nabla} \delta(\vec{r}') ] \quad , \end{aligned} \quad (2.4)$$

where  $\vec{r}$  ,  $\vec{r}'$  are the relative coordinates of the two nucleons.

Thus we can anticipate that the simplicity of the Skyrme form will be due to the expansion of the range and nonlocality of the potential as differential operators. The  $t_0$  term can be rewritten  $t_0(1+\chi_0 P_\sigma) \delta(\vec{r}-\vec{r}') \delta(\vec{r})$ , so it is a local, zero-range force. Since this term acts only in s waves; it has strength  $t_0(1-\chi_0)$  for like nucleons ( singlet spin states ), while it has strength  $t_0(1+\chi_0)$  for unlike nucleons ( triplet spin states ). The  $t_1$  term acts in s-d states and the  $t_2$  term acts in p states;  $W_0$  is the strength of the spin-orbit force. In all of our applications we will be investigating bulk nuclear dynamics. Since these spin-orbit forces cause single-particle effects which are unlikely to significantly alter the bulk dynamics, we assume a spin-saturated system and neglect the spin-orbit force. Therefore, each orbital is occupied by two protons or two neutrons, one spin up and the other spin down.

The three-body interaction contains only the first term of an expansion like the above. In coordinate space, it is

$$V^{(3)} = t_3 \delta(\vec{r}_1 - \vec{r}_2) \delta(\vec{r}_2 - \vec{r}_3) \quad , \quad (2.5)$$

a zero-range, three-body interaction. Since the potential between two nucleons depends on the presence of another nucleon, this term introduces a local density dependence.

In Appendix A2, the expectation values of these potentials are derived for a spin-saturated Slater determinant, showing that the three-body potential above is equivalent to a two-body potential (VAU 72)

$$v^{(2)} = \frac{1}{6} t_3 (1 + P_\sigma) \delta(\vec{r}_1 - \vec{r}_2) \rho \left( \frac{\vec{r}_1 + \vec{r}_2}{2} \right) \quad . \quad (2.6)$$

The result, from Appendix A2, for the nuclear energy density is (EN 75)

$$\begin{aligned}
 H_s(\vec{r}) = & \frac{\hbar^2}{2m} \tau + \frac{1}{2} t_0 \left[ \frac{1}{2} (1 - \chi_0) (\rho_p^2 + \rho_n^2) + (2 + \chi_0) \rho_p \rho_n \right] + \frac{t_3}{4} (\rho_p + \rho_n) \rho_p \rho_n \\
 & + \frac{(t_1 + 3t_2)}{8} [\rho_p \tau_p - \vec{j}_p^2 + \rho_n \tau_n - \vec{j}_n^2] + \frac{(t_1 + t_2)}{4} [\rho_p \tau_n + \rho_n \tau_p - 2\vec{j}_p \cdot \vec{j}_n] \\
 & + \frac{3(t_2 - t_1)}{32} [\rho_p \nabla^2 \rho_p + \rho_n \nabla^2 \rho_n] + \frac{(t_2 - 3t_1)}{16} [\rho_p \nabla^2 \rho_n + \rho_n \nabla^2 \rho_p] .
 \end{aligned} \tag{2.7}$$

The particle, kinetic energy and current densities for each isospin species q ( p for protons, n for neutrons ) are defined as:

$$\begin{aligned}
 \rho_q(\vec{r}) &= \sum_{\substack{i \text{ with} \\ q_i = q}} |\psi_i(\vec{r}, q_i)|^2 , \\
 \tau_q(\vec{r}) &= \sum_{\substack{i \text{ with} \\ q_i = q}} |\vec{\nabla} \psi_i(\vec{r}, q_i)|^2 , \text{ and} \\
 \vec{j}_q(\vec{r}) &= \sum_{\substack{i \text{ with} \\ q_i = q}} \text{Im}[\psi_i^*(\vec{r}, q_i) \vec{\nabla} \psi_i(\vec{r}, q_i)] ,
 \end{aligned} \tag{2.8}$$

where the  $\psi_i$  are the occupied single-particle orbitals and the sums are over all these orbitals with isospin q. Densities without isospin subscripts refer to total densities;  $\rho = \rho_p + \rho_n$ ,  $\tau = \tau_p + \tau_n$ , and  $\vec{j} = \vec{j}_p + \vec{j}_n$ . ( For notational convenience the time dependence of the above orbitals and densities has not been explicitly included.)

For light systems, where the Coulomb potential is weak, which have equal numbers of protons and neutrons an assumption of isospin degeneracy seems a reasonable approximation. Since this assumption considerably simplifies calculations, it was used in many of the early calculations (BO 76a, BO 76b, BO 78, DAV 78a, DAV 78b, FL 78, KO 76, KO 77) and we use it for some of our calculations. With this assumption, each spatial orbital is effectively occupied by an alpha particle. Setting each of the proton and neutron densities to one-half the total density gives

$$H_s(\vec{r}) = \frac{\hbar^2}{2m} \tau + \frac{3}{8} t_0 \rho^2 + \frac{1}{16} t_3 \rho^3 + \frac{(3t_1 + 5t_2)}{16} (\rho \tau - \vec{j}^2) + \frac{(5t_2 - 9t_1)}{64} \rho \nabla^2 \rho . \tag{2.9}$$

The  $\rho \tau - \vec{j}^2$  term gives rise to a non-locality ( effective mass ) in the mean field.

The  $\rho \nabla^2 \rho$  term, which is sometimes rewritten after integration by parts as  $-|\vec{\nabla} \rho|^2$ , can be identified with the surface energy since the density varies rapidly only at the surface.

The determination of the five Skyrme parameters  $t_0, \chi_0, t_1, t_2,$  and  $t_3$  is somewhat ambiguous and has led to a variety of Skyrme potentials. Of course, a saturating internucleon force demands  $t_0$  negative and  $t_3$  positive. Four of the conditions used to determine the coefficients are the nuclear volume, surface and symmetry energies (as determined from the semi-empirical mass formula) and the saturation density. One linear combination is then undetermined, essentially the balance between the effective mass and the density dependence in producing saturation. A more refined approach uses these values as estimates and adjusts the parameters slightly to give better fits to the binding energies and charge radii of magic nuclei when used in static HF calculations (BEI 75). All of these potentials give accurate fits to both the binding energies and charge radii of magic nuclei and reasonable densities when used in these static HF calculations. However, with very different effective masses the different potentials give different single-particle level densities near the Fermi surface (BEI 75). The level density decreases with decreasing  $m^*$  ( increasing  $t_3$  ). This determines the last parameter. Presently the two favored forces are Skyrme II and III with effective masses in nuclear matter of .58 and .76 respectively. Another force, the BKN force (BO 76a), is sometimes used for isospin degenerate systems because of its simplicity. For these systems, there is only one nonlocal term, so with a choice of  $3t_1 + 5t_2 = 0$  one can select a purely local potential. This expression is approximately true for Skyrme VI with  $t_1 = 271.67$  and  $t_2 = -138.33$  so a slight readjustment of these parameters yields a local mean-field potential. Therefore, use of this force, the BKN force, greatly simplifies calculations. However, for the nondegenerate case only the trivial choice  $t_1 = t_2 = 0$  can eliminate

both of the nonlocal terms. This choice is completely unreasonable since it also eliminates the surface energy terms ( $\rho \nabla^2 \rho$ ).

The modification of the Skyrme form mentioned earlier consists of replacing these surface energy terms by direct Yukawa interactions. (BO 76a, NE 78) There are two reasons for this change. First, the finite range of the nuclear force is more accurately approximated (HOO 77). The expansion of the exchange term is the crucial simplification which makes the Skyrme form so useful, but there is no technical reason to eliminate the convolution of the density with a finite range interaction occurring in the direct term. Second, when the calculations are done in coordinate space (as ours are) the evolution with  $\nabla^2$  terms is unstable (BO 76a). That is, the wavefunctions develop a periodicity equal to the number of points in the discretization formula for  $\nabla^2$ . The connection between the surface energy terms and a Yukawa energy can be seen by a Taylor series expansion of the Yukawa energy.

$$E_{qq'} = \int \int d\vec{r} d\vec{r}' \frac{\exp(-|\vec{r}-\vec{r}'|/a)}{|\vec{r}-\vec{r}'|/a} \rho_q(\vec{r}) \rho_{q'}(\vec{r}') \quad (2.10)$$

$$= 4\pi a^3 \left[ \int d\vec{r} \rho_q(\vec{r}) \rho_{q'}(\vec{r}) + \frac{1}{2} a^2 \int d\vec{r} [\rho_q(\vec{r}) \nabla^2 \rho_{q'}(\vec{r}) + \rho_{q'}(\vec{r}) \nabla^2 \rho_q(\vec{r})] + \dots \right]$$

Therefore, the surface energy terms are replaced by

$$E_Y = \frac{V_L}{2} (E_{pp} + E_{nn}) + V_U E_{pn} \quad (2.11)$$

where  $\frac{V_L}{2} 4\pi a^5 = \frac{3}{32} (t_2 - t_1)$  and  $V_U \frac{4\pi a^5}{2} = \frac{1}{16} (t_2 - 3t_1)$ .

$V_L$  and  $V_U$  are the strengths of the interaction between like and unlike nucleons respectively and  $a$  is the range of the force. Since we choose  $a$  to approximate the range of the G matrix in nuclear matter (BO 76a), the selection of a set of Skyrme constants determines  $V_L$  and  $V_U$ . The presence of the first term above requires adjusting the parameters  $t_0$  and  $\chi_0$  of the zero-range component of the potential. Therefore, the parameters  $t_0$  and  $\chi_0$  are replaced by  $\tilde{t}_0$  and  $\tilde{\chi}_0$  satisfying

$$\frac{1}{4}\tilde{t}_0(1-\tilde{\chi}_0) = \frac{1}{4}t_0(1-\chi_0) - 4\pi a^3 \frac{V_L}{2} \quad (2.12)$$

and

$$\frac{1}{2}\tilde{t}_0(2+\tilde{\chi}_0) = \frac{1}{2}t_0(2+\chi_0) - 4\pi a^3 V_Y \quad . \quad ^+$$

For the isospin degenerate case we need only one Yukawa interaction,

$$E_Y = \frac{V}{2} \int d\vec{r} d\vec{r}' \exp\left(\frac{-|\vec{r}-\vec{r}'|/a}{|\vec{r}-\vec{r}'|/a}\right) \rho(\vec{r})\rho(\vec{r}') \quad (2.13)$$

The surface energy terms can be replaced by choosing

$$\frac{V}{2} 4\pi a^5 = \frac{5t_2 - 9t_1}{64} \quad (2.14)$$

and replacing  $t_0$  by  $\tilde{t}_0$  satisfying

$$\frac{3}{8}\tilde{t}_0 = \frac{3}{8}t_0 - 4\pi a^3 \frac{V}{2} \quad (2.15)$$

For the Coulomb energy we will use only the direct Coulomb contribution,

$$E_C = \frac{1}{2}e^2 \int d\vec{r} d\vec{r}' \frac{1}{|\vec{r}-\vec{r}'|} \rho_p(\vec{r})\rho_p(\vec{r}') \quad (2.16)$$

TDHF studies of light ion systems have shown the inclusion of the exchange energy has negligible effect on experimental observables (KRI 78). Studies of heavy ion systems have shown that the exchange energy is approximately 30 times smaller than the direct and that it fluctuates little throughout the collision (DAV).<sup>++</sup>

Therefore, in summary, for the isospin non-degenerate systems we will use the energy functional,

<sup>+</sup> Although the contribution of higher-order terms causes small changes in the results of static HF calculations (HOO 77, BO 76a), no one has attempted to readjust the parameters to maintain the same accuracy of fit to energies and radii for each set of Skyrme parameters. This adjustment would require a whole new set of static HF calculations, and the changes in the parameters would be very small compared to the differences for different Skyrme forces.

<sup>++</sup> All these TDHF studies approximate the exchange energy as the first term (Slater term) of a density-matrix expansion (NE 72),

$$H_C(\text{exchange}) = -\frac{3}{4} \left(\frac{3}{\pi}\right)^{\frac{1}{3}} e^2 \int d^3r [\rho_p(\vec{r})]^{\frac{4}{3}}$$

since an exact treatment would destroy the simplicity of the Skyrme form. Previous static HF calculations (TI 74) showed that this is accurate to better than 10% and the discrepancy varies slowly with nucleon number. These studies also showed that the exchange contribution is less than 10% of the direct contribution.

$$\begin{aligned}
 \langle H \rangle = \int d\vec{r} & \left[ \frac{\hbar^2}{2m} (\tau_p + \tau_n) + \frac{T_{0L}}{2} (\rho_p^2 + \rho_n^2) + T_{0U} \rho_p \rho_n + T_3 (\rho_n^2 \rho_p + \rho_p^2 \rho_n) \right. \\
 & + C_L (\rho_p \tau_p - \vec{j}_p^2 + \rho_n \tau_n - \vec{j}_n^2) + C_U (\rho_p \tau_n + \rho_n \tau_p - 2\vec{j}_p \cdot \vec{j}_n) \\
 & + \int d\vec{r}' O_Y(|\vec{r} - \vec{r}'|) \left[ \frac{V_L}{2} [\rho_p(\vec{r}) \rho_p(\vec{r}') + \rho_n(\vec{r}) \rho_n(\vec{r}')] + V_U \rho_p(\vec{r}) \rho_n(\vec{r}') \right] \\
 & \left. + \frac{1}{2} \int d\vec{r}' O_C(|\vec{r} - \vec{r}'|) \rho_p(\vec{r}) \rho_p(\vec{r}') \right] .
 \end{aligned} \tag{2.17}$$

where  $O_Y = \frac{\exp(-|\vec{r} - \vec{r}'|/a)}{|\vec{r} - \vec{r}'|/a}$  and  $O_C = \frac{e^2}{|\vec{r} - \vec{r}'|}$ . The coefficients are given by

$$\begin{aligned}
 T_{0L} &= \tilde{t}_0 \frac{1}{2} (1 - \tilde{\chi}_0) = \frac{1}{2} t_0 (1 - \chi_0) - \frac{3}{16a^2} (t_2 - t_1) \\
 T_{0U} &= \tilde{t}_0 (1 + \frac{1}{2} \tilde{\chi}_0) = t_0 (1 + \frac{1}{2} \chi_0) - \frac{1}{8a^2} (t_2 - 3t_1) \\
 T_3 &= \frac{t_3}{4} \\
 C_U &= \frac{t_1 + t_2}{4} \quad C_L = \frac{t_1 + 3t_2}{8} \\
 V_L &= \frac{3}{32} (t_2 - t_1) \frac{1}{2\pi a^5} \quad V_U = \frac{1}{16} (t_2 - 3t_1) \frac{1}{2\pi a^5}
 \end{aligned}$$

with parameters chosen from Skyrme III.

For the isospin degenerate systems we will use the energy functional,

$$\begin{aligned}
 \langle H \rangle = \int d\vec{r} & \left[ \frac{\hbar^2}{2m} \tau + \frac{3}{8} \tilde{t}_0 \rho^2 + \frac{1}{16} t_3 \rho^3 + \frac{V}{2} \int d\vec{r}' O_Y(|\vec{r} - \vec{r}'|) \rho(\vec{r}) \rho(\vec{r}') \right. \\
 & \left. + \frac{1}{8} \int d\vec{r}' O_C(|\vec{r} - \vec{r}'|) \rho(\vec{r}) \rho(\vec{r}') \right] .
 \end{aligned} \tag{2.18}$$

The coefficients are given by  $\frac{V}{2} = \left( \frac{5t_2 - 9t_1}{64} \right) \frac{1}{4\pi a^5}$  and  $\tilde{t}_0 = t_0 - \frac{8}{3} 4\pi a^3 \frac{V}{2}$  with parameters of the BKN force. The values of both sets of parameters are shown in Table 1.

Table 1					
Skyrme Parameters					
Force	$t_0$	$t_1$	$t_2$	$t_3$	$\chi_0$
	MeV-fm <sup>3</sup>	MeV-fm <sup>5</sup>	MeV-fm <sup>5</sup>	MeV-fm <sup>6</sup>	
II	-1169.9	586.6	-27.1	9331.1	0.34
III	-1128.8	395.0	-95.0	14000.0	0.45
BKN	-1089.0	250.0	-150.0	17270.0	-

Nuclear Matter Results				
Force	E/A	$k_F$	K	$\frac{m^*}{m}$
	MeV	fm <sup>-1</sup>	MeV	
II	-16.00	1.30	342	0.58
III	-15.87	1.29	356	0.76
BKN	-15.77	1.29	368	1.0

Derived with range a=0.45979				
Force	$\tilde{t}_0$	$\tilde{\chi}_0$	$V_U$	$V_L$
	MeV-fm <sup>3</sup>		MeV	MeV
II	-104.49	4.01	-868.53	-444.85
III	-334.52	1.74	-619.60	-355.79
BKN	-497.73	-	-363.04	

We derive the mean field,  $h_q$ , to use in the evolution of the single-particle wavefunctions,  $i\hbar \frac{\partial}{\partial t} \psi_{iq} = h_q \psi_{iq}$ , by the variation of the energy functional,  $\frac{\delta \langle H \rangle}{\delta \psi_{iq}^*(\vec{r})} = h_q \psi_{iq}$ . As before q labels the isospin and i the orbital. In the isospin nondegenerate case this mean field will, of course, be different for protons and neutrons. Terms in  $\langle H \rangle$  involving the variation of the density will be very simple. With  $\rho_q = \sum_i |\psi_{iq}|^2$ ,

$$\frac{\delta \rho_q(\vec{r}')}{\delta \psi_{iq}^*(\vec{r})} = \delta_{qq} \delta(\vec{r} - \vec{r}') \psi_{iq}(\vec{r}) \quad (2.19)$$

Variation of the kinetic energy or current densities will require integration by parts. Thus, with  $\tau_q = |\vec{\nabla} \psi_{iq}|^2$ ,

$$\delta \tau_q = \sum_i [\vec{\nabla} \delta \psi_{iq} \cdot \vec{\nabla} \psi_{iq} + \vec{\nabla} \psi_{iq} \cdot \vec{\nabla} \delta \psi_{iq}] \quad (2.20)$$

Therefore, integration by parts gives

$$\int d\vec{r}' F(\vec{r}') \frac{\delta \tau_q(\vec{r}')}{\delta \psi_{iq}^*(\vec{r})} = \delta_{qq} [-\vec{\nabla} F(\vec{r}) \cdot \vec{\nabla} \psi_{iq}(\vec{r})] \quad (2.21)$$

where the operator  $\vec{\nabla}$  acts on all functions to its right. Similarly for

$$\vec{j}_q = \frac{1}{2i} \sum_i (\psi_{iq}^* \vec{\nabla} \psi_{iq} - \psi_{iq} \vec{\nabla} \psi_{iq}^*),$$

$$\delta \vec{j}_q = \frac{1}{2i} \sum_i (\delta \psi_{iq}^* \vec{\nabla} \psi_{iq} + \psi_{iq}^* \vec{\nabla} \delta \psi_{iq} - \delta \psi_{iq} \vec{\nabla} \psi_{iq}^* - \psi_{iq} \vec{\nabla} \delta \psi_{iq}^*) \quad (2.22)$$

Therefore,

$$\int d\vec{r}' \vec{F}(\vec{r}') \cdot \frac{\delta \vec{j}_q(\vec{r}')}{\delta \psi_{iq}^*(\vec{r})} = \delta_{qq'} \frac{1}{2i} [\vec{F}(\vec{r}') \cdot \vec{\nabla} \psi_{iq}(\vec{r}) + \vec{\nabla} \cdot \vec{F}(\vec{r}') \psi_{iq}(\vec{r})] \quad (2.23)$$

Combining these formulas and defining  $q' \neq q$  gives the result (EN 75, NE 78)

$$\begin{aligned} h_q(\vec{r}) = & -\frac{\hbar^2}{2m} \nabla^2 + T_{0L} \rho_q + T_{0Y} \rho_{q'} + T_S (\rho_q^2 + 2\rho_q \rho_{q'}) \\ & + C_L (\tau_q - \vec{\nabla} \cdot \rho_q \vec{\nabla} + i [\vec{j}_q \cdot \vec{\nabla} + \vec{\nabla} \cdot \vec{j}_q]) \\ & + C_Y (\tau_{q'} - \vec{\nabla} \cdot \rho_{q'} \vec{\nabla} + i [\vec{j}_{q'} \cdot \vec{\nabla} + \vec{\nabla} \cdot \vec{j}_{q'}]) \\ & + V_L U_{Yq} + V_Y U_{Yq'} + U_C \delta_{qp} \quad (2.24) \end{aligned}$$

where the Yukawa potential is

$$U_{Yq} = \int d\vec{r}' O_Y(|\vec{r} - \vec{r}'|) \rho_q(\vec{r}') \quad (2.25)$$

and the Coulomb potential is

$$U_C = \int d\vec{r}' O_C(|\vec{r} - \vec{r}'|) \rho_p(\vec{r}') \quad (2.26)$$

and the differential operators  $\vec{\nabla}$  act on all functions to the right including the wavefunction.

We can see now that the nonlocality of the mean field, contained in the terms  $C_L$  and  $C_Y$ , has been expressed as a second-order differential operator - just like the kinetic energy. By rearranging the terms slightly, we can define an effective mass,

$$\frac{\hbar^2}{2m_q^*(\vec{r})} = \frac{\hbar^2}{2m} + C_L \rho_q + C_Y \rho_{q'} \quad (2.27)$$

which will appear in the mean field as  $-\vec{\nabla} \cdot \frac{\hbar^2}{2m_q^*(\vec{r})} \vec{\nabla}$ .

For the isospin degenerate case, with the BKN force, the mean field is quite simple and can be written immediately (BO 76a).

$$h(\vec{r}) = -\frac{\hbar^2}{2m}\nabla^2 + \frac{3}{4}t_0\tilde{\rho} + \frac{3}{16}t_3\rho^2 + VU_Y + \frac{1}{2}U_C \quad (2.28)$$

where

$$U_Y = \int d\vec{r}' O_Y(|\vec{r} - \vec{r}'|) \rho(\vec{r}') \quad (2.29)$$

and

$$U_C = \int d\vec{r}' O_C(|\vec{r} - \vec{r}'|) \frac{\rho(\vec{r}')}{2} \quad (2.30)$$

Therefore, this BKN force results in a local mean-field potential. Although a local two-body interaction with finite range will give rise to a nonlocal Hartree-Fock potential (as shown in Appendix A1, Part III), we see that we can choose a nonlocal two-body interaction which will result in a local Hartree-Fock potential for spin-saturated systems.

### Section 3: Brief Review of Heavy-Ion Reactions

(For a recent review see (LE 78). )

The early heavy-ion beams of about 20 years ago were confined primarily to  ${}^7\text{Li}$ ,  ${}^{12}\text{C}$ ,  ${}^{14}\text{N}$ , and  ${}^{16}\text{O}$  at energies less than 10 MeV/nucleon. Scattering studies were done to probe the optical potential between nuclei, and resonances revealed the occurrence of transient nuclear molecules (BR 60). Compound nucleus formation and decay was used to study the behavior of highly excited nuclei with large angular momentum. Then, about 10 years ago, with the use of heavier beams, a new phenomenon called deep-inelastic reactions was discovered. Two fragments similar to the target and projectile are emitted, but with pronounced damping of the initial kinetic energy (LE 73). In the most dramatic cases, there can even be complete energy relaxation; the two fragments are emitted with energies corresponding to Coulomb repulsion, just like a fissioning compound nucleus. However, the masses of the fragments are completely different from the expectations of a fissioning compound nucleus. The lack of a fissioning compound nucleus was convincingly demonstrated when reactions leading to nearly the same composite system had different final fragments (TA 75).

Thus, the energy damping and mass exchange show that a composite system is formed, but the entrance channel dependence shows that the system splits again before complete equilibration can be reached. These reactions, therefore, allow the study of interaction times and equilibration times of different degrees of freedom for a tremendous variety of targets, projectiles, and energies. This opens a new field of collective phenomenology correlating the scattering angle, energy loss, mass of the products, and the charge of the products. We can then develop models using parameters such as interaction potentials, viscosity coefficients, friction tensors, and diffusion coefficients (NO 76).

Or, in our case, we try to describe all these collective phenomena from a microscopic approximation using a previously determined nucleon-nucleon interaction.

The application of classical concepts, like that of an ion-ion trajectory, to the problem is justified since the wavelength associated with the relative motion of the nuclei is small. This wavelength is (NO 76 p.3)

$$\lambda = \frac{\hbar}{\mu v} \approx \left( \frac{A_1 + A_2}{A_1 A_2} \frac{20}{E_{cm}} \right)^{1/2} ; \quad (3.1)$$

where  $v$  is the relative velocity,  $\mu$  is the reduced mass,  $\lambda$  is in fm,  $E_{cm}$  is the center of mass kinetic energy in MeV, and  $A_1, A_2$  are the atomic mass numbers of the target, projectile. Thus, for some of the cases we will be describing later, this wavelength can range from .2 fm, for  $^{16}\text{O} + ^{16}\text{O}$  at  $E_{cm} = 55$  MeV, to .004 fm, for  $^{86}\text{Kr} + ^{139}\text{La}$  at  $E_{cm} = 312$  MeV.

Also, the Sommerfeld parameter,  $\eta$ , is large for these collisions (NO 76 p.19).

$$\eta = \frac{1}{2} \frac{d_{\min}}{\lambda} = \frac{Z_1 Z_2 e^2}{2 E_{cm} \lambda} \quad (3.2)$$

Here  $d_{\min}$  is the distance of closest approach on a Coulomb trajectory; and  $Z_1, Z_2$  are the charges of the two nuclei. This parameter ranges from about 5, for our O+O case, to about 400, for our Kr+La case. This means the scattering can be described with a classical deflection function, and that classical Rutherford scattering is expected when the minimum distance of approach lies significantly outside the sum of the radii of the two nuclei.

Therefore, at large impact parameters Rutherford scattering is expected. At smaller impact parameters, the attractive nuclear interaction bends these trajectories forward in angle (WI 73). For still smaller impact parameters, when the nuclei touch, the damping of kinetic energy begins along with mass, charge, and angular momentum transfer. Also, the temporary sticking and rotation of the system bends the trajectories further forward in angle. At still smaller

impact parameters, with significant overlap of the two nuclei, a composite system is formed; in some cases, a compound nucleus.

For the formation of a compound nucleus the target and projectile must completely lose their individual characteristics, and the system must exhibit equipartition in the occupation of all accessible degrees of freedom. Then, the decay process will be independent of the formation process, except for such restrictions as the conservation of energy and angular momentum. The system is still considered fused into a compound nucleus if a few pre-equilibrium nucleons or alpha particles are emitted. For light nuclei fusion is quite clear because the composite system is stable against fission. Therefore, we observe an evaporation residue together with light particles: mainly protons and neutrons, with alpha particles if the system has high angular momentum. Thus, for light systems, with small  $Z_1 Z_2$ , the complete-fusion cross section is a large part of the total reaction cross section; and only a small fraction of the reaction goes into the inelastic, grazing collisions.

For heavier systems the situation is much more complex. These systems can be unstable and fission - either because they are simply too large, or because they have too much excitation energy and angular momentum - so the complete-fusion cross section goes to zero. Evidence of fusion-fission behavior is the complete relaxation of the kinetic energy of the system, and mass and charge distributions of the fragments which are independent of the initial fragments. However, these same factors, which would cause the compound nucleus to fission, will inhibit its formation; causing the system to break apart before becoming completely equilibrated. Thus, for heavier systems even the fusion-fission cross section decreases, and the deep-inelastic reactions become more important.

For later sections, it is useful to discuss in general terms some of the final-

fragment correlations we will be looking at, and the type of information we can learn. For instance, as mentioned earlier, the correlation between energy and mass led to the discovery of deep-inelastic reactions. Thus, contours of the number of events versus the total kinetic energy and mass of the fragments show two schematic possibilities, (Fig. 1a and 1b), both of which have been observed (TA 75). Both of these reactions show quasi-elastic peaks at the initial masses and energy. Fig. 1a shows evidence of fusion-fission since the energy-relaxed products are centered about the average mass. Fig. 1b shows evidence of the deep-inelastic reaction since the energy-relaxed products still maintain nearly their original identities.

Thus, using the previously discussed classical concepts, we would say that for the system in Fig. 1a a certain range of impact parameters have interaction times longer than the equilibration times for both mass and energy. For the system in Fig. 1b the energy equilibration is much more rapid than the mass equilibration, and a certain range of impact parameters have interaction times which are between these two equilibration times. No impact parameters have interaction times as long as the equilibration time for the mass. By looking in more detail at this correlation, we can relate the amount of energy damping, mass transfer, and the spread of these two distributions (HU 76). Thus, for example, a certain increase in energy damping corresponds to a certain increase in mass transfer; but the time scale, so far, is completely undetermined.

Looking for correlations with scattering angle proves very useful because this allows the estimation of an interaction time (SC 77); and thus, sets a definite time scale for the equilibration processes. For a given angular momentum (or impact parameter) the deviation from Coulomb scattering is a measure of the rotation of the composite system. Therefore, a knowledge of the angular momentum and moment-of-inertia of the composite system gives an estimate of

the interaction time,  $\tau_{int} = \frac{I}{L} \Delta\vartheta$ ; where  $I$  is the moment-of-inertia,  $L$  the angular momentum, and  $\Delta\vartheta$  the deviation from Coulomb scattering. Typical interaction times range from  $10^{-22}$  to several times  $10^{-21}$  sec. (SC 77).

Thus, for instance, a gradual energy loss as interaction time increases would lead to a classical trajectory in  $E$  vs.  $\vartheta$  like that in Fig. 2a (WI 73); except, of course, that we can't differentiate between positive and negative angle scattering, so the trajectory folds back at  $\vartheta=0^\circ$ . Since each point in the trajectory corresponds to a particular angular momentum, we can also plot  $E$  vs.  $l$  and  $\vartheta$  vs.  $l$ . From the plot of  $\vartheta$  vs.  $l$ , we can derive an interaction time,  $\tau_{int}$  vs.  $l$ . These are also shown in Figs. 2b, 2c, and 2d for the same system as in Fig. 2a.

In a realistic case, showing spread in both  $E$  and  $\vartheta$ , the trajectory in  $E$  vs.  $\vartheta$  becomes a ridge in contours of the cross section. The example in Fig. 2 is fairly typical of moderately light systems (GA 76), but the variation of both interaction times and equilibration rates causes the shape of these contours to vary for different systems. For heavier systems, the trajectory drops more steeply in energy (SC 77).

In summary, we can make a few general comments about these heavy-ion reactions. First, the widths of the mass and energy distributions increase as the mass transfer or energy damping increases (HU 76). This shows that these deep-inelastic reactions are relaxation phenomena. Second, the kinetic energy equilibrates much more rapidly than the masses of the fragments (LE 73). Third, looking at different isotopes shows that the neutron excess, or ratio  $N/Z$ , equilibrates even more rapidly than energy ( $\tau_{N/Z} \approx 10^{-22}$  sec.) (GA 75, KRA 77). And fourth, the large variation in all these rates and interaction times for different systems leads to quite different collective behavior, and presents a formidable challenge to a unified, microscopic theory.

#### Section 4: Application of TDHF to Heavy-Ion Reactions

The application of the TDHF method to heavy-ion collisions requires large scale numerical calculations. We write the TDHF equations in coordinate space and use finite difference methods to follow the evolution of the single-particle orbitals. These orbitals are described by their values on a uniformly spaced Cartesian mesh within a rectangular box. Vanishing boundary conditions are imposed outside this box. We use a coordinate space representation rather than an expansion in a set of basis functions as in static calculations because it more uniformly describes the wide variety of shapes which occur and because the matrices are sparse. Our discrete space-time mesh has a typical spacing,  $\Delta x$ , of approximately 1 fm and a time step,  $\Delta t$ , of approximately  $5 \times 10^{-24}$  sec. Therefore, two separated nuclei require a spatial box approximately  $30 \times 30 \times 16$  (the smaller dimension is perpendicular to the scattering plane) and the evolution to the final state requires on the order of 100 time steps. For our heaviest nuclei, with approximately 100 wave functions, the computational effort is substantial. Storage requirements exceed that available on a CDC 7600, requiring tapes and substantial input/output; the computing time can be as high as 5 hours for a single impact parameter. Fortunately, the Cray we used most recently can meet the storage requirements and also decrease the computing time to about one hour per run. In our calculations, we impose a reflection symmetry with respect to the reaction plane, thus cutting our numerical work in half. For collisions of identical nuclei, we also impose a point reflection symmetry through the center of mass of the total system, cutting our numerical work by another factor of two.

Since the TDHF equations,  $i\hbar \frac{\partial}{\partial t} \psi_j = h \psi_j$ , are first order in time, they can be solved formally by using a time evolution operator,

$$\psi_j(t) = U(t, t_0) \psi_j(t_0) \quad , \quad (4.1)$$

where  $U$  is the unitary operator

$$U(t, t_0) = T \exp\left[\frac{-i}{\hbar} \int_{t_0}^t d\tau h(\tau)\right] \quad (4.2)$$

and  $T$  is the time-ordering operator. Therefore, we only need to know the set of single-particle wavefunctions at one time to solve the problem. Our discrete approximation to this operator,  $U(t + \Delta t, t)$ , is discussed in Appendix A6. The calculation of  $h\psi_j$ , required for the evolution, is considerably simplified because the only nonlocal terms are differential operators. Therefore, the discretization, as discussed in Appendices A3 and A4, results in a sparse matrix for  $h$  with nonzero elements only near the diagonal.

Our initial condition is an impending collision between two nuclei. At a large separation, when nuclear forces between nuclei and Coulomb induced distortion are negligible, the system is completely described by the nuclei, their energies (kinetic plus Coulomb) and their impact parameter (or angular momentum). We choose two static Hartree-Fock solutions at positions which result in a large separation without either nucleus getting too close to the walls of our spatial box. We can generate a translating HF solution,  $\Psi$ , by  $\Psi = \exp[i\vec{k} \cdot \vec{R}] \Phi$ , where  $\Phi$  is the static HF solution, composed of single-particle wavefunctions  $\varphi_j$  and  $\vec{R} = \sum_j \frac{\vec{r}_j}{A}$  is the center of mass coordinate of the nucleus. ( $A$  is the mass number of the nucleus.) The nucleus then has a total momentum  $\hbar\vec{k}$ . The existence of these translating solutions is intimately connected with the conservation of momentum. The time-dependent single-particle wavefunctions of  $\Psi$  are  $\psi_j$  where

$$\psi_j(\vec{r}, t) = \exp\left[-i\left(e_j + \frac{\hbar^2}{2m} k^2\right) \frac{t}{\hbar}\right] \exp[i\vec{k} \cdot \vec{r}] \varphi_j(\vec{r} - \vec{v}t) \quad , \quad (4.3)$$

where  $\vec{v} = \frac{\hbar\vec{k}}{m} = \frac{\hbar\vec{K}}{mA}$  and  $m$  is the nucleon mass. We do our calculations in the center-of-mass frame, so we choose  $\vec{K}_1 = -\vec{K}_2 = \vec{K}$  and our initial state becomes

$$\Psi = \exp[i\vec{K} \cdot \vec{R}_1] \Phi_1 \exp[-i\vec{K} \cdot \vec{R}_2] \Phi_2 , \quad (4.4)$$

two translating static HF solutions. The total kinetic energy is given by

$$TKE = \frac{(\hbar\vec{K})^2}{2\mu} , \quad (4.5)$$

with reduced mass  $\mu = m \frac{A_1 A_2}{(A_1 + A_2)}$ . The total energy is

$$E = TKE + \frac{Z_1 Z_2 e^2}{|\vec{R}_1 - \vec{R}_2|} , \quad (4.6)$$

and the total angular momentum is given by

$$\vec{L} = \hbar\vec{K} \times (\vec{R}_1 - \vec{R}_2) \quad (4.7)$$

(or equivalently the impact parameter is  $|\vec{R}_1 - \vec{R}_2| \sin\vartheta$  where  $\vartheta$  is the angle between  $\vec{K}$  and  $\vec{R}_1 - \vec{R}_2$ ).<sup>†</sup>

The static HF solutions are calculated using the same energy functional as the TDHF solutions. (Otherwise they would not be the ground state of the nuclei in the collision.) These solutions are obtained by an imaginary time step method (FL 7B). We use an operator similar to the actual evolution operator,  $U(t, t_0)$ , but with  $t$  replaced by  $-i\tau$ . This results in an exponential decrease,  $\exp(\frac{-\Delta E \tau}{\hbar})$ , of higher states relative to the ground state of the static solution. Since this operator is nonunitary, we also renormalize the wavefunctions after each time step. This procedure enables us to use a code almost identical to our TDHF code and results in very rapid convergence to the ground state static HF solution. For the exact solution, we can easily show that the imaginary time step method will result in the lowest energy state which has any overlap with the initial trial state. Any  $\Psi$  can be expanded  $\Psi(0) = \sum_i a_i \Phi_i$  where the  $\Phi_i$  are the complete set of eigenstates  $H\Phi_i = E_i \Phi_i$ . The exact evolution of  $\Psi$  is given by

$$\Psi(t) = \sum_i a_i \exp[-i\omega_i t] \Phi_i \quad (4.8)$$

<sup>†</sup> Different discretization errors for the different wavefunctions result in slightly different boosts. Since all wavefunctions are coupled by the mean field, this results in a small initial transfer of collective kinetic energy to internal excitation.

where  $\omega_i = \frac{E_i}{\hbar}$ . Replacing  $t$  by  $-i\tau$  gives

$$\Psi(-i\tau) = \exp[-\omega_0\tau] \sum_i a_i \exp[-(\omega_i - \omega_0)\tau] \Phi_i \quad (4.9)$$

Renormalizing  $\Psi$  as a function of time gives

$$\Psi(-i\tau) = \left[ \sum_i |a_i|^2 \exp[-2(\omega_i - \omega_0)\tau] \right]^{-\frac{1}{2}} \sum_i a_i \exp[-(\omega_i - \omega_0)\tau] \Phi_i \quad (4.10)$$

and

$$\lim_{\tau \rightarrow \infty} \Psi(-i\tau) = \Phi_0 \quad (4.11)$$

For the HF solution the method is very similar,

$$\Psi(-i\tau) = N(\tau) T \exp\left[ \frac{-1}{\hbar} \int_0^\tau d\tau' h(i\tau') \right] \Psi(0) \quad (4.12)$$

but the dependence of  $h$  on the wavefunction  $\Psi$  means that a tiny overlap of the initial guess  $\Psi(0)$  with the ground state,  $\Phi_0$ , is no longer a sufficient condition for convergence to the ground state. If the initial guess is bad enough so the mean field  $h(0)$  looks nothing like the mean field in the ground state,  $h_0$ , it is possible that the self-consistency will result in an excited state, similar to  $\Psi(0)$ , with a mean field similar to  $h(0)$ . In practice, this is not a problem because we always know the approximate ground state. The resulting mean field is always close enough to  $h_0$  so that  $\Psi$  evolves closer to  $\Phi_0$  and the convergence is very rapid.

This initial state is evolved by our discrete approximation to the evolution operator (in both space and time) until some final time. The complete set of wavefunctions  $\{\psi_j(t)\}$  contains far too much information, as we are primarily interested in the proton and neutron densities. We observe one of two possibilities, either the density separates into two fragments again rather quickly or stays as one fragment long enough to be considered fused. This fusion criterion can be improved by considering the mean radius of the system (or a collective coordinate describing fragment separation as discussed later) although in some cases the determination can be ambiguous.

As an example, we will jump ahead to some data which are discussed more fully later. The root mean square radius of the system,  $(\frac{\langle r^2 \rangle}{A})^{1/2}$ , for four angular momenta is plotted in Fig. 3. All show a rapid decrease initially, as the two nuclei approach one another, followed by a slower increase. For the peripheral angular momentum,  $L=165$ , this increase is very steady with the density separating into two fragments at about  $r=9.16$  fm and the fragments moving apart at a speed somewhat slower than the initial speed. The curve for  $L = 80$  is a typical deep-inelastic event. The rms radius can oscillate several times before beginning a steady increase leading to separation into two fragments at about  $r = 8.9$  fm. The lowest curve for,  $L = 50$ , is an unambiguous fusion event. The rms radius shows oscillations, indicative of the excitation of the system, but no net increase. The curve for  $L=5$  is one of the most ambiguous cases since the rms radius shows a slow but definite increase. Extrapolation of this increase would result in the system reaching a typical separation radius of 9 fm at a time approximately  $160 \times 10^{-22}$  sec, far beyond our calculations. However, in any system interacting this long, the two-body collisions will become important. The excitation of these additional internal modes will damp the energy in collective modes and result in fusion. Therefore, events such as this are considered fused and we can use plots such as these to determine whether or not to continue our calculation a little farther to look for separation.

For the angular momenta which lead to fusion, we can learn little except that the system fuses. The behavior of the system after fusion is better described by traditional statistical models (NO 76 p.224). We can calculate a fusion cross section,  $\sigma_F$ , by a sharp cutoff formula

$$\sigma_F = \frac{\pi}{k^2} \sum_{l_j} (2l+1) \quad , \quad (4.13)$$

where  $\hbar k$  is the relative momentum of the nuclei and the sum is over all  $l$  which

fuse,  $l_F$ . When fusion occurs, it occurs for a range of  $l$  from  $l_<$  to  $l_>$ . Then we can do the sum,

$$\sigma_F = \frac{\pi}{k^2} [l_>(l_>+1) - l_<(l_<+1)] = \frac{\pi}{k^2} [(l_> + \frac{1}{2})^2 - (l_< + \frac{1}{2})^2] \quad (4.14)$$

The classical correspondence is most obvious from the first formula. Since the total angular momentum squared  $L^2 = \hbar^2 l(l+1) = (\hbar kb)^2$ , where  $b$  is the classical impact parameter, substituting above gives  $\sigma_F = \pi(b_>^2 - b_<^2)$ , the area between these impact parameters. For lighter nuclei at low energies, fusion dominates and the fusion cross section is the main result.

For heavier nuclei, scattering becomes more important. For the angular momenta which separate, we get much more information, primarily from the densities. By integrating the densities over each fragment separately, we can calculate their mass numbers ( $A_1, A_2$ ), charge numbers ( $Z_1, Z_2$ ) and centers of mass ( $\vec{R}_1, \vec{R}_2$ ) at each time. (After separation the masses and charges are very nearly constant.) The motion of the centers of mass determines the important dynamic quantities in the center of mass frame:

$$TKE = \frac{1}{2} m \left( \frac{A_1 A_2}{A_1 + A_2} \right) (\dot{\vec{R}}_1 - \dot{\vec{R}}_2)^2 \quad (4.15)$$

$$E = TKE + \frac{Z_1 Z_2 e^2}{|\vec{R}_1 - \vec{R}_2|} \quad \text{and}$$

$$\vec{L} = m A_1 \dot{\vec{R}}_1 \times (\vec{R}_1 - \vec{R}_2) = m A_2 \dot{\vec{R}}_2 \times (\vec{R}_2 - \vec{R}_1) \quad .$$

These quantities are actually estimated at the half time step,  $t - \frac{1}{2}\Delta t$ , by

$$\dot{\vec{R}}_i = \frac{\vec{R}_i(t) - \vec{R}_i(t - \Delta t)}{\Delta t} \quad (4.16)$$

and

$$\vec{R}_i = \frac{\vec{R}_i(t) + \vec{R}_i(t - \Delta t)}{2} \quad .$$

We also calculate the orientation of the principal axis of inertia and various moments of the density distribution for both the total system and the fragments. In addition, we define fragments even when they aren't separated, as

discussed in Appendix A7. Although this procedure is somewhat arbitrary when the fragments overlap greatly, it determines possibly useful collective coordinates throughout the evolution.

To calculate the scattering angle, we need to translate our initial nuclei back to infinity and our final nuclei forward to infinity along Rutherford trajectories (GO 50). Therefore, the change in angle before the calculation begins is

$$\Delta\vartheta_b = \cos^{-1}\left[\frac{-1}{\varepsilon_i}\left(\frac{1}{\alpha_i r_i} + 1\right)\right] - \cos^{-1}\left[\frac{-1}{\varepsilon_i}\right] , \quad (4.17)$$

and the change after the calculation ends is

$$\Delta\vartheta_a = \cos^{-1}\left[\frac{-1}{\varepsilon_f}\left(\frac{1}{\alpha_f r_f} + 1\right)\right] - \cos^{-1}\left[\frac{-1}{\varepsilon_f}\right] ,$$

where

$$\varepsilon = \left[1 + \frac{2E}{\mu} \left(\frac{L}{Z_1 Z_2 e^2}\right)^2\right]^{1/2} , \quad (4.18)$$

$$\alpha = \frac{\mu Z_1 Z_2 e^2}{L^2} \quad \text{and} \quad r = |\vec{R}_1 - \vec{R}_2| .$$

In general, these three quantities are different for the final state because  $E$ ,  $L$ ,  $Z_1$ ,  $Z_2$ ,  $A_1$ , and  $A_2$  are all different. (Of course  $A_1 + A_2 = A_T$  and  $Z_1 + Z_2 = Z_T$  and the total mass and charge are not changed.) Therefore, the scattering angle is given by

$$\vartheta_s = 180^\circ - (\vartheta_f - \vartheta_i + \Delta\vartheta_b + \Delta\vartheta_a) . \quad (4.19)$$

The ambiguity in the sign of  $\Delta\vartheta$  due to the multiple values of  $\cos^{-1}x$  is resolved by choosing  $\cos^{-1}x$  between  $0^\circ$  and  $180^\circ$ . This results in  $\Delta\vartheta > 0$  as we would expect for a repulsive potential.

For scattered events, we also define two moments, contact and separation, from the pictures of the density projected onto the scattering plane. Thus, we consider the fragments to be separated when a line in the scattering plan dividing the density distribution has a maximum projected density,  $\rho_{pr} = \int dz \rho$ , less than  $\rho_{cr} = .1 \text{fm}^{-2}$ . (This would correspond to a neck width of .6 fm at

$\rho_{sat} = .17 \text{fm}^{-3}$ .) Defining these events allows us to approximate the interaction time by  $\tau_{int} = t(\text{separation}) - t(\text{contact})$  and allows comparison of other quantities, like the rms radius of the system, at contact and separation.

The last results we obtain require more information from the wavefunctions than the total proton and neutron density. These are the single-particle energies and the mass and charge widths of the fragments. The single-particle energies,

$$e_j = \langle \psi_j | h | \psi_j \rangle \quad (4.20)$$

are obtained quite simply since  $h | \psi_j \rangle$  is calculated for the evolution of  $\psi_j$  (see Appendix A6, Part IV). The mass and charge widths can be obtained by defining a number operator for particles in a particular fragment (BO 76a)

$$\hat{N}^R = \int d\tau \vartheta(\tau) \Psi^\dagger(\tau) \Psi(\tau) \quad (4.21)$$

where  $\Psi^\dagger, \Psi$  are creation, annihilation operators for a particle of position  $\tau$  and  $\tau'$  is a Heaviside function (MA 70) so the integral extends only over one fragment (as defined by the split in Appendix A7).

$$\begin{aligned} \langle \hat{N}^R \rangle &= \int d\tau \vartheta(\tau) \sum_i \psi_i(\tau) \psi_i^*(\tau) \\ &= \sum_i w_{ii} \end{aligned} \quad (4.22)$$

The dispersion of this number operator is given by

$$\sigma_{\hat{N}^R}^2 = \langle \hat{N}^{R^2} \rangle - \langle \hat{N}^R \rangle^2 \quad (4.23)$$

The first term gives

$$\begin{aligned} \langle \hat{N}^{R^2} \rangle &= \int d\tau \vartheta(\tau) \Psi^\dagger(\tau) \Psi(\tau) + \int d\tau d\tau' \vartheta(\tau) \vartheta(\tau') \Psi^\dagger(\tau) \Psi^\dagger(\tau') \Psi(\tau') \Psi(\tau) \\ &= \sum_i w_{ii} + \sum_{ij} (w_{ii} w_{jj} - w_{ij} w_{ji}) \end{aligned} \quad (4.24)$$

Since

$$\langle \hat{N}^R \rangle^2 = \sum_{ij} w_{ii} w_{jj} \quad , \quad (4.25)$$

$$\sigma_{\hat{N}^R}^2 = \sum_i w_{ii} - \sum_{ij} |w_{ij}|^2 \quad . \quad (4.26)$$

Thus for a Gaussian distribution, we can define a full-width half-maximum for

charge or mass by

$$\Gamma = \sqrt{8 \ln 2} \sigma \quad (4.27)$$

where the sums over  $ij$  include only protons for the charge width and both isospins for the mass widths.

We note that this width is inherently limited by the one-body nature of TDHF (DAS 79). (Since this  $\Gamma$  is a two-body operator, the TDHF results will be less accurate.) Performing a unitary transformation to diagonalize  $w_{ij}$  gives

$$\sigma_{NR}^2 = \sum_i w_{ii} (1 - w_{ii}) \quad (4.28)$$

so with  $\sum_i w_{ii} \equiv A_R$

$$\sigma_{NR}^2 \leq A_R \left(1 - \frac{A_R}{A}\right) \quad (4.29)$$

and the absolute maximum is

$$\sigma_{NR}^2(\max) = \frac{A}{4} . \quad (4.30)$$

### Section 5: Brief Review of Earlier Calculations

The earliest investigation of TDHF for nuclear collisions was a one-dimensional calculation of the dynamics of slabs of nuclear matter, infinite and homogeneous in two directions but finite in the other direction (BO 76a). These authors introduced the BKN force and ignored Coulomb forces. These slabs showed nearly constant saturation density in the interior with surfaces about 2 fm thick. Single slab dynamics were studied, both breathing mode oscillations and the interaction with an external barrier. However, for our purposes their calculations of slab collisions are more important. These revealed a wide range of phenomena - fusion, resonances, deep inelastic scattering and fragmentation as the bombarding energy was increased. At the lowest energies, up to 1 MeV per nucleon, the nuclei fused. The coherent translational energy went into internal excitation, that is, oscillations of the system. At higher energies, these oscillations became more vigorous and could lead to scission. In this energy range, from 1 - 2 MeV/A, a delicate interplay between single particle effects (orbitals bouncing between the walls) and collective effects (scission of the walls) caused resonances, sometimes fusion, sometimes inelastic scattering. From 2 - 15 MeV/A, there was deep-inelastic scattering where the fragments separated with reduced relative kinetic energies (sometimes only 10% of the initial) and internal excitation. At still higher energies fragmentation was observed with 3 or 4 outgoing fragments.

These results encouraged the first realistic calculations: two dimensions with axial symmetry. These calculations were first done for head-on collisions (BO 76b, KO 76) but were very soon extended to any impact parameter by the use of a rotating frame approximation (KO 77). This approximation reduced TDHF to two dimensions ( $r, z$ ) by requiring axial symmetry about the rotating line between mass centers. It then added a rotational energy to the Hamiltonian

$$H' = H + \frac{L^2}{2I(\rho)} \quad (5.1)$$

where  $L$  was the conserved relative orbital momentum and  $I$  was the moment of inertia, a prescribed functional of the density. This added a centrifugal term to the HF potential

$$W' = W - \frac{1}{2}\omega^2 \frac{\delta I}{\delta \rho} \quad (5.2)$$

where  $\omega = \frac{d\vartheta}{dt} = \frac{L}{I}$ . At large separation  $I$  was taken to be that of two point masses, and, when the nuclei coalesced, it was taken to be that of a rigid rotor. The wavefunctions were evolved with  $W'$  while simultaneously  $\omega$  was integrated to give the orientation of the symmetry axis in space,  $\vartheta$ . This approximation should be best for peripheral or head-on collisions and at lower energies. These first calculations for symmetric collisions of  $^{16}\text{O}$  or  $^{40}\text{Ca}$  showed inelastic scattering and fusion similar to the experimental data but with too little dissipation and too little fusion.

Since these deficiencies could be due to either TDHF itself, the effective interaction, or the two dimensional approximation, it was important to do full three-dimensional calculations. Calculations were done for the same systems, yielding fusion cross sections at various energies (BO 78) and detailed scattering results at one energy (FL 78). The results at large and small impact parameters agreed with the axially symmetric results but significant differences appeared at intermediate impact parameters, where nonaxial deformations were large. In some cases, the axial asymmetry,  $\frac{\langle z^2 - y^2 \rangle}{\langle z^2 + y^2 \rangle}$ , was as large as 0.2. The 3D calculations provided a microscopic realization of tangential dissipation which decreased both the angular momentum and energy in collective modes, particularly at higher energies, and led to increased fusion.

The scattered solutions for  $^{16}\text{O}$  at one energy, showed a behavior typical of our later calculations. The highest angular momenta showed no energy loss and

Coulomb scattering. Smaller angular momenta led to decreasing scattering angle (becoming negative when nuclear attraction dominated Coulomb repulsion) and increasing energy loss until the system fused. This behavior is to be expected (see section 3) although the details can be compared with experiment. The unexpected result was that at the lowest angular momentum there were also scattered solutions with nearly constant energy loss (about 35 MeV of the original 52.5 MeV) and little loss of angular momentum.

The fusion calculation for  $^{16}\text{O}$  showed that this low- $l$  "cutoff" appeared at  $E_{lab}=54$  MeV and persisted at higher energies. This lower angular momentum limit occurred because too much energy was transferred to a single collective mode, in this case a vibrational mode. For TDHF calculations this mode is strongly excited because the long mean free path of the nucleons results in an "almost transparent" nucleus, but it has been shown to be a more general phenomenon (BR 78, TS 74, SI 76) occurring even in drops of water (AD 68). Thus, the upper and lower angular momentum limits can be thought of as rotational and vibrational limits. Both the upper- and lower- $l$  cutoffs were approximately proportional to  $\sqrt{E-E_T}$ , though with different proportionality constants and energy thresholds,  $E_T$ . This can be interpreted as a limitation of radial kinetic energy since  $E_{rad}=E_T$  will result in  $l=[\frac{2I}{7R^2}(E-E_T)]^{\frac{1}{2}}$ . For the upper- $l$  cutoff this means the nuclei can climb in over the fusion barrier, for the low- $l$  cutoff this means that a more compact configuration (smaller  $I$ ) can climb out over the fission barrier.

These  $^{16}\text{O}$  fusion cross sections fit the data very well up to  $E_{lab} = 120$  MeV, in contrast to optical model predictions which greatly overestimate the fusion cross section above about 60 MeV. (The potential fit elastic scattering for  $E_{lab}\leq 70$  MeV.) The higher cutoff was in excellent agreement with the optical model up to 80 MeV and showed only a slight lowering above this energy due to

the onset of peripheral deep inelastic processes. This discrepancy between the optical model and experiment was then resolved in TDHF by the existence of a low- $l$  cutoff. The fusion calculations for  $^{40}\text{Ca}$  showed the same general behavior of the upper limit but they showed no lower cutoff. The energies were all below the threshold since a low- $l$  cutoff was seen in the higher energy 2D calculations which should be exact for  $l=0$ . These cross sections were less accurate and showed some sensitivity to the interaction parameters. However, all of the forces were local forces so these calculations may give us more information about the effective interaction. The experimental search for this low- $l$  cutoff is as yet unresolved and work is continuing. More will be said about this later for our specific calculations.

The need to extend these calculations to more realistic forces (even if still the Skymre type) and heavier nuclei led to a renewed investigation of 2D approximations (DAV 78a,79,80) since the 3D calculations were already saturating computer capabilities. Heavier nuclei are important both because the increase in deep inelastic events will yield information about equilibration processes in TDHF and because the classical concepts we are using will be more appropriate. Refinements to the axially symmetric approximation were made by changes in the moment of inertia (DAV 78b). Several prescriptions were tried which permitted angular momentum to be transferred to internal excitation, thus allowing tangential dissipation. These results were a better approximation to 3D results than the previous 2D results and agreed quite well at lower energies. However, at higher energies, above the threshold of the low- $l$  cutoff, there is no escaping the importance of nonaxial deformations for intermediate impact parameters.

## Section 6: Separable Approximation

The deficiencies of axially symmetric approximations and the intractability of full 3D calculations prompt the investigation of other approximations which can limit the number of variables treated explicitly but still retain those degrees of freedom necessary for an accurate solution. Once such approximation, the separable approximation (DE 78a,78b), is tested in the first published paper included here (KO 78). The separable approximation reduces the calculation to two dimensions by forbidding motion perpendicular to the scattering plane. However, it imposes no restrictions on motion in the scattering plane and will allow the important features of nonaxial deformations and tangential dissipation to be calculated self-consistently.

The freezing of the wavefunctions in this transverse direction is motivated by the mean-field dynamics which govern their evolution in the TDHF approximation. The saturation of nuclear forces results in a nearly constant density and thus a nearly constant mean field in the nuclear interior. Therefore, the orbitals which are initially moving in the scattering plane will continue to move predominantly in the scattering plane during the collision.

The separable approximation constrains the single-particle wavefunctions to the factorized form,

$$\psi_i(\vec{r}, t) = \varphi_i(x, y, t) \chi_i(z) \quad , \quad (6.1)$$

where  $z$  is the coordinate normal to the reaction plane and  $x, y$  are coordinates in this plane. The functions  $\chi_i$  are real and time independent so only the 2D complex wavefunctions  $\varphi_i$  need to be evolved in time. The time evolution is obtained from the TDHF equation,  $i\hbar \frac{\partial}{\partial t} \psi_j = h \psi_j$ . Since  $\chi_j$  is time independent, the equation becomes

$$\chi_j i\hbar \frac{\partial}{\partial t} \varphi_j = h \chi_j \varphi_j \quad . \quad (6.2)$$

The functions  $\chi_j$  are normalized so we can write the evolution equation as

$$i\hbar \frac{\partial}{\partial t} \varphi_j(x, y) = (h'_j \varphi_j)(x, y) \quad (6.3)$$

(in general  $h$  and  $h'$  will be nonlocal) with the projected Hamiltonian given by

$$h'(x, x', y, y') = \int dz dz' \chi_j(z) h(x, x', y, y', z, z') \chi_j(z') \quad (6.4)$$

This equation can also be derived from a variational principle with,

$$\frac{\delta \langle H \rangle}{\delta \varphi_j^*(x, y)} = (h'_j \varphi_j)(x, y) \quad (6.5)$$

(Variation of only  $\varphi_j^*$  would leave a  $\chi_j$  on the left-hand side of the Hamiltonian and give the same result as Eq. (6.4)) Notice that this projected Hamiltonian is, in general, different for different orbitals.

Since the mean field (that is, the same field for all wavefunctions) is important for maintaining the orthogonality of the single-particle wavefunctions  $\psi_j$ , we must check the orthogonality in the separable approximation. At the initial time  $\langle \varphi_j | \varphi_i \rangle \langle \chi_j | \chi_i \rangle = \delta_{ij}$  can be satisfied with either  $\langle \chi_j | \chi_i \rangle = \delta_{ij}$  or  $\langle \varphi_j | \varphi_i \rangle = \delta_{ij}$  permitting a natural grouping of the  $\psi_j$ . The orthogonality of the  $\psi_j$  is trivially preserved for wavefunctions with  $\langle \chi_j | \chi_i \rangle = 0$  since these functions are independent of time. However, maintaining the orthogonality of the  $\varphi_j$  for the other wavefunctions with  $\langle \chi_j | \chi_i \rangle \neq 0$  is not trivial since  $i\hbar \frac{\partial}{\partial t} \langle \varphi_j | \varphi_i \rangle = \langle \varphi_j | h_i - h_j | \varphi_i \rangle$ . Orthogonality requires  $h_i = h_j$  and  $\chi_i = \chi_j$  if  $\langle \chi_j | \chi_i \rangle \neq 0$ . Therefore, we need a set of orthogonal functions in the  $z$  direction,  $B_\alpha(z)$ , and there is a group of wavefunctions  $\varphi_j$  for each  $\alpha$ . For a symmetric collision, like those considered in this first paper, this is the obvious thing to do. However, in asymmetric collisions, like those considered later in Sections 7 and 8, this requires that the same set of orthogonal functions be used for the two different nuclei.

We choose these wavefunctions,  $B_\alpha(z)$ , to be one-dimensional harmonic oscillator functions. For the  $^{16}\text{O}$  and  $^{40}\text{Ca}$  nuclei considered in this first paper, oscillator states are a fairly accurate approximation to the ground state

wavefunctions and for oscillator states the factorization,  $\psi_j(\vec{r}) = \varphi_j(x,y)\chi_j(z)$  is exact. For heavier nuclei we might consider other possibilities for the transverse wavefunctions but the 3D HF wavefunctions can't generally be factored as above. Fortunately, as shown in the paper, factoring and using oscillator states doesn't cause much change from the 3D results. The static HF calculations begin with 3D oscillator states, so we simply freeze these wavefunctions in one direction and use the imaginary time step method with the separable approximation to find the ground state wavefunctions  $\varphi_j(x,y)$ . We then choose the time independent oscillator frequency to minimize the energy of the static solution.

The actual incorporation of this approximation into the computer code and the savings obtained are discussed in Appendix A5 for the full nonlocal Skyrme force (protons and neutrons treated separately). For this paper, we use the much simpler BKN force, isospin degenerate and without the  $(\rho\tau - j^2)$  term, but otherwise the discussion is applicable. The major computational effort, both in time and storage, is the evolution of the wavefunctions. This evolution is reduced to a 2D problem resulting in considerable savings. However, the entire problem is not two dimensional and the calculation of the energy and potential will still require 3 dimensions.

The results we obtain with this approximation for symmetric collisions of  $^{16}\text{O}$  or  $^{40}\text{Ca}$  and the comparisons to the 3D results are described in detail in the paper. The conclusion is that this approximation is not only better than the axially symmetric approximation, but is surprisingly accurate. Therefore, we will use this approximation for more TDHF calculations with heavier nuclei and more realistic nonlocal Skyrme forces.

The insensitivity of the results to the choice of oscillator parameter is also important. For both O and Ca, runs done at the most sensitive angular

momenta, those at the fusion limits, showed that a 10% change in the oscillator parameter would lead to, at most, one unit ( $\hbar$ ) of angular momentum difference in the fusion cross section or in comparable trajectories. This is undoubtedly related to the success of the approximation, since even small motion in the transverse direction could be important if the results were sensitive to the shape in this direction. It is also fortunate since the transverse wavefunctions for heavier nuclei are more complicated than harmonic oscillator functions, and the factorized form limits the accuracy of the descriptions of these heavy nuclei in the  $z$  direction. Also, this insensitivity is almost a necessity for the calculation of asymmetric systems since the requirement of one set of wavefunctions  $B_a(z)$  in the transverse direction limits the accuracy of the shapes of the two different nuclei.

A SEPARABLE APPROXIMATION TO TIME-DEPENDENT  
HARTREE-FOCK CALCULATIONS

S. Koonin, B. Flanders, H. Flocard, and M. Weiss  
Phys. Lett. 77B, 13 (1978)

A SEPARABLE APPROXIMATION TO TIME-DEPENDENT  
HARTREE-FOCK CALCULATIONS\*

S. KOONIN<sup>†</sup> and B. FLANDERS

W. K. Kellogg Radiation Laboratory

California Institute of Technology, Pasadena, California 91125 USA

H. FLOCARD

Division de Physique Théorique

Institut de Physique Nucleaire, B.P. N<sup>o</sup> 1, 91406 Orsay, France

and

M. WEISS

Lawrence Livermore Laboratory

University of California, Livermore, California 94550 USA

Abstract

We discuss an approximation to three-dimensional (3-D) TDHF calculations for heavy-ion reactions which neglects motion normal to the scattering plane. Quantitative comparisons with 3-D results indicate the accuracy of this method and an order-of-magnitude reduction in computation time.

---

\* Supported in part by the National Science Foundation [PHY76-83685, PHY77-21602] and U.S. Energy Research and Development Contract No. W-7405-Eng-48.]

<sup>†</sup> Alfred P. Sloan Foundation Fellow.

---

Numerical applications of the time-dependent Hartree-Fock method [1] to heavy-ion reactions [2-5] and fission [6] provide a microscopic description of large-amplitude nuclear dynamics. Several calculations have approximated these systems in two non-trivial spatial dimensions by constraining the TDHF determinant to be axially symmetric [2,3,6]. However, recent fully three-dimensional (3-D) solutions for heavy-ion reactions have shown that tangential degrees of freedom are important for realizing fully the dissipation inherent in a mean-field approach [4,5]. There are also indications that tri-axiality is essential for an accurate TDHF description of fission dynamics [6]. Since "exact" 3-D solutions presently involve a great deal of computational effort for large systems, it is desirable to seek approximations which limit the number of variables to be treated explicitly, but which retain those degrees of freedom necessary for an accurate solution. This Letter explores one such approximation for heavy-ion reactions, in which motion normal to the scattering plane is forbidden [7]. By direct comparison with 3-D calculations for  $^{16}\text{O} + ^{16}\text{O}$  and  $^{40}\text{Ca} + ^{40}\text{Ca}$  reactions we show that the resulting solutions are surprisingly accurate. The associated order-of-magnitude reduction in computation time therefore opens the possibility for meaningful calculations of larger systems using more sophisticated effective interactions.

The motivation and specifics of a TDHF approach to nuclear dynamics have been discussed elsewhere [1,2,4]. The fundamental feature new to this work is that the complex time-dependent single-particle wavefunctions are constrained to be of the factorized form proposed by Devi and Strayer [7]

$$\psi_i(\vec{r}, t) = \varphi_i(x, y, t) \chi_i(z). \quad (1)$$

The coordinate normal to the reaction plane is  $z$ , while  $(x, y)$  are the

coordinates in this plane. The real functions  $\chi$  are time independent, so that only the complex functions  $\varphi$  involving two spatial variables must be evolved in time. The ansatz (1) is thus comparable to the axially symmetric factorization used previously [2,3,6], although here the coordinate  $z$  is "frozen" rather than the azimuthal angle about the symmetry axis. Note that non-axial configurations are still permitted by the form of (1).

The motivation for the above factorization can be found in features of mean-field dynamics familiar from previous calculations [2,4]. In a TDHF approach, the evolution of the single-particle wavefunctions is governed only by their common, time-dependent mean field. Initially, the determinant is constructed to represent approaching, self-consistent static HF solutions for the colliding ions. During the collision, as orbitals propagate freely in the nearly constant mean-field of the nuclear interior [1], their motion is predominantly in the scattering plane. This can readily be seen in fig. 2 of ref. [2], which represents a  $^{40}\text{Ca} + ^{40}\text{Ca}$  collision. There, despite the dramatic dynamics along the symmetry axis, the transverse extent of the system changes little during the collision. There is consequently little tendency to deform the system normal to the plane, and an approximate self consistency in this direction is maintained.

The equations of motion for the functions  $\varphi$  follow from the TDHF equations. For an effective interaction which results in a local HF potential  $W$ , they are of the form

$$i\hbar \frac{\partial \varphi_j}{\partial t} = \left[ -\frac{\hbar^2}{2m} \left( \frac{\partial^2}{\partial x^2} + \frac{\partial^2}{\partial y^2} \right) + \langle T_z \rangle_j + W_j(x, y) \right] \varphi_j \quad (2)$$

Here,  $W_j$  is the projected HF potential

$$W_j(x, y) = \int_{-\infty}^{\infty} dz |\chi_j(z)|^2 W(x, y, z), \quad (3)$$

and  $\langle T_z \rangle_j$  is the kinetic energy of  $\chi_j$ :

$$\langle T_z \rangle_j = \frac{\hbar^2}{2m} \int_{-\infty}^{\infty} dz \left| \frac{d\chi_j}{dz} \right|^2. \quad (4)$$

Our calculations employ the energy functional of refs. [2,4,5]. This includes zero-range two- and three-body forces, a finite range Yukawa interaction, and the direct Coulomb energy. It is known to give a fair reproduction of the ground-state properties of  $^{16}\text{O}$  and  $^{40}\text{Ca}$  [1,5] and results in a local HF potential. The functions  $\chi$  are chosen to be one-dimensional harmonic-oscillator functions and are assigned to the wavefunctions  $\psi$  at  $t = 0$  according to the three-dimensional harmonic-oscillator classification of the static HF solutions.

The time-independent oscillator frequency is chosen to minimize the energy of the individual static HF solutions before collision. Finite difference approximations to the equations (2) are derived by variation of a discretized "5-point" energy functional defined on a uniform 1 fm cartesian mesh, as described in refs. [2,4]. The Poisson and Helmholtz equations for the one-body Coulomb and Yukawa potentials are solved by the conjugate-gradient method discussed in ref. [4], and the functions  $\varphi$  are evolved in time using the exponential method of that reference. Time steps of  $\Delta t = 0.002-0.004 \times 10^{-21}$  sec are used and energy and norm conservation for the entire system are equal to or better than the values quoted in ref. [4] for the 3-D calculations.

One evidently necessary condition for the accuracy of the separable approximation (1) is that it reproduce adequately the exact static HF

solutions, at least in the reaction plane. The properties of these solutions for several oscillator closed-shell nuclei ( $N = Z = 8, 20, 40, 70$ ) are shown in Table 1. Both the separable and 3-D solutions have been obtained with the imaginary time-step technique of ref. [4]. For each separable solution, the oscillator frequency for the functions  $\chi, \chi\omega$ , has been chosen to maximize the binding energy per nucleon,  $BE/A$ . The binding energies of the separable solutions are consistently somewhat smaller than the 3-D values since they correspond to a more restricted class of variational wavefunction. The discrepancy increases with mass as oscillator states become a poorer approximation to the exact HF wavefunctions, although even for  $A = 140$  it amounts to only 0.3 MeV per nucleon. The root-mean-square radii,  $\langle r^2 \rangle^{\frac{1}{2}}$ , of the two solutions agree to within 1% for all values of  $A$ . The values of  $Q/A\langle r^2 \rangle$ , where  $Q$  is the mass quadrupole moment, show that even though the separable approximation treats one cartesian coordinate differently from the other two, it results in only slightly oblate solutions. Note that the deformations listed for the 3-D solutions indicate the accuracy of our finite-difference techniques, since these should be zero in the exact HF solution.

In fig. 1 we show the coordinate-space densities of the separable and 3-D static solutions. In the reaction plane ( $z = 0$ ), the separable results agree well with the 3-D calculation, particularly in the surface region. In the direction normal to the reaction plane ( $x = y = 0$ ), where the separable approximation is expected to be worst, the agreement is poor. However, this appears to be of small significance for dynamical TDHF calculations, which depend strongly only on those properties of the ions within the reaction plane.

In fig. 2 we compare separable and 3-D time-dependent trajectories for the  $^{40}\text{Ca} + ^{40}\text{Ca}$  system at  $E_{\text{cm}} = 139$  MeV. The fragment separation and angular coordinates used are defined in ref. [4] in terms of the over-all mass-quadrupole tensor

of the system and the centers-of-mass of the two fragments. The results as a function of impact parameter follow a pattern familiar from previous 3-D calculations [4,5]: highly inelastic events at small impact parameters, fusion at intermediate angular momenta, and inelastic scattering for peripheral collisions. The overall qualitative behavior of the separable approximation agrees excellently with the 3-D calculations. The relatively minor discrepancies in the  $L = 20 \hbar$  (highly inelastic) and  $L = 30 \hbar$  (fusion) trajectories indicate that the nuclei are somewhat too "stiff" in the separable approximation, and scission is therefore more difficult. This trend is confirmed in the  $L = 80 \hbar$  trajectory (inelastic scattering), although the discrepancy here is actually smaller than it appears since the deflection function is changing rapidly with  $L$  in this region. Trajectory plots for  $^{40}\text{Ca} + ^{40}\text{Ca}$  at other bombarding energies and for  $^{16}\text{O} + ^{16}\text{O}$  collisions show similar agreement between the separable and 3-D calculations.

Final-state results for some  $^{16}\text{O} + ^{16}\text{O}$  and  $^{40}\text{Ca} + ^{40}\text{Ca}$  collisions are quantitatively compared in Table 2. Separable values for the final orbital angular momentum, final fragment kinetic energies, and center-of-mass scattering angle are generally in very good agreement with the 3-D calculations. Note particularly that in every case save one ( $^{40}\text{Ca} + ^{40}\text{Ca}$ ,  $E_i = 96$  MeV,  $L_i = 10 \hbar$ ) the fusion region is reproduced by the separable approximation, in contrast to the axially symmetric approximation where no fusion is found at all in these collisions [2]. Note also that the apparently large discrepancies in  $E_f$  for  $^{40}\text{Ca} + ^{40}\text{Ca}$  at  $E_i = 400$  MeV amount to only some 20 MeV out of over 300 MeV dissipated in the collisions. The largest differences between the separable and 3-D results generally occur where the final state is very sensitive to the initial conditions. Thus, the separable solution for  $^{40}\text{Ca} + ^{40}\text{Ca}$  at  $E_i = 96$  MeV,  $L_i = 10 \hbar$  crosses the outer barrier to scission with less than 2 MeV of radial

collective kinetic energy, while the 3-D calculation is just above the low-L cutoff for fusion. Similarly, the slight discrepancies at  $E_i = 96$  MeV,  $L_i = 60 \hbar$  and  $E_i = 192$  MeV,  $L_i = 80 \hbar$  may be attributed to the rapid change of scattering angle with impact parameter in the region just above orbiting. Since such singular regions of L-space are only a very small part of the total cross section, the separable approximation accurately reproduces both the 3-D fusion cross section and the deflection function. We have also investigated the sensitivity of several of our calculations to choices of  $\hbar\omega$  other than that which minimizes the energy of the static solutions. The separable results presented in Table 2 are relatively insensitive to variations of  $\pm 20\%$  in this parameter.

In summary, a quantitative study of  $^{16}\text{O} + ^{16}\text{O}$  and  $^{40}\text{Ca} + ^{40}\text{Ca}$  collisions has demonstrated the accuracy of a separable approximation to the 3-D TDHF equations. The time-independence of the wavefunction in the coordinate normal to the reaction plane results in almost an order-of-magnitude decrease in computational time. The techniques presented here may be extended immediately to Skyrme-like forces having an effective mass and allowing for isospin degrees of freedom. Large-scale calculations with these methods for mass symmetric systems should then provide a decisive test of mean-field theories for heavy-ion reactions. Furthermore, while there appears to be no need to do so at present, the separable determinant can be made somewhat more flexible by allowing for a simple time-dependence in the transverse coordinate; e.g., a time-dependent oscillator frequency. Self-consistent equations describing such motion can readily be derived from the time-dependent variational principle [8]. The method can be simply extended to moderately mass-asymmetric systems by using the same  $\hbar\omega$  for each nucleus; the relative insensitivity of the results in Table 2 to  $\hbar\omega$  favors such an approach. However, the extension

of this technique to strongly asymmetric systems is not at all obvious and work in this direction is in progress.

We are grateful for discussions with Drs. Paul Bonche and John Negele during these calculations.

References

- [1] P. Bonche, S. Koonin and J. W. Negele, Phys. Rev. C13 (1976) 1226.
- [2] S. E. Koonin, K. T. R. Davies, V. Maruhn-Rezwani, H. Feldmeier, S. J. Krieger and J. W. Negele, Phys. Rev. C15 (1977) 1359.
- [3] V. Maruhn-Rezwani, K. T. R. Davies and S. E. Koonin, Phys. Lett. 67B (1977) 134; A. Kerman, to be published in Proceedings of the International Conference on Nuclear Structure, Tokyo, 1977.
- [4] H. Flocard, S. E. Koonin and M. S. Weiss, Phys. Rev. C, in press.
- [5] P. Bonche, B. Grammaticos and S. E. Koonin, Phys. Rev. C, in press.
- [6] J. W. Negele, S. E. Koonin, P. Möller, J. R. Nix and A. J. Sierk, Phys. Rev. C, in press.
- [7] K. R. Sandhya Devi and M. R. Strayer, Phys. Lett. 77B, 135 (1978).
- [8] A. K. Kerman and S. E. Koonin, Ann. Phys. (N.Y.) 100 (1976) 332.

Table 1  
 Properties of the static solutions

	BE/A (MeV)	$\langle r^2 \rangle^{\frac{1}{2}}$ (fm)	Q/A $\langle r^2 \rangle$	$\hbar\omega$ (MeV)
$^{16}_0$	7.29	2.61	-0.014	13.9
	(7.43)	(2.60)	(-0.006)	—
$^{40}_{Ca}$	8.11	3.38	-0.003	10.9
	(8.30)	(3.35)	(-0.003)	—
A = 80	7.84	4.17	-0.022	9.1
	(8.10)	(4.14)	(-0.001)	—
A = 140	6.91	5.00	-0.020	7.6
	(7.23)	(4.96)	(-0.000)	—

Values in parentheses correspond to the 3-D solutions.

Table 2

Comparison of final states in separable and 3-D TDHF calculations

	$L_f(\hbar)$	$E_f$ (MeV)	$\Theta_f$ (degrees)		$L_f(\hbar)$	$E_f$ (MeV)	$\Theta_f$ (degrees)
$^{16}\text{O} + ^{16}\text{O}$ $E_i = 55.6$ MeV					$^{40}\text{Ca} + ^{40}\text{Ca}$ $E_i = 139$ MeV		
$L_i = 10\hbar$	11	18	80		$L_i = 0\hbar$	0	58
	8	17	90			0	58
$L_i = 20\hbar$	← fusion →				$L_i = 10\hbar$	11	59
	← fusion →					10	58
$L_i = 30\hbar$	25	37	-1		$L_i = 20\hbar$	17	58
	23	29	-29			17	59
$^{40}\text{Ca} + ^{40}\text{Ca}$ $E_i = 96$ MeV					$L_i = 30-70\hbar$	← fusion →	
$L_i = 0\hbar$	0	59	180			← fusion →	
	0	54	180		$L_i = 80\hbar$	65	89
$L_i = 10\hbar$	6	55	143			66	88
	← fusion →				$L_i = 90\hbar$	84	122
$L_i = 20-50\hbar$	← fusion →					83	120
	← fusion →				$^{40}\text{Ca} + ^{40}\text{Ca}$ $E_i = 400$ MeV		
$L_i = 60\hbar$	52	79	28		$L_i = 10\hbar$	9	69
	50	72	19			14	93
$L_i = 70\hbar$	65	89	45		$L_i = 30\hbar$	28	83
	65	89	45			32	103

$E_i$  and  $L_i$  are the initial c.m. energy and orbital angular momentum;  $L_f$ ,  $E_f$ , and  $\Theta_f$  are the final orbital angular momentum, c.m. fragment kinetic energy, and c.m. scattering angle. 3-D results are given below the separable values.

Figure Captions

Fig. 1. Comparison between separable and 3-D static HF solutions for several oscillator closed-shell nuclei. Curves labeled by  $z = 0$  ( $x = y = 0$ ) are the separable solutions in (normal to) the reaction plane. The fully 3-D solutions are the solid lines.

Fig. 2. Comparison between separable and 3-D trajectories for  $^{40}\text{Ca} + ^{40}\text{Ca}$  collisions at a center-of-mass energy  $E_1 = 139$  MeV. In cases where the 3-D trajectory is not shown, it is too close to the separable result to be plotted.

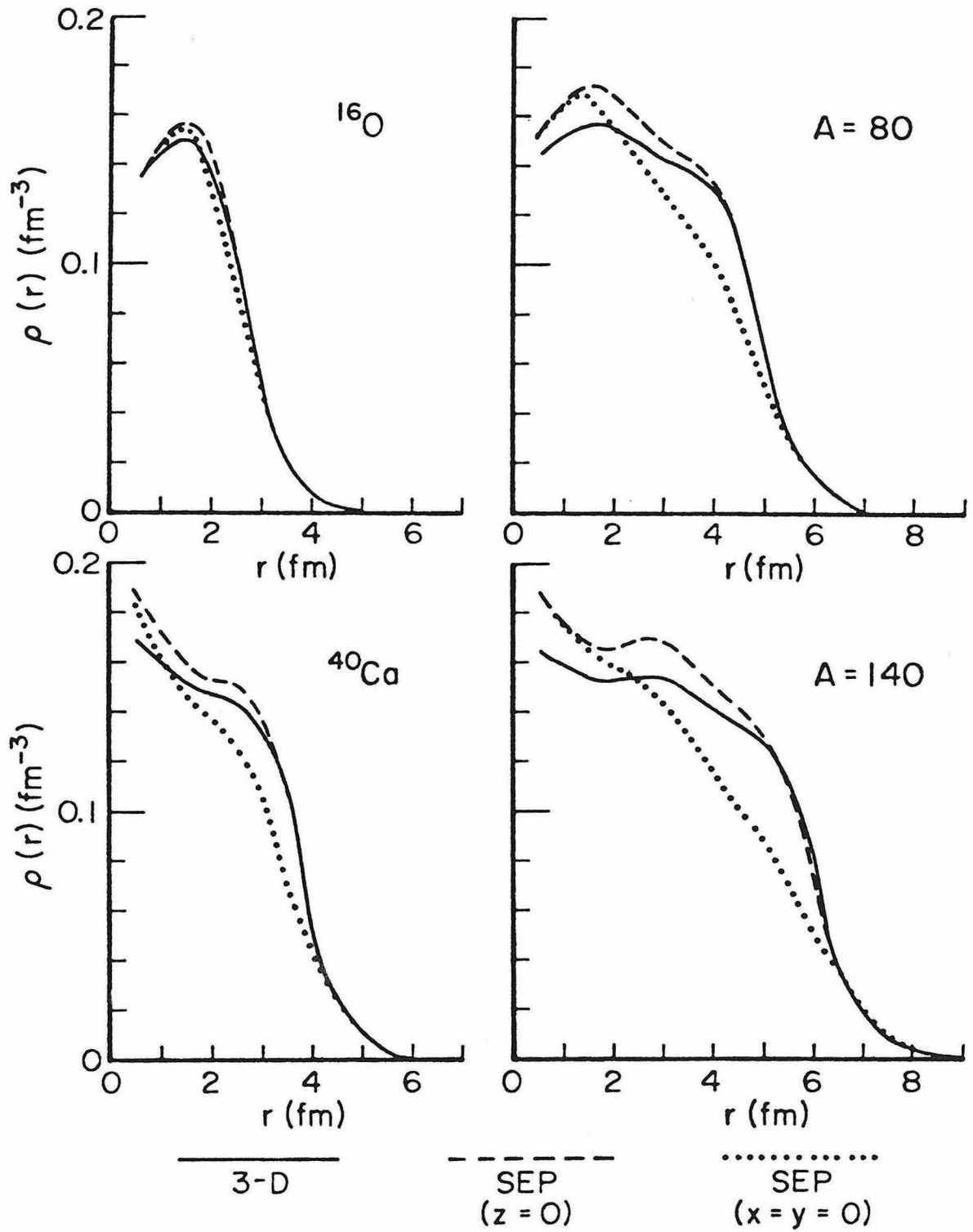


Fig. 1

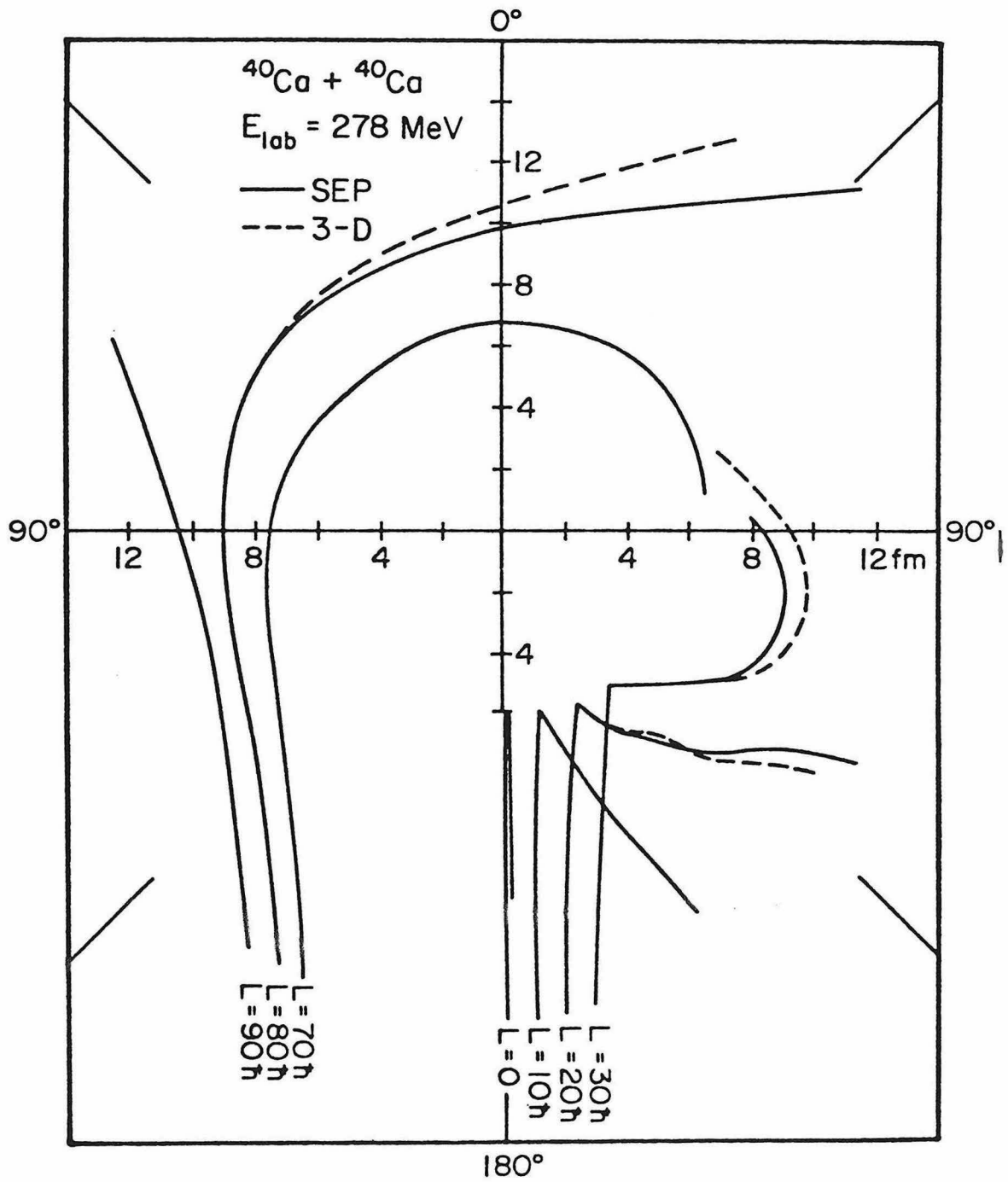


Fig. 2

### Section 7: The Filling Approximation

The previous calculations were for closed shell nuclei,  $^{16}\text{O}$  and  $^{40}\text{Ca}$ . For open shell nuclei, however, the static HF solutions will be deformed. Therefore, the previous initial conditions are ambiguous because we must also specify the initial orientation of the ions. Different orientations have been shown to lead to substantial differences in the fusion cross sections calculated for  $^{12}\text{C} + ^{12}\text{C}$  [Nilsson, Dhar, Koonin unpublished], so a plausible presumption is to average over all such orientations. However, heavier nuclei are relatively less deformed than was  $^{12}\text{C}$  in these calculations ( $\beta = \frac{2(a-b)}{a+b} \approx 0.4$  with  $a, b$  the major and minor axes) so that such orientation effects are probably small for energies not too near the Coulomb barrier. Averaging over orientation would substantially increase the computation involved, even beyond the need to perform several runs, at different orientations, for each energy and angular momentum. Lack of reflection symmetry with respect to the reaction plane would double the size of our spatial box; and, in fact, a general orientation would no longer permit the separable approximation to be made since the values of the wavefunctions out of the plane will depend on both the values in the plane and the tilt of the nucleus. Therefore, we adopt a filling approximation in which the valence nucleons are uniformly distributed throughout the valence shell, resulting in spherical HF solutions. This represents a crude orientation averaging.

In the filling approximation, the density matrix is generalized as

$$\rho(\vec{r}, \vec{r}', t) = \sum_j n_j \psi_j(\vec{r}, t) \psi_j^*(\vec{r}', t) \quad . \quad (7.1)$$

where the  $n_j$  are time-independent occupation numbers determined by the ground states of the colliding ions. These  $n_j$  are one for filled shells and a fractional value for the partially filled shells. Since these  $n_j$  are not all zero or one, the many-body wavefunction cannot be expressed as a single Slater determinant

and these calculations are no longer true HF or TDHF calculations. (In effect, this creates a wavepacket of different orientations and binds them together by the use of a common mean field.) However, once the densities have been defined, the TDHF evolution scheme is still applicable. Since the particles are independent, moving in a mean field and conserving their normalization, the evolution should be just like TDHF as long as the contribution of each particle to the mean field is properly normalized. Therefore, we regard the filling approximation as only a slight generalization of the ordinary theory.

To actually incorporate this approximation into the computer code, it is much more convenient to normalize the  $\psi_j$  to  $n_j$  rather than 1,  $\langle \psi_j | \psi_j \rangle = n_j$ . Therefore, the calculation of the densities  $\rho_q$ ,  $\tau_q$ , and  $\vec{j}_q$  doesn't need to be changed. Instead, relatively minor changes are made in the code: in the normalization routine, the calculation of single particle energies, and the calculation of the mass and charge dispersion. The single particle energies become

$$e_j = \frac{1}{n_j} \langle \psi_j | h | \psi_j \rangle \quad (7.2)$$

and the total single particle energy becomes

$$ESPT = \sum_j n_j e_j \quad (7.3)$$

The dispersion of proton (or neutron) number becomes

$$\sigma_{L_q}^2 = \sum_i \langle \psi_i | O_L | \psi_i \rangle - \sum_j \frac{1}{n_j} |\langle \psi_i | O_L | \psi_j \rangle|^2 \quad (7.4)$$

where the operator  $O_L$  means that the integral in  $r$  is done over only one fragment (see Eq. (4.22)) and the sums are over only protons (or neutrons).

Use of the filling approximation results in static solutions with smaller binding energy. For the case considered in the next published paper (BO 79),  $^{28}\text{Si}$ , this difference is quite large. Shown in Table 2 are energies for several systems calculated with the BKN force.

Table 2		
nucleus	exp.	sep. approx.
$^{16}\text{O}$	-127.6	-116.9
$^{40}\text{Ca}$	-342.1	-324.9
$^{28}\text{Si}$ prolate	-236.5	-208.4
$^{28}\text{Si}$ oblate		-205.0
$^{28}\text{Si}$ filling		-185.2

Oxygen is a closed shell nucleus, in an oscillator basis ( $n_x, n_y, n_z$ ) the occupied states are (000), (100), (010) and (001). Calcium is the next closed shell nucleus, including the states (110), (101), (011), (200), (020) and (002). The first two silicon solutions used  $n_j=1$  and included only 3 of these valence states; prolate about the z axis used (101), (011), and (002), while oblate used (110), (200), and (020). (The HF solution using the separable approximation will retain the oscillator states in the z direction and the symmetry of the wavefunctions in the x-y plane.) The third silicon solution used  $n_j=1/2$  for all six states in the valence shell. Therefore, the binding energy discrepancy mentioned in the paper is due to the filling approximation rather than the force or the separable approximation.

The second paper included here describes in detail calculations for two systems  $^{16}\text{O}+^{40}\text{Ca}$  and  $^{28}\text{Si}+^{28}\text{Si}$ . These would lead to the same compound nucleus  $^{56}\text{Ni}$  but use of the filling approximation for  $^{28}\text{Si}$  results in a different system. Although both systems have 28 protons and neutrons, the  $^{16}\text{O}+^{40}\text{Ca}$  calculation uses 14 wavefunctions whereas the  $^{28}\text{Si}+^{28}\text{Si}$  calculation uses 20 wavefunctions. Therefore, the silicon system has more degrees of freedom to dissipate energy, but it also has more total energy and more energy to dissipate at a given bombarding energy because the nuclei are less tightly bound. The energy differences seem to dominate, resulting in both a smaller maximum angular momentum for fusion and the opening of the low- $l$  window for fusion at a smaller energy. This seems reasonable since some of the degrees of freedom in the silicon case are, in a sense, fractional degrees of freedom. Regardless of their

relative size, however, these two effects obscure any entrance channel effects which could be discovered by a detailed comparison of these calculations. (Just as possible entrance channel effects throw uncertainty into the comparison of the two effects above.)

Both of these calculations can be compared with experiment and both give reasonable agreement, as discussed in the paper. The  $^{16}\text{O}+^{40}\text{Ca}$  calculations are compared with  $^{16}\text{O}+^{40}\text{Ca}$  experiments. The fusion cross sections show quite good agreement but the experiments don't extend to high enough energies to give evidence of the low- $l$  fusion window. The  $^{28}\text{Si}+^{28}\text{Si}$  calculations are compared with  $^{32}\text{S}+^{27}\text{Al}$  experiments since there were no data for  $^{28}\text{Si}+^{28}\text{Si}$  at the time of publication. This can be done because single-particle effects aren't calculated properly anyway and the bulk dynamics should be very similar for these two systems. The experiment doesn't measure fusion cross sections but does give evidence of a high- $l$  and low- $l$  cutoff for fusion in quantitative agreement with the calculated results. The calculation also gives quantitative agreement for the energies of scattered products just above and below these fusion cutoffs.

The experimental references of this paper (24,25) have since been published (VI 79, NA 79). The major addition is that  $^{16}\text{O}+^{40}\text{Ca}$  seems to have too few deep-inelastic events for the low- $l$  cutoff to be correct, however, no numbers are quoted. There are at least two experimental groups actively looking for low- $l$  cutoffs in systems relevant to TDHF predictions. R. Vandenbosch, et al are studying  $^{16}\text{O}+^{16}\text{O}$ , and J. Barrette, et al are studying  $^{28}\text{Si}+^{28}\text{Si}$ . The problem is difficult, however, especially because of the small cross section at these low  $l$ .

TDHF CALCULATIONS OF FUSION CROSS  
SECTIONS FOR  $^{16}\text{O} + ^{40}\text{Ca}$  AND  $^{28}\text{Si} + ^{28}\text{Si}$

P. Bonche, K.T.R. Davies, B. Flanders, H. Flocard,  
B. Grammaticos, S.E. Koonin, S.J. Krieger, and M.S. Weiss

Phys. Rev. C 20, 641 (1979)

TDHF CALCULATIONS OF FUSION CROSS  
SECTIONS FOR  $^{16}\text{O} + ^{40}\text{Ca}$  AND  $^{28}\text{Si} + ^{28}\text{Si}$

P. Bonche<sup>a)</sup>, K.T.R. Davies<sup>b)</sup>, B. Flanders<sup>c)</sup>, H. Flocard<sup>d)</sup>,  
B. Grammaticos<sup>e)</sup>, S.E. Koonin<sup>f)</sup>, S.J. Krieger<sup>g)</sup>, and M.S. Weiss<sup>h)</sup>

- a) Service de Physique Théorique, CEN Saclay, BP n°2, 91190 Gif-sur-Yvette, France
- b) Physics Division, Oak Ridge National Laboratory, Oak Ridge, TN 37830
- c) W.K. Kellogg Radiation Laboratory, California Institute of Technology, Pasadena, CA 91125
- d) Division de Physique Théorique, Institut de Physique Nucléaire, BP n°1, 91406, Orsay, France
- e) Service de Physique Théorique, CRN de Strasbourg, BP n°20, Cro, 67037 Strasbourg, France
- f) Alfred P. Sloan Foundation Fellow, W.K. Kellogg Radiation Laboratory, California Institute of Technology, Pasadena, CA 91125
- g) Department of Physics, University of Illinois at Chicago Circle, Chicago, IL 60680
- h) Lawrence Livermore Laboratory, University of California, Livermore, CA 94550

NUCLEAR REACTIONS  $^{16}\text{O}(^{40}\text{Ca},x)$  and  $^{28}\text{Si}(^{28}\text{Si},x)$  in time-dependent Hartree-Fock approximation. Fusion and strongly damped collisions.

#### ABSTRACT

Time-dependent Hartree-Fock calculations are carried out for the systems  $^{16}\text{O} + ^{40}\text{Ca}$  and  $^{28}\text{Si} + ^{28}\text{Si}$ . Cross sections for the formation of  $^{56}\text{Ni}$  are qualitatively similar in both cases, although there exist significant quantitative differences which reflect the importance of the entrance channel. Both systems exhibit an angular momentum window for fusion. The results of the calculations are compared with currently available experimental data.

## I. INTRODUCTION

Although the time-dependent Hartree-Fock (TDHF) approximation was formulated<sup>1)</sup> 50 years ago, it is the last 3 years in which the approximation has been seriously applied to the calculation of physical quantities in heavy ion collisions. In this brief span, we have witnessed a remarkably rapid evolution from the early one-dimensional calculations<sup>2),3)</sup>, which reproduced the qualitative features of colliding heavy ions, to increasingly more ambitious two-dimensional calculations<sup>4)-14)</sup>, and finally to three-dimensional calculations<sup>12)-18)</sup> which yield quantitatively accurate descriptions of certain experimental data. In the present work, the TDHF approach is applied to the calculation of fusion cross sections for two systems,  $^{16}\text{O} + ^{40}\text{Ca}$ , and  $^{28}\text{Si} + ^{28}\text{Si}$ , both of which lead to the compound nucleus  $^{56}\text{Ni}$ . Although the primary purpose of this work is to compare the results of the TDHF calculations with experimental data, we shall also discuss the accuracy of the two-dimensional rotating frame and separable approximations to the fully three-dimensional TDHF calculations. In addition, we shall discuss the effect of removing the isospin symmetry restriction on the nuclear wave function, and of varying the parameters of the nuclear potential.

## II. METHOD OF CALCULATION

Most of the calculations presented here employ the parameterization of the Skyrme potential<sup>19)</sup> referred to as Force I in ref. 18). In this version of the potential, the non-local terms in the mean field proportional to the Skyrme parameters  $t_1$  and  $t_2$  are identically zero. At the highest energies, the full Skyrme potential, including the non-local

terms, has also been used to calculate the fusion cross section. The effect on the fusion cross section of varying the Skyrme parameters is also discussed in ref. 18), and in ref. 11).

The calculations have been carried out using the two-dimensional separable approximation<sup>12),14)</sup>, and the two-dimensional rotating frame approximation<sup>4),5),13)</sup> to the TDHF equations. In addition, in order to verify the accuracy of the separable approximation, the  $^{16}\text{O} + ^{40}\text{Ca}$  fusion cross section has also been calculated at selected energies using the fully three-dimensional TDHF code<sup>13),17)</sup>. It should be noted that in effecting this comparison we have employed codes, both the separable code and the three-dimensional code, which enforce isospin symmetry. That is, neutrons and protons which occupy the same orbital are constrained to be degenerate. This degeneracy is not enforced in the rotating frame approximation<sup>4),5),13)</sup> code, and we shall therefore be able to comment upon the effect of lifting the isospin degeneracy. As the various numerical methods which are employed to solve the TDHF equations have been discussed extensively in the references cited, we shall not comment upon them further here.

The fusion cross sections for  $^{16}\text{O} + ^{40}\text{Ca}$  and  $^{28}\text{Si} + ^{28}\text{Si}$  have been calculated as follows. For each of the energies studied, the maximum value of angular momentum for which fusion takes place,  $l_u \hbar$ , and the minimum value of angular momentum for which fusion takes place,  $l_c \hbar$ , are separately determined to a precision of approximately  $2\hbar$ . The fusion cross section is then calculated at each energy by the sharp cut-off formula<sup>18)</sup>,

$$\sigma_{\text{fusion}} = \frac{\pi}{k^2} \sum_{l=l_c}^{l_u} (2l+1) \quad , \quad (2.1)$$

in which  $k$  represents the relative wave number in the entrance channel. For the asymmetric system  $^{16}_0 + ^{40}\text{Ca}$ , the sum extends over all partial waves for which fusion occurs. For the symmetric system  $^{28}\text{Si} + ^{28}\text{Si}$ , the sum in eq. 2.1 is replaced by twice the sum over all even partial waves for which fusion occurs. The values of  $\ell$  for which fusion does occur are determined at each energy by evolving the system at various impact parameters for a sufficiently long period of time to offer convincing evidence that the system will not undergo prompt fission. A more detailed discussion of the latter point may be found in ref. 11). Although the sums to which we refer above may easily be evaluated exactly, it is consistent with the nature of the approximation to use, for either symmetric or asymmetric systems, the result

$$\begin{aligned} \sigma_{\text{fusion}} &\simeq \frac{\pi}{k^2} [ (\ell_{\text{r}} + 1)^2 - (\ell_{\text{c}} + 1)^2 ] \\ &= \frac{\pi \hbar^2}{2\mu E_{\text{CM}}} [ (\ell_{\text{r}} + 1)^2 - (\ell_{\text{c}} + 1)^2 ] \quad , \quad (2.2) \end{aligned}$$

in which  $\mu$  represents the reduced mass of the system under consideration.

### III. RESULTS

#### A. $^{16}_0 + ^{40}\text{Ca}$

We have performed calculations for the  $^{16}_0 + ^{40}\text{Ca}$  system for laboratory bombarding energies from 40 MeV to 350 MeV. The calculations have been carried out in the two-dimensional separable approximation<sup>12),14),30)</sup>, and in the two-dimensional rotating frame approximation<sup>4),5),13)</sup>. In addition, selected points have been calculated using the fully three-dimensional TDHF code<sup>13),17)</sup>. In all cases which have been compared, the separable fusion cross sections have been in complete agreement with the

fully three-dimensional TDHF calculations. A graphic demonstration of this agreement is given in fig. 1, in which the fragment separation coordinate  $r$ , defined as in ref. 5), is plotted as a function of time for a collision at a laboratory energy of 290 MeV, in which the initial angular momentum,  $l$ , is equal to 48. The results of the two-dimensional separable approximation are in very good agreement with the results of the fully three-dimensional calculation, until  $t \approx 9 \times 10^{-22}$  s, by which time the system has fused. Plots of the quadrupole moments of the mass distribution exhibit similar behavior.

The angular momenta for which the  $^{16}_0 + ^{40}_{\text{Ca}}$  system fuses are depicted as a function of the center of mass energy in fig. 2. The values plotted are derived from calculations which employ the separable two-dimensional code with degenerate neutron and proton orbitals. The maximum angular momentum which the fused system can sustain is approximately 60 units of  $\hbar$ . This value is in good agreement with the prediction 58  $\hbar$  of the liquid drop model<sup>20)</sup> for the  $A = 56$  system. The fact that there exists a minimum angular momentum,  $l_{\text{c}}(E)$ , for which the  $^{16}_0 + ^{40}_{\text{Ca}}$  system fuses, represents a dramatic prediction of the TDHF calculations<sup>27)</sup>. Referring again to fig. 2, we note that as the center of mass energy increases above 100 MeV,  $l_{\text{c}}$  likewise increases. This reflects the inability of the colliding ions to convert sufficient translational energy to internal excitation energy. The inability of the transient fused system to dissipate more radial kinetic energy than a certain amount is an essential feature of the mean field dynamics<sup>21)</sup>. The increase of  $l_{\text{c}}$  with energy causes the fusion cross section to decrease more rapidly than  $1/E_{\text{CM}}$ , which represents the energy dependence of Eq. (2.2) in the absence of  $l_{\text{c}}$ , for energies greater than  $E_{\text{CM}} \sim 160$  MeV. At the latter

energy, the saturation angular momentum,  $l \sim 60$ , has been reached, and, in the absence of  $l_c$ , the energy dependence is given simply by the kinematical factor  $1/E_{CM}$ . The actual existence of a lower fusion limit could thus be inferred from the decrease with energy of the experimental fusion cross section for energies  $E_{CM} > 160$  MeV.

The  $^{16}_0 + ^{40}_{Ca}$  fusion cross section, as given by Eq. (2.2) is compared with the experimental cross section in fig. 3. The theoretical results presented have been calculated using both the results of the two-dimensional, separable approximation with constrained neutron and proton orbitals, and the two-dimensional rotating frame approximation in which no isospin symmetry has been enforced. As we have previously noted, the separable results are in complete agreement with the results of fully three-dimensional TDHF calculations (with the same enforced isospin symmetry). The cross section computed using the results of the rotating frame approximation exceeds the cross section calculated using the results of the separable approximation by approximately 120 mb in the energy range from just above the fusion barrier to  $E_{CM} \sim 100$  MeV. This difference may be attributed entirely to the enforced neutron-proton degeneracy in the separable calculations. At center of mass energies above 100 MeV, a significant amount of the dissipated energy excites non-axial modes, and the rotating frame approximation breaks down. Thus, although the upper limit for fusion,  $l_s \sim 50$ , is accurately given by the rotating frame approximation at  $E_{CM} \sim 100$  MeV, the approximation incorrectly indicates that the system will not fuse at  $l = 15$ . The latter results are qualitatively the same as those found in ref. (11), in which the lifting of the isospin restriction on the nuclear wave function resulted in an increase of approximately 200 mb in the  $^{40}_{Ca} + ^{40}_{Ca}$  fusion

cross section, and the excitation of non-axial modes caused the rotating frame approximation to break down in the  $^{40}\text{Ca} + ^{40}\text{Ca}$  system at a center of mass energy on the order of 100 MeV, the approximate energy at which the angular momentum window appears in the three-dimensional calculations.

Referring to fig. 3, in which the fusion cross section is plotted as a function of the energy, we note that the theoretical results are in good agreement with the experimental results at low energy. This agreement at low energy affirms the facts that the nuclear sizes and the inter-ion potential are accurately given by the TDHF wave functions and the nucleon-nucleon interaction. However at energies  $E_{\text{CM}} \approx 100$  MeV, the theoretical cross section exceeds the measured cross section by  $\approx 25\%$ . In discussing the discrepancy between theory and experiment it should be noted that a significant amount of fusion followed by fission is consistent with the prediction of the liquid drop model<sup>22)</sup> for the mass 56 system. Moreover such events would not have been observed in the evaporation residue experiments with which we are making our comparison. However, separate investigations<sup>23)</sup> do not indicate that there exists sufficient fusion-fission cross section to account for the discrepancy between the theoretical and experimental results. The fact that the TDHF cross section exceeds the experimental cross section especially warrants further study, since corrections to TDHF would be expected, at least naively, to result in an increased fusion cross section.

We have also performed a single calculation at  $E_{\text{CM}} = 208$  MeV, using the separable approximation with the full Skyrme interaction<sup>11)</sup>, and the isospin symmetry restriction removed. The fusion cross section computed on the basis of this calculation is  $823^{+121}$  mb. Referring to fig.3,

we note that the cross section at this energy, as calculated using the results of the separable calculation with the local Skyrme interaction and degenerate neutron and proton orbitals is approximately 600 mb. The difference in cross section of the calculations is thus  $220 \pm 120$  mb. Since approximately 120 mb of this difference can be attributed to the removal of the isospin symmetry restriction, no definitive statement can be made as to the effect of the non-local terms in the Skyrme potential.

B.  $^{28}\text{Si} + ^{28}\text{Si}$

We have performed calculations for the  $^{28}\text{Si} + ^{28}\text{Si}$  system for laboratory bombarding energies from 70 MeV to 220 MeV. The calculations have been carried out in the two-dimensional separable approximation, with the initial, static wave function for the system determined in a filling approximation, in which the occupation of each  $1s-0d$  orbital of the separated  $^{28}\text{Si}$  ions is set equal to 0.5. In essence, this approximation represents an average over the possible initial orientations of the deformed Slater determinants of the separated  $^{28}\text{Si}$  ions. As such it is a physically reasonable (and computationally necessary) approximation to the actual scattering. It nevertheless represents a departure from, and approximation to, a true TDHF calculation.

The angular momenta for which the  $^{28}\text{Si} + ^{28}\text{Si}$  system fuses are depicted as a function of the energy in fig. 4. The maximum angular momentum which the fused system can sustain can be inferred to be approximately 50  $\hbar$ . Since the fused  $^{16}\text{O} + ^{40}\text{Ca}$  system has been calculated to sustain 60  $\hbar$ , it might appear that the maximum angular momentum depends upon the entrance channel, and is not a function only of the total charge and mass of the system, as given by the liquid drop model. This conclusion, however, is considerably obscured by the fact that the  $^{28}\text{Si} + ^{28}\text{Si}$  calculation has been effected in the filling approximation. We shall discuss this point more fully at the conclusion of this section. As in the case of the  $^{16}\text{O} + ^{40}\text{Ca}$  system, we find a fusion window in the  $^{28}\text{Si} + ^{28}\text{Si}$  vs.  $E_{\text{CM}}$  plot. For center of mass energies greater than 54 MeV, the  $^{28}\text{Si} + ^{28}\text{Si}$  system exhibits no fusion when the angular momentum of the system is less than a cut-off value,  $l_c(E)$ , which increases as a function of bombarding energy. An unexpected result of the  $^{28}\text{Si} + ^{28}\text{Si}$  calculations is the

partial closing of the fusion window in the energy range above 100 MeV. This effect is manifest in fig. 4, in which the fusion region in the angular momentum-energy plane is plotted for the  $^{28}\text{Si} + ^{28}\text{Si}$  system. The results of the calculations effected in this energy range have been explicitly plotted. Thus, the crosses represent calculations in which the  $^{28}\text{Si}$  ions scatter, and the dots represent calculations in which the  $^{28}\text{Si}$  ions fuse. An island of non-fusion events is clearly visible in this energy range. While such dramatic variation, associated with only minor changes in the initial conditions did occur in the very first one-dimensional calculations<sup>2)</sup>, it is more probable that the appearance of the island signals a breakdown of the two-dimensional separable approximation. For a fully three-dimensional calculation effected in the center of the island of non-fusion events indeed leads to fusion. It is thus possible that the two-dimensional separable approximation breaks down at high energy, where the fusion cross section goes to zero. Accordingly, we shall assume that the island of non-fusion events is spurious, and shall ignore it in the computation of the fusion cross sections.

The fusion cross section for  $^{28}\text{Si} + ^{28}\text{Si}$  is plotted as a function of energy in fig. 5. The behavior of the cross section is qualitatively similar to that of  $^{16}\text{O} + ^{40}\text{Ca}$ , although the latter system exhibits a more pronounced plateau at intermediate energies, and drops more precipitously at high energy. A comparison of fig. 2 and fig. 4 shows that the faster decrease of the  $^{16}\text{O} + ^{40}\text{Ca}$  cross section is due to the more rapid closing of the fusion window of the latter reaction. As the energy increases,  $l_c$  increases more rapidly for the  $^{16}\text{O} + ^{40}\text{Ca}$  system than for the  $^{28}\text{Si} + ^{28}\text{Si}$  system. It should be noted, however, that this high

energy comparison may be complicated by the unexpected behavior of the  $^{28}\text{Si} + ^{28}\text{Si}$  system at energies above  $E_{\text{CM}} = 100$  MeV, as given by the separable approximation.

In fig. 6, the center of mass energy loss and scattering angle, as calculated in the separable approximation, are plotted as functions of angular momentum for  $^{28}\text{Si} + ^{28}\text{Si}$  at  $E_{\text{CM}} = 111$  MeV. The curves are qualitatively similar to results obtained<sup>5)</sup> for  $^{16}\text{O} + ^{16}\text{O}$  and  $^{40}\text{Ca} + ^{40}\text{Ca}$ . However, an important distinction is the fact that the systems and energies investigated in ref. 5) did not lead to fusion. As discussed above, the scattering events observed in reactions in which the angular momentum of the system is in the range  $27 \leq \ell \leq 39$  are quite possibly spurious. Fully three-dimensional calculations would likely lead to fusion in this interval.

Although experimental data are not available for the  $^{28}\text{Si} + ^{28}\text{Si}$  system, measurements have recently been made<sup>25)</sup> on the similar  $^{32}\text{S} + ^{27}\text{Al}$  system. In their investigation of the latter system at a laboratory energy of 175 MeV, Natowitz et al<sup>25)</sup> can explain the observed spectrum by assuming the existence of two strongly damped components in the energy spectrum of the reaction products. One component is inferred to correspond to an angular momentum  $\ell \approx 48$ , not inconsistent with the liquid drop expectation that the  $A = 59$  system will not support angular momentum  $\geq 58$ . In contrast, the second component is inferred to correspond to very low values of angular momentum,  $\ell \leq 15$ . As a result of their analysis, Natowitz et al<sup>25)</sup> conclude that the observation of scissioning nuclei with such small angular momenta can be explained if the lowest partial waves in the entrance channel lead to strongly damped collisions, rather than to fusion. This situation is precisely that found in the

$^{28}\text{Si} + ^{28}\text{Si}$  system. At  $E_{\text{CM}} = 80$  MeV, the same center of mass energy as in the  $^{32}\text{S} + ^{27}\text{Al}$  experiment, we find that the  $^{28}\text{Si} + ^{28}\text{Si}$  fusion window is open for angular momenta  $17 \leq \ell \leq 48$ . Further comparison can be made with the fragment energies for collisions at angular momenta just outside the window. Natowitz, et al<sup>25)</sup> find a center of mass fragment kinetic energy of 16.6 MeV for the  $\ell \approx 15$  component, and a fragment kinetic energy of 26.4 MeV for the  $\ell \approx 48$  component. TDHF calculations of the  $^{28}\text{Si} + ^{28}\text{Si}$  system at  $E_{\text{CM}} = 80$  MeV show that the fragments in collisions with  $\ell = 16$  carry 16 MeV kinetic energy, and fragments in collisions with  $\ell = 49$  carry 28 MeV kinetic energy. The results of the  $^{28}\text{Si} + ^{28}\text{Si}$  calculations are thus consistent with this interpretation of the  $^{32}\text{S} + ^{27}\text{Al}$  data.

We mentioned above that any conclusion as to the existence of entrance channel effects is significantly obscured by the fact that the filling approximation has been employed in the calculations for the  $^{28}\text{Si} + ^{28}\text{Si}$  system. One such consideration is the fact that the Q value of the reaction is considerably affected by the filling approximation. Thus, while the total binding energy of the separated  $^{16}\text{O}$  and  $^{40}\text{Ca}$  ions, as computed using the local Skyrme interaction, is 442 MeV, 28 MeV less than the experimental value, the total binding energy of the separated  $^{28}\text{Si}$  ions is but 370 MeV, 103 MeV less than the experimental value. The 75 MeV discrepancy in binding energy of the two systems can be used to explain, at least in a qualitative sense, the reason why the low angular momentum cut-off occurs at a much lower energy in the  $^{28}\text{Si} + ^{28}\text{Si}$  system than in the  $^{16}\text{O} + ^{40}\text{Ca}$  system. Other effects must be considered as well. Thus, for the  $^{16}\text{O} + ^{40}\text{Ca}$  system,  $\frac{1}{4}(16+40) = 14$  orbitals are involved in the calculation, while for the

$^{28}\text{Si} + ^{28}\text{Si}$  system, because of the filling approximation,  $\frac{1}{4}(40+40) = 20$  orbitals are involved in the calculation. The intent of this discussion is to emphasize that no clear-cut statement as to the importance of entrance channel effects is possible on the basis of the present calculations.

#### IV. SUMMARY

We have calculated fusion cross sections for the systems  $^{16}\text{O} + ^{40}\text{Ca}$  and  $^{28}\text{Si} + ^{28}\text{Si}$ , both of which lead to the compound system  $^{56}\text{Ni}$ . Both systems exhibit an angular momentum window for fusion. The  $^{16}\text{O} + ^{40}\text{Ca}$  results are in reasonable agreement with experiment<sup>24)</sup>, and the  $^{28}\text{Si} + ^{28}\text{Si}$  results are consistent with the experimental data<sup>25)</sup> on the similar  $^{32}\text{S} + ^{27}\text{Al}$  system.

The fusion results are qualitatively similar for the  $^{16}\text{O} + ^{40}\text{Ca}$  and  $^{28}\text{Si} + ^{28}\text{Si}$  systems, but do display significant quantitative differences<sup>26)</sup>. Thus, the  $^{16}\text{O} + ^{40}\text{Ca}$  system can fuse with an angular momentum  $\ell = 62$ , while the maximum angular momentum with which the  $^{28}\text{Si} + ^{28}\text{Si}$  system is calculated to fuse is  $\ell = 50$ . For comparison, the limiting angular momentum which the  $A = 56$  system can sustain is given by the liquid drop model as  $\ell = 58$ .

The results calculated using the two-dimensional separable approximation are in very good agreement with the results of the fully three-dimensional calculations, except in the case of the most energetic of the  $^{28}\text{Si} + ^{28}\text{Si}$  reactions. The rotating frame approximation, as in past calculations, is accurate just above the Coulomb barrier, but breaks down for energies greater than that at which a fusion window develops. The effect of removing the neutron-proton degeneracy increases the

$^{16}_0 + ^{40}\text{Ca}$  fusion cross section by approximately 120 mb over the energy range studied. The effect of the non-local terms in the Skyrme interaction is not clear at the single energy at which comparison was attempted. The difference in fusion cross section, as computed using the full Skyrme and local Skyrme interactions is not inconsistent with the difference which could be attributed to the fact that the full Skyrme calculation does not enforce isospin symmetry.

Perhaps the most striking result of the TDHF calculations remains the prediction of an angular momentum window for fusion. While both the  $^{16}_0 + ^{40}\text{Ca}$  and  $^{28}\text{Si} + ^{28}\text{Si}$  results are consistent with experiment, it would be exciting if a definitive experiment could determine whether such a window indeed does exist.

ACKNOWLEDGEMENTS

This research was supported in part by the National Science Foundation [PHY77-21602, PHY76-83685, NSF77-12879], and by the Division of Physical Research, U.S. Department of Energy, under contract W-7405-eng-26 with the Union Carbide Corporation.

REFERENCES

1. P.A.M. Dirac, Proc. Cam. Phil. Soc. 26, 376 (1930).
2. P. Bonche, S. Koonin, and J.W. Negele, Phys. Rev. C13, 1226 (1976).
3. P. Bonche, J. de Physique 37 Colloque C5, 213 (1976).
4. S. Koonin, Phys. Lett. 61B, 227 (1976).
5. S.E. Koonin, K.T.R. Davies, V. Maruhn-Rezwani, H. Feldmeier, S.J. Krieger, and J.W. Negele, Phys. Rev. C15, 1359 (1977).
6. V. Maruhn-Rezwani, K.T.R. Davies, and S.E. Koonin, Phys. Lett. 67B, 134 (1977).
7. R.Y. Cusson and J. Maruhn, Phys. Lett. 62B, 134 (1976).
8. J.A. Maruhn and R.Y. Cusson, Nucl. Phys. A270, 437 (1976).
9. J.W. Negele, S.E. Koonin, P. Moller, J.R. Nix, and A.J. Sierk, Phys. Rev. C17, 1098 (1978).
10. K.T.R. Davies, V. Maruhn-Rezwani, S.E. Koonin, and J.W. Negele, Phys. Rev. Letts. 41, 632 (1978).
11. S.J. Krieger and K.T.R. Davies, Phys. Rev. C18, 2567 (1978).
12. K.R. Sandhya Devi and M.R. Strayer, J. Phys. G4, L97 (1978); Phys. Letts. 77B, 135 (1978).
13. K.T.R. Davies, H.T. Feldmeier, H. Flocard, and M.S. Weiss, Phys. Rev. C18, 2631 (1978).
14. S.E. Koonin, B. Flanders, H. Flocard, and M.S. Weiss, Phys. Letts. 77B, 13 (1978).
15. R.Y. Cusson, R.K. Smith, and J. Maruhn, Phys. Rev. Lett. 36, 1166 (1976).
16. R.Y. Cusson, J.A. Maruhn, and H.W. Meldner, Phys. Rev. C18, 2589 (1978).
17. H. Flocard, S.E. Koonin, and M.S. Weiss, Phys. Rev. C17, 1682 (1978).
18. P. Bonche, B. Grammaticos, and S.E. Koonin, Phys. Rev. C17, 1700 (1978).

19. T.H.R. Skyrme, Phil. Mag.. 1, 1043 (1956); Nucl. Phys. 9, 615 (1959).
20. S. Cohen, F. Plasil, and W.J. Swiatecki, Annals of Phys. 82, 557 (1974).
21. While the actual value of  $\ell_c$  does depend upon the symmetries imposed upon the TDHF wave function, it is likely that the limit would remain in a totally unrestricted TDHF calculation. Although it is true that the removal of enforced symmetries, such as axial symmetry, and neutron-proton degeneracy, can enlarge the fusion window, our experience suggests that the limit will remain in a purely mean field calculation.
22. Referring to fig. 15 of ref. 20), we note that for values of  $\ell \geq 42$ , the fission barrier for  $A = 56$  is calculated to be less than 8 MeV. Thus, on the basis of the liquid drop model, the  $A = 56$  system is expected to fission for angular momenta  $42 < \ell < 58$ .
23. D.G. Kovar, unpublished; F. Plasil, unpublished.
24. S.E. Vigdor, D.G. Kovar, P. Sperr, J. Mahoney, A. Menchaca-Rocha, C. Olmer, and M.S. Zisman, unpublished.
25. J.B. Natowitz, G. Doukellis, B. Kolb, G. Rosner, and Th. Walcher, unpublished.
26. It should be iterated that the initial  $^{28}\text{Si}$  wave functions are not pure HF wave functions, but are calculated in the filling approximation. Thus, as discussed at the conclusion of section III, no clear cut conclusion can be drawn as to the importance of entrance channel effects.

27. The dynamical inhibition of fusion at low impact parameters has also been observed in Ca + Ca calculations based on the excitation of damped surface modes<sup>28)</sup>, and in other macrophysics studies<sup>29)</sup>.
28. R.A. Broglia, C.H. Dasso, G. Pollarolo, and A. Winther, Phys. Rev. Lett. 40, 707 (1978).
29. C.F. Tsang, Physica Scripta 10A, 90 (1974).  
K. Siwek-Wilczynska and J. Wilczynski, Nucl. Phys. A264, 115 (1976).
30. In the separable approximation, the required orthogonality of the orbitals (as a function of the coordinate perpendicular to the reaction plane) demands that the same harmonic oscillator parameter be used for both the <sup>16</sup>O ion and the <sup>40</sup>Ca ion. In the present calculation, the parameter employed is the mean of that appropriate to the individual ions. Since the latter parameters differ by but 10%, the effect upon the calculation is negligible. This point will be fully discussed in the forthcoming publication by B. Flanders, P. Donche, S.E. Koonin, and M.S. Weiss.

FIGURE CAPTIONS

- Fig. 1 Comparison, as a function of time, of the fragment separation coordinate in a collision between  $^{16}\text{O}$  and  $^{40}\text{Ca}$  ions at a laboratory energy of 290 MeV with  $\ell = 48$ . The solid line gives the result of the two-dimensional separable approximation, and the dashed line gives the result of the fully three-dimensional calculation. In both calculations, the neutron and proton orbitals are degenerate.
- Fig. 2 Fusion region in the angular momentum-energy plane for the system  $^{16}\text{O} + ^{40}\text{Ca}$ . The calculations have been effected with the separable code using the local Skyrme interaction, and with neutron and proton orbitals degenerate.
- Fig. 3 Comparison of the calculated fusion cross section with the results of experiment<sup>24)</sup> for  $^{16}\text{O} + ^{40}\text{Ca}$ . Plotted are the results of calculations using the separable code with the local Skyrme interaction and degenerate neutron and proton orbitals, the results of calculations using the rotating frame approximation with the local Skyrme interaction and unrestricted neutron and proton orbitals, and the result of a single calculation at 208 MeV using the separable code with the full Skyrme interaction and unrestricted neutron and proton orbitals.
- Fig. 4 Fusion region, in the angular momentum-energy plane, for the system  $^{28}\text{Si} + ^{28}\text{Si}$ . The calculations have been effected with the separable code using the local Skyrme interaction, and with neutron and proton orbitals degenerate. For energies above 100 MeV, the results of the calculations have been explicitly plotted, with crosses used to indicate events in which the  $^{28}\text{Si}$  ions scatter, and dots used to indicate events in which the  $^{28}\text{Si}$  ions fuse.

Fig. 5 Calculated fusion cross section for  $^{28}\text{Si} + ^{28}\text{Si}$ . The calculations have been effected using the code as described in fig. 4.

Fig. 6 Deflection and energy loss functions for  $^{28}\text{Si} + ^{28}\text{Si}$  at a center of mass energy of 111 MeV. The calculations have been effected using the code as described in fig. 4.

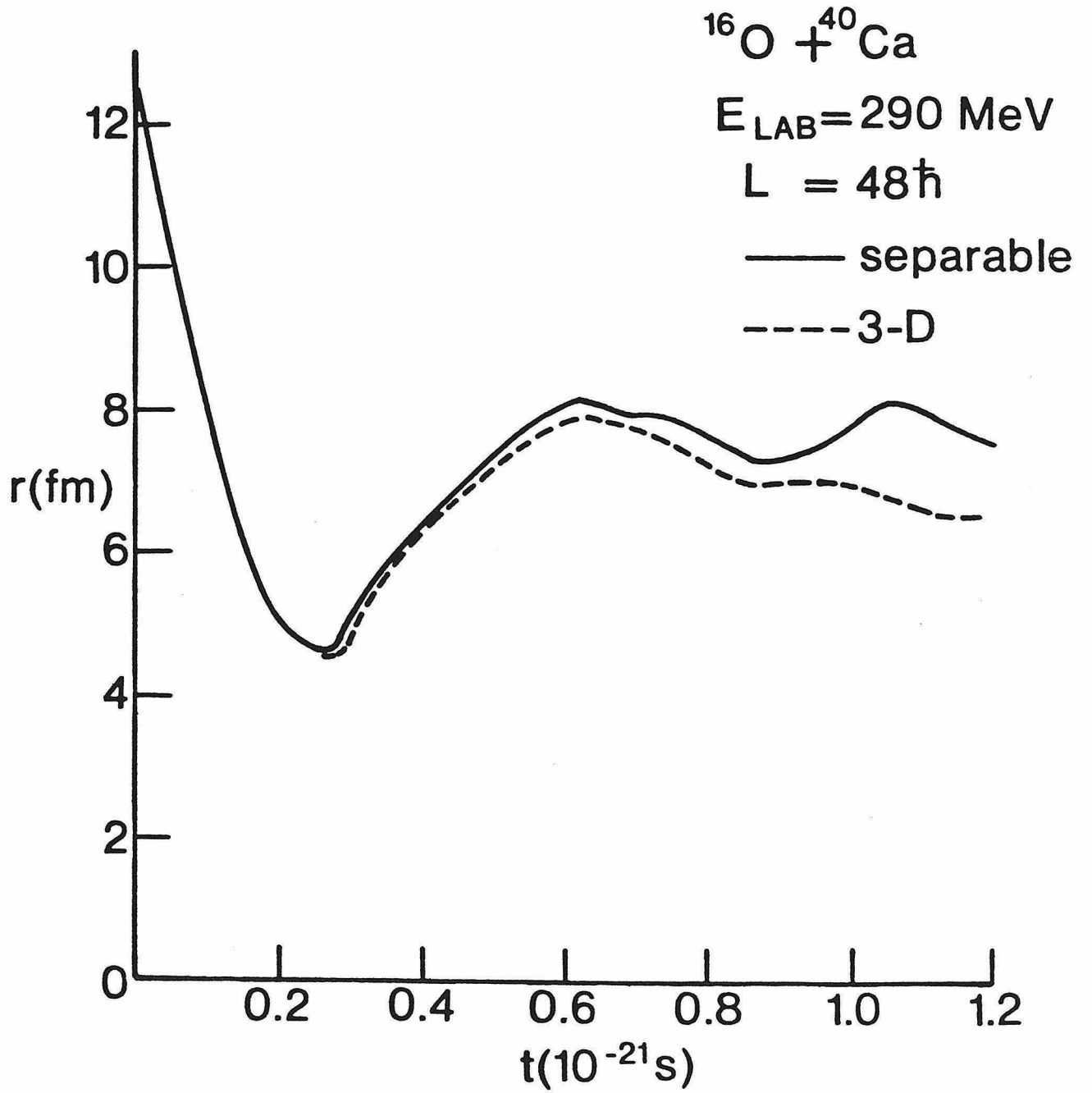
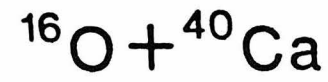


Fig. 1



FUSION REGION

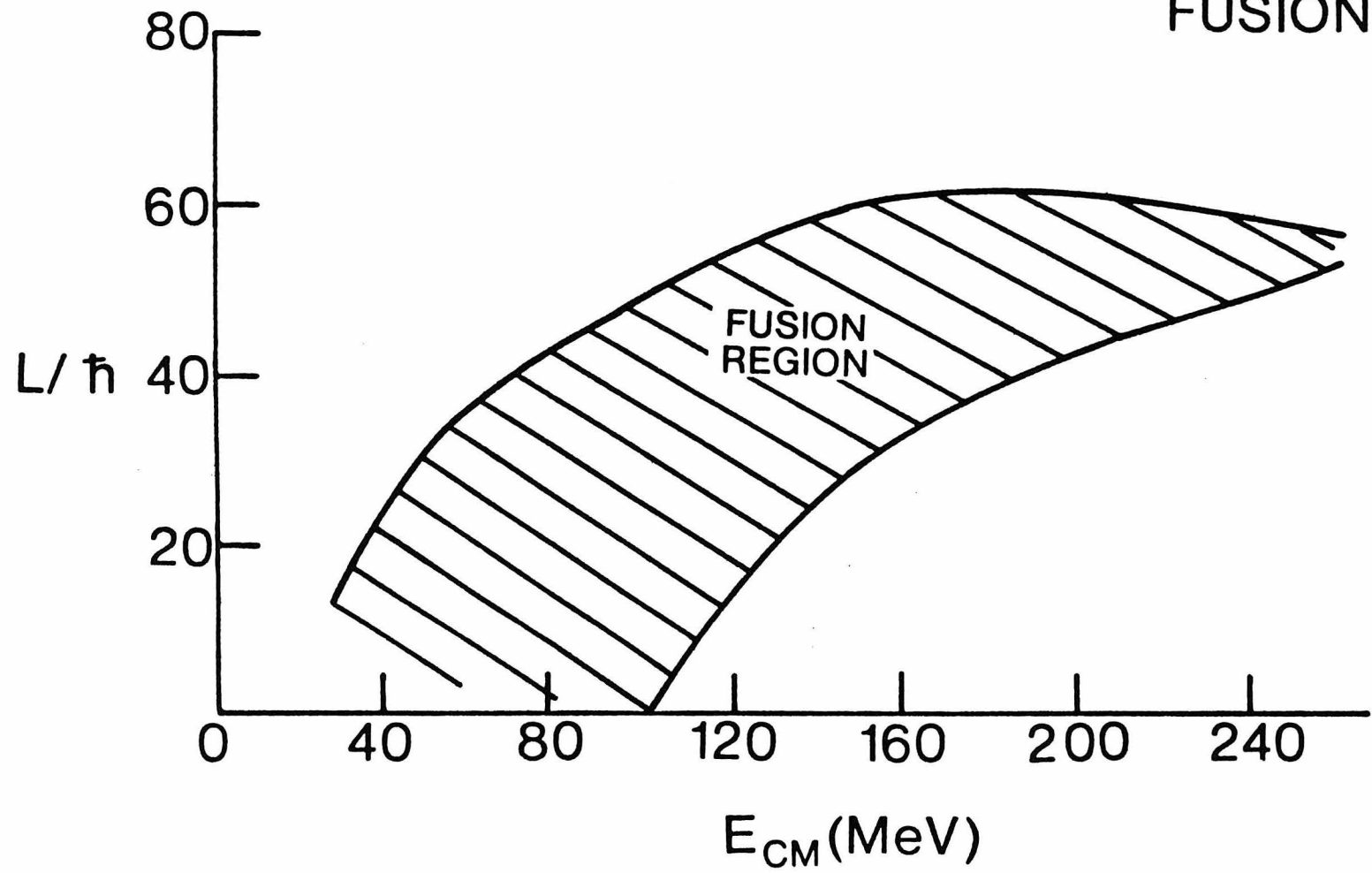


Fig. 2

# $^{16}\text{O} + ^{40}\text{Ca}$ FUSION CROSS SECTION

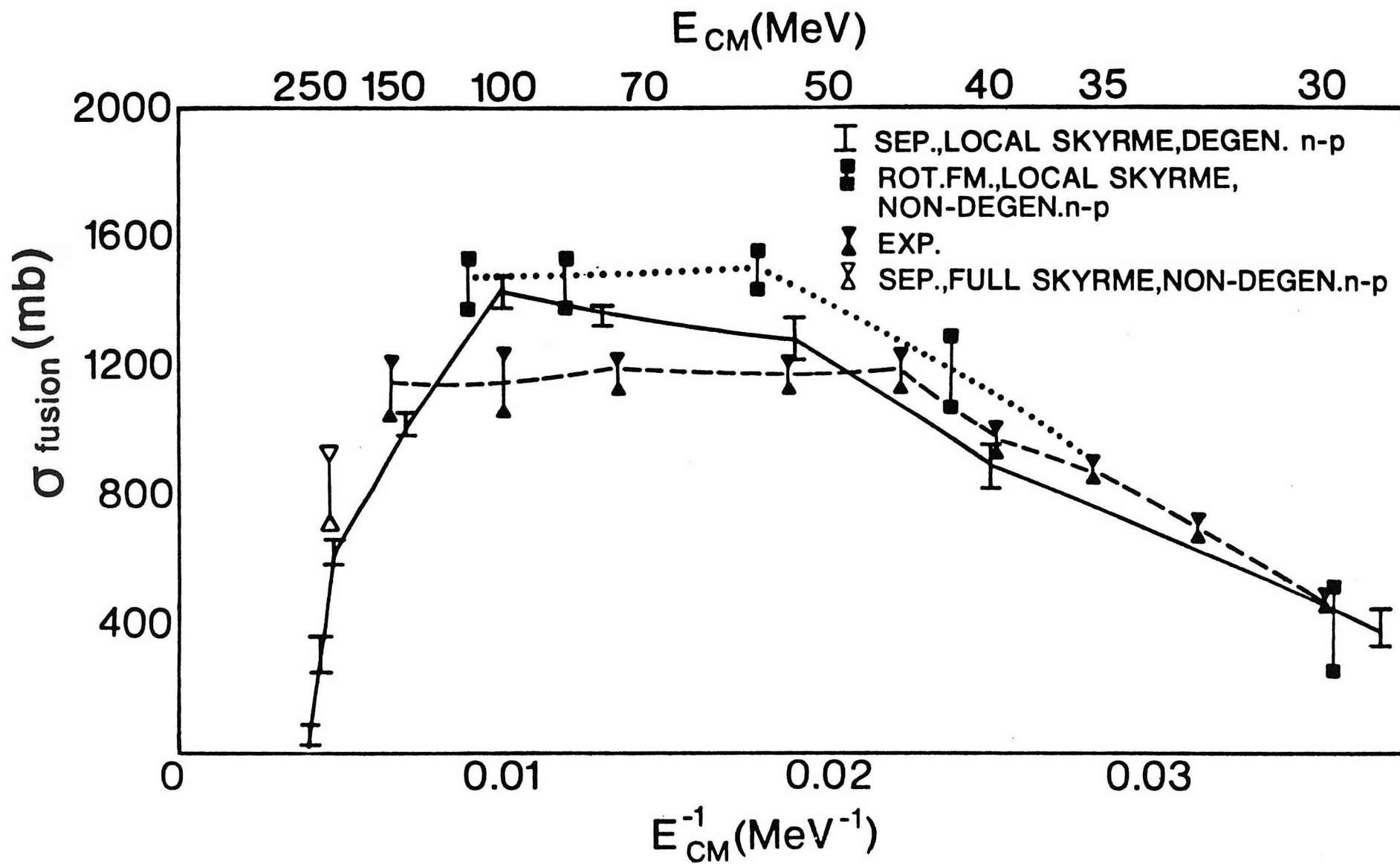


Fig. 3

$^{28}\text{Si} + ^{28}\text{Si}$   
FUSION REGION

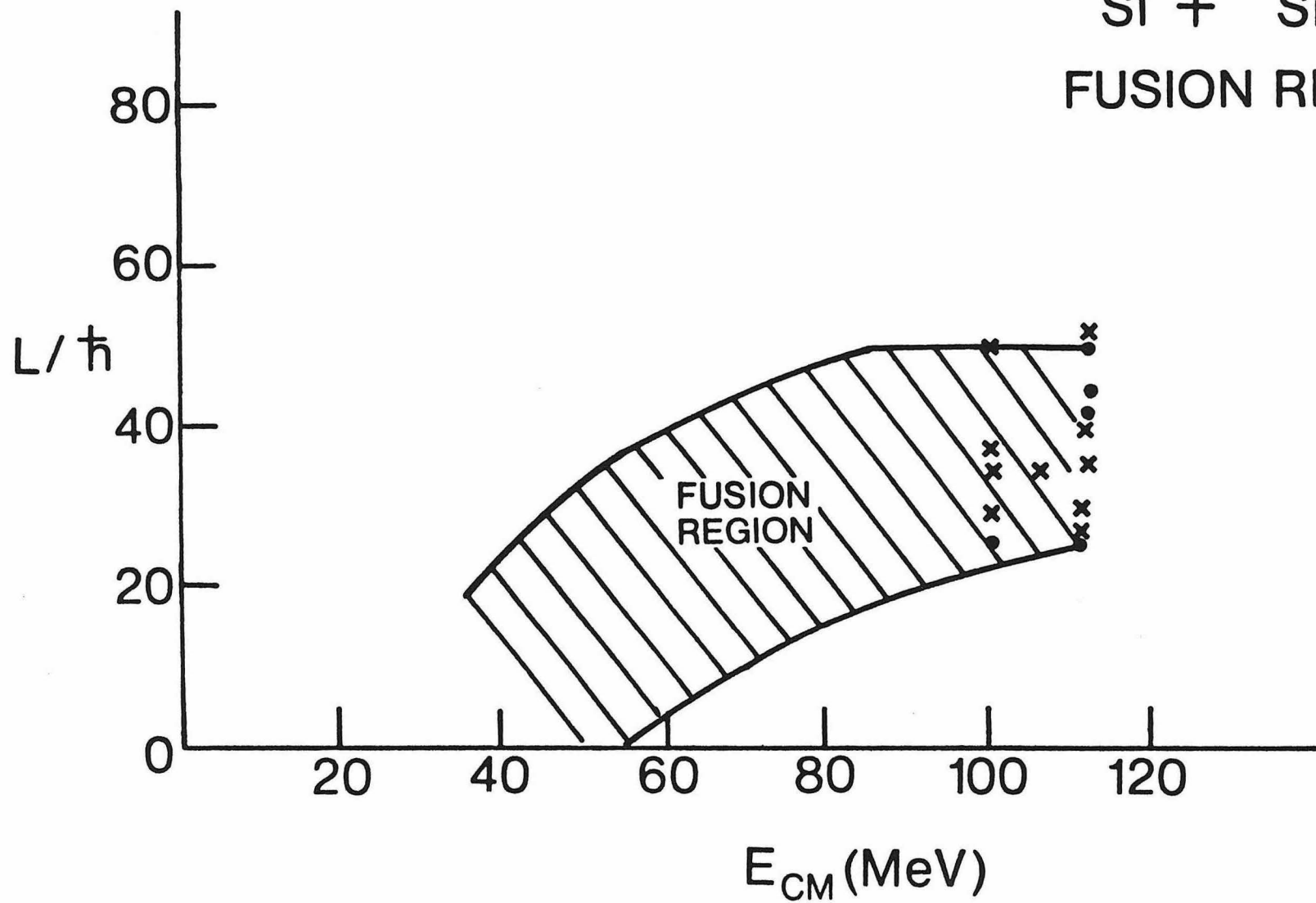


Fig. 4

# $^{28}\text{Si}+^{28}\text{Si}$ FUSION CROSS SECTION

$E_{\text{CM}}$  (MeV)

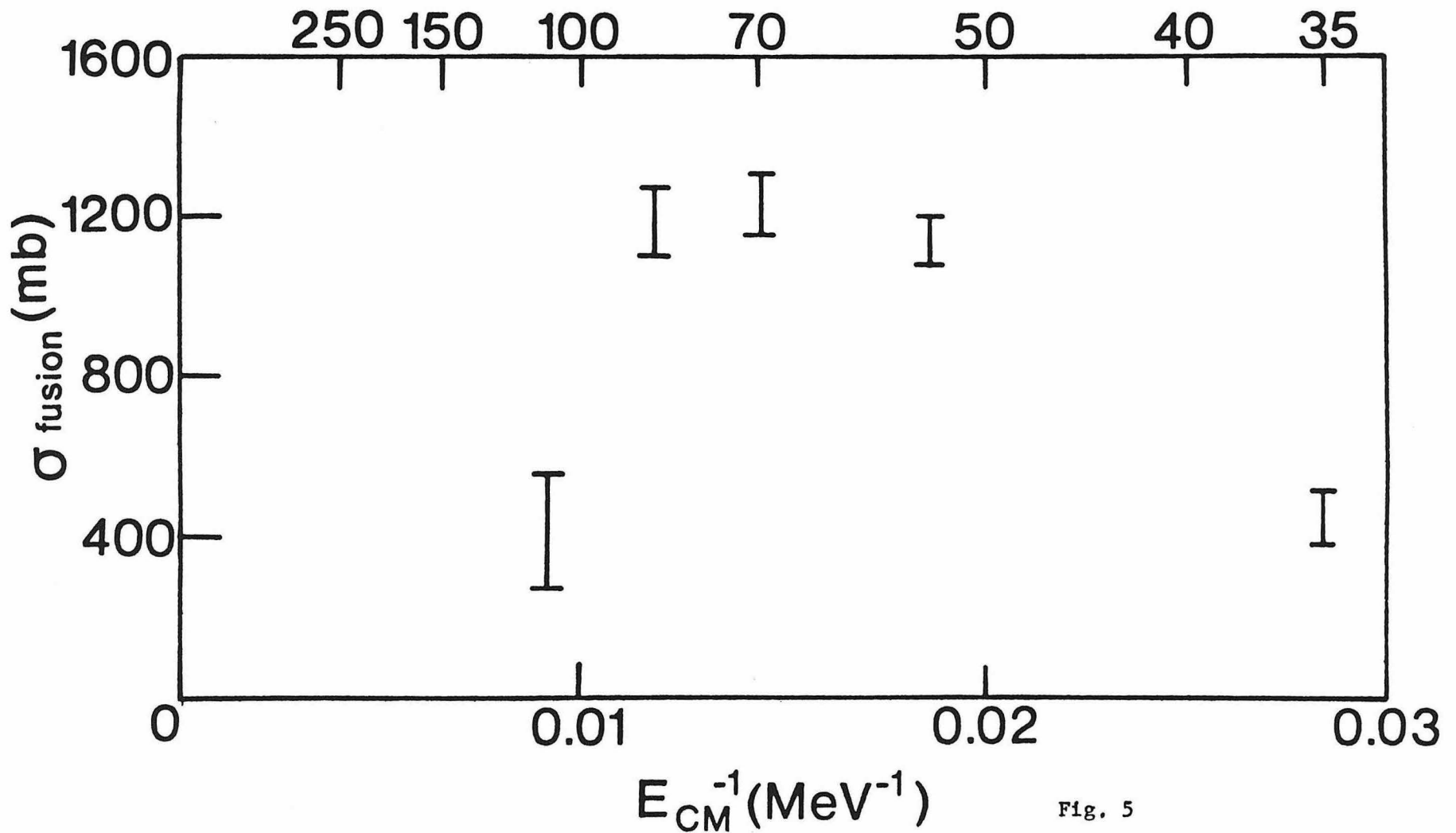


Fig. 5

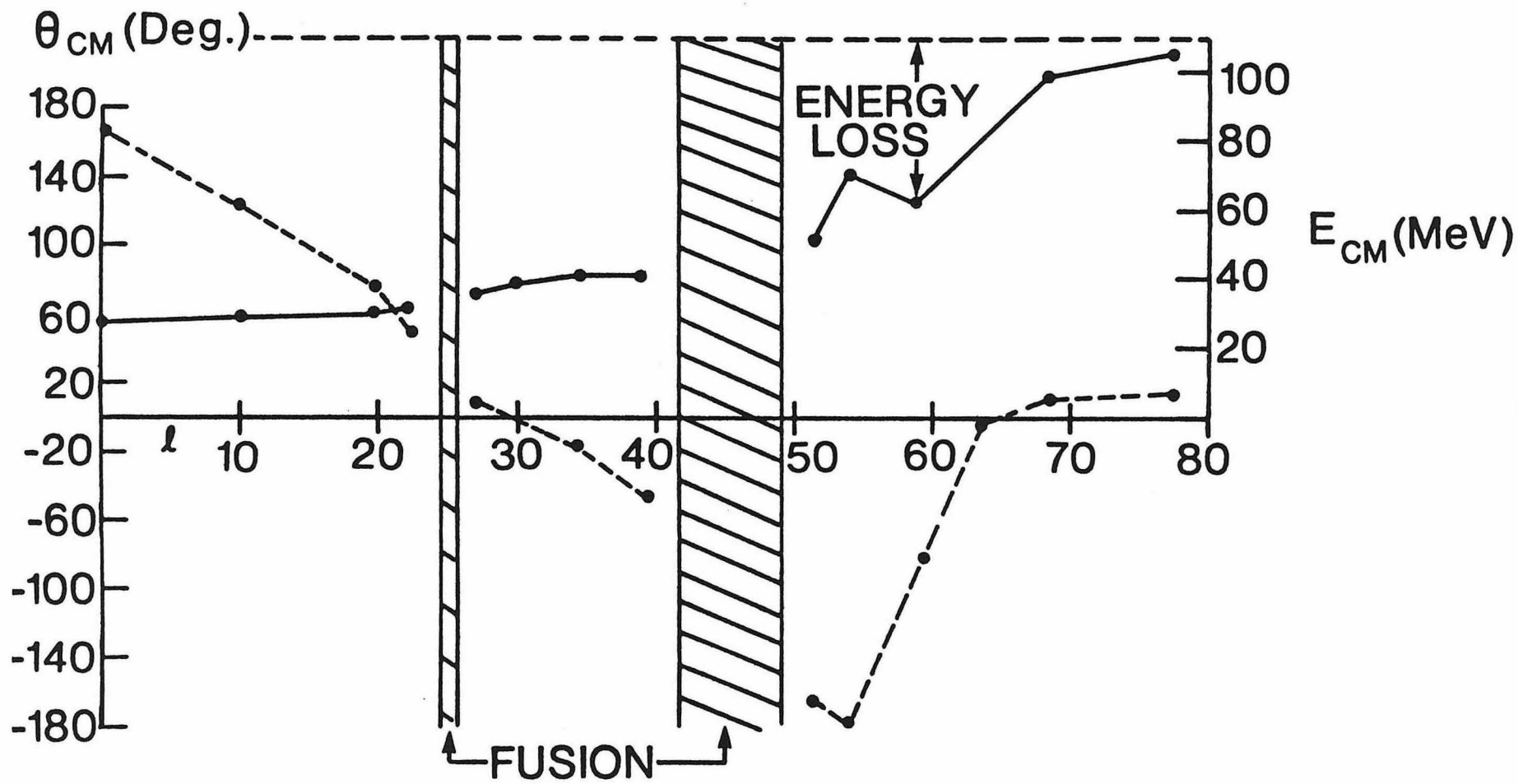


Fig. 6

### Section 8: Results for $^{86}\text{Kr} + ^{139}\text{La}$

The final calculations presented here are separable, 2-D calculations for the heavier system,  $^{86}\text{Kr} + ^{139}\text{La}$ , using the Skyrme III force. This system is heavy enough so that deep-inelastic processes dominate and the TDHF predictions for the various equilibration processes can be obtained. For this larger system, the classical approximations discussed previously are more accurate and the bulk dynamics is less influenced by single-particle behavior. This system has also been studied experimentally (VAN 78, DY 80) and with axially symmetric TDHF calculations (DAV 79,80), providing ample results for comparison with our predictions. The experimental results do show substantial deep-inelastic scattering but also show some fusion-fission events.

For this system, the full, nonlocal modified Skyrme force must be used (again neglecting the spin-orbit force and occupying each orbital with two nucleons of opposite spin) as in Eq. (2.17) and (2.24). Since neither of these nuclei have closed shells in an oscillator basis, we also use the filling approximation. Thus, for  $^{86}\text{Kr}$  the 36 protons fill the lowest three shells and the fractional occupation of the fourth shell is 0.8, while the 50 neutrons fill the lowest four shells and the fractional occupation of the fifth shell is  $1/3$ . For  $^{139}\text{La}$ , the 57 protons result in a fractional occupation for the fifth shell of  $17/30$  while the 82 neutrons result in a fractional occupation for the sixth shell of  $6/21$ . (However, for real nuclei, including the spin-orbit force, both of these nuclei would have closed neutron shells  $N = 50, 82$ .)

Static HF solutions for each nucleus are obtained by the imaginary time step method. For an oscillator parameter  $\hbar\omega = 4.10$ , which maximizes the total binding energy of the system, the binding energies and rms radii of the two nucleons are given in Table 3.

Table 3			
nucleus	BE	rms <sub>p</sub>	rms <sub>n</sub>
	(MeV)	(fm)	(fm)
<sup>86</sup> Kr	671.4	4.24	4.41
<sup>139</sup> La	1032.5	4.86	5.01

The experimental values are  $BE_{Kr} = 749.2$  and  $BE_{La} = 1159.5$ . (All energies are in MeV.) From Table 1 of the first paper, we expect that the separable approximation would cause about 20 MeV and 40 MeV less binding, respectively, than the full 3-D calculation. Because of this difference in binding energies, our calculations will have an extra 200 MeV of total energy at a given bombarding energy (collective kinetic energy). However, to the extent that it is the initial relative velocity of the ions which determines the dynamics, this should be unimportant. The spherical aspect of the filling approximation should not present this kind of problem, however, since both nuclei have small deformations. ( $\beta < .1$  see page 56.) This is related to the closure of the neutron shells.

For the TDHF evolution of the system, a spacing  $\Delta x = 1.2$  fm and a box size  $35 \times 34 \times 16$  are used. The discretization errors can be estimated from the kinetic energy in the z direction (odd multiples of  $1/2 \hbar\omega$ ). These range from 0.3% for the first level to almost 6% for the sixth level. Indeed, discretization errors in the boost result in a rapid initial transfer of about 16 MeV, or 5%, from collective kinetic energy to internal excitation. This is worse than for lighter systems because higher orbitals with more rapid spatial variation are included. These errors, however, are not related to the conservation of the discrete total energy because the operator  $\hbar$  was derived from a variational principle. The conservation of energy (and norm) are dependent on the accuracy of the time evolution operator. Using  $\Delta t = .08$  or  $.09 \times 10^{-22}$  sec. and 2(4) terms in the exponential in the first (second) time step, total energy is conserved to 1 part in 600 and the normalization to 1 part in 5,000. A partial test run with  $\Delta t$  smaller

by a factor of 2 showed less than 1 part in 900 difference in the physical observables: kinetic energy and the total and fragment rms radii.

A set of calculations was performed at  $E_{lab} = 505$  MeV to determine both the fusion region and the characteristics of the scattering, and two runs were performed at  $E_{lab} = 710$  MeV to check the existence of a fusion region.

Looking first at the fusion regions for  $E_{lab} = 505$  MeV, our results predict fusion for  $l=5$  through  $l=60$  (in units of  $\hbar$ ) while  $l=0$  and  $l=80$  scatter. Thus, we would predict a fusion cross section  $190 \pm 50$  mb. This agrees quite well with the experimental value of  $170 \pm 50$  mb ( $l_{crit} = 66 \pm 10$ ) which is identified as fusion-fission yield from both charge and angular distributions. In contrast, the axially symmetric (AS) calculation shows no fusion at this energy. However, the Skyrme II force was used in these calculations and a single run at  $l=0$  with Skyrme III did fuse.

The scattering at  $l=0$  differed from that in lighter systems because the lighter nuclei bounced back from the heavier nuclei rather than passing through it. This is undoubtedly due to the greater strength of the Coulomb potential. However, since the AS calculation should be exact for  $l=0$ , this effect is probably due to the slightly increased stiffness of nuclei in the separable approximation. This is demonstrated by comparing the rms radii of the systems. The AS result for  $l=0$  has a minimum rms radius approximately 6.4 fm whereas our results have a minimum rms radius about 6.75 fm for any  $l \leq 80$ . (This corresponds to a fragment separation about 9.8 fm.) At slightly larger  $l$ , the impact of the two nuclei is somewhat more gradual, giving the nuclear shapes more time to adjust.

Runs performed at  $E_{lab} = 710$  MeV show fusion for both  $l=0$  and  $l=50$ . This is consistent with both the experimental determination,  $77 \pm 12$ , and with AS calculations using Skyrme II, which show fusion for  $l \leq 65$ . (For these two runs, our minimum rms radius is about 6.4 fm whereas AS calculations give about 6.2 fm.)

Figure 4 shows results for the final total kinetic energy and scattering angle in the center of mass. Our results are compared with both the axial calculations and the experimental contours for the double differential cross section. (The TDHF results are labelled by the initial angular momentum.) Both calculations reproduce the general characteristics of the experimental contours but with less energy dissipation, particularly for the fully damped events. The separable calculations provide slightly more dissipation in general than the axially symmetric calculations but the principle difference seems to be a much larger small-angle contribution from the separable calculations.

Experimental values are quoted for partially damped and fully damped cross sections - fully damped events are defined to be those below and to the left of the dashed line in Figure 4. These values are  $\sigma(\text{fully damped}) = 1020 \pm 200$  mb and  $\sigma(\text{partially damped}) = 770 \pm 165$  mb. The axial results are quoted as  $\sigma_{FD} \approx 975$  mb ( $l=0-100$  and  $125-175$ ) and  $\sigma_{PD} \approx 745$  mb. Our results show  $l=0-90$  and  $110-180$  in the full damping region yielding  $\sigma_{FD} \approx 1100$  mb. The partially damped region is hard to estimate in TDHF calculations because of the "energy damping" due to the numerical errors, so that even at  $l=250$ , when the nuclei pass without getting closer than 14.6 fm (their combined radii are only about 11.4 fm), there is some energy loss. Although an energy loss of almost 20 MeV is not particularly good, it must be remembered that this is only 2% of the total energy of -1380 MeV. Both predictions of the fully damped cross section are consistent with the experiment. For small angle events ( $\vartheta_{cm} < 42^\circ$ ) the difference between the two TDHF calculations is much more dramatic. Our results indicate  $l=110-180$  in this region giving a cross section  $\approx 800$  mb. We also expect that fusion-fission events (with an angular distribution  $\frac{d\sigma}{d\Omega} = \frac{1}{\sin^3 \vartheta}$ ), will fall in this region approximately a quarter of the time, contributing another 40 mb. For the axially symmetric calculations, the comparable estimate is only

about 600 mb. Unfortunately, the comparable experimental number was not published.

Figure 5 shows the total kinetic energy in the center of mass,  $E_{cm}$ , the scattering angle in the center of mass,  $\vartheta_s$ , and the interaction time,  $\tau_{int}$  as functions of the initial angular momentum for  $l \geq 80$ . The fusion region and the run at  $l=0$ , which should have fused, have been omitted. We see that  $E_{cm}$  drops below the Coulomb barrier very quickly.

The experimental Coulomb barrier is about  $E_{cm} = 250$  MeV, in agreement with the estimate

$$\frac{Z_1 Z_2 e^2}{r_0 (A_1^{\frac{1}{3}} + A_2^{\frac{1}{3}})} \quad (8.1)$$

The final states have energy below the barrier because they scission with a very deformed shape (not two tangent spheres). Full energy dissipation is reached in about  $2 \times 10^{-21}$  sec.

The scattering angle,  $\vartheta_s$ , is characteristic of a heavier system with a stronger Coulomb force. Thus, it is predominantly positive, like the AS results, although in contrast to these, there is a small region of negative angle scattering. For the highest  $l$ ,  $\vartheta_s$  is very close to pure Coulomb scattering. Our interaction times are generally larger than the AS calculation - sometimes by as large as a factor of two.

Figure 6 shows the changes in charge and mass numbers,  $\Delta Z$  and  $\Delta A$ , the charge to mass ratio  $Z/A$  and the widths of the number distributions,  $\Gamma_Z$  and  $\Gamma_A$ . Since the AS results for the width are quoted as full-width half-maximum,  $\Gamma$ , and the experimental results as dispersion,  $\sigma^2$ , both labels are used for the axis, where  $\Gamma = \sqrt{8 \ln 2} \sigma$ . The AS results are quoted for  $\Delta A$  and  $\Gamma_A$  while experimental results are quoted for  $\Delta Z$  and  $\Gamma_Z$ .

Our calculations show more mass transfer to the larger fragment with a typical  $\Delta A \approx 3$  for events with intermediate damping, compared to  $\Delta A \leq 1$  for the AS calculations. The experimental values are given for two amounts of energy damping:  $Q = -125$  MeV gives  $\Delta Z \approx -1$  and  $Q = -175$  MeV gives  $\Delta Z \approx +1$ . Therefore, we seem to slightly overestimate mass and charge transfer, while AS calculations underestimate them. We never show mass transfer to the light fragment as do the most highly damped experimental events, but none of our calculations show as much damping either; our  $Q_{\max} \approx -110$  MeV.

Our value for  $A/Z$  shows an initial rise due to a greater transfer of neutrons to the heavy fragment and never seems to equilibrate to the  $Z/A$  of the total system, denoted  $(Z/A)_T$ . The AS results show the expected behavior with  $Z/A$  approaching and then fluctuating about  $(Z/A)_T$ .

Our results for the widths are somewhat smaller than the AS results, but they use a slightly different prescription for calculating the widths in the filling approximation because of ambiguities in the implementation. The AS calculations (DAV ) use

$$\sigma^2 = \sum_i n_i w_{ii} - \sum_{ij} n_i n_j |w_{ij}|^2 , \quad (8.2)$$

but since this isn't zero for the initial  $^{86}\text{Kr}$  nucleus, it is modified to

$$\sigma^2(\text{true}) = \sigma^2 - \sigma_{\text{Kr}}^2 \text{ at } t=0 . \quad (8.3)$$

In either case, the results are lower than the experimental values. These values are  $\sigma_{\text{Z}}^2 = 7$  for  $Q = -125$  MeV and  $\sigma_{\text{Z}}^2 = 20$  for  $Q = -175$  MeV. Thus, for intermediate damping, we are about a factor of 4 too low, while for the full damping (which we do not get in our results), we are a factor of 10 too low. For comparison, the absolute limit on  $\sigma_{\text{Z}}^2$  for an independent-particle wavefunction ((DAS 79) and Section 4) is about 20 (depending on how the filling approximation changes the widths) close to the value observed experimentally. This underestimation of the widths is a common feature of TDHF calculations and is related to the fact that

$\sigma^2$  is a two-body operator.

## Section 9: Summary

In conclusion, a one-body microscopic theory, TDHF using the Skyrme interaction, calculates quite successfully the gross properties of many different types of nuclear behavior for collisions of nuclei up to several MeV/nucleon above the Coulomb barrier.

The separable approximation yields substantial agreement with both full 3D TDHF calculations and experimental results. Fusion cross sections are generally within about 10% of the experimental values for systems from  $^{16}\text{O}+^{16}\text{O}$  to  $^{86}\text{Kr}+^{139}\text{La}$ . In heavier systems, the predictions of these separable approximations for the deep-inelastic scattering are also quite accurate for energy vs. scattering angle and for the mean charges and masses of the fragments, except at the most fully damped events. The most fully damped events in these calculations show too little energy dissipation. The widths of the distributions, however, are not accurately given. The calculations predict widths smaller by a factor of 2 to 4 (for the most fully damped events). This isn't surprising since the widths are expectation values of two-body operators.

The inadequacies of these calculations are generally assumed to be due to the TDHF approximation itself. However, in the absence of full 3-D calculations including the spin-orbit force and averaging over orientations, we cannot, with certainty, know how much of the inadequacy is indeed due to the TDHF approximation itself. These calculations will, however, have to wait for more powerful computers or more powerful computer budgets. Indeed, they may be inappropriate because of the use of an effective interaction and the inherent limitations of the TDHF description.

PART II

A STABILITY CRITERION

FOR

TDHF CALCULATIONS

## Section 1: Introduction

Large-scale numerical calculations have shown that the TDHF approximation can successfully describe the gross features of heavy-ion collisions. The situation remains unsatisfying, however, for two related reasons: there are as yet no quantitative criteria which might be applied to signal the break-down of the mean-field approximation in any given physical situation, and tractable, systematic corrections to TDHF which become important when such a break-down occurs have yet to be developed. Although we can offer no guidance in solving the second problem, this contribution is relevant to the first problem, namely the development of a necessary criterion for the validity of TDHF solutions.

Our approach rests on the following general considerations. It is well known that the TDHF equations for a system of  $A$  nucleons may be derived from a variational principle (KE 76), in which the action is made stationary with respect to the functional variation of the  $A$  complex single-particle wavefunctions parametrizing the TDHF determinant. However, the variational principle makes no statement about the second variation of the action, which is connected with the stability of the TDHF solution under small perturbations. Consider, for example, the situations shown in Fig. 7. Let  $\Phi(t)$  be a solution to the TDHF equation (one which makes the action stationary), and suppose that at some time  $t=0$ ,  $\Phi(0)$  is perturbed to a new determinant  $\Psi(0)$  which differs only slightly from  $\Phi(0)$ . The subsequent evolution of  $\Psi$  can then lead to one of two situations. In Fig. 7a,  $\Psi(t)$  remains "near"  $\Phi(t)$  for all  $t>0$  and so  $\Phi(t)$  is stable. Fig. 7b,  $\Phi(t)$  is unstable, and  $\Psi(t)$  diverges from  $\Phi(t)$ . Of course, the stability or instability of  $\Phi$  may change with time, and might depend upon the type of perturbation applied to generate  $\Psi$  (conditional stability).

The standard interpretation of the TDHF wavefunction is that expectation values of one- or few-body operators generated from it correspond to the aver-

age evolution of the exact Schroedinger wavepacket. Consistency in this interpretation requires that this mean evolution (and hence the TDHF path) be well defined; i.e., that  $\Phi$  lie in a "valley" as in Fig. 7a, rather than on a "ridge", as in Fig. 7b. We, therefore, propose that the stability of TDHF solution with respect to small perturbations is a necessary (although not sufficient) criterion for the validity of the TDHF approximation. The RPA theory (TH 61) has been used to test the stability of static HF solutions; we propose a time-dependent generalization to test the stability of TDHF solutions.

## Section 2: RPA Theory

Ordinary RPA theory attempts to calculate the energies of collective states which are similar to the Hartree-Fock ground state. The theory looks for periodic solutions for states "close" to the HF state. Because of the condition that these states be "close" to the HF state, about which we will be specific later, we are actually calculating the curvature of the energy surface for determinantal wavefunctions at the HF state. This curvature is the important property to test the local stability of the HF state. If all the normal modes have periodic solutions, the HF state must be a local minimum and it will be stable. However, if any mode does not have a periodic solution, because its frequency is imaginary, then the HF state will be unstable with respect to that mode.

As in the derivation of TDHF, we minimize the action

$$\int dt \langle \Psi | i\hbar \frac{\partial}{\partial t} - H | \Psi \rangle \quad (2.1)$$

with respect to variations in  $\Psi^*$  in order to derive equations of motion for  $\Psi$ . For the state  $\Psi$  we want to use a general Slater determinant. Thouless (TH 61) showed that any N-particle Slater determinant not orthogonal to the Hartree-Fock determinant  $\Phi$  can be written in the representation appropriate for  $\Phi$  as

$$|\Psi\rangle = \eta^{-1/2} \exp\left(\sum_{ph} c_{ph} a_p^\dagger a_h\right) |\Phi\rangle \quad (2.2)$$

$\eta$  is a normalization constant and  $a^\dagger$  and  $a$  are creation and annihilation operators, respectively. The subscripts  $p$  or  $h$  refer to states which are not occupied or occupied, respectively, in the original HF state

$$|\Phi\rangle = \prod_{h=1}^N a_h^\dagger |0\rangle \quad (2.3)$$

To show that  $\Psi$  is a determinant, we need to use the fact that all terms in which the same creation or annihilation operator occurs more than once vanish.

$$\exp\left(\sum_{ph} c_{ph} a_p^\dagger a_h\right) |\Phi\rangle = \left[1 + \sum_{n=1}^{\infty} \frac{1}{n!} \left(\sum_{ph} c_{ph} a_p^\dagger a_h\right)^n\right] |\Phi\rangle \quad (2.4)$$

Since there are only  $N$  different occupied states  $h$  we can stop the sum over  $n$  at  $N$  and rewrite the sum as a product of  $N$  terms,

$$|\Psi\rangle = \left[ \prod_h \left( 1 + \sum_p c_{ph} a_p^\dagger a_h \right) \right] \left[ \prod_{h'} a_{h'}^\dagger |0\rangle \right] . \quad (2.5)$$

Each term in  $h$  will give 0 unless  $h' = h$ . Therefore,

$$|\Psi\rangle = \prod_h \left( a_h^\dagger + \sum_p c_{ph} a_p^\dagger \right) |0\rangle . \quad (2.6)$$

Thus, we can see that  $\Psi$  is a determinant of the wavefunctions

$$\chi_h = \phi_h + \sum_p c_{ph} \phi_p . \quad (2.7)$$

Since unitary transformations among occupied states will not change the Slater determinant of the wavefunctions, we see that the state  $\Psi$  is a general determinant not orthogonal to  $\Phi$ . States orthogonal to  $\Phi$  can be constructed by using one or more wavefunctions of the type  $Z_h = \sum_p d_{ph} \phi_p$ .

We now see that we are calculating the TDHF evolution of the state  $\Psi$  where its time dependence is contained completely in  $c_{ph}$ , the particle-hole occupation numbers. We write the action in terms of  $c_{ph}$ ,  $\dot{c}_{ph}$ , and  $c_{ph}^\circ$  and accomplish the variation with respect to  $\Psi^\circ$  by a variation of  $c_{ph}^\circ$ , so the evolution of  $\Psi$  is described by the equation for  $\dot{c}_{ph}$  as a function of  $c_{ph}$  and  $c_{ph}^\circ$ . To study the local stability of the HF state, we assume  $c_{ph}$  is small and truncate the calculations of  $\Psi$  and the action to second order in  $c_{ph}$ . Therefore, after the variation, the equation for  $\dot{c}_{ph}$  will be linear in  $c_{ph}$  and  $c_{ph}^\circ$ . We look for periodic solutions by assuming

$$c_{ph} = X_{ph} e^{-i\omega t} + Y_{ph}^\circ e^{+i\omega t} , \quad (2.8)$$

and then solve for the normal modes and their frequencies  $\omega$ . These must all be real for the solution  $c_{ph}$  in Eq. (2.8) to be periodic. Of course, a larger  $\omega$  will imply a sharper local minimum and a more sharply confined HF state.

### Section 3: Time-Dependent Generalization of the RPA Theory

For our time-dependent generalization of the RPA theory, we again minimize the action for a general determinantal wavefunction,

$$|\Psi\rangle = \eta^{-1/2} \exp\left(\sum_{ph} c_{ph} a_p^\dagger a_h\right) |\Phi\rangle \quad (3.1)$$

but in this case, the state  $\Phi$  and the creation and annihilation operators for particles and holes also evolve in time. We define an operator  $A_{ph}^\dagger \equiv a_p^\dagger a_h$  which creates a particle-hole pair and write

$$\sum_{ph} c_{ph} A_{ph}^\dagger = \vec{c} \cdot \vec{A}^\dagger \quad (3.2)$$

Since we are still concerned with local stability, we still truncate the expressions for  $\Psi$  and the action to second order in  $c_{ph}$ :

$$|\Psi\rangle = \eta^{-1/2} [1 + \vec{c} \cdot \vec{A}^\dagger + \frac{1}{2}(\vec{c} \cdot \vec{A}^\dagger)^2] |\Phi\rangle \quad (3.3)$$

We also evaluate  $\eta$  to second order, by setting  $\langle \Psi | \Psi \rangle = 1$ . (See Appendix B1 for details.)

$$\eta = 1 + \vec{c}^* \cdot \vec{c} \quad (3.4)$$

so that

$$|\Psi\rangle = [1 - \frac{1}{2} \vec{c}^* \cdot \vec{c} + \vec{c} \cdot \vec{A}^\dagger + \frac{1}{2}(\vec{c} \cdot \vec{A}^\dagger)^2] |\Phi\rangle \quad (3.5)$$

For the action we need  $\langle \Psi | H | \Psi \rangle$  and  $\langle \Psi | i \frac{\partial}{\partial t} | \Psi \rangle$ . ( $\hbar \equiv 1$ ) The first is straightforward.

$$\begin{aligned} \langle \Psi | H | \Psi \rangle = & (1 - \vec{c}^* \cdot \vec{c}) \langle H \rangle + \langle H \vec{c} \cdot \vec{A}^\dagger \rangle + \langle \vec{c}^* \cdot \vec{A} H \rangle \\ & + \langle \vec{c}^* \cdot \vec{A} H \vec{c} \cdot \vec{A}^\dagger \rangle + \frac{1}{2} \langle (\vec{c}^* \cdot \vec{A})^2 H \rangle + \frac{1}{2} \langle H (\vec{c} \cdot \vec{A}^\dagger)^2 \rangle \end{aligned} \quad (3.6)$$

We assume a second-quantized Hamiltonian

$$H = \sum_{\alpha\beta} t_{\alpha\beta} a_\alpha^\dagger a_\beta + \frac{1}{4} \sum_{\alpha\beta\gamma\delta} \tilde{V}_{\alpha\beta\gamma\delta} a_\alpha^\dagger a_\beta^\dagger a_\delta a_\gamma \quad (3.7)$$

where  $\{\alpha\}$  is a complete single-particle basis,

$$t_{\alpha\beta} = \langle \alpha | t | \beta \rangle \quad (3.8)$$

are the matrix elements of the one-body kinetic energy, and

$$\tilde{V}_{\alpha\beta\gamma\delta} = \langle \alpha\beta | V | \gamma\delta - \delta\gamma \rangle \quad (3.9)$$

are the antisymmetrized matrix elements of the two-body interaction.

The second expression,  $\langle \Psi | i \frac{\partial}{\partial t} | \Psi \rangle$ , is more complicated because the generalization must agree with the RPA theory for  $\Phi$  an HF state. If we evolved each wavefunction  $\varphi_h$  with the standard HF operator  $h$  as  $i\dot{\varphi}_h = h\varphi_h$ , we would get  $\varphi_h = e^{-ie_h t} \varphi_{hHF}$ , where  $h\varphi_{hHF} = e_h \varphi_{hHF}$ . This would result in a time dependent

$$|\Phi\rangle = \exp(-i \sum_h e_h t) |\Phi_{HF}\rangle \quad (3.10)$$

rather than the time independent  $|\Phi_{HF}\rangle$  needed to agree with ordinary RPA theory. Since this time-dependent phase is unobservable, the correct operator  $\bar{h}$  must include only the physically relevant changes in  $\Phi$ . The usual  $h$  in the single-particle wavefunction evolution  $i\dot{\varphi}_\alpha = h_{\alpha\beta} \varphi_\beta$ , with  $h_{\alpha\beta} = t_{\alpha\beta} + \sum_h V_{\alpha h \beta h}$  (since  $\rho_{\alpha\beta} = \delta_{\alpha\beta} \delta_{\alpha h}$  see Appendix A1) is a unitary transformation mixing all the various states. However, since unitary transformations among hole states or among particle states will not produce any observable changes, we want to take the hole-hole and particle-particle components out of  $h$ . To do this, we can use the one-body density matrix  $\rho = \sum_h |\varphi_h\rangle \langle \varphi_h|$ , which is a projector for  $|\Phi\rangle$ . If we remove the hole-hole components,  $\rho h \rho$  and the particle-particle components,  $(1-\rho)h(1-\rho)$  we are left with

$$\bar{h} = \rho h (1-\rho) + (1-\rho) h \rho \quad (3.11)$$

so that

$$\begin{aligned} \bar{h}_{pp} &= 0 = \bar{h}_{hh} \\ \bar{h}_{ph} &= h_{ph} \quad \text{and} \quad \bar{h}_{hp} = h_{hp} \end{aligned} \quad (3.12)$$

Since we now include only the physically relevant changes  $\Phi$  is orthogonal to its time derivative.

$$\langle \Phi | \frac{\partial}{\partial t} | \Phi \rangle = -i \langle \Phi | \rho h (1-\rho) + (1-\rho) h \rho | \Phi \rangle = 0 \quad (3.13)$$

With this evolution operator, the static  $\Phi_{HF}$  is a solution to the evolution equation

$$i \frac{\partial}{\partial t} |\Phi_{HF}\rangle = \bar{h} |\Phi_{HF}\rangle = 0 \quad (3.14)$$

We can now evaluate the other term from the action,

$$\begin{aligned} \langle \Psi | i \frac{\partial}{\partial t} | \Psi \rangle = & i \left[ -\frac{1}{2} \frac{\partial}{\partial t} (\vec{c}^* \cdot \vec{c}) + \vec{c}^* \cdot \dot{\vec{c}} + \langle \vec{c} \cdot \vec{A}^+ \rangle + \langle \vec{c}^* \cdot \vec{A} \vec{c} \cdot \vec{A}^+ \rangle \right. \\ & + \frac{1}{2} (\langle \vec{c} \cdot \vec{A}^+ \vec{c} \cdot \vec{A}^+ \rangle + \langle \vec{c}^* \cdot \vec{A}^+ \vec{c} \cdot \vec{A}^+ \rangle) \\ & \left. + \langle \Phi | 1 - \vec{c}^* \cdot \vec{c} + \vec{c}^* \cdot \vec{A} + \vec{c} \cdot \vec{A}^+ + \vec{c}^* \cdot \vec{A} \vec{c} \cdot \vec{A}^+ + \frac{1}{2} (\vec{c}^* \cdot \vec{A})^2 + \frac{1}{2} (\vec{c} \cdot \vec{A}^+)^2 | \Phi \rangle \right] \end{aligned} \quad (3.15)$$

We now know the correct evolution operator to use, so

$$\begin{aligned} i |\dot{\Phi}\rangle &= \bar{h} |\Phi\rangle \\ i a_p^{\dot{+}} &= [\bar{h}, a_p^+] ; \text{ and } i a_h^{\dot{-}} = [\bar{h}, a_h] \\ i A_{ph}^{\dot{+}} &= [\bar{h}, \vec{A}^+] \end{aligned} \quad (3.16)$$

Therefore, the net result is

$$\begin{aligned} \langle \Psi | i \frac{\partial}{\partial t} | \Psi \rangle = & i \left[ -\frac{1}{2} \frac{\partial}{\partial t} (\vec{c}^* \cdot \vec{c}) + \vec{c}^* \cdot \dot{\vec{c}} \right] + (1 - \vec{c}^* \cdot \vec{c}) \langle \bar{h} \rangle + \langle \bar{h} \vec{c} \cdot \vec{A}^+ \rangle \\ & + \langle \vec{c}^* \cdot \vec{A} \bar{h} \rangle + \langle \vec{c}^* \cdot \vec{A} \bar{h} \vec{c} \cdot \vec{A}^+ \rangle + \frac{1}{2} \langle \bar{h} (\vec{c} \cdot \vec{A}^+)^2 \rangle + \frac{1}{2} \langle (\vec{c}^* \cdot \vec{A})^2 \bar{h} \rangle \end{aligned} \quad (3.17)$$

We can notice that after the first two terms, the right-hand side looks precisely like  $\langle \Psi | H | \Psi \rangle$  but with  $H$  replaced by  $\bar{h}$ .

Now we want to minimize the action by varying  $c_{ph}^{\dot{+}}$  but remembering that the total derivatives, such as  $\frac{\partial}{\partial t} (\vec{c}^* \cdot \vec{c})$  do not vary since the endpoints are fixed.

$$\begin{aligned} \frac{\delta}{\delta c_{ph}^{\dot{+}}} \langle \Psi | H | \Psi \rangle = & -c_{ph} \langle H \rangle + \langle A_{ph} H \rangle + \langle A_{ph} H \vec{c} \cdot \vec{A}^+ \rangle \\ & + \frac{1}{2} (\langle A_{ph} \vec{c}^* \cdot \vec{A} H \rangle + \langle \vec{c}^* \cdot \vec{A} A_{ph} H \rangle) \end{aligned} \quad (3.18)$$

and

$$\begin{aligned} \frac{\delta}{\delta c_{ph}^{\dot{-}}} \langle \Psi | i \frac{\partial}{\partial t} | \Psi \rangle = & i \dot{c}_{ph} - c_{ph} \langle \bar{h} \rangle + \langle A_{ph} \bar{h} \rangle + \langle A_{ph} \bar{h} \vec{c} \cdot \vec{A}^+ \rangle \\ & + \frac{1}{2} (\langle A_{ph} \vec{c}^* \cdot \vec{A} \bar{h} \rangle + \langle \vec{c}^* \cdot \vec{A} A_{ph} \bar{h} \rangle) \end{aligned} \quad (3.19)$$

Since the stability of the TDHF path is determined by the curvature of the energy surface normal to the path, another modification of the ordinary RPA theory is needed. We require that the initial perturbation of  $\Phi$  be orthogonal to

the TDHF path. (An initial perturbation along the path would be equivalent to a shift in time.) The direction of the path is given by  $\frac{\partial}{\partial t}\Phi$ , so that  $\Phi$  is also orthogonal to the path and the perturbed wavefunction  $\Psi$  is orthogonal to  $\frac{\partial}{\partial t}\Phi$ .

$$i\langle \frac{\partial \Phi}{\partial t} | \Psi \rangle = 0 = \langle \Phi | \bar{h} (1 - \frac{1}{2} \vec{c}^* \cdot \vec{c} + \vec{c} \cdot \vec{A}^+ + \frac{1}{2} (\vec{c} \cdot \vec{A}^+)^2) | \Phi \rangle \quad (3.20)$$

Only the  $\vec{c} \cdot \vec{A}^+$  terms contribute (See Appendix B1 for details.) The orthogonality condition on  $\Psi$  becomes

$$\sum_{ph} h_{ph}^* c_{ph} = 0 = \sum_{ph} h_{ph} c_{ph}^* \quad (3.21)$$

These conditions are most simply imposed by the method of LaGrange multipliers, adding the terms

$$-\lambda \sum_{ph} c_{ph}^* h_{ph} - \lambda^* \sum_{ph} c_{ph} h_{ph}^* \quad (3.22)$$

to the action. The final result for the variation of the action with this constraint is

$$i\dot{c}_{ph} = -c_{ph} (\langle H \rangle - \langle \bar{h} \rangle) + \langle A_{ph} (H - \bar{h}) \rangle + \langle A_{ph} (H - \bar{h}) \vec{c} \cdot \vec{A}^+ \rangle + \frac{1}{2} [\langle A_{ph} \vec{c}^* \cdot \vec{A} (H - \bar{h}) \rangle + \langle \vec{c}^* \cdot \vec{A} A_{ph} (H - \bar{h}) \rangle] - \lambda h_{ph} \quad (3.23)$$

The evaluation of these expectation values in Appendix B1 gives the result

$$i\dot{c}_{ph} = \sum_{p'h'} [A_{ph,p'h'} c_{p'h'} + B_{ph,p'h'} c_{p'h'}^*] - \lambda h_{ph} \quad (3.24)$$

where the matrix

$$A_{ph,p'h'} \equiv h_{pp'} \delta_{hh'} - \delta_{pp'} h_{hh'} + \tilde{V}_{ph,hp'} \quad (3.25)$$

is hermitian and the matrix

$$B_{ph,p'h'} \equiv \tilde{V}_{pp',hh'} \quad (3.26)$$

is symmetric.

We can see that for a static HF solution with  $h_{ph} = 0$ ,  $h_{pp'} = \epsilon_p \delta_{pp'}$ , and  $h_{hh'} = \epsilon_h \delta_{hh'}$ , where the  $\epsilon$ 's are the single particle energies; this equation reduces to the usual RPA equation. To test the stability (or measure the curvature of the energy surface) at a particular point along the TDHF path of  $\Phi$ , we must imagine

suspending the evolution of  $\Phi$  and studying the motion of  $\Psi$  constrained to be perpendicular to this frozen direction of motion for  $\Phi$ . Thus  $A$ ,  $B$ , and  $h$  depend on the TDHF wavefunction  $\Phi$  and vary from point to point in parameter space. However, while testing the hypothetical motion of  $\Psi$  in a particular direction, at a particular point these are constant. Note that we are only able to equate choosing a particular point in parameter space with freezing the time evolution of  $\Phi$ ,  $A$ ,  $B$ , and  $h_{ph}$  because we have chosen the correct evolution operator  $\bar{h}$  to isolate only physically relevant changes. This means that Eq. (3.21) becomes

$$\sum_{ph} \dot{c}_{ph}(t) h_{ph}^*(t_F) = 0 \quad (3.27)$$

for all times  $t$  in the motion of  $\Psi$  and any particular time we choose to freeze the motion of  $\Phi$ ,  $t_F$ . Therefore,

$$\sum_{ph} \dot{c}_{ph}(t) h_{ph}^*(t_F) = 0 \quad (3.28)$$

also and we can solve for  $\lambda$  by multiplying Eq. (3.23) by  $h_{ph}^*$  and summing over  $ph$ . This gives

$$\lambda(t) = \frac{1}{\sum_{ph} h_{ph}^*(t_F) h_{ph}(t_F)} \sum_{php'h'} [h_{ph}^*(t_F) A_{ph,p'h'}(t_F) c_{p'h'}(t) + h_{ph}^*(t_F) B_{ph,p'h'}(t_F) c_{p'h'}(t)] \quad (3.29)$$

and substituting  $\lambda$  back into Eq. (3.23) gives

$$i\dot{c}_{ph} = \sum_{p'h'p'e_{h'e}} [P_{ph,p'e_{h'e}} A_{p'e_{h'e},p'h'} c_{p'h'} + P_{ph,p'e_{h'e}} B_{p'e_{h'e},p'h'} c_{p'h'}] \quad (3.30)$$

where

$$P_{ph,p'e_{h'e}} = \delta_{pp'} \delta_{hh'} - \frac{h_{ph} h_{p'e_{h'e}}^*}{\sum_{p'h'} h_{p'h} h_{p'h'}^*} \quad (3.31)$$

We can put this equation into a more elegant form by noticing that  $P$  is hermitian and that it is a projector off the TDHF path, i.e.

$$\sum_{p'h'} P_{ph,p'h'} c_{p'h'} = c_{ph} \quad \text{with} \quad P^2 = P \quad (3.32)$$

We can write the equation as

$$i\dot{c}_{ph} = \sum_{p'h'} [\bar{A}_{ph;p'h} c_{p'h} + \bar{B}_{ph;p'h} c_{p'h}^*] \quad (3.33)$$

where  $\bar{A}=PAP$  is hermitian and  $\bar{B}=PBP^*$  is symmetric, just like the RPA matrices  $A$  and  $B$ .

We look for periodic solutions by setting

$$c_{ph}(t) = X_{ph} e^{-i\omega t} + Y_{ph}^* e^{+i\omega t} \quad (3.34)$$

and assuming  $\omega$  is real. Equating terms with  $e^{-i\omega t}$  gives

$$\omega X_{ph} = \sum_{p'h'} [\bar{A}_{ph;p'h} X_{p'h} + \bar{B}_{ph;p'h} Y_{p'h}^*] \quad (3.35)$$

and equating terms with  $e^{+i\omega t}$  gives

$$-\omega Y_{ph} = \sum_{p'h'} [\bar{A}_{ph;p'h} Y_{p'h}^* + \bar{B}_{ph;p'h} X_{p'h}^*] \quad (3.36)$$

In the usual RPA matrix notation, these equations are written.

$$\omega \begin{pmatrix} X \\ Y \end{pmatrix} = \begin{pmatrix} \bar{A} & \bar{B} \\ -\bar{B}^* & -\bar{A}^* \end{pmatrix} \begin{pmatrix} X \\ Y \end{pmatrix} \quad (3.37)$$

If all the eigenvalues  $\omega$  are real, then the TDHF path for  $\Phi$  lies in a valley and the path is stable. Once again larger  $|\omega|$  imply a more sharply confined path.

Although a specific evolution operator  $\bar{h}$  was chosen to facilitate the derivation of these equations, we would suspect that unitary transformations among particles or among holes would not change the eigenvalues,  $\omega$ . In Appendix B2 we show that these transformations would result merely in a similarity transformation of the matrix

$$\begin{pmatrix} \bar{A} & \bar{B} \\ -\bar{B}^* & -\bar{A}^* \end{pmatrix}$$

and thus, we prove that the eigenvalues are not changed. This is important because the time evolution can still be defined merely by the particle-hole and hole-particle elements,  $h_{ph}$  and  $h_{hp}$ , as in TDHF. Therefore, we will not need to evolve any additional wavefunctions or parameters to do the stability analysis.

#### Section 4: TDHF for the SU(3) Model

To test our ideas about stability, we apply them to an exactly soluble model. We consider the SU(3) generalization (LI 70, HOL 74) of the familiar SU(2) (Lipkin) model (LIP 65). Although the TDHF approximation for SU(2) has been investigated in some detail (KRI 77), it is not sufficiently complex for our purposes. There is only one collective coordinate and associated velocity (the rotation angles  $\vartheta, \varphi$ ) and hence, no collective degrees of freedom exist normal to the TDHF path.

The SU(3) model consists of N distinguishable identical particles, labeled by the index  $n$ , each of which can be in three single-particle states having energy  $\varepsilon_i$ . The Hamiltonian is

$$H = \sum_k \varepsilon_k G_{kk} + \sum_{kl} V_{kl} G_{lk}^2 \quad (4.1)$$

where  $V_{kl}$  is the strength of the two-body interaction between states  $k$  and  $l$ .

$$V_{kl} = V_{lk} \quad \text{and} \quad V_{kk} = 0 \quad (4.2)$$

with

$$G_{kl} = \sum_n a_{nk}^\dagger a_{nl} \quad (4.3)$$

The operators  $a^\dagger$  and  $a$  are creation and annihilation operators so that each term of  $G_{kl}$  takes a particle,  $n$ , out of state  $l$  and into state  $k$  and each  $G_{kk}$  counts the particles in state  $k$ .

We want to write a general collective determinant, i.e., in which all particles behave identically. We define new creation, annihilation operators  $\alpha^\dagger, \alpha$  by

$$\alpha_{nk}^\dagger = \sum_j A_{kj}^{-1} a_{nj}^\dagger \quad (4.4)$$

where  $A$  is a unitary matrix independent of  $n$ . Now  $\alpha_{n1}^\dagger$  creates the occupied TDHF orbital;  $\alpha_{n2}^\dagger$  and  $\alpha_{n3}^\dagger$  create the remaining two particle orbitals. Thus, a general collective determinant is written

$$|\Phi\rangle = \prod_n \alpha_{n1}^\dagger |0\rangle \quad (4.5)$$

and the matrix elements  $A_{ij}$  determine the actual occupied and unoccupied states. Since these  $A$ 's may be complex, six parameters would be required to completely define the TDHF orbital; however, since both wavefunctions (created by  $\alpha^+$  or  $\alpha^+$ ) are normalized and the overall phase can be ignored, we are left with four parameters needed to define the TDHF state.

Since the operators  $\alpha^+$  are in a fixed basis, the time dependence of the operators  $\alpha^+$  and ultimately of the TDHF state is contained completely in the matrix elements of  $A$ . Therefore, the TDHF equation governing the evolution of  $\Phi$  must be transformed into equations governing the evolution of the matrix elements of  $A$  and the parameters used to characterize  $A$ . The TDHF equations are

$$i \frac{\partial}{\partial t} \varphi_n = h \varphi_n \quad , \quad (4.6)$$

where  $h$  is a one-body operator

$$h = \sum_{kl} h_{kl} \sum_n \alpha_{nk}^+ \alpha_{nl} \quad . \quad (4.7)$$

The matrix elements  $h_{kl}$  are independent of  $n$  because the particles are identical. We write the TDHF equation in terms of the  $\alpha^+$ 's as

$$i \frac{\partial}{\partial t} \varphi_n = i \dot{\alpha}_{n1}^+ |0\rangle \quad (4.8)$$

and

$$h \varphi_n = \sum_{kl} h_{kl} \sum_{n'} \alpha_{n'k}^+ \alpha_{n'l} \alpha_{n1}^+ |0\rangle = \sum_k h_{k1} \alpha_{nk}^+ |0\rangle \quad . \quad (4.9)$$

Therefore, the equation for the operators  $\alpha^+$  becomes

$$i \dot{\alpha}_{n1}^+ = \sum_k h_{k1} \alpha_{nk}^+ \quad . \quad (4.10)$$

We know that the time dependence of  $\alpha$  is contained completely in the matrix  $A$ .

$$\dot{\alpha}_{nk}^+ = \sum_l A_{kl}^{-1} \dot{\alpha}_{nl}^+ = \sum_{lm} A_{kl}^{-1} A_{lm} \alpha_{nm}^+ \quad (4.11)$$

Thus, if we define a matrix

$$T = A^{-1} A \quad , \quad (4.12)$$

we can write Eq. (4.10) as

$$iT_{1k} = h_{k1} \quad (4.13)$$

We can easily show that  $iT$  is hermitian, just as  $h$  is hermitian.

If we ignore the winding phase, given by the purely imaginary  $T_{11}$ , we again need just 4 parameters for the two complex equations with  $k = 2$  or  $3$ . For our time-dependent generalization of the RPA theory, we have shown that we can ignore hole-hole and particle-particle components of the evolution operator,  $T_{11}$ ,  $T_{22}$ ,  $T_{23}$  and  $T_{33}$ . Therefore, throughout the calculation we need only the four parameters used for a normalized general TDHF orbital (ignoring the overall phase). Using the matrix elements of  $h$ , which are calculated in Appendix B3, the TDHF equations can be written as two equations for matrix elements of  $A$  :

$$\sum_k iA_{1k}^{-1} A_{kj} = \sum_k \varepsilon_k A_{kj} A_{k1}^* + \sum_{kl} 2V_{kl} (N-1) (A_{k1}^*)^2 A_{l1} A_{lj} \quad (4.14)$$

for  $j=2,3$ .

We choose, for our model Hamiltonian, equal level spacing ( $\varepsilon_1 = -\varepsilon$ ,  $\varepsilon_2 = 0$ , and  $\varepsilon_3 = \varepsilon$ ) and equal interaction strengths ( $V_{kl} = \frac{V}{2}$  for  $k \neq l$ ). We choose to parameterize the matrix  $A$  in terms of four rotation angles  $\vartheta_1, \vartheta_2, \psi_1$ , and  $\psi_2$  and write  $A$  as

$$A = \begin{pmatrix} \cos\vartheta_1 & \cos\vartheta_2 \sin\vartheta_1 e^{i\psi_1} & -\sin\vartheta_2 \sin\vartheta_1 e^{i\psi_2} \\ \cos\vartheta_2 \sin\vartheta_1 e^{-i\psi_1} & 1 + \cos^2\vartheta_2 (\cos\vartheta_1 - 1) & \sin\vartheta_2 \cos\vartheta_2 (\cos\vartheta_1 - 1) e^{-i(\psi_1 - \psi_2)} \\ \sin\vartheta_2 \sin\vartheta_1 e^{-i\psi_2} & \sin\vartheta_2 \cos\vartheta_2 (\cos\vartheta_1 - 1) e^{i(\psi_1 - \psi_2)} & 1 + \sin^2\vartheta_2 (\cos\vartheta_1 - 1) \end{pmatrix} \quad (4.15)$$

Note that this  $A$  is defined to be the inverse of the transformation matrix in (KRI 77). So for  $\vartheta_2=0$  this choice results in the same definitions: my  $\vartheta_1$  is his  $\alpha$ , my  $\psi_1$  is his  $\psi$ . The physical meaning of the "coordinates"  $\vartheta_1$  and  $\vartheta_2$  is quite clear. Since we can easily confirm that  $A$  is unitary in Eq. (4.15), we can write the occupied TDHF orbital

$$\alpha_{n1}^{\dagger} = \cos\vartheta_1 \alpha_{n1}^{\dagger} + \cos\vartheta_2 \sin\vartheta_1 e^{i\psi_1} \alpha_{n2}^{\dagger} + \sin\vartheta_2 \sin\vartheta_1 e^{i\psi_2} \alpha_{n3}^{\dagger} \quad (4.16)$$

Therefore, the probability of finding  $n$  in the first level is  $\cos^2\vartheta_2$ , in the second level is  $\cos^2\vartheta_2\sin^2\vartheta_1$  and in the third level is  $\sin^2\vartheta_2\sin^2\vartheta_1$ . Since all particles behave the same in the collective state, multiplying the above probabilities by the number of particles,  $N$ , gives the mean number of particles in each level for the TDHF state  $\Phi$  (in agreement with  $\langle G_{kk} \rangle$  as calculated in Appendix B3). The meaning of the "associated velocities"  $\psi_1$  and  $\psi_2$  is less clear but we can see from the evolution equations following, that  $\psi_1=\psi_2=0$  will imply  $\dot{\vartheta}_1=\dot{\vartheta}_2=0$ .

In Appendix B4 we transform the TDHF equations for the matrix elements of  $A$  into four coupled nonlinear first-order differential equations for the four angles.

$$\dot{\vartheta}_1 = \varepsilon \chi \cos\vartheta_1 \sin\vartheta_1 [\sin 2\psi_1 \cos^2\vartheta_2 + \sin 2\psi_2 \sin^2\vartheta_2] \quad (4.17)$$

$$\dot{\vartheta}_2 = \varepsilon \chi \cos\vartheta_2 \sin\vartheta_2 [-\sin 2\psi_1 \cos^2\vartheta_1 + \sin 2\psi_2 \cos^2\vartheta_1 - \sin 2(\psi_1 - \psi_2) \sin^2\vartheta_1]$$

$$\dot{\psi}_1 = -\varepsilon (1 + \chi [\cos 2\psi_1 (-\cos^2\vartheta_1 + \cos^2\vartheta_2 \sin^2\vartheta_1) + \cos 2\psi_2 \sin^2\vartheta_2 \sin^2\vartheta_1 - \cos 2(\psi_1 - \psi_2) \sin^2\vartheta_2 \sin^2\vartheta_1])$$

$$\dot{\psi}_2 = -\varepsilon (2 + \chi [\cos 2\psi_1 \cos^2\vartheta_2 \sin^2\vartheta_1 + \cos 2\psi_2 (-\cos^2\vartheta_1 + \sin^2\vartheta_2 \sin^2\vartheta_1) - \cos 2(\psi_1 - \psi_2) \cos^2\vartheta_2 \sin^2\vartheta_1])$$

Note that for  $\vartheta_2=0$  these agree with (KRI 77)'s TDHF equations. Here  $\chi$  is the usual strength parameter

$$\chi = -\frac{V(N-1)}{\varepsilon} \quad (4.18)$$

The determinant characterized by these four angles has a total energy

$$H(\vartheta_1, \vartheta_2, \psi_1, \psi_2) = N\varepsilon (\sin^2\vartheta_2 \sin^2\vartheta_1 - \cos^2\vartheta_1 - \chi \sin^2\vartheta_1 [\cos^2\vartheta_1 (\cos^2\vartheta_2 \cos 2\psi_1 + \sin^2\vartheta_2 \cos 2\psi_2) + \cos^2\vartheta_2 \sin^2\vartheta_2 \sin^2\vartheta_1 \cos 2(\psi_1 - \psi_2)]) \quad (4.19)$$

(see Appendix B4). The TDHF evolution of  $\Phi$  must conserve energy and substitution of the TDHF equations for the four angles into  $\frac{\partial H}{\partial t}$  shows that indeed,

$\frac{\partial H}{\partial t}=0$ . We can also notice that for  $\chi$  positive, an attractive potential between particles in different states, the minimum energy for a given  $\vartheta_1, \vartheta_2$  occurs at  $\psi_1=\psi_2=0$ . Thus,  $H(\vartheta_1, \vartheta_2, 0, 0)$  can be viewed as the potential energy and we can orient ourselves by following the position of the TDHF state,  $\vartheta_1$  and  $\vartheta_2$  on a contour plot of the potential energy surface.

### Section 5: TDRPA for the SU(3) Model

To apply our ideas for a time-dependent generalization of the RPA theory, we must cast our general equations (3.30-3.33) into the specific form suitable for this SU(3) model. Thus, a normally occupied state, previously denoted by  $h$ , will now be denoted by a particle  $n$  in state 1. A normally unoccupied state, previously  $p$ , will now be a particle  $n$  in state  $\sigma=2,3$ . Thus, our particle-hole creation operator  $A_{ph}^+ = a_p^+ a_h$ , now becomes  $K_{n\sigma 1} = \alpha_{n\sigma}^+ \alpha_{n1}$  and its adjoint  $A_{ph}$  now becomes  $K_{n1\sigma}$ . Our particle-hole occupation numbers,  $c_{ph}$ , become  $c_{n\sigma 1}$ , or dropping the irrelevant 1,  $c_{n\sigma}$ . The previous sums over  $p$  and  $h$  now become sums over  $n$  and  $\sigma$ . Thus, our perturbed state becomes

$$|\Psi\rangle = \eta^{1/2} \exp\left(\sum_{n\sigma} c_{n\sigma} \alpha_{n\sigma}^+ \alpha_{n1}\right) |\Phi\rangle \quad (5.1)$$

with the TDHF state

$$|\Phi\rangle = \prod_{n=1}^N \alpha_{n1}^+ |0\rangle \quad (5.2)$$

Of course, for  $|\Psi\rangle$  to also be a collective state, all particles must behave identically and  $c_{n\sigma}$  must be independent of  $n$ , i.e.  $c_{n\sigma} = \frac{1}{N} C_\sigma$  where  $C_\sigma = \sum_n c_{n\sigma}$ . This restriction on the perturbation of  $|\Psi\rangle$  will be used only after the equations have been solved. We now need only a prescription for  $h_{ph}$  in order to write down the TDRPA equations for the SU(3) model.

Before  $h_{ph} = \bar{h}_{ph} = \langle A_{ph} \bar{h} \rangle$ . Now this equation becomes

$$h_{n\sigma 1} = \langle K_{n1\sigma} H \rangle = \langle K_{n1\sigma} \bar{h} \rangle \quad (5.3)$$

Since all particles,  $n$ , are identical in our full Hamiltonian  $H$ , these  $h_{n\sigma 1}$  must also be independent of  $n$  and are written  $h_{\sigma 1}$ . The term  $\langle K_{n1\sigma} (H - \bar{h}) \rangle$  vanishes again just like  $\langle A_{ph} (H - \bar{h}) \rangle$  and the hole-hole and particle-particle components of  $\bar{h}$  must vanish. With these substitutions, the TDRPA equations for  $c_{n\sigma}$  become

$$i\dot{c}_{n\sigma} = \sum_{n'\sigma'} c_{n'\sigma'} (-\delta_{nn'} \delta_{\sigma\sigma'} (\langle H \rangle - \langle \bar{h} \rangle) + \langle K_{n1\sigma} (H - \bar{h}) K_{n'\sigma'1} \rangle) \quad (5.4)$$

$$+ \sum_{n'\sigma'} c_{n'\sigma'} \frac{1}{2} (2 \langle K_{n1\sigma} K_{n'\sigma'1} (H - \bar{h}) \rangle) - \lambda h_{\sigma 1}$$

After the evaluation of these expectation values, as discussed in Appendix B3, we get

$$i\dot{c}_{n\sigma} = \sum_{n'\sigma'} A_{n\sigma;n'\sigma'} c_{n'\sigma'} + \sum_{n'\sigma'} B_{n\sigma;n'\sigma'} c_{n'\sigma'} - \lambda h_{\sigma 1} \quad (5.5)$$

where

$$A_{n\sigma;n'\sigma'} = \delta_{nn'} (h_{\sigma\sigma'} - \delta_{\sigma\sigma'} h_{11}) + \tilde{V}_{\sigma 11\sigma'} (1 - \delta_{nn'}) \quad (5.6)$$

$$B_{n\sigma;n'\sigma'} = \tilde{V}_{\sigma\sigma'11} (1 - \delta_{nn'})$$

and

$$\tilde{V}_{ijkl} = \sum_{ij} 2 V_{ij} A_{jk} A_{jl} A_{im}^* A_{iq}^* \quad (5.7)$$

$$h_{ik} = \sum_i A_{ik} A_{ii}^* + \sum_{ij} 2 V_{ij} (N-1) A_{j1} A_{i1}^* A_{jk} A_{ii}^* = h_{ik}^*$$

Because the  $n$  dependence of the matrices  $A$  and  $B$  is of the simple forms 1 or  $\delta_{nn'}$ , we can rewrite the above equation, using  $C_\sigma$  as

$$i\dot{c}_{n\sigma} = \sum_{\sigma'} (h_{\sigma\sigma'} - \delta_{\sigma\sigma'} h_{11} - \tilde{V}_{\sigma 11\sigma'}) c_{n\sigma'} + \tilde{V}_{\sigma 11\sigma'} C_{\sigma'} \quad (5.8)$$

$$+ \sum_{\sigma'} (-\tilde{V}_{\sigma\sigma'11}) c_{n'\sigma'} + \sum_{\sigma'} \tilde{V}_{\sigma\sigma'11} C_{\sigma'} - \lambda h_{\sigma 1}$$

With the equation in this form, we see that all the coupling between different  $n$ 's occurs in the collective terms  $C_{\sigma'}$  and  $C_{\sigma'}$ .

The constraint  $\sum_{ph} h_{ph}^*(t_F) c_{ph}(t) = 0$  now becomes

$$\sum_{\sigma} h_{1\sigma}(t_F) C_{\sigma}(t) = 0 \quad (5.9)$$

Just as in the general case, we solve for  $\lambda$  by

$$\sum_{\sigma} h_{1\sigma} \dot{C}_{\sigma} = 0 \quad (5.10)$$

We find the expression for  $\dot{C}_{\sigma}$  by adding the equations for each  $n$ . Thus, we get

$$i\dot{C}_{\sigma} = \sum_{\sigma'} A_{\sigma\sigma'} C_{\sigma'} + \sum_{\sigma'} B_{\sigma\sigma'} C_{\sigma'} - \lambda N h_{\sigma 1} \quad (5.11)$$

with

$$\begin{aligned} A_{\sigma\sigma'} &= h_{\sigma\sigma'} - \delta_{\sigma\sigma'} h_{11} + \tilde{V}_{\sigma 11\sigma'}(N-1) = A_{\sigma'\sigma}^* \\ \text{and} \quad B_{\sigma\sigma'} &= \tilde{V}_{\sigma\sigma'11}(N-1) = B_{\sigma'\sigma} \end{aligned} \quad (5.12)$$

The matrices A and B have the usual RPA symmetries,  $A=A^+$  and  $B=B^{Tr}$ . Using the constraint from Eq. (5.10) to find  $\lambda$  in Eq. (5.11) gives

$$\lambda = \frac{1}{N \sum_{\sigma} h_{1\sigma} h_{\sigma 1}} \sum_{\sigma\sigma'} (h_{1\sigma} A_{\sigma\sigma'} C_{\sigma'} + h_{1\sigma} B_{\sigma\sigma'} C_{\sigma'}^*) \quad (5.13)$$

Now to solve the TDRPA equations, we first solve the collective equation for  $\dot{C}_{\sigma}$ .

$$i\dot{C}_{\sigma} = \sum_{\sigma'\sigma''} \left[ \delta_{\sigma\sigma''} - \frac{h_{\sigma 1} h_{1\sigma''}}{h^2} \right] [A_{\sigma'\sigma''} C_{\sigma'} + B_{\sigma'\sigma''} C_{\sigma'}^*] \quad (5.14)$$

where  $h^2 \equiv \sum_{\sigma} h_{1\sigma} h_{\sigma 1}$ . Because there are only two values for  $\sigma$ , the constraint

$\sum_{\sigma} h_{1\sigma} C_{\sigma}$  can be used to solve for

$$C_3 = -\frac{h_{12}}{h_{13}} C_2 \quad (5.15)$$

This fortunate circumstance occurs because the one-body HF Hamiltonian couples the hole state to one linear combination of our two particle states. Excitation of the other linear combination is the single RPA mode transverse to the TDHF path whose stability we are testing. Thus, the equation for  $\sigma=2$  is

$$i\dot{C}_2 = AC_2 + BC_2^* \quad (5.16)$$

where

$$A = \frac{h_{31} h_{13}}{h^2} A_{22} - \frac{h_{21} h_{13}}{h^2} A_{32} - \frac{h_{12} h_{31}}{h^2} A_{23} + \frac{h_{21} h_{12}}{h^2} A_{33} \quad (5.17)$$

(which is real) and

$$B = \frac{h_{31} h_{13}}{h^2} B_{22} - \frac{h_{21} h_{13}}{h^2} B_{32} - \frac{h_{21} h_{13}}{h^2} B_{23} + \frac{h_{21}^2 h_{13}}{h_{31} h^2} B_{33} \quad (5.18)$$

(which is complex).

We now look for periodic solutions

$$C_2 = X_2 e^{-i\omega t} + Y_2^* e^{+i\omega t} \quad (5.19)$$

with  $\omega$  real. When we separately equate terms with  $e^{-i\omega t}$  and terms with  $e^{+i\omega t}$ ,

we get

$$\omega \begin{bmatrix} X_2 \\ Y_2 \end{bmatrix} = \begin{bmatrix} A & B \\ -B^* & -A^* \end{bmatrix} \begin{bmatrix} X_2 \\ Y_2 \end{bmatrix} \quad (5.20)$$

Therefore, our collective mode has a frequency  $\omega$  given by setting

$$\begin{vmatrix} A-\omega & B \\ -B^* & -A^*-\omega \end{vmatrix} = 0 \quad (5.21)$$

Notice that a real frequency  $\omega$  is only possible for A real, as it is in this case, so

$$\omega^2 = A^2 - |B|^2 \quad (5.22)$$

Of course, we could just as well have substituted for  $C_2$  in the equation for  $\dot{C}_3$ .

This would give

$$i\dot{C}_3 = \tilde{A}C_3 + \tilde{B}C_3^* \quad (5.23)$$

with

$$\tilde{A} = A \quad \text{and} \quad \tilde{B} = \frac{h_{12}h_{31}}{h_{21}h_{13}} B \quad (5.24)$$

Thus, we would get the same value for  $\omega^2$  verifying that we have found a normal mode. This is the one collective mode normal to the TDHF path.

Of course, the matrix equation above also has the trivial solution,  $X_2 = Y_2 = 0$  meaning  $C_2 = C_3 = 0$ . This also means that  $\lambda = 0$  and the constraint  $\sum_{\sigma} h_{1\sigma} C_{\sigma} = 0$  becomes trivial. Now we can look back to our equations for the individual  $\dot{c}_{n\sigma}$  and try noncollective perturbations for which  $c_{n\sigma}$  is dependent on  $n$  and  $\sum_n c_{n\sigma} = 0$  with  $c_{n\sigma} \neq 0$ . With  $C_{\sigma} = 0$  our equations for  $\dot{c}_{n\sigma}$  become uncoupled, i.e. single-particle like. The equations are

$$i\dot{c}_{n\sigma} = \sum_{\sigma'} A'_{\sigma\sigma'} c_{n\sigma'} + \sum_{\sigma'} B'_{\sigma\sigma'} c_{n\sigma'}^* \quad (5.25)$$

with  $A'$  and  $B'$  independent of  $n$ ;

$$\begin{aligned} A'_{\sigma\sigma'} &= h_{\sigma\sigma'} - \delta_{\sigma\sigma'} h_{11} - \tilde{V}_{\sigma 11 \sigma'} = A'_{\sigma'\sigma} \\ B'_{\sigma\sigma'} &= -\tilde{V}_{\sigma\sigma' 11} = B'_{\sigma'\sigma} \end{aligned} \quad (5.26)$$

Making the periodic assumption and separating terms as before gives modes with frequencies  $\omega$  given by

$$\omega^2 = D \pm \sqrt{D^2 - E} \quad (5.27)$$

where

$$D = \frac{1}{2}(A'_{22}{}^2 + A'_{33}{}^2 + 2A'_{23}A'_{23}{}^* - (B'_{22}B'_{22}{}^* + B'_{33}B'_{33}{}^* + 2B'_{23}B'_{23}{}^*)) \quad (5.28)$$

and

$$E = \det \begin{vmatrix} A' & B' \\ B'{}^* & A'{}^* \end{vmatrix} \quad (5.29)$$

Thus, we get two values for  $\omega^2$  for the two normal modes of noncollective oscillations. However, the exact Hamiltonian H, which treats all particles identically, would not mix these states with any collective state. This means that this instability will not be apparent in a comparison of TDHF with the exact evolution of a collective state. This instability will instead cause doubts about the appropriateness of a collective state description of the many-body wavefunction.

### Section 6: Exact Solution for the SU(3) Model

We choose a two-body Hamiltonian which is exactly soluble (LI 70)

$$H = \sum_i \epsilon_i G_{ii} + \sum_{ij} V_{ij} G_{ji}^2 \quad (6.1)$$

where

$$\begin{aligned} V_{ij} &= V_{ji} \quad , \quad V_{ii} = 0 \quad , \\ G_{ij} &= \sum_n a_{ni}^\dagger a_{nj} \quad , \end{aligned} \quad (6.2)$$

$a_{ni}^\dagger$  creates a particle  $n$  in state  $i$ , and  $a_{ni}$  annihilates a particle  $n$  from state  $i$ .

Applying the usual fermion anti-commutation rules, we get

$$[G_{ij}, G_{kj}] = \delta_{ij} G_{kj} - \delta_{jk} G_{ij} \quad (6.3)$$

and the nine operators  $G_{ij}$  are generators for U(3). Remembering number conservation,  $\sum_i G_{ii} = N$ , this becomes SU(3).

In order to find the eigenstates and eigenvalues to solve the problem exactly, we need to find a complete set of basis states. Group theoretic methods have been published (LI 70) which derive this basis set, but for our purposes physical intuition will suffice. First, we must remember that we are only interested in collective states, that is, states with all particles,  $n$ , behaving the same. Therefore, we need not worry about each particle and its mean occupation of each level, but only the mean number of particles in each level. This is analogous to Krieger's (KRI 77) using only states with  $J = \frac{1}{2}N$  like the state with  $N$  in lowest level. In our case,  $H$  will not mix a collective state like this state with any noncollective states since  $H$  treats all particles alike.

Thus, a natural basis can be written  $|pq\rangle$  meaning  $p$  particles in the second level,  $q$  in the third level and, of course,  $N-p-q$  in the first level. To calculate the number of basis states  $|pq\rangle$  for a given  $N$ , we can pick any number from 0 to  $N$  for  $p$  and then pick any number from 0 to  $N-p$  for  $q$ . The number in the first level is then determined,  $N-p-q$ . Thus, for  $q$  we have  $N-p+1$  choices

after  $p$  is chosen, with  $N+1$  choices for  $p$ . Thus, the number of states  $NS$  is

$$NS = \sum_{p=0}^N (N+1-p) = \frac{(N+1)(N+2)}{2} , \quad (6.4)$$

that is, the number of choices for  $p$  times the average number of choices for  $q$ ,  $(\frac{N+1}{2}+1)$ .

We define

$$|00\rangle \equiv \prod_n a_n^+ |0\rangle , \quad (6.5)$$

so that  $|00\rangle$  is all  $N$  particles in the lowest level. We can write the general basis state

$$|pq\rangle = c(p,q) G_{21}^p G_{31}^q |00\rangle \quad (6.6)$$

with  $c(p,q)$  a normalizing constant since  $G_{ij}$  is the collective operator to move a particle from state  $j$  to state  $i$ . To calculate  $c(p,q)$  or any of the other expectation values we will need ( $\langle G_{ij} \rangle$  and  $\langle H \rangle$ ), we need to learn how to manipulate these  $G_{ij}$ 's to arbitrary powers. (Note that since  $[G_{21}, G_{31}] = 0$  the  $G_{21}$ 's in Eq. (6.6) can all be grouped together as can the  $G_{31}$ 's.) For  $q=0$  these states  $|p0\rangle$  are identical to the basis states of (KRI 77) since  $G_{21}$  is his  $J_+$ .

We know that  $G_{ij}|00\rangle = 0$  unless  $j=1$  and  $G_{11}|00\rangle = N|00\rangle$ . Therefore, to evaluate  $G_{ij}|pq\rangle$ , we can commute the  $G_{ij}$  through  $G_{21}$   $p$  times, and through  $G_{31}$   $q$  times, collecting  $G_{21}$ 's and  $G_{31}$ 's to the left and moving the other  $G_{ij}$ 's toward the right. For instance, to verify the meaning of the states above, we need to show  $G_{22}|pq\rangle = p|pq\rangle$  and  $G_{33}|pq\rangle = q|qp\rangle$ . From the commutation relation derived earlier we get

$$[G_{11}, G_{21}] = -G_{21} \quad (6.7)$$

and therefore

$$[G_{11}, G_{21}^p] = -pG_{21}^p . \quad (6.8)$$

Similarly,

$$[G_{11}, G_{31}^q] = -q G_{31}^q \quad ; \quad (6.9)$$

so

$$G_{11} |pq\rangle = (N - p - q) |pq\rangle \quad (6.10)$$

For  $G_{22}$  we get

$$[G_{22}, G_{21}] = G_{21} \quad \text{so} \quad [G_{22}, G_{21}^p] = p G_{21}^p \quad (6.11)$$

and

$$[G_{22}, G_{31}] = 0 \quad \text{so} \quad [G_{22}, G_{31}^q] = 0 \quad (6.12)$$

Therefore,

$$G_{22} |pq\rangle = p |pq\rangle \quad (6.13)$$

Similar relations show that

$$\begin{aligned} [G_{33}, G_{21}^p] &= 0 \\ [G_{33}, G_{31}^q] &= q G_{31}^q \end{aligned} \quad (6.14)$$

and

$$G_{33} |pq\rangle = q |pq\rangle \quad (6.15)$$

Thus, we have chosen our basis to be eigenstates of these number operators  $G_{ii}$ . Since  $G_{ii} |pq\rangle$  was proportional to  $|pq\rangle$  we didn't need to evaluate  $c(p, q)$  yet. However, for the other elements of  $G_{ij}$ , we need to know  $c(p, q)$ ; for instance

$$G_{21} |pq\rangle = \frac{c(p, q)}{c(p+1, q)} |p+1, q\rangle \quad (6.16)$$

Before finishing these calculations, we must evaluate all the other  $G_{ij} |pq\rangle$ . By a similar repeated application of the commutation rule in Eq. (6.3), we calculate the following commutators:

$$\begin{aligned} [G_{11}, G_{21}^p] &= -p G_{21}^p & [G_{11}, G_{31}^q] &= -q G_{31}^q & (6.17) \\ [G_{22}, G_{21}^p] &= p G_{21}^p & [G_{22}, G_{31}^q] &= 0 \\ [G_{33}, G_{21}^p] &= 0 & [G_{33}, G_{31}^q] &= q G_{31}^q \\ [G_{12}, G_{21}^p] &= p G_{21}^{p-1} (G_{11} - G_{22}) - p(p-1) G_{21}^{p-1} \\ [G_{13}, G_{31}^q] &= q G_{31}^{q-1} (G_{11} - G_{33}) - q(q-1) G_{31}^{q-1} \\ [G_{13}, G_{21}^p] &= -p G_{21}^{p-1} G_{23} & [G_{12}, G_{31}^q] &= -q G_{31}^{q-1} G_{32} \\ [G_{32}, G_{21}^p] &= p G_{21}^{p-1} G_{31} & [G_{23}, G_{31}^q] &= q G_{21} G_{31}^{q-1} \end{aligned}$$

$$\begin{aligned} [G_{21}, G_{21}^{\rho}] &= 0 & [G_{31}, G_{31}^{\rho}] &= 0 \\ [G_{31}, G_{21}^{\rho}] &= 0 & [G_{21}, G_{31}^{\rho}] &= 0 \\ [G_{23}, G_{21}^{\rho}] &= 0 & [G_{32}, G_{31}^{\rho}] &= 0 \end{aligned}$$

These relations then give net results for the action on the states  $|pq\rangle$  of

$$\begin{aligned} G_{11}|pq\rangle &= (N-p-q)|pq\rangle & (6.18) \\ G_{22}|pq\rangle &= p|pq\rangle \\ G_{33}|pq\rangle &= q|pq\rangle \\ G_{12}|pq\rangle &= \frac{c(p,q)}{c(p-1,q)} p(N-q-(p-1))|p-1,q\rangle \\ G_{21}|pq\rangle &= \frac{c(p,q)}{c(p+1,q)} |p+1,q\rangle \\ G_{13}|pq\rangle &= \frac{c(p,q)}{c(p,q-1)} q(N-(q-1)-p)|p,q-1\rangle \\ G_{31}|pq\rangle &= \frac{c(p,q)}{c(p,q+1)} |p,q+1\rangle \\ G_{23}|pq\rangle &= \frac{c(p,q)}{c(p+1,q-1)} q|p+1,q-1\rangle \\ G_{32}|pq\rangle &= \frac{c(p,q)}{c(p-1,q+1)} p|p-1,q+1\rangle \end{aligned}$$

We can calculate  $c(p,q)$  by a repeated application of these rules to evaluate  $\langle 00|G_{13}^{\rho}G_{12}^{\rho}G_{21}^{\rho}G_{31}^{\rho}|00\rangle$ . Thus

$$G_{12}^{\rho}G_{21}^{\rho}G_{31}^{\rho}|00\rangle = \frac{p!(N-q)!}{(N-p-q)!} G_{31}^{\rho}|00\rangle \quad (6.19)$$

A similar relation for  $G_{13}^{\rho}$  resulting in a factor  $\frac{q!N!}{(N-q)!}$  gives

$$\langle 00|G_{13}^{\rho}G_{12}^{\rho}G_{21}^{\rho}G_{31}^{\rho}|00\rangle = \frac{N!p!q!}{(N-p-q)!} \quad (6.20)$$

Substituting into the previous Eqs. (6.18), the net result is

$$\begin{aligned} G_{12}|pq\rangle &= \sqrt{p(N-q-p+1)}|p-1,q\rangle & (6.21) \\ G_{13}|pq\rangle &= \sqrt{q(N-q-p+1)}|p,q-1\rangle \\ G_{21}|pq\rangle &= \sqrt{(p+1)(N-p-q)}|p+1,q\rangle \\ G_{31}|pq\rangle &= \sqrt{(q+1)(N-p-q)}|p,q+1\rangle \\ G_{23}|pq\rangle &= \sqrt{(p+1)q}|p+1,q-1\rangle \\ G_{32}|pq\rangle &= \sqrt{(q+1)p}|p-1,q+1\rangle \end{aligned}$$

Now we can immediately write down the one-body density matrix elements

$$\langle p'q'|\rho_{\psi}|pq\rangle = \frac{1}{N}\langle p'q'|G_{\psi}|pq\rangle \quad (6.22)$$

for each  $ij$  by writing the above factors and appropriate delta functions. By setting  $q=0$  and  $p=1/2N+m$ ,  $G_{21}$  agrees with (KRI 77)'s  $J_+$  and  $G_{22}$  agrees with his  $\sum_p a_p^\dagger a_p$ , although there is a misprint in his Eq. 2.12. We must look to his Eq. 2.14 to see that Eq. 2.12 should be  $(\frac{1}{2} + \frac{N}{m})\delta_{mm}$ .

Now we can calculate expectation values of  $H$  and thus, eigenvalues and eigenstates of  $H$ . We need  $G_{ij}^2$  acting on  $|pq\rangle$ ; that is, two applications of the rules in Eq. (6.21). Thus, with  $\varepsilon_1=-\varepsilon$ ,  $\varepsilon_2=0$ ,  $\varepsilon_3=+\varepsilon$  and  $V_{ij}=\frac{V}{2}(1-\delta_{ij})$ , the result is

$$\langle p'q' | H | pq \rangle = \varepsilon(-N+p+2q)\delta_{pp'}\delta_{qq'} + \frac{V}{2}A \quad (6.23)$$

where

$$\begin{aligned} A = & \sqrt{p(p-1)(N-p-q+1)(N-p-q+2)}\delta_{p-2,p'}\delta_{qq'} \\ & + \sqrt{(p+1)(p+2)(N-p-q)(N-p-q-1)}\delta_{p+2,p'}\delta_{qq'} \\ & + \sqrt{q(q-1)(N-p-q+1)(N-p-q+2)}\delta_{pp'}\delta_{q-2,q'} \\ & + \sqrt{(q+1)(q+2)(N-p-q)(N-p-q-1)}\delta_{pp'}\delta_{q+2,q'} \\ & + \sqrt{(p+1)(p+2)q(q-1)}\delta_{p+2,p'}\delta_{q-2,q'} \\ & + \sqrt{(q+1)(q+2)p(p-1)}\delta_{p-2,p'}\delta_{q+2,q'} \end{aligned} \quad (6.24)$$

$H$  is hermitian, in fact, with the choice made for  $V_{ij}$  and phase of  $c(p,q)$ , it is real and symmetric. To make this more apparent, we can rewrite some of the terms, for instance  $p+2=p'$  as  $p=p'-2$ . Now switching  $p$  with  $p'$  and  $q$  with  $q'$  obviously leaves  $A$  unchanged.

For any given number of particles  $N$  we can set up the complete basis states, write down the matrix elements of  $H$  and then diagonalize  $H$  to find its eigenvalues (real) and its eigenvectors (real and orthogonal). For even a moderately large  $N$  the dimensions of  $H$  will be very large (greater than  $\frac{N^4}{4}$ ). However,  $H$  connects only states with  $\Delta p=0, \pm 2$  and  $\Delta q=0, \pm 2$  which makes the problem easier. First, we group states with  $p, q$  even;  $p$  even,  $q$  odd;  $p$  odd,  $q$  even; and  $p, q$  odd. This means that  $\langle H \rangle$  becomes block diagonal containing 4

blocks which can be diagonalized separately, each approximately 1/16 the size of the full  $\langle H \rangle$ . Regardless of the size of  $N$ , there can be no more than 7 non-zero elements in any row or column - all quite close to the diagonal for many reasonable schemes of ordering the states. For this kind of sparse matrix, the standard routines for eigenvalues and eigenvectors of a matrix work very well and very quickly.

Eigenvalues are labeled  $e_\lambda$  and eigenvectors  $|\lambda\rangle$ . An arbitrary state can be expanded

$$|\psi(0)\rangle = \sum_{\lambda} |\lambda\rangle \langle \lambda | \psi(0)\rangle \quad (6.25)$$

and its time dependence is straightforward.

$$|\psi(t)\rangle = \sum_{\lambda} |\lambda\rangle \exp(-ie_\lambda t) \langle \lambda | \psi(0)\rangle \quad (6.26)$$

Now for any given wavefunction, we can follow its evolution exactly.

## Section 7: How to Compare Exact and TDHF Calculations

Our purpose is, of course, to compare with the Hartree-Fock approximation. At this point, we can compare our ground state energy, the smallest  $e_\lambda$ , with the energy of the Hartree-Fock state (and perhaps higher states to periodic TDHF solutions if these can be found), but we want to compare the evolution of an arbitrary TDHF state to its exact evolution. To do this, we must expand an arbitrary TDHF state in terms of these eigenvectors and, secondly, we must identify the 4 parameters characterizing a TDHF state from an arbitrary state.

Although the eventual goal is to expand a TDHF state  $|\psi\rangle$  in terms of the eigenstates  $|\lambda\rangle$ ; these are not known yet and are different for each  $N, V$  different. Therefore, we expand  $|\psi\rangle$  in our basis states  $|pq\rangle$ ;

$$|\psi\rangle = \sum_{pq} |pq\rangle \langle pq | \psi \rangle . \quad (7.1)$$

Our general TDHF state was defined as

$$|\psi\rangle = \prod \alpha_{n1}^\dagger |0\rangle , \quad (7.2)$$

a general determinantal state, where the states created by  $\alpha$  are linear combinations of the three levels, an obvious set of basis states. Thus, using the definitions of  $\alpha$  and  $|pq\rangle$ , we get

$$\langle pq | \psi \rangle = \langle 0 | \prod_n \alpha_{n1} G_{13}^q G_{12}^p \prod_{n' i=1}^3 A_{1i}^\dagger \alpha_{n'i} | 0 \rangle c(p, q) . \quad (7.3)$$

We need to expand  $\prod_{n' i} A_{1i}^\dagger \alpha_{n'i}$ . Thus, we get a general term of the structure

$$(A_{11}^\dagger)^{N-n-m} (A_{12}^\dagger)^n (A_{13}^\dagger)^m \prod_{(N-n-m)} \alpha_{n'1}^\dagger \prod_{(n)} \alpha_{n'2}^\dagger \prod_{(m)} \alpha_{n'3}^\dagger , \quad (7.4)$$

where the number in parantheses under the product is the number of  $n'$ 's in the product.

The different choices of particles for each level give terms of identical structure. First, we need to choose from  $N$  particles  $N-n-m$  to be in the first level; this gives the standard binomial coefficient  $\frac{N!}{(N-n-m)!(n+m)!}$ . Then

with  $n+m$  particles left, we need to choose  $n$  for the second level -  $\frac{(n+m)!}{n!m!}$  choices. The net result is then

$$\langle pq | \psi \rangle = \sum_{\substack{n,m \\ n+m < N}} (A_{11}^\dagger)^{N-n-m} (A_{12}^\dagger)^n (A_{13}^\dagger)^m \frac{N!}{(N-n-m)!n!m!} I \quad (7.5)$$

where

$$I = \langle 0 | \prod_n a_{n1} G_{13}^q G_{12}^p \prod_{(N-n-m)} a_{n'1}^\dagger \prod_{(n)} a_{n'2}^\dagger \prod_{(m)} a_{n'3}^\dagger | 0 \rangle \quad (7.6)$$

$G_{12} = \sum_{n''} a_{n''2}^\dagger a_{n''2}$  commutes with  $a_{n'1}^\dagger$  and acts on  $a_{n'2}^\dagger$ . Terms with  $n'' \neq n'$  give zero since  $a_{n''2}^\dagger | 0 \rangle = 0$ . Terms  $n'' = n'$  leave  $a_{n'1}^\dagger$ . Since there are  $n$  factors of  $a_{n'2}^\dagger$ , there will be  $n$  terms left, each with one less  $G_{12}$ , one less  $a_{n'2}^\dagger$  and one more  $a_{n'1}^\dagger$ . Multiplying all the  $G_{12}$  through gives

$$\delta_{pn} n! \langle 0 | \prod_n a_{n1} G_{13}^q \prod_{(N-m)} a_{n'1}^\dagger \prod_{(m)} a_{n'3}^\dagger | 0 \rangle \quad (7.7)$$

The  $G_{13}$ 's behave similar to the  $G_{12}$ 's leaving

$$I = \delta_{pn} n! \delta_{qm} m! \quad (7.8)$$

The net result for  $\langle pq | \psi \rangle$  is

$$\langle pq | \psi \rangle = \left( \frac{N!}{(N-p-q)!p!q!} \right)^{\frac{1}{2}} (A_{11}^\dagger)^{N-p-q} (A_{21}^\dagger)^p (A_{31}^\dagger)^q \quad (7.9)$$

This can be checked quite simply to be sure  $\langle \psi | pq \rangle \langle pq | \psi \rangle = 1$ . Note also that if we constrain  $q=0$  in Eq. (7.9), the result agrees with Krieger's results for SU(2) (KRI 77).

Now that we can expand any TDHF state in terms of our basis states for the exact solution, we can evolve any TDHF state exactly. We need, however, to compare this exact solution with the TDHF evolution. Since the TDHF states form only a restricted set of many-body wavefunctions, namely determinantal wavefunctions, there will be no way to uniquely match wavefunctions in general. In particular the wavefunctions themselves can not be matched since for a TDHF state  $\psi(t)$

$$\langle pq | \psi(t) \rangle = \sum_{\lambda p'q'} \langle pq | \lambda \rangle \exp(-ie_{\lambda}t) \langle \lambda | p'q' \rangle \langle p'q' | \psi(0) \rangle . \quad (7.10)$$

The TDHF state (or its expansion parameters) depends only on the 4 parameters used to specify  $A_{n1}$ . The one-body density matrix  $\rho_{ij} = \frac{1}{N} \langle G_{ij} \rangle$  for the TDHF state also depends only on these 4 parameters  $\rho_{ij} = A_{i1} A_{j1}^*$ . We use this one-body density matrix to compare to the exact evolution. Of course, the exact  $\langle G_{ij} \rangle$  depends on more than 4 parameters. A general 3 x 3 complex matrix would require 18 parameters, an hermitian matrix half of this or 9 parameters, and since the  $\text{Tr}\rho=1$ , we are left with 8 parameters for  $\langle G_{ij} \rangle$ . This number is reduced to 4 for the TDHF state by the condition that for determinantal wavefunctions  $\rho^2 = \rho$ .

Thus, there is ambiguity in determining the relevant 4 parameters for comparison. We also want to know  $\text{Tr}(\rho^2 - \rho)$  for the exact state since the deviation from the TDHF value of 0 gives us an idea of the deviation of the exact wavefunction from a determinantal wavefunction and an idea of the ambiguity involved in matching  $\rho$  to determine the 4 parameters.

Although the choice of which elements to match may vary in specific cases, generally, the most physically relevant property of these states is the mean occupation of the various levels. Therefore, we want to use the diagonal elements  $\rho_{ii}$  to calculate the magnitudes of the  $A_{n1}$  and thus, the parameters  $\vartheta_1$  and  $\vartheta_2$ . (We can also check on some of the numerics involved in the calculation by checking  $\text{Tr}\rho=1$ .) This means that in general, the magnitude of the off-diagonal elements will not match. To compare the phases relative to the first level, we use  $\rho_{12}$  and  $\rho_{13}$  to calculate the phases  $\psi_1$  and  $\psi_2$ , but now the phase of  $\rho_{23}$  will not match  $\psi_1 - \psi_2$ . Therefore, we define

$$\begin{aligned} \vartheta_1(\text{exact}) &= \cos^{-1}(\sqrt{\langle G_{11} \rangle / N}) \\ \vartheta_2(\text{exact}) &= \tan^{-1}(\sqrt{\langle G_{33} \rangle / \langle G_{22} \rangle}) \\ \psi_1(\text{exact}) &= \frac{1}{2} \cos^{-1}(\text{Re}[\langle G_{12} \rangle / \langle G_{21} \rangle]) \times \text{Sign}(\text{Im}[\langle G_{12} \rangle]) \end{aligned} \quad (7.11)$$

$$\psi_2(\text{exact}) = \frac{1}{2} \cos^{-1}(\text{Re}[\langle G_{13} \rangle / \langle G_{31} \rangle]) \times \text{Sign}(\text{Im}[\langle G_{13} \rangle]) .$$

We also check that

$$(\langle G_{11} \rangle + \langle G_{22} \rangle + \langle G_{33} \rangle) \frac{1}{N} = 1 . \quad (7.12)$$

Since there are many exact states which result in these same 4 parameters, the prescription for finding  $\langle pq | \psi \rangle$  can be thought of as finding the unique exact state which gives these 4 parameters and the auxiliary condition  $\rho^2 - \rho = 0$ . (This state must be unique since we find a unique expansion.)

We also find this prescription useful to compare our lowest energy eigenvector to the Hartree-Fock state. Since  $H$  mixes states with  $\Delta p, \Delta q = 0, \pm 2$  and  $G$  mixes states with  $\Delta p, \Delta q = 0, \pm 1$  only the diagonal elements  $\langle G_{ii} \rangle$  will be nonzero for any eigenvector. Thus, the phases of the off-diagonal elements are zero just like static HF solutions. We compare  $\psi_1$  and  $\psi_2$  by the prescription in Eq. (7.11) and also compare  $\text{Tr}(\rho^2 - \rho)$ .  $\text{Tr}(\rho^2 - \rho)(\text{exact}) = \rho_{11}^2 - \rho_{22}^2 - \rho_{33}^2 - 1$  since  $\rho$  is diagonal.

### Section 8: TDRPA Results

For orientation, contours of the energy surface (Eq. (4.19) with  $\psi_1=\psi_2=0$ ) are plotted in Figures 8-13 for values of  $\chi = .5, 2.5, 5, 10, 20$  and  $100$  (attractive forces). The surface is relatively flat and featureless for  $\chi=.5$  but as  $\chi$  increases, it develops rather deep valleys and quite a deep minimum. Static HF calculations can be performed analytically (HOL 74), yielding the position and depth of the minimum, as well as saddle points and maxima. For  $\chi \leq 1$ , the minimum energy lies along the line  $\vartheta_1=0$  (all particles in the lowest level) and has a value  $E/n\varepsilon=1$ . When  $\chi$  increases past 1, the strength of the attraction between different levels becomes strong enough to decrease the energy by beginning to populate the second level. The position and energy of the minimum are then given by

$$\begin{aligned} \vartheta_1 &= \frac{1}{2} \cos^{-1} \left( \frac{1}{\chi} \right) ; \quad \vartheta_2 = 0 ; \\ E/n\varepsilon &= -\frac{1}{4} \left( \chi + \frac{1}{\chi} \right) - \frac{1}{2} . \end{aligned} \tag{8.1}$$

At  $\chi=3$ , the potential is strong enough to begin populating the third level also, and the minimum moves off the  $\vartheta_2$  axis. Its position and energy are then given by

$$\begin{aligned} \vartheta_1 &= \sin^{-1} \left( \left[ \frac{2\chi-3}{3\chi} \right]^{1/2} \right) ; \quad \vartheta_2 = \frac{1}{2} \cos^{-1} \left( \frac{3}{2\chi-3} \right) ; \\ E/n\varepsilon &= -\left( \frac{\chi}{3} + \frac{1}{\chi} \right) . \end{aligned} \tag{8.2}$$

The TDHF calculations can be checked by calculating the evolution near this minimum in energy. The solutions should then be approximately equal to those of the ordinary RPA calculations, which can be solved analytically. Since the time-dependent generalization agrees with ordinary RPA theory for static HF solutions, these positions can be substituted into Eq. (5.22). The solution involves only straightforward but rather messy algebra and trigonometry. We are most interested in  $\chi \geq 3$  where the energy surface has a more interesting

topology. In this case, the RPA frequencies are

$$\left(\frac{\omega}{\varepsilon}\right)^2 = 4\left(\frac{\chi^2 - 3}{3} \pm \left[\frac{\chi^2 + 3}{3}\right]^{1/2}\right) . \quad (8.3)$$

Therefore, we expect an average period

$$\varepsilon T = \frac{4\pi\varepsilon}{(\omega_+ + \omega_-)} , \quad (8.4)$$

and beats in the amplitude with a period

$$\varepsilon T_b = \frac{2\pi\varepsilon}{(\omega_+ - \omega_-)} . \quad (8.5)$$

Table 4 shows the two periods and the beat period for several values of  $\chi$ . Figure 14 shows that the TDHF solutions do oscillate with these periods.

Table 4				
Period	$\chi=5$	$\chi=10$	$\chi=20$	$\chi=100$
$\varepsilon T_+$	0.975	0.508	0.262	0.054
$\varepsilon T_-$	1.519	0.611	0.286	0.055
$\varepsilon T_b$	2.721	3.035	3.126	3.142

Figures 15-18 show results for the TDRPA frequencies for several paths to compare with our expectations from the contours of the energy surface. Beginning with a case of extreme topography,  $\chi=100$ , the first example is not plotted in this way although the details of the motion are shown in Figure 26. For this path near the minimum,  $\omega^2$  is positive and large everywhere. The path is a small ellipse and  $\left(\frac{\omega}{\varepsilon}\right)^2$  varies only between  $+1.32 \times 10^4$  and  $+1.42 \times 10^4$ . Figure 15 shows a TDHF path moving down a valley. The frequency is initially negative because the motion is from the side of the valley down into it. However, once the path begins moving along the valley, the frequency becomes positive and large, and it stays positive and large.

Figure 16 shows a path which is unstable almost everywhere. At this higher

energy, the path moves closer to the maxima where the peaks flatten and the curvature of the surface is negative. The few points where the frequency is positive, mostly on the inner loop, cross the ridge closer to the minimum where the curvature of the top of the ridge is positive. Thus, there can be a ridge effect (if the ridge has a saddle shape) since the direction in which stability is being tested changes from across the ridge to along the ridge.

The next example, Figure 17, shows a path with more nearly equal stable and unstable regions. The central right region in the vicinity of the minimum, where the curvature of  $V$  is positive, has positive frequencies and should be stable. The upper right region shows another ridge effect. The path is unstable while moving along either side of the ridge, but appears stable briefly as the top of the ridge is crossed and the direction of the stability test crosses along the top of the ridge. The lower left region shows interesting behavior where two paths cross the initial rightward path. The inner loop, lying closer to the minimum, is stable but the outer loop isn't. The initial rightward path tests stability in a different direction and is unstable. Therefore, in the vicinity of the inner loop, the surface must have a saddle shape.

These features persist at other values of  $\chi$  with less drastic topology as seen in Figure 18 for  $\chi=5$ . Here, the path is unstable while moving back and forth across the valley (at either end), but is stable while moving along the valley. Just as for ordinary RPA theory, the values of  $\omega^2$  scale like  $\chi^2$  - on the order of  $10^4$  for  $\chi=100$  and 25 for  $\chi=5$ .

Therefore, the value of  $\omega^2$  does, indeed, describe the local curvature of the potential energy surface in the direction normal to the TDHF path and can thereby identify relative minima, ridges, valleys and saddle shapes. In this case, we could easily draw contours of the energy surface; however, in more realistic cases there are far too many parameters to allow the construction of this kind

of energy surface, so the smallest values of  $\omega^2$  could prove useful.

We next compare these TDRPA calculations with exact calculations, first checking the HF results. Figure 19 shows that the energies of the exact ground states agree quite well for  $N \geq 15$ . (Lines are to guide the eye since  $N$  is an integer.) However, comparing the positions and  $\text{Tr}(\rho^2 - \rho)$  for these states gives poorer agreement. The trace, shown in Figure 20, shows that none of these states looks much like HF (independent particle) states which have  $\text{Tr}=0$ . However, the important quantity for comparison is the position  $\vartheta_1, \vartheta_2$ . This comparison is made in Figure 21 for  $\chi = 5, 10, 20$ . For  $\chi=5$ , agreement is quite poor. As  $\chi$  increases, the agreement gets much better and also seems to agree for smaller values of  $N$ . For  $\chi=100$ , both  $N=10$  and  $15$  give good agreement with the position of the ground state.

This is a problem because the method of comparing the evolution of TDHF and exact states is to compare these angular positions. Indeed, for calculations with small  $\chi$ , the exact solution doesn't look like TDHF regardless of the value of  $\omega^2$ . Thus, in Figure 22, for  $\chi=5$ , the direction of motion seems to be right when  $\omega^2 > 0$  and wrong when  $\omega^2 < 0$ , but neither of the exact results agrees well with the TDHF results. (Notice that the TDHF path moves so slowly relative to the exact, that it is drawn for twice as long a time so that it can be seen more clearly.)

The exact solutions, of course, depend on the number of particles  $N$  and TDHF is accurate only for large  $N$ . Therefore, the agreement could be poor because TDHF is a poor approximation to the exact behavior or because  $N$  is too small to give this limiting behavior for large  $N$ . For the  $SU(2)$  case (KRI 77),  $N=40$  particles could be solved exactly since the number of basis states is proportional to  $N$ , and the agreement was very good. In our case, with an extra level populated, we would expect to need  $N > 40$  to be sure of a similar comparison. However, since the number of basis states is proportional to  $N^2$ , we

simply can't run  $N > 15$  for any length of time.

From the change in the exact results from  $N=10$  to  $N=15$ , the stability parameter seems to work. That is, a prediction of stability results in exact solutions which approach the TDHF solution as  $N$  increases while a prediction of instability seems to result in an approach to something different than the TDHF result. The real test, however, comes from increasing  $\chi$  so that the limiting behavior of the exact solutions for large  $N$  can be reached at a smaller value of  $N$  (as for the static solutions described earlier). Thus, we look for solutions near the minimum, which are always predicted to be stable and increase  $\chi$  until the exact solution agrees fairly well with the TDHF solution. Figures 23-26 plot  $\vartheta_1$  and  $\vartheta_2$  as functions of time for the TDHF solution and two exact solutions  $N=10$  and  $N=15$ . These show the progression from poor agreement for  $\chi=5$  to very good agreement for a full period in both  $\vartheta_1$  and  $\vartheta_2$  for  $\chi=100$  with  $N=15$ . A plot of  $\text{Tr}(\rho^2 - \rho)$  in Figure 27 also shows that the exact state in this case is approaching an independent particle state with  $\text{Tr}=0$ .

For an unstable example at  $\chi=100$ , we test the path from Figure 16. In Figures 28-30, plots of both  $\vartheta_1$  and  $\vartheta_2$  vs. time and a trajectory plot of  $\vartheta_1$  vs.  $\vartheta_2$  show that TDHF is a poor approximation to the exact solution. Figure 31 also shows that the  $\text{Tr}(\rho^2 - \rho)$  climbs quickly to a relatively large value, .6, and then levels off - a state far removed from a TDHF state. We also notice that all these results in Figures 28-31 don't vary much from  $N=10$  to  $N=15$  so that these calculations probably are in the "large  $N$  regime" where the exact solutions have reached their limiting behavior.

### Section 9: Summary

This TDRPA frequency can be used in a qualitative way to get fairly accurate ideas of the shape of the energy surface, and might, therefore, prove useful in more complex models. It also works well for predicting the reliability of TDHF calculations in extreme cases, with  $\chi=100$ . However, because of the scaling of the frequency with  $\chi$ , this means the frequency has only proven reliable for  $|\frac{\omega}{\epsilon}| \approx 100$ . The motion of the exact solutions as  $N$  increases shows that  $\omega^2$  seems to be a good indicator of the reliability of TDHF calculations in general. However, even this relatively simple model can't be solved exactly for a large enough number of particles to permit quantitative testing of this criterion or the development of quantitative ideas about its meaning. The results also suggest another possible use for this frequency. Its magnitude might give a qualitative idea of the number of particles which can be considered large in a given situation.

APPENDICES

## Appendix A1: Derivation of the TDHF Equations

### I. Variational Derivation (KE 76)

We begin with the definition of the action,

$$I = \int dt \langle \Psi | i\hbar \frac{\partial}{\partial t} - H | \Psi \rangle, \quad (\text{A1.1})$$

and parametrize the many-body wavefunction,  $\Psi$ , as a Slater determinant of single-particle wavefunctions,  $\psi_j$ ,

$$\Psi = \frac{1}{\sqrt{(A!)}} \det\{\psi_1(\alpha_1) \cdots \psi_A(\alpha_A)\} ; \quad (\text{A1.2})$$

where the  $\alpha_j$  refer to spatial, spin, and isospin nucleon coordinates and  $A$  is the total number of nucleons. These single-particle wavefunctions will be orthonormal,

$$\langle \psi_i | \psi_j \rangle = \delta_{ij} . \quad (\text{A1.3})$$

The calculation of  $\langle \Psi | \Psi \rangle$  checks that the many-body wavefunction is normalized.

$$\langle \Psi | \Psi \rangle = \frac{1}{A!} \det\{\psi_j^*\} \det\{\psi_j\} \quad (\text{A1.4})$$

Each determinant has  $A!$  terms so the product has  $A!$  terms where the coordinates pair identical single-particle wavefunctions,

$$\langle \psi_1 | \psi_1 \rangle \langle \psi_2 | \psi_2 \rangle \cdots \langle \psi_A | \psi_A \rangle = 1 . \quad (\text{A1.5})$$

The other terms include at least two mismatched wavefunctions, with  $\langle \psi_i | \psi_{i \neq j} \rangle = 0$ ; and thus, do not contribute. Therefore,

$$\langle \Psi | \Psi \rangle = 1 . \quad (\text{A1.6})$$

In a similar way, we can rewrite  $\langle \Psi | i\hbar \frac{\partial}{\partial t} | \Psi \rangle$ . As above, this product has  $(A!)^2$  terms. Of these,  $A!$  properly match the single-particle wavefunctions and the rest mismatch at least two of them. The derivative of each of the product terms can be expressed as a sum involving derivatives of single-particle wavefunctions,

$$i\hbar \frac{\partial}{\partial t} \prod_j \psi_j = \sum_j (i\hbar \frac{\partial}{\partial t} \psi_j) \prod_{i \neq j} \psi_i . \quad (\text{A1.7})$$

Thus, any of the mismatched terms still have at least one mismatch, with  $\langle \psi_i | \psi_{j \neq i} \rangle = 0$ , and do not contribute. Each of the  $A!$  matched terms gives

$$\sum_j \langle \psi_j | i\hbar \frac{\partial}{\partial t} | \psi_j \rangle \prod_{i \neq j} \langle \psi_i | \psi_i \rangle = \sum_j \langle \psi_j | i\hbar \frac{\partial}{\partial t} | \psi_j \rangle . \quad (\text{A1.8})$$

Thus, our net result is

$$\langle \Psi | i\hbar \frac{\partial}{\partial t} | \Psi \rangle = \sum_j \langle \psi_j | i\hbar \frac{\partial}{\partial t} | \psi_j \rangle , \quad (\text{A1.9})$$

and the variation with respect to  $\psi_j^*$  will give  $i\hbar \frac{\partial}{\partial t} \psi_j$ . We then arrive at the TDHF equations in the form

$$i\hbar \frac{\partial}{\partial t} \psi_j = \frac{\delta \langle H \rangle}{\delta \psi_j^*} . \quad (\text{A1.10})$$

To see that Eq. (A1.10) results in a mean-field formulation,  $i\hbar \frac{\partial}{\partial t} \psi_j = h \psi_j$ , with  $h$  a one-body operator, we calculate  $\frac{\delta \langle H \rangle}{\delta \psi_j^*}$  for a two-body Hamiltonian. The generalization for higher-body potentials is straightforward. A two-body Hamiltonian can be written in second-quantized notation as,

$$H = \sum_{\alpha\beta} t_{\alpha\beta} a_\alpha^\dagger a_\beta + \frac{1}{2} \sum_{\alpha\beta\gamma\delta} V_{\alpha\beta\gamma\delta} a_\alpha^\dagger a_\beta^\dagger a_\delta a_\gamma . \quad (\text{A1.11})$$

The greek labels refer to the spatial, spin, and isospin nucleon coordinates; and the annihilation and creation operators satisfy the usual fermion anti-commutation rules:

$$\{a_\alpha^\dagger, a_\beta^\dagger\} = \{a_\alpha, a_\beta\} = 0 \quad \text{and} \quad \{a_\alpha^\dagger, a_\beta\} = \delta_{\alpha\beta} . \quad (\text{A1.12})$$

Since  $H$  is hermitian,

$$t_{\alpha\beta} = t_{\beta\alpha} \quad \text{and} \quad V_{\alpha\beta\gamma\delta} = V_{\beta\alpha\delta\gamma} = V_{\gamma\delta\alpha\beta}^* . \quad (\text{A1.13})$$

With  $\Psi$  a Slater determinant as in Eq. (A1.2),

$$\begin{aligned} \langle H \rangle = & \sum_{\alpha\beta} t_{\alpha\beta} \psi_j^*(\alpha) \psi_j(\beta) \\ & + \frac{1}{2} \sum_{\alpha\beta\gamma\delta} V_{\alpha\beta\gamma\delta} \psi_i^*(\alpha) \psi_j^*(\beta) [\psi_i(\gamma) \psi_j(\delta) - \psi_i(\delta) \psi_j(\gamma)] . \end{aligned} \quad (\text{A1.14})$$

The variation of  $\langle H \rangle$  with respect to  $\psi_k^*$  gives

$$\begin{aligned} \frac{\delta \langle H \rangle}{\delta \psi_k^*(\varepsilon)} &= \sum_{\alpha\beta j} t_{\alpha\beta} \delta_{jk} \delta_{\alpha\varepsilon} \psi_j(\beta) + \frac{1}{2} \sum_{\alpha\beta\gamma\delta ij} V_{\alpha\beta\gamma\delta} \{ \delta_{ik} \delta_{\alpha\varepsilon} \psi_j^*(\beta) + \delta_{jk} \delta_{\beta\varepsilon} \psi_i^*(\alpha) \} \times \\ &\quad \{ \psi_i(\gamma) \psi_j(\delta) - \psi_i(\delta) \psi_j(\gamma) \} , \\ &= \sum_{\beta} t_{\varepsilon\beta} \psi_k(\beta) + \sum_{\beta\gamma\delta} \tilde{V}_{\varepsilon\beta\gamma\delta} [ \sum_j \psi_j^*(\beta) \psi_j(\delta) ] \psi_k(\gamma) , \\ &= \sum_{\beta} h_{\varepsilon\beta} \psi_k(\beta) ; \end{aligned} \quad (A1.15)$$

where  $\tilde{V}$  are the antisymmetrized elements of  $V$ ,  $\tilde{V}_{\alpha\beta\gamma\delta} = V_{\alpha\beta\gamma\delta} - V_{\alpha\beta\delta\gamma}$ ;  $h = t + W$ ; and the mean-field potential,  $W$ , a one-body operator, is given by

$$W_{\alpha\beta} = \sum_{\gamma\delta} \tilde{V}_{\alpha\gamma\beta\delta} [ \sum_j \psi_j^*(\gamma) \psi_j(\delta) ] . \quad (A1.16)$$

For  $\Psi$  a Slater determinant, we can write the one-body density matrix,

$$\rho_{\alpha\beta} \equiv \langle \Psi | a_{\beta}^{\dagger} a_{\alpha} | \Psi \rangle = \sum_j \psi_j^*(\beta) \psi_j(\alpha) , \quad (A1.17)$$

and rewrite Eq. (A1.16) as

$$W_{\alpha\beta} = \sum_{\gamma\delta} \tilde{V}_{\alpha\gamma\beta\delta} \rho_{\delta\gamma} . \quad (A1.18)$$

We can also rewrite Eq. (A1.14) for  $\langle H \rangle$  in terms of the mean field and density as

$$\begin{aligned} \langle H \rangle &= \sum_{\alpha\beta} t_{\alpha\beta} \rho_{\beta\alpha} + \frac{1}{2} \sum_{\alpha\beta\gamma\delta} \tilde{V}_{\alpha\beta\gamma\delta} \rho_{\gamma\alpha} \rho_{\delta\beta} , \\ &= \sum_{\alpha\beta} [ t_{\alpha\beta} + \frac{1}{2} W_{\alpha\beta} ] \rho_{\beta\alpha} . \end{aligned} \quad (A1.19)$$

Similarly, for a general n-body potential,  $V_{\alpha_1 \dots \alpha_n \beta_1 \dots \beta_n}$ ;

$$\langle H \rangle = \frac{1}{n!} \sum_{\alpha\beta} \tilde{V}_{\alpha_1 \dots \alpha_n \beta_1 \dots \beta_n} \rho_{\beta_1 \alpha_1} \dots \rho_{\beta_n \alpha_n} ; \quad (A1.20)$$

where  $\tilde{V}_{\alpha_1 \dots \alpha_n \beta_1 \dots \beta_n}$  is completely antisymmetrized with respect to interchanges of the  $\alpha$ 's and interchanges of the  $\beta$ 's. The variation gives

$$\begin{aligned} \frac{\delta \langle H \rangle}{\delta \psi_j^*(\gamma)} &= \frac{n}{n!} \sum_{\alpha\beta} \tilde{V}_{\gamma\alpha_2 \dots \alpha_n \beta_2 \dots \beta_n} \rho_{\beta_2 \alpha_2} \dots \rho_{\beta_n \alpha_n} \psi_j(\delta) \\ &= \sum_{\delta} W_{\gamma\delta} \psi_j(\delta) . \end{aligned} \quad (A1.21)$$

Thus the mean field,

$$W_{\gamma\delta} = \frac{1}{(n-1)!} \sum_{\alpha\beta} \tilde{V}_{\gamma\alpha_2 \dots \alpha_n \delta\beta_2 \dots \beta_n} \rho_{\beta_2\alpha_2} \dots \rho_{\beta_n\alpha_n} \quad , \quad (A1.22)$$

and

$$\langle H \rangle = \frac{1}{n} \sum_{\gamma\delta} W_{\gamma\delta} \rho_{\delta\gamma} \quad . \quad (A1.23)$$

## II. Derivation by Truncation (KO 79a)

This derivation begins with the definitions of the density matrices.

$$\rho_{\alpha\beta} \equiv \langle \Psi | a_\beta^\dagger a_\alpha | \Psi \rangle \quad , \quad (A1.24)$$

$$\rho_{\alpha\beta\gamma\delta}^{(2)} \equiv \langle \Psi | a_\gamma^\dagger a_\delta^\dagger a_\alpha a_\beta | \Psi \rangle \quad , \quad (A1.25)$$

*etc.*

We once again use a two-body Hamiltonian, as in Eq. (A1.11), so

$$\langle H \rangle = \sum_{\alpha\beta} t_{\alpha\beta} \rho_{\beta\alpha} + \frac{1}{2} \sum_{\alpha\beta\gamma\delta} V_{\alpha\beta\gamma\delta} \rho_{\delta\gamma\alpha\beta}^{(2)} \quad . \quad (A1.26)$$

The exact equation for the evolution of the one-body density is

$$\begin{aligned} i\hbar \frac{\partial}{\partial t} \rho_{\alpha\beta} &= \langle \Psi | -H a_\beta^\dagger a_\alpha + a_\beta^\dagger a_\alpha H | \Psi \rangle \quad , \\ &= \sum_{\gamma\delta} t_{\gamma\delta} \langle \Psi | [a_\beta^\dagger a_\alpha, a_\gamma^\dagger a_\delta] | \Psi \rangle \\ &\quad + \frac{1}{2} \sum_{\gamma\delta\epsilon\zeta} V_{\gamma\delta\epsilon\zeta} \langle \Psi | [a_\beta^\dagger a_\alpha, a_\gamma^\dagger a_\delta^\dagger a_\epsilon a_\zeta] | \Psi \rangle \quad . \end{aligned} \quad (A1.27)$$

Using the anti-commutation rules from Eq. (A1.12), we get

$$[a_\beta^\dagger a_\alpha, a_\gamma^\dagger a_\delta] = \delta_{\alpha\gamma} a_\beta^\dagger a_\delta - \delta_{\beta\delta} a_\gamma^\dagger a_\alpha \quad \text{and} \quad (A1.28)$$

$$\begin{aligned} [a_\beta^\dagger a_\alpha, a_\gamma^\dagger a_\delta^\dagger a_\epsilon a_\zeta] &= \delta_{\alpha\gamma} a_\beta^\dagger a_\delta^\dagger a_\epsilon a_\zeta - \delta_{\alpha\delta} a_\beta^\dagger a_\gamma^\dagger a_\epsilon a_\zeta \\ &\quad + \delta_{\zeta\beta} a_\gamma^\dagger a_\delta^\dagger a_\epsilon a_\alpha - \delta_{\epsilon\beta} a_\gamma^\dagger a_\delta^\dagger a_\zeta a_\alpha \quad . \end{aligned} \quad (A1.29)$$

Therefore,

$$i\hbar \frac{\partial}{\partial t} \rho_{\alpha\beta} = \sum_{\delta} (t_{\alpha\delta} \rho_{\delta\beta} - \rho_{\alpha\delta} t_{\delta\beta}) + \frac{1}{2} \sum_{\delta\epsilon\zeta} (\tilde{V}_{\alpha\delta\epsilon\zeta} \rho_{\zeta\epsilon\beta\delta}^{(2)} - \rho_{\zeta\alpha\epsilon\delta}^{(2)} \tilde{V}_{\epsilon\delta\beta\zeta}) \quad . \quad (A1.30)$$

This equation gives the exact evolution of  $\rho_{\alpha\beta}$  for a two-body potential in terms of a two-body dynamical quantity  $\rho_{\alpha\beta\gamma\delta}^{(2)}$ . Of course, higher-body potentials would involve higher-body dynamical quantities. The evolution of  $\rho^{(2)}$  can be described by a similar equation involving  $\rho^{(3)}$  (or higher for higher-body poten-

tials). The hierarchy terminates at  $\rho^{(A)}$  and is equivalent to the exact Schroedinger equation.

We make the independent-particle approximation by saying that the only two-body correlation is the necessary antisymmetry,

$$\rho_{\alpha\beta\gamma\delta}^{(2)} = \rho_{\alpha\delta}\rho_{\beta\gamma} - \rho_{\beta\delta}\rho_{\alpha\gamma} \quad , \quad (A1.31)$$

and we ignore all the higher-body equations. Eq. (A1.31) is true for  $\Psi$  a Slater determinant since a comparison of Eqs. (A1.26) and (A1.14) shows that  $\rho_{\alpha\beta} = \sum_j \psi_j^*(\beta)\psi_j(\alpha)$  and  $\rho_{\delta\gamma\alpha\beta}^{(2)} = \sum_{ij} \psi_i^*(\alpha)\psi_j^*(\beta)[\psi_i(\gamma)\psi_j(\delta) - \psi_i(\delta)\psi_j(\gamma)]$ . However, it can also be shown that the assumption of Eq. (A1.31) leads to a Slater determinant wavefunction. Setting  $\delta = \alpha$  and summing over  $\alpha$  in Eq. (A1.31) gives

$$\sum_{\alpha} \rho_{\alpha\beta\gamma\alpha}^{(2)} = \left( \sum_{\alpha} \rho_{\alpha\alpha} \right) \rho_{\beta\gamma} - \sum_{\alpha} \rho_{\beta\alpha} \rho_{\alpha\gamma} = \langle \Psi | a_{\gamma}^{\dagger} \left( \sum_{\alpha} a_{\alpha}^{\dagger} a_{\alpha} \right) a_{\beta} | \Psi \rangle \quad . \quad (A1.32)$$

Since the number operator is  $N = \sum_{\alpha} a_{\alpha}^{\dagger} a_{\alpha}$ ,  $\sum_{\alpha} \rho_{\alpha\alpha} = \langle N \rangle = A$  the total number of particles and  $\langle a_{\gamma}^{\dagger} N a_{\beta} \rangle = (A-1) \langle a_{\gamma}^{\dagger} a_{\beta} \rangle$ . Therefore,  $\rho^2 = \rho$  and  $\rho$  is a projector. This means it has  $A$  eigenvalues of 1, the rest zero. Therefore, we can write a spectral expansion for  $\rho_{\alpha\beta}$ ,

$$\rho_{\alpha\beta} = \sum_{j=1}^A \psi_j^*(\beta)\psi_j(\alpha) \quad ;$$

where the functions  $\psi_j$  span the space of unit eigenvalues  $\sum_{\beta} \rho_{\alpha\beta}\psi_j(\beta) = \psi_j(\alpha)$  and are orthonormal  $\sum_{\beta} \psi_j^*(\beta)\psi_k(\beta) = \delta_{jk}$ . The above expression for  $\rho$  is then consistent with a Slater determinant many-body wavefunction as in Eq. (A1.2).

Substituting this approximation, Eq. (A1.31), into our exact expression gives

$$\begin{aligned} i\hbar \frac{\partial}{\partial t} \rho_{\alpha\beta} &= \sum_{\delta} (t_{\alpha\delta} \rho_{\delta\beta} - \rho_{\alpha\delta} t_{\delta\beta}) + \sum_{\delta\epsilon\zeta} (\tilde{V}_{\alpha\delta\epsilon\zeta} \rho_{\zeta\delta} \rho_{\epsilon\beta} - \rho_{\alpha\epsilon} \rho_{\zeta\delta} \tilde{V}_{\epsilon\delta\beta\zeta}) \quad , \\ &= \sum_{\delta} [(t_{\alpha\delta} + W_{\alpha\delta}) \rho_{\delta\beta} - \rho_{\alpha\delta} (t_{\delta\beta} + W_{\delta\beta})] \quad , \\ &= [h, \rho]_{\alpha\beta} \quad ; \end{aligned} \quad (A1.33)$$

where  $h$  and  $W$  are the same as the previous definitions in Eqs. (A1.15) through

(A1.18).

Similarly for an n-body potential

$$V^{(n)} = \frac{1}{n!} \sum_{\alpha\beta} V_{\alpha_1 \dots \alpha_n \beta_1 \dots \beta_n} a_{\alpha_1}^+ \dots a_{\alpha_n}^+ a_{\beta_n} \dots a_{\beta_1} \quad (\text{A1.34})$$

we get

$$\begin{aligned} \langle [a_\gamma^+ a_\delta, V^{(n)}] \rangle &= \frac{1}{n!} [\hat{V}_{\delta\alpha_2 \dots \alpha_n \beta_1 \dots \beta_n} \rho_{\beta_n}^{(n)} \dots \beta_1 \gamma \alpha_2 \dots \alpha_n \\ &\quad - \rho_{\beta_n}^{(n)} \dots \beta_2 \delta \alpha_1 \dots \alpha_n \hat{V}_{\alpha_1 \dots \alpha_n \gamma \beta_2 \dots \beta_n}] \end{aligned} \quad (\text{A1.35})$$

where  $\hat{V}$  is antisymmetric under permutations of  $\delta$  through the  $\alpha$ 's or equivalently  $\gamma$  through the  $\beta$ 's while keeping the  $\alpha$ 's or  $\beta$ 's in order. For Slater determinant wavefunctions  $\rho^{(n)}$  is written as an antisymmetric combination of one-body  $\rho$ 's, with  $n!$  terms. Thus there are  $n$  terms where  $\gamma$  is permuted through the  $\alpha$ 's and the  $\alpha$ 's remain in the same order. Because of the symmetry of  $\hat{V}$  these all give the same result. The  $(n-1)!$  permutations of the  $\alpha$ 's for each position of  $\gamma$  form the completely antisymmetric matrix elements  $\tilde{V}$ . Therefore,

$$\begin{aligned} \langle [a_\gamma^+ a_\delta, V^{(n)}] \rangle &= \frac{1}{(n-1)!} \sum_{\alpha\beta} (\tilde{V}_{\delta\alpha_2 \dots \alpha_n \beta_1 \dots \beta_n} \rho_{\beta_1} \rho_{\beta_2} \dots \rho_{\beta_n} \alpha_n \\ &\quad - \rho_{\delta\alpha_1} \tilde{V}_{\alpha_1 \dots \alpha_n \gamma \beta_2 \dots \beta_n} \rho_{\beta_2} \dots \rho_{\beta_n} \alpha_n) \\ &= \sum_{\beta_1} (W_{\delta\beta_1} \rho_{\beta_1 \gamma} - \rho_{\delta\beta_1} W_{\beta_1 \gamma}) \end{aligned} \quad (\text{A1.36})$$

with  $W$  in agreement with Eq. (A1.22). Therefore,

$$i\hbar \frac{\partial}{\partial t} \rho_{\alpha\beta} = [W, \rho]_{\alpha\beta} \quad (\text{A1.37})$$

### III. Hartree Potential and Fock Potential

The traditional Hartree and Fock terms can be calculated by evaluating this mean field,  $W$ , for a local, Galilean-invariant two-body potential,  $V$ , dependent only on the relative position of the particles.

$$V_{\alpha\beta\gamma\delta} \rightarrow V(\vec{r}_1, \vec{r}_2, \vec{r}_3, \vec{r}_4) = \delta\left(\frac{\vec{r}_1 + \vec{r}_2}{2} - \frac{\vec{r}_3 + \vec{r}_4}{2}\right) \delta(\vec{r}_1 - \vec{r}_2 - [\vec{r}_3 - \vec{r}_4]) v(\vec{r}_1 - \vec{r}_2) \quad (\text{A1.38})$$

Ignoring the spins of the particles, Eq. (A1.18) gives a mean field

$$W(\vec{r}_1, \vec{r}_3) = \int d\vec{r}_2 d\vec{r}_4 \rho(\vec{r}_4, \vec{r}_2) [V(\vec{r}_1, \vec{r}_2, \vec{r}_3, \vec{r}_4) - V(\vec{r}_1, \vec{r}_2, \vec{r}_4, \vec{r}_3)] \quad (A1.39)$$

In this first term, the two  $\delta$  functions require  $\vec{r}_1 = \vec{r}_3$  and  $\vec{r}_2 = \vec{r}_4$ . Thus, the first term, the direct term, gives

$$\begin{aligned} U_H(\vec{r}_1, \vec{r}_3) &= \delta(\vec{r}_1 - \vec{r}_3) \int d\vec{r}_2 \rho(\vec{r}_2, \vec{r}_2) v(\vec{r}_1 - \vec{r}_2) \quad , \\ &= \delta(\vec{r}_1 - \vec{r}_3) \int d\vec{r}_2 \rho(\vec{r}_2) v(\vec{r}_1 - \vec{r}_2) \quad , \end{aligned} \quad (A1.40)$$

the local Hartree term.

In the second term, the exchange term, the two  $\delta$  functions require  $\vec{r}_1 = \vec{r}_4$  and  $\vec{r}_2 = \vec{r}_3$ . This gives

$$U_F(\vec{r}_1, \vec{r}_3) = -\rho(\vec{r}_1, \vec{r}_3) v(\vec{r}_1 - \vec{r}_3) \quad , \quad (A1.41)$$

the nonlocal Fock term.

#### IV. Conservation Laws

We want to show that for a one-body operator the TDHF equations conserve any expectation values conserved by the exact  $H$ , but that this is not true for many-body operators. The time evolution of  $\langle O \rangle$  for the TDHF state is given by

$$i\hbar \frac{\partial}{\partial t} \langle O \rangle = \sum_{j\alpha} \left[ \frac{\delta \langle O \rangle}{\delta \psi_j(\alpha)} \frac{\delta \langle H \rangle}{\delta \psi_j^*(\alpha)} - \frac{\delta \langle O \rangle}{\delta \psi_j^*(\alpha)} \frac{\delta \langle H \rangle}{\delta \psi_j(\alpha)} \right] \quad (A1.42)$$

Using the results from Part I, for a general n-body operator we get

$$\begin{aligned} i\hbar \frac{\partial}{\partial t} \langle O \rangle &= \sum_{j\gamma\delta\delta'} (\psi_j^*(\delta) \bar{O}_{\delta\gamma} \bar{H}_{\gamma\delta'} \psi_j(\delta') - \psi_j^*(\delta) \bar{H}_{\delta\gamma} \bar{O}_{\gamma\delta'} \psi_j(\delta')) \\ &= \sum_{\delta\delta'} [\bar{O}, \bar{H}]_{\delta\delta'} \rho_{\delta\delta'} \\ &= \langle [\bar{O}, \bar{H}] \rangle \end{aligned} \quad (A1.43)$$

where  $\bar{O}$  and  $\bar{H}$  are one-body operators defined by Eq. (A1.22). Of course, the exact evolution would be

$$i\hbar \frac{\partial}{\partial t} \langle O \rangle = \langle [O, H] \rangle \quad (A1.44)$$

Therefore, we must compare these two commutators from Eqs. (A1.43-44).

For a one-body operator  $O$  and an n-body  $H$ , the expectation value of the commutator is

$$\langle [O, H] \rangle = \sum_{\gamma\delta} O_{\gamma\delta} \langle [a_{\gamma}^{\dagger} a_{\delta}, H] \rangle \quad (A1.45)$$

Using Eq. (A1.36) from Part II this gives

$$\langle [O, H] \rangle = \sum_{\gamma\delta} O_{\gamma\delta} [\bar{H}, \rho]_{\delta\gamma} \quad (A1.46)$$

which can be rewritten

$$= \sum_{\beta\gamma} [O, \bar{H}]_{\gamma\beta} \rho_{\beta\gamma} \quad (A1.47)$$

Since  $\bar{O} = O$  for a one-body operator, the TDHF evolution with the one-body  $h \equiv \bar{H}$  conserves all expectations of one-body operators which are conserved by the exact n-body Hamiltonian, in addition to the energy and normalization.

However, it will not conserve expectations of many-body operators. For instance, with both  $O$  and  $H$  two-body operators and  $\tilde{H}$  the antisymmetrized elements of  $H$  the commutator is

$$\begin{aligned} [O, H] = \frac{1}{4} \sum_{\alpha_1 \beta_1 \gamma_1 \delta_1} O_{\alpha_1 \beta_1 \gamma_1 \delta_1} & (\tilde{H}_{\gamma_1 \beta_2 \gamma_2 \delta_2} a_{\alpha_1}^{\dagger} a_{\beta_1}^{\dagger} a_{\delta_1} a_{\beta_2}^{\dagger} a_{\delta_2} a_{\gamma_2} \\ & - \tilde{H}_{\alpha_2 \beta_2 \alpha_1 \delta_2} a_{\alpha_2}^{\dagger} a_{\beta_2}^{\dagger} a_{\delta_2} a_{\beta_1}^{\dagger} a_{\delta_1} a_{\gamma_1} \\ & + \tilde{H}_{\delta_1 \beta_2 \gamma_2 \delta_2} a_{\alpha_1}^{\dagger} a_{\beta_1}^{\dagger} a_{\beta_2}^{\dagger} a_{\delta_2} a_{\gamma_2} a_{\gamma_1} \\ & - \tilde{H}_{\alpha_2 \beta_2 \beta_1 \delta_2} a_{\alpha_2}^{\dagger} a_{\beta_2}^{\dagger} a_{\alpha_1}^{\dagger} a_{\delta_2} a_{\delta_1} a_{\gamma_1}) \quad (A1.48) \end{aligned}$$

where the sum is over all repeated indices. Collecting all  $a^{\dagger}$ 's to the left yields two-body and three-body pieces. The three-body pieces can be paired by defining an antisymmetrized  $\tilde{O}$ . The expectation values for a Slater determinant many-body wavefunction are antisymmetric combinations of one-body density matrices. For the two-body pieces, the two pairs of terms can be combined by changing  $O$  to  $\tilde{O}$ . For each three-body piece, the terms form two groups: 4 terms have only one  $\rho$  with one index from each  $\tilde{O}$  and  $\tilde{H}$ , while 2 terms have all 3  $\rho$  with one index from each. Within each group the terms are equal because of the symmetries of  $\tilde{O}$  and  $\tilde{H}$ . The four terms with only one mixed  $\rho$  give

$$\sum \tilde{O}_{\alpha_1 \beta_1 \gamma_1 \delta_1} \rho_{\gamma_1 \alpha_1} \tilde{H}_{\delta_1 \beta_2 \gamma_2 \delta_2} \rho_{\delta_2 \beta_2} \rho_{\gamma_2 \beta_1} = \bar{O}_{\beta_1 \delta_1} \bar{H}_{\delta_1 \gamma_2} \rho_{\gamma_2 \beta_1} \quad (A1.49)$$

Therefore, the difference in expectation values is

$$\begin{aligned} \langle [O, H] \rangle - \langle [\bar{O}, \bar{H}] \rangle = & \frac{1}{4} \sum (\tilde{O}_{\alpha_1 \beta_1 \gamma_1 \delta_1} \tilde{H}_{\gamma_1 \delta_1 \gamma_2 \delta_2} - \tilde{H}_{\alpha_1 \beta_1 \gamma_1 \delta_1} \tilde{O}_{\gamma_1 \delta_1 \gamma_2 \delta_2} \quad (A1.50) \\ & + 2 \tilde{O}_{\alpha_1 \beta_1 \gamma_1 \delta_1} \rho_{\gamma_1 \beta_2} \tilde{H}_{\delta_1 \beta_2 \gamma_2 \delta_2} - 2 \tilde{H}_{\alpha_1 \beta_1 \gamma_1 \delta_1} \rho_{\gamma_1 \beta_2} \tilde{O}_{\delta_1 \beta_2 \gamma_2 \delta_2}) \rho_{\delta_2 \beta_1} \rho_{\gamma_2 \alpha_1} \end{aligned}$$

## Appendix A2: $\langle H \rangle$ for the Skyrme Potential

### I. Introduction and Kinetic Energy Term

We want to evaluate the energy functional,  $H_s(\vec{r})$ , defined by  $\langle H \rangle = \int d\vec{r} H_s(\vec{r})$ , for a Skyrme potential and a Slater determinant wavefunction. For a Slater determinant wavefunction

$$\begin{aligned} \langle H \rangle = & \sum_i \langle i | T | i \rangle + \frac{1}{2} \sum_{ij} \langle ij | V^{(2)} | ij - ji \rangle \\ & + \frac{1}{6} \sum_{ijk} \langle ijk | V^{(3)} | ijk + jki + kij - jik - kji - ikj \rangle , \end{aligned} \quad (\text{A2.1})$$

where  $T$  is the one-body, kinetic energy operator, and  $V^{(2)}$  (or  $V^{(3)}$ ) is the two- (or three-) body potential. In coordinate space,  $T(\vec{r}) = -\frac{\hbar^2}{2m} \nabla^2$  or

$$T(\vec{r}_1, \vec{r}_2) = \delta(\vec{r}_1 - \vec{r}_2) \left[ -\frac{\hbar^2}{2m} \nabla_{\vec{r}_1}^2 \right] . \quad (\text{A2.2})$$

Similarly in coordinate space, the Skyrme potentials are:

$$\begin{aligned} V^{(2)}(\vec{r}, \vec{r}') = & t_0 (1 + \chi_0 P_\sigma) \delta(\vec{r}) \delta(\vec{r}') - \frac{t_1}{2} [\nabla_{\vec{r}}^2 \delta(\vec{r}) \delta(\vec{r}') + \nabla_{\vec{r}'}^2 \delta(\vec{r}') \delta(\vec{r})] \\ & + t_2 [\vec{\nabla}_{\vec{r}} \delta(\vec{r})] \cdot [\vec{\nabla}_{\vec{r}'} \delta(\vec{r}')] + iW_0 (\vec{\sigma}_1 + \vec{\sigma}_2) \cdot [\vec{\nabla}_{\vec{r}} \delta(\vec{r})] \times [\vec{\nabla}_{\vec{r}'} \delta(\vec{r}')] , \end{aligned} \quad (\text{A2.3})$$

or

$$V^{(2)}(\vec{r}_1, \vec{r}_2, \vec{r}_3, \vec{r}_4) = \delta(\vec{R} - \vec{R}') V^{(2)}(\vec{r}, \vec{r}') ,$$

where  $\vec{r} = \vec{r}_1 - \vec{r}_2$ ,  $\vec{r}' = \vec{r}_3 - \vec{r}_4$ ,  $\vec{R} = \frac{\vec{r}_1 + \vec{r}_2}{2}$ , and  $\vec{R}' = \frac{\vec{r}_3 + \vec{r}_4}{2}$ ;

and

$$V^{(3)}(\vec{r}_1, \vec{r}_2, \vec{r}_3) = t_3 \delta(\vec{r}_1 - \vec{r}_2) \delta(\vec{r}_2 - \vec{r}_3) , \quad (\text{A2.4})$$

or

$$V^{(3)}(\vec{r}_1, \vec{r}_2, \vec{r}_3, \vec{r}_4, \vec{r}_5, \vec{r}_6) = t_3 \delta(\vec{r}_1 - \vec{r}_2) \delta(\vec{r}_2 - \vec{r}_3) \delta(\vec{r}_1 - \vec{r}_4) \delta(\vec{r}_2 - \vec{r}_5) \delta(\vec{r}_3 - \vec{r}_6) .$$

In these expressions:  $P_\sigma = \frac{1}{2}(1 + \vec{\sigma}_1 \cdot \vec{\sigma}_2)$ , the spin-exchange operator, and  $\vec{\sigma}_1, \vec{\sigma}_2$  are Pauli spin matrices. The rewriting of the expressions above is to make Galilean invariance ( conservation of total momentum ) manifest ; that is, the potentials only depend on the relative coordinates and do not change the

centers of mass.

A general state,  $|i\rangle$ , is  $|\varphi_i(\vec{r})\rangle$ , a four component spinor in spin, isospin space.

$$|\varphi_i(\vec{r})\rangle = \varphi_i(\vec{r}, \alpha_i, q_i) |\alpha_i\rangle |q_i\rangle \quad . \quad (\text{A2.5})$$

where  $\varphi_i(\vec{r}, \alpha_i, q_i)$  is a wavefunction characterized by position  $\vec{r}$ , spin  $\alpha_i$ , and isospin  $q_i$ , and  $|\alpha_i\rangle$ ,  $|q_i\rangle$  are each two component spinors, in spin and isospin, respectively. Since each single-particle state is either a proton or a neutron, specifying  $|i\rangle$  also specifies its isospin  $q_i$  (either p or n) and the spinors  $|q_i\rangle$  are eigenstates of the isospin operator,  $Q_z$ . (The more traditional  $\tau$  is being used for the kinetic energy density.) Therefore, the spinors are orthogonal,

$$\langle q_i | q_j \rangle = \delta_{q_i q_j} \quad . \quad (\text{A2.6})$$

We consider only spin-saturated systems, so that for each  $|i\rangle$  as above there is a corresponding state  $|i'\rangle$  with opposite spin, but with the same isospin. We also neglect the spin-orbit force, so the state  $|i'\rangle$  has the same spatial orbital as the state  $|i\rangle$ .

$$\varphi_i(\vec{r}) = \varphi_i(\vec{r}, \alpha_i', q_i') |\alpha_i'\rangle |q_i'\rangle = \varphi_i(\vec{r}, -\alpha_i, q_i) |-\alpha_i\rangle |q_i\rangle \quad , \quad (\text{A2.7})$$

where

$$\langle \alpha_i | \vec{\sigma} | \alpha_i \rangle = - \langle -\alpha_i | \vec{\sigma} | -\alpha_i \rangle \quad \text{and} \quad \varphi_i(\vec{r}, -\alpha_i, q_i) = \varphi_i(\vec{r}, \alpha_i, q_i) \quad . \quad (\text{A2.8})$$

These two states,  $|\alpha_i\rangle$  and  $|-\alpha_i\rangle$ , form a complete set of spin states, so

$$\sum_{\alpha_i} f(\alpha_i) = f(\alpha_i) + f(-\alpha_i) \quad . \quad (\text{A2.9})$$

Therefore,

$$\begin{aligned} \sum_{\alpha_i} \langle \alpha_i | \vec{\sigma} | \alpha_i \rangle &= 0 \quad , \\ \sum_{\alpha_i} |\alpha_i\rangle \langle \alpha_i| &= 1 \quad , \end{aligned} \quad (\text{A2.10})$$

and

$$\sum_{\alpha_i} \langle \alpha_i | \alpha_i \rangle = 2 \quad .$$

Since  $\varphi_i(\vec{r}, \alpha_i, q_i)$  is independent of the spin  $\alpha_i$ , it can be rewritten  $\varphi_i(\vec{r}, q_i)$  and

the sum over  $i$  can be replaced by a sum over  $i$  and  $\alpha_i$ . The ability to sum over the spinors,  $|\alpha_i\rangle$ , without weighting factors from  $\varphi_i(\vec{r}, \alpha_i, q_i)$  is a crucial simplification in dealing with spin-saturated systems.

The one-body piece,  $\sum_i \langle i | T | i \rangle$ , can be evaluated as follows.

$$\begin{aligned}
 \sum_i \langle i | T | i \rangle &= \sum_{i\alpha_i} \int d\vec{r}_1 \int d\vec{r}_2 \varphi_i^*(\vec{r}_2, q_i) \langle \alpha_i | \langle q_i | \delta(\vec{r}_1 - \vec{r}_2) \left( -\frac{\hbar^2}{2m} \nabla_{\vec{r}_1}^2 \right) \varphi_i(\vec{r}_1, q_i) | \alpha_i \rangle | q_i \rangle \\
 &= \sum_{i\alpha_i} \int d\vec{r}_1 \varphi_i^*(\vec{r}_1, q_i) \left( -\frac{\hbar^2}{2m} \nabla_{\vec{r}_1}^2 \right) \varphi_i(\vec{r}_1, q_i) \langle \alpha_i | \alpha_i \rangle \langle q_i | q_i \rangle \\
 &= 2 \sum_i \int d\vec{r}_1 \varphi_i^*(\vec{r}_1, q_i) \left( -\frac{\hbar^2}{2m} \nabla_{\vec{r}_1}^2 \right) \varphi_i(\vec{r}_1, q_i) \\
 &= 2 \int d\vec{r} \frac{\hbar^2}{2m} \sum_i |\vec{\nabla} \varphi_i(\vec{r}, q_i)|^2 \\
 &= \int d\vec{r} \frac{\hbar^2}{2m} \tau(\vec{r}) \tag{A2.11}
 \end{aligned}$$

where

$$\tau_q(\vec{r}) \equiv 2 \sum_{\substack{i \text{ with} \\ q_i=q}} |\vec{\nabla} \varphi_i(\vec{r}, q_i)|^2 \quad \text{and} \quad \tau \equiv \tau_p + \tau_n \tag{A2.12}$$

## II. Two-Body Terms

Since the two-body potential has been written in terms of the relative coordinates,  $\vec{r}$  and  $\vec{r}'$ , and the center of mass coordinates,  $\vec{R}$  and  $\vec{R}'$ ; the expectation value is calculated by setting  $\vec{r}_1 = \vec{R} + \frac{1}{2}\vec{r}$ ,  $\vec{r}_2 = \vec{R} - \frac{1}{2}\vec{r}$ ,  $\vec{r}_3 = \vec{R}' + \frac{1}{2}\vec{r}'$ , and  $\vec{r}_4 = \vec{R}' - \frac{1}{2}\vec{r}'$ . Therefore, the integral  $\int d\vec{r}_1 d\vec{r}_2 d\vec{r}_3 d\vec{r}_4$  becomes  $\int d\vec{r} d\vec{r}' d\vec{R} d\vec{R}'$ . The integral  $\int d\vec{R}' \delta(\vec{R} - \vec{R}')$  can be done by replacing  $\vec{R}'$  by  $\vec{R}$  in the rest of the expression. Since none of the terms in  $V^{(2)}$  involve any isospin operators, the inner product of the isospin spinors can be done very easily for any term. The direct terms give  $\langle q_i | q_i \rangle \langle q_j | q_j \rangle = 1$ , and the exchange terms give  $\langle q_i | q_j \rangle \langle q_j | q_i \rangle = \delta_{q_i q_j}$ . The two-body contribution is evaluated term by term, neglecting the spin-orbit term.

The  $t_0$  term from Eq. (A2.3) gives

$$V_0 = \frac{1}{2} \sum_{ij} \int d\vec{r} d\vec{r}' d\vec{R} \varphi_i^*(\vec{R} + \frac{1}{2}\vec{r}', q_i) \varphi_j^*(\vec{R} - \frac{1}{2}\vec{r}', q_j) \delta(\vec{r}) \delta(\vec{r}') \quad (\text{A2.13})$$

$$\left[ \sum_{\alpha_i \alpha_j} t_0 (\langle \alpha_i | \alpha_i \rangle \langle \alpha_j | \alpha_j \rangle + \chi_0 \langle \alpha_i | \langle \alpha_j | P_\sigma | \alpha_i \rangle | \alpha_j \rangle) \varphi_i(\vec{R} + \frac{1}{2}\vec{r}', q_i) \varphi_j(\vec{R} - \frac{1}{2}\vec{r}', q_j) - \right. \\ \left. \delta_{q_i q_j} \sum_{\alpha_i \alpha_j} t_0 (\langle \alpha_i | \alpha_j \rangle \langle \alpha_j | \alpha_i \rangle + \chi_0 \langle \alpha_i | \langle \alpha_j | P_\sigma | \alpha_j \rangle | \alpha_i \rangle) \varphi_i(\vec{R} - \frac{1}{2}\vec{r}', q_j) \varphi_j(\vec{R} + \frac{1}{2}\vec{r}', q_i) \right]$$

The simplest way to evaluate the contribution from  $P_\sigma$  is simply to regard it as a spin-exchange operator, so  $P_\sigma | \alpha_i \rangle | \alpha_j \rangle = | \alpha_j \rangle | \alpha_i \rangle$ . Therefore,

$$\langle \alpha_i | \langle \alpha_j | P_\sigma | \alpha_i \rangle | \alpha_j \rangle = \langle \alpha_i | \alpha_j \rangle \langle \alpha_j | \alpha_i \rangle \quad (\text{A2.14})$$

and

$$\langle \alpha_i | \langle \alpha_j | P_\sigma | \alpha_j \rangle | \alpha_i \rangle = \langle \alpha_i | \alpha_i \rangle \langle \alpha_j | \alpha_j \rangle .$$

Since  $\sum_{\alpha_i \alpha_j} \langle \alpha_i | \alpha_i \rangle \langle \alpha_j | \alpha_j \rangle = 2 \times 2 = 4$  and  $\sum_{\alpha_i \alpha_j} \langle \alpha_i | \alpha_j \rangle \langle \alpha_j | \alpha_i \rangle = \sum_{\alpha_i} \langle \alpha_i | \alpha_i \rangle = 2$ ,

the contribution from the  $t_0$  term is

$$V_0 = \frac{1}{2} \sum_{ij} \int d\vec{r} d\vec{r}' d\vec{R} \varphi_i^*(\vec{R} + \frac{1}{2}\vec{r}', q_i) \varphi_j^*(\vec{R} - \frac{1}{2}\vec{r}', q_j) \left[ t_0 (4 + 2\chi_0) \varphi_i(\vec{R} + \frac{1}{2}\vec{r}', q_i) \varphi_j(\vec{R} - \frac{1}{2}\vec{r}', q_j) \right. \\ \left. - \delta_{q_i q_j} t_0 (2 + 4\chi_0) \varphi_i(\vec{R} - \frac{1}{2}\vec{r}', q_j) \varphi_j(\vec{R} + \frac{1}{2}\vec{r}', q_i) \right] \delta(\vec{r}) \delta(\vec{r}') , \\ = \frac{1}{2} \sum_{ij} \int d\vec{R} \varphi_i^*(\vec{R}, q_i) \varphi_j^*(\vec{R}, q_j) \left[ t_0 (4 + 2\chi_0) \varphi_i(\vec{R}, q_i) \varphi_j(\vec{R}, q_j) \right. \\ \left. - \delta_{q_i q_j} t_0 (2 + 4\chi_0) \varphi_i(\vec{R}, q_j) \varphi_j(\vec{R}, q_i) \right] . \quad (\text{A2.15})$$

With

$$\rho_q(\vec{R}) \equiv \sum_{\substack{i \text{ with} \\ q_i = q}} \varphi_i^*(\vec{R}, q_i) \varphi_i(\vec{R}, q_i) = 2 \sum_{\substack{i \text{ with} \\ q_i = q}} \varphi_i^*(\vec{R}, q_i) \varphi_i(\vec{R}, q_i) \quad (\text{A2.16})$$

and

$$\rho(\vec{R}) \equiv \rho_p(\vec{R}) + \rho_n(\vec{R}) .$$

Eq. (A2.15) can be written

$$V_0 = \frac{1}{2} \int d\vec{R} \left[ t_0 (4 + 2\chi_0) (\frac{1}{2}\rho)^2 - t_0 (2 + 4\chi_0) [(\frac{1}{2}\rho_p)^2 + (\frac{1}{2}\rho_n)^2] \right] , \\ = \int d\vec{R} \frac{1}{2} t_0 \left[ (1 + \frac{1}{2}\chi_0) (\rho_p + \rho_n)^2 - (\frac{1}{2} + \chi_0) (\rho_p^2 + \rho_n^2) \right] , \\ = \int d\vec{R} \frac{1}{2} t_0 \left[ \frac{1}{2} (1 - \chi_0) (\rho_p^2 + \rho_n^2) + (2 + \chi_0) \rho_p \rho_n \right] . \quad (\text{A2.17})$$

The  $t_1$  term from Eq. (A2.3) gives

$$V_1 = -\frac{t_1}{4} \sum_{ij} \int d\vec{r} d\vec{r}' d\vec{R} \varphi_i^*(\vec{R} + \frac{1}{2}\vec{r}', q_i) \varphi_j^*(\vec{R} - \frac{1}{2}\vec{r}', q_j) \left[ [\nabla_{\vec{r}'}^2 \delta(\vec{r}')] \delta(\vec{r}') + [\nabla_{\vec{r}}^2 \delta(\vec{r})] \delta(\vec{r}) \right] \times \\ \left[ 4\varphi_i(\vec{R} + \frac{1}{2}\vec{r}, q_i) \varphi_j(\vec{R} - \frac{1}{2}\vec{r}, q_j) - \delta_{q_i q_j} 2\varphi_i(\vec{R} - \frac{1}{2}\vec{r}, q_j) \varphi_j(\vec{R} + \frac{1}{2}\vec{r}, q_i) \right] . \quad (\text{A2.18})$$

Since  $\vec{r}$  and  $\vec{r}'$  are independent variables, integrating by parts twice for each  $\nabla_{\vec{r}'}^2$  and  $\nabla_{\vec{r}}^2$  gives

$$V_1 = -\frac{t_1}{4} \sum_{ij} \int d\vec{r} d\vec{r}' d\vec{R} \delta(\vec{r}) \delta(\vec{r}') \left[ \varphi_i^*(\vec{R} + \frac{1}{2}\vec{r}', q_i) \varphi_j^*(\vec{R} - \frac{1}{2}\vec{r}', q_j) \left[ 4\nabla_{\vec{r}'}^2 [\varphi_i(\vec{R} + \frac{1}{2}\vec{r}', q_i) \varphi_j(\vec{R} - \frac{1}{2}\vec{r}', q_j)] \right. \right. \\ \left. \left. - 2\delta_{q_i q_j} \nabla_{\vec{r}'}^2 [\varphi_i(\vec{R} - \frac{1}{2}\vec{r}', q_j) \varphi_j(\vec{R} + \frac{1}{2}\vec{r}', q_i)] \right] + \nabla_{\vec{r}}^2 [\varphi_i^*(\vec{R} + \frac{1}{2}\vec{r}', q_i) \varphi_j^*(\vec{R} - \frac{1}{2}\vec{r}', q_j)] \right] \times \\ \left[ 4\varphi_i(\vec{R} + \frac{1}{2}\vec{r}, q_i) \varphi_j(\vec{R} - \frac{1}{2}\vec{r}, q_j) - 2\delta_{q_i q_j} \varphi_i(\vec{R} - \frac{1}{2}\vec{r}, q_j) \varphi_j(\vec{R} + \frac{1}{2}\vec{r}, q_i) \right] ; \quad (\text{A2.19})$$

where  $\nabla^2[\varphi_i \varphi_j]$  is shorthand for  $\nabla^2[\varphi_i \varphi_j] = (\nabla^2 \varphi_i) \varphi_j + 2(\vec{\nabla} \varphi_i) \cdot (\vec{\nabla} \varphi_j) + \varphi_i (\nabla^2 \varphi_j)$ , and  $\vec{\nabla}_r \varphi_i(\vec{R} \pm \frac{1}{2}\vec{r}, q) = \pm \frac{1}{2} \vec{\nabla} \varphi_i(\vec{R} \pm \frac{1}{2}\vec{r}, q)$ .

Therefore the contribution from  $t_1$  is

$$V_1 = -\frac{t_1}{4} \sum_{ij} \int d\vec{R} \left[ 4 \left( \frac{1}{4} \right) \left[ \nabla^2 \varphi_i(\vec{R}, q_i) \varphi_j(\vec{R}, q_j) - 2(\vec{\nabla} \varphi_i(\vec{R}, q_i)) \cdot (\vec{\nabla} \varphi_j(\vec{R}, q_j)) + \varphi_i(\vec{R}, q_i) \nabla^2 \varphi_j(\vec{R}, q_j) \right] \right. \\ \left. - 2\delta_{q_i q_j} \left( \frac{1}{4} \right) \left[ \nabla^2 \varphi_i(\vec{R}, q_j) \varphi_j(\vec{R}, q_i) - 2(\vec{\nabla} \varphi_i(\vec{R}, q_j)) \cdot (\vec{\nabla} \varphi_j(\vec{R}, q_i)) + \varphi_i(\vec{R}, q_j) \nabla^2 \varphi_j(\vec{R}, q_i) \right] \right] \\ + \frac{1}{4} \left[ (\nabla^2 \varphi_i^*(\vec{R}, q_i)) \varphi_j^*(\vec{R}, q_j) - 2(\vec{\nabla} \varphi_i^*(\vec{R}, q_i)) \cdot (\vec{\nabla} \varphi_j^*(\vec{R}, q_j)) + \varphi_i^*(\vec{R}, q_i) \nabla^2 \varphi_j^*(\vec{R}, q_j) \right] \times \\ \left[ 4\varphi_i(\vec{R}, q_i) \varphi_j(\vec{R}, q_j) - 2\delta_{q_i q_j} \varphi_i(\vec{R}, q_j) \varphi_j(\vec{R}, q_i) \right] . \quad (\text{A2.20})$$

The sums over  $i$  and  $j$  can be done, to express this result in terms of densities, by defining a current density

$$\vec{j}_q \equiv \text{Im} \sum_{\substack{i \alpha_i \text{ with} \\ q_i = q}} \varphi_i^*(\vec{r}, q_i) \vec{\nabla} \varphi_i(\vec{r}, q_i) = \frac{1}{i} \sum_{\substack{i \text{ with} \\ q_i = q}} (\varphi_i \vec{\nabla} \varphi_i - \varphi_i^* \vec{\nabla} \varphi_i^*) \quad (\text{A2.21})$$

and rearranging the terms in Eq. (A2.20) as follows:

(A2.22)

$$\begin{aligned}
 V_1 = & -\frac{t_1}{4} \int d\vec{R} \sum_{ij} \left\{ \left[ \varphi_i(\vec{R}, q_i) \nabla^2 \varphi_i(\vec{R}, q_i) + \nabla^2 \varphi_i(\vec{R}, q_i) \varphi_i(\vec{R}, q_i) \right] \varphi_j(\vec{R}, q_j) \varphi_j(\vec{R}, q_j) \times 2 \right. \\
 & - 2 \left[ \varphi_i(\vec{R}, q_i) \vec{\nabla} \varphi_i(\vec{R}, q_i) \cdot \varphi_j(\vec{R}, q_j) \vec{\nabla} \varphi_j(\vec{R}, q_j) + \vec{\nabla} \varphi_i(\vec{R}, q_i) \varphi_i(\vec{R}, q_i) \cdot \vec{\nabla} \varphi_j(\vec{R}, q_j) \varphi_j(\vec{R}, q_j) \right] \\
 & - \frac{1}{2} \delta_{q_i q_j} \left[ \left[ \varphi_i(\vec{R}, q_i) \nabla^2 \varphi_i(\vec{R}, q_j) + \nabla^2 \varphi_i(\vec{R}, q_i) \varphi_i(\vec{R}, q_j) \right] \varphi_j(\vec{R}, q_j) \varphi_j(\vec{R}, q_i) \times 2 \right. \\
 & \left. \left. - 2 \left[ \varphi_i(\vec{R}, q_i) \vec{\nabla} \varphi_i(\vec{R}, q_j) \cdot \varphi_j(\vec{R}, q_j) \vec{\nabla} \varphi_j(\vec{R}, q_i) + \varphi_i(\vec{R}, q_j) \vec{\nabla} \varphi_i(\vec{R}, q_i) \cdot \varphi_j(\vec{R}, q_i) \vec{\nabla} \varphi_j(\vec{R}, q_j) \right] \right] \right\} .
 \end{aligned}$$

where the extra factors of two come from terms with i and j switched. With

$$\rho = 2 \sum_i \varphi_i(\vec{r}, q_i) \varphi_i(\vec{r}, q_i),$$

$$\vec{\nabla} \rho = 2 \sum_i \left( \vec{\nabla} \varphi_i(\vec{r}, q_i) \varphi_i(\vec{r}, q_i) + \varphi_i(\vec{r}, q_i) \vec{\nabla} \varphi_i(\vec{r}, q_i) \right) , \text{ and} \quad (\text{A2.23})$$

$$\nabla^2 \rho = 2 \sum_i \left[ \nabla^2 \varphi_i(\vec{r}, q_i) \varphi_i(\vec{r}, q_i) + 2 \vec{\nabla} \varphi_i(\vec{r}, q_i) \cdot \vec{\nabla} \varphi_i(\vec{r}, q_i) + \varphi_i(\vec{r}, q_i) \nabla^2 \varphi_i(\vec{r}, q_i) \right] .$$

Therefore,

$$\sum_i \left[ \nabla^2 \varphi_i(\vec{r}, q_i) \varphi_i(\vec{r}, q_i) + \varphi_i(\vec{r}, q_i) \nabla^2 \varphi_i(\vec{r}, q_i) \right] = \frac{1}{2} \nabla^2 \rho - \tau , \text{ and} \quad (\text{A2.24})$$

$$\sum_i \varphi_i(\vec{r}, q_i) \vec{\nabla} \varphi_i(\vec{r}, q_i) = \frac{1}{4} (\vec{\nabla} \rho + 2i\vec{j}) .$$

The contribution from the  $t_1$  term becomes

$$\begin{aligned}
 V_1 = & -\frac{t_1}{4} \int d\vec{R} \left\{ \left( \frac{1}{2} \nabla^2 \rho - \tau \right) \rho - 2 \left[ \frac{1}{16} (\vec{\nabla} \rho + 2i\vec{j})^2 + \frac{1}{16} (\vec{\nabla} \rho - 2i\vec{j})^2 \right] \right. \\
 & \left. - \frac{1}{2} \sum_q \left( \frac{1}{2} \nabla^2 \rho_q - \tau_q \right) \rho_q - 2 \left[ \frac{1}{16} (\vec{\nabla} \rho_q + 2i\vec{j}_q)^2 + \frac{1}{16} (\vec{\nabla} \rho_q - 2i\vec{j}_q)^2 \right] \right\} . \\
 = & -\frac{t_1}{4} \int d\vec{R} \left[ \left( \frac{1}{2} \nabla^2 \rho - \rho \tau - \frac{1}{4} |\vec{\nabla} \rho|^2 + j^2 \right) \right. \\
 & \left. - \frac{1}{2} \sum_q \left( \frac{1}{2} \nabla^2 \rho_q - \rho_q \tau_q - \frac{1}{4} |\vec{\nabla} \rho_q|^2 + j_q^2 \right) \right] .
 \end{aligned} \quad (\text{A2.25})$$

Doing an integration by parts on  $|\vec{\nabla} \rho|^2$ , and combining terms gives,

$$\begin{aligned}
 V_1 = & \int d\vec{R} \left\{ \frac{t_1}{4} \left[ -\frac{3}{4} (\rho_p \nabla^2 \rho_n + \rho_n \nabla^2 \rho_p) + \rho_p \tau_n + \rho_n \tau_p - 2\vec{j}_p \cdot \vec{j}_n \right] \right. \\
 & \left. + \frac{t_1}{8} \left[ -\frac{3}{4} (\rho_p \nabla^2 \rho_p + \rho_n \nabla^2 \rho_n) + \rho_p \tau_p + \rho_n \tau_n - j_p^2 - j_n^2 \right] \right\} .
 \end{aligned} \quad (\text{A2.26})$$

The contribution from the  $t_2$  term is

$$\begin{aligned}
V_2 &= \frac{1}{2} \sum_{ij} \int d\vec{r} d\vec{r}' d\vec{R} \varphi_i^*(\vec{R} + \frac{1}{2}\vec{r}', q_i) t_2 \vec{\nabla}_r \delta(\vec{r}) \cdot \vec{\nabla}_r' \delta(\vec{r}') \times \\
&\quad \left[ \sum_{\alpha_i, \alpha_j} \langle \alpha_i | \alpha_i \rangle \langle \alpha_j | \alpha_j \rangle \varphi_i(\vec{R} + \frac{1}{2}\vec{r}', q_i) \varphi_j(\vec{R} - \frac{1}{2}\vec{r}', q_j) \right. \\
&\quad \left. - \delta_{q_i q_j} \sum_{\alpha_i \alpha_j} \langle \alpha_i | \alpha_j \rangle \langle \alpha_j | \alpha_i \rangle \varphi_i(\vec{R} - \frac{1}{2}\vec{r}', q_j) \varphi_j(\vec{R} + \frac{1}{2}\vec{r}', q_i) \right] . \\
&= \frac{1}{2} \sum_{ij} \int d\vec{r} d\vec{r}' d\vec{R} t_2 \delta(\vec{r}) \delta(\vec{r}') \vec{\nabla}_r \cdot [\varphi_i^*(\vec{R} + \frac{1}{2}\vec{r}', q_i) \varphi_j(\vec{R} - \frac{1}{2}\vec{r}', q_j)] \cdot \\
&\quad [4 \vec{\nabla}_r (\varphi_i(\vec{R} + \frac{1}{2}\vec{r}', q_i) \varphi_j(\vec{R} - \frac{1}{2}\vec{r}', q_j)) - 2 \delta_{q_i q_j} \vec{\nabla}_r (\varphi_i(\vec{R} - \frac{1}{2}\vec{r}', q_j) \varphi_j(\vec{R} + \frac{1}{2}\vec{r}', q_i))] . \\
&= \frac{t_2}{2} \int d\vec{R} \sum_{ij} \frac{1}{2} [\vec{\nabla} \varphi_i^*(\vec{R}, q_i) \varphi_j(\vec{R}, q_j) - \varphi_i^*(\vec{R}, q_i) \vec{\nabla} \varphi_j(\vec{R}, q_j)] \cdot \\
&\quad \frac{1}{2} [4 (\vec{\nabla} \varphi_i(\vec{R}, q_i) \varphi_j(\vec{R}, q_j) - \varphi_i(\vec{R}, q_i) \vec{\nabla} \varphi_j(\vec{R}, q_j)) \\
&\quad - 2 \delta_{q_i q_j} (-\vec{\nabla} \varphi_i(\vec{R}, q_j) \varphi_j(\vec{R}, q_i) + \varphi_i(\vec{R}, q_j) \varphi_j(\vec{R}, q_i))] . \\
&= \frac{t_2}{8} \int d\vec{R} \left[ 2 \rho \tau - \frac{1}{2} (\vec{\nabla} \rho + 2i\vec{j}) \cdot (\vec{\nabla} \rho - 2i\vec{j}) + \frac{1}{2} \sum_q [2 \rho_q \tau_q - \frac{1}{2} (\vec{\nabla} \rho_q + 2i\vec{j}_q) \cdot (\vec{\nabla} \rho_q - 2i\vec{j}_q)] \right] \\
&= \int d\vec{R} \left\{ \frac{t_2}{8} [\frac{1}{2} (\rho_n \nabla^2 \rho_p + \rho_p \nabla^2 \rho_n) + 2 (\rho_n \tau_p + \rho_p \tau_n - 2 \vec{j}_p \cdot \vec{j}_n)] \right. \\
&\quad \left. + \frac{3t_2}{16} [\frac{1}{2} (\rho_p \nabla^2 \rho_p + \rho_n \nabla^2 \rho_n) + 2 (\rho_p \tau_p + \rho_n \tau_n - \vec{j}_p^2 \cdot \vec{j}_n^2)] \right\} \quad (A2.27)
\end{aligned}$$

### III. Three-Body Term and Density-Dependent Two-Body Term

The three-body contribution can be written quite easily since  $t_3 \delta(\vec{r}_1 - \vec{r}_2) \delta(\vec{r}_2 - \vec{r}_3)$  requires all three particles in the same place. This means that three nucleons must be two like nucleons, one spin up and one spin down, and an unlike nucleon in either spin state. The density in a particular spin state is  $\frac{1}{2}\rho$ . Therefore, the total three-body contribution is

$$t_3 \left[ \left( \frac{\rho_n}{2} \right)^2 \rho_p + \left( \frac{\rho_p}{2} \right)^2 \rho_n \right] = \frac{t_3}{4} (\rho_p + \rho_n) \rho_p \rho_n \quad (A2.28)$$

The full calculation verifies this result.

Adding all these contributions gives

$$\begin{aligned}
 H_S(\vec{r}) = & \frac{\hbar^2}{2m} \tau + \frac{1}{2} t_0 \left[ \frac{1}{2} (1 - \chi_0) (\rho_p^2 + \rho_n^2) + (2 + \chi_0) \rho_p \rho_n \right] + \frac{t_3}{4} \rho \rho_n \rho_p \\
 & + \frac{1}{16} (t_2 - 3t_1) (\rho_n \nabla^2 \rho_p + \rho_p \nabla^2 \rho_n) + \frac{3}{32} (t_2 - t_1) (\rho_p \nabla^2 \rho_n + \rho_n \nabla^2 \rho_p) \\
 & + \frac{1}{4} (t_1 + t_2) (\rho_n \tau_p + \rho_p \tau_n - 2\vec{j}_p \cdot \vec{j}_n) + \frac{1}{8} (t_1 + 3t_2) (\rho_p \tau_p + \rho_n \tau_n - \vec{j}_p^2 - \vec{j}_n^2)
 \end{aligned} \tag{A2.29}$$

The density-dependent two-body potential

$$v^2 = \frac{t_3}{8} (1 + P_\sigma) \delta(\vec{r} - \vec{r}') \delta(\vec{r}) \rho(\vec{R}) \delta(\vec{R} - \vec{R}') \tag{A2.30}$$

is Galilean-invariant and local with zero range. Its expectation value  $\langle v^2 \rangle$  is

$$\frac{1}{2} \sum_{\vec{q}} \int d\vec{R} \frac{t_3}{8} \rho(\vec{R}) \varphi_i^*(\vec{R}, \vec{q}_i) \varphi_j^*(\vec{R}, \vec{q}_j) (6\varphi_i(\vec{R}, \vec{q}_i) \varphi_j(\vec{R}, \vec{q}_j) - 6\delta_{\vec{q}_i \vec{q}_j} \varphi_i(\vec{R}, \vec{q}_j) \varphi_j(\vec{R}, \vec{q}_i)) \tag{A2.31}$$

since

$$6 = \langle \alpha_i | \langle \alpha_j | (1 + P_\sigma) | \alpha_i \rangle | \alpha_j \rangle = \langle \alpha_i | \langle \alpha_j | (1 + P_\sigma) | \alpha_j \rangle | \alpha_i \rangle \tag{A2.32}$$

Therefore,

$$\begin{aligned}
 \langle v^2 \rangle = & \frac{t_3}{2} \int d\vec{R} \rho(\vec{R}) \left[ \left( \frac{\rho(\vec{R})}{2} \right)^2 - \sum_{\vec{q}} \left( \frac{\rho_{\vec{q}}(\vec{R})}{2} \right)^2 \right] \\
 = & \frac{t_3}{4} \int d\vec{R} \rho \rho_n \rho_p
 \end{aligned} \tag{A2.33}$$

It is therefore equivalent to the three-body potential above.

## Appendix A3: Spatial Discretization of the Energy Functional

### I. Introduction and Zero-Range Terms

We solve the TDHF equations by finite difference methods in coordinate space. We obtain the discrete representation of the TDHF Hamiltonian by the variation of a discrete approximation to the energy functional with respect to the values of the single-particle wavefunctions at the mesh points. This procedure guarantees a hermitian approximation to the single-particle Hamiltonian and would yield exact conservation of the discrete approximation to the energy if we could use an evolution operator which is exact in time. We split the energy functional,  $H$ , into zero-range,  $H_Z$ ; kinetic,  $H_K$ ; nonlocal,  $H_{NL}$ ; Yukawa,  $H_Y$ ; and Coulomb,  $H_C$ , energies.

$$H = H_Z + H_K + H_{NL} + H_Y + H_C \quad (\text{A3.1})$$

Our TDHF equations are

$$i\hbar \frac{\partial}{\partial t} \psi_{\lambda q}(i, j, k) = h_q(i, j, k) \quad \text{where} \quad h_q(i, j, k) = \frac{\delta H}{\delta \psi_{\lambda q}^*(i, j, k)}. \quad (\text{A3.2})$$

We use a uniformly-spaced cartesian mesh within a rectangular box. Vanishing boundary conditions are imposed outside of this box and the separable approximation allows some simplification. We use a relatively large mesh spacing (typically 1 fm in all directions) because of computing time and storage considerations; so we need care to obtain an accurate representation of the energy functional.

We begin with the wavefunctions at each mesh point  $\psi_{\lambda q}(i, j, k)$ . Since  $\psi_{\lambda q} \equiv 0$  outside the box, we must be sure nothing gets too close to the edges. From these wavefunctions we calculate the proton and neutron densities at each mesh point

$$\rho_q(i, j, k) = \sum_{\lambda} |\psi_{\lambda q}(i, j, k)|^2 \quad (\text{A3.3})$$

Previous work has shown that the zero-range terms,  $H_Z$ , involving  $\tilde{t}_0$  and  $t_3$  are accurately discretized by a simple trapezoidal approximation to the integrals.

$$\int d\vec{\tau} \rho_q^2(\vec{\tau}) = \sum_{ijk} \rho_q^2(i, j, k) (\Delta x)^3 \quad (\text{A3.4})$$

and

$$\int d\vec{\tau} \rho_q^2(\vec{\tau}) \rho_q(\vec{\tau}) = \sum_{ijk} \rho_q^2(i, j, k) \rho_q(i, j, k) (\Delta x)^3 \quad (\text{A3.5})$$

Therefore, the discretized expression for  $H_Z$  is

$$H_Z = \sum_{ijk} \left\{ \frac{1}{2} \tilde{t}_0 \left[ \frac{1}{2} (1 - \tilde{\chi}_0) (\rho_p^2(i, j, k) + \rho_n^2(i, j, k)) + (2 + \tilde{\chi}_0) \rho_p(i, j, k) \rho_n(i, j, k) \right] + \frac{t_3}{4} (\rho_p(i, j, k) + \rho_n(i, j, k)) \rho_p(i, j, k) \rho_n(i, j, k) \right\} \quad (\text{A3.6})$$

## II. Kinetic Energy Term

The kinetic energy term,  $H_K$ , is more difficult because of the gradient operator. The treatment here is described in (FL 7B). Instead of first approximating  $\tau = |\nabla\psi|^2$  at each mesh point and then summing the contributions, it is more accurate to directly approximate the integral of  $\tau$  over each interval and sum these contributions. The difference in accuracy is shown by Taylor's expansions in the above reference. This method consists of approximating the integral

$$\frac{1}{2} \int_{x_1 - (\Delta x)}^{x_1 + (\Delta x)} dx \tau(x) = \frac{1}{2} (\tau^+ + \tau^-) (\Delta x) \quad (\text{A3.7})$$

where

$$\tau^\pm = |b_\mp \psi(i-1) + b_0 \psi(i) + b_\pm \psi(i+1)|^2 \quad (\text{A3.8})$$

with

$$b_0 = \frac{2}{\sqrt{3}} \frac{1}{(\Delta x)} \quad (\text{A3.9})$$

$$\text{and } b_\pm = \left( \frac{-1}{\sqrt{3}} \pm \frac{1}{2} \right) \frac{1}{(\Delta x)}$$

This approximation is the simplest of the most accurate group of formulas

involving only the points at  $i, i \pm 1$ . We can see that this is an application of Gauss' method, using the two points at  $i \pm \frac{1}{\sqrt{3}}$  with equal weightings =  $\frac{1}{2}$ , from the Taylor expansion for  $\tau$ .

$$\begin{aligned} b_{\mp}\psi(i-1)+b_0\psi(i)+b_{\pm}\psi(i+1) &= \pm\psi'(i) - \frac{(\Delta x)}{\sqrt{3}}\psi''(i) \pm \frac{(\Delta x)^2}{3!}\psi''' + \dots \quad (A3.10) \\ &= \pm\psi'(i - \frac{1}{\sqrt{3}}) \quad \text{with error=order } ((\Delta x)^3) \end{aligned}$$

Thus in 3D,

$$H_K = \frac{\hbar^2}{2m} \sum_{ijk} \frac{1}{2} [\tau_x^+(i, j, k) + \tau_x^-(i, j, k) + \tau_y^+(i, j, k) + \tau_y^-(i, j, k) + \tau_z^+(i, j, k) + \tau_z^-(i, j, k)] \quad (A3.11)$$

where

$$\tau_{qx}^{\mp}(i, j, k) = \sum_{\lambda} |b_{\mp}\psi_{\lambda q}(i-1, j, k) + b_0\psi_{\lambda q}(i, j, k) + b_{\pm}\psi_{\lambda q}(i+1, j, k)|^2 \quad (A3.12)$$

and  $\tau = \tau_{\rho} + \tau_n$ .

### III. Nonlocal Terms

The nonlocal term  $H_{NL}$  is the new feature, so its discretization is described in more detail. The fundamental quantity of interest is again the one-dimensional integral over an interval of  $\pm(\Delta x)$ . Just as for the kinetic energy, we first discretize the integral for each component of  $\tau$  and  $j$  in that direction and then perform a simple sum, like for the zero-range terms, in the directions not involving the differential operator.

We look at the general case  $\int dx fg$ . The Taylor expansion for the integral is then

$$\frac{1}{2} \int_{x_i - (\Delta x)}^{x_i + (\Delta x)} dx fg = (\Delta x) [fg + \frac{(\Delta x)^2}{3!} (f^2g + 2f'g' + fg^2) + \dots] |_{x=x_i} \quad (A3.13)$$

Once again we want to use a formula involving only the 3 points  $i, i \pm 1$ . The values of  $f$  and  $g$  at these points can also be expanded. We will find that the best formula is similar to that for  $\tau$ . We define  $f^{\pm} \approx f(x_i \pm \frac{\Delta x}{\sqrt{3}})$  and  $g^{\pm} \approx g(x_i \pm \frac{\Delta x}{\sqrt{3}})$

and approximate the integral

$$\frac{1}{2} \int_{x_i - (\Delta x)}^{x_i + (\Delta x)} dx f g = \frac{(\Delta x)}{2} (f^+(i)g^+(i) + f^-(i)g^-(i)) \quad (\text{A3.14})$$

If we try a simpler formula involving only one combination of  $f$ 's and  $g$ 's, our error will be order  $((\Delta x)^2)$ .

$$\begin{aligned} & (b_- f(i-1) + b_0 f(i) + b_+ f(i+1))(a_- g(i-1) + a_0 g(i) + a_+ g(i+1)) \quad (\text{A3.15}) \\ & = (b_- + b_0 + b_+)(a_- + a_0 + a_+) f(i)g(i) \\ & + (\Delta x)[(b_+ - b_-)(a_- + a_0 + a_+) f'(i)g(i) + (a_+ - a_-)(b_- + b_0 + b_+) f(i)g'(i)] \\ & + \frac{(\Delta x)^2}{2} [(b_+ + b_-)(a_- + a_0 + a_+) f^2(i)g(i) + 2(b_+ - b_-)(a_+ - a_-) f'(i)g'(i) \\ & + (a_+ + a_-)(b_- + b_0 + b_+) f(i)g^2(i) + \dots \end{aligned}$$

Thus, setting the first coefficient to 1 and the next two coefficients to 0 requires  $b_+ - b_- = 0 = a_+ - a_-$  and we can't match the middle term of order  $(\Delta x)^2$ . If we use two combinations, we can use symmetry to remove all odd powers of  $(\Delta x)$  just as in the expansion of the integral. We can then match all the terms of order  $(\Delta x)^2$  and be left with an error of order  $(\Delta x)^4$ . Because the odd powers have a factor  $(a_+ - a_-)$  we simply add two terms with  $a_+$  and  $a_-$  switched. (Each with weighting  $\frac{1}{2}$  and  $b$  from the previous formula replaced by  $a$ .) Thus, we eliminate all odd powers of  $(\Delta x)$  and are left with simple equations for the coefficients  $a$ .

$$(a_- + a_0 + a_+)^2 = 1 \quad (\text{A3.16})$$

Choosing  $(a_- + a_0 + a_+) = 1$  simplifies the other equations to become

$$\begin{aligned} (a_+ + a_-) &= \frac{1}{3} \quad (\text{A3.17}) \\ (a_+ - a_-) &= \pm \frac{1}{\sqrt{3}} \end{aligned}$$

Choosing the minus sign above gives

$$a_0 = \frac{2}{3} \quad a_{\mp} = \frac{1}{2} \left( \frac{1}{3} \pm \frac{1}{\sqrt{3}} \right) \quad (\text{A3.18})$$

Now if we substitute these coefficients into

$$f^{\mp} = a_{\mp} f(i-1) + a_0 f(i) + a_{\pm} f(i+1) \quad (\text{A3.19})$$

and do a Taylor's expansion, we see that we have derived an approximation for

$f(i \mp \frac{1}{\sqrt{3}})$  with error of order  $(\Delta x)^3$ .

$$f^{\mp} = f(i) + \frac{(\Delta x)}{\sqrt{3}} f'(i) + \frac{(\Delta x)^2}{2 \times 3} f''(i) + \dots \quad (\text{A3.20})$$

$$\approx f(i \mp \frac{1}{\sqrt{3}})$$

There is some ambiguity, however, to applying this rule to integrating functions of  $\psi$  from the values of  $\psi$  at the mesh points. For instance, in calculating the kinetic energy, we calculated  $\nabla\psi$  at the points  $\pm \frac{(\Delta x)}{\sqrt{3}}$  and then squared. We could also imagine using  $\nabla\psi$  at the mesh points, squaring and then interpolating to the points  $\pm \frac{(\Delta x)}{\sqrt{3}}$ . Of course, this would be foolish in this case since  $\nabla\psi$  isn't known at the mesh points. Calculating it at the points  $\pm(\Delta x)$  from the three allowed points,  $x_i, x_i \pm(\Delta x)$  would be less accurate than calculating it inside the interval, for instance at  $x_i \pm \frac{(\Delta x)}{\sqrt{3}}$ . This method would also require two successive numerical approximations and would be more complex. Thus, for both  $\tau$  and  $j$  we want to approximate the gradients directly at the relevant points  $\pm \frac{(\Delta x)}{\sqrt{3}}$ .

$$\tau^{\mp} = |b_{\mp}\psi(i-1) + b_0\psi(i) + b_{\pm}\psi(i+1)|^2 \quad (\text{A3.21})$$

and

$$j^{\mp} = \text{Im}[(a_{\mp}\psi(i-1) + a_0\psi(i) + a_{\pm}\psi(i+1)) \cdot (b_{\mp}\psi(i-1) + b_0\psi(i) + b_{\pm}\psi(i+1))] \quad (\text{A3.22})$$

For calculating  $\rho^{\mp}$  there is no clear difference between the accuracy of the methods

$$\rho^{\mp}(i) = a_{\mp}\rho(i-1) + a_0\rho(i) + a_{\pm}\rho(i+1) \quad (\text{A3.23})$$

$$\rho^{\mp}(i) = |a_{\mp}\psi(i-1) + a_0\psi(i) + a_{\pm}\psi(i+1)|^2 \quad (\text{A3.24})$$

However, since we are already calculating the densities at the mesh points (it is our primary result, in fact), and the resulting formulas for both the energy functional and the TDHF Hamiltonian will be much simpler (involving no cross terms

like  $\psi^*(i-1)\psi(i)$ , we interpolate the densities at the mesh points.

$$\rho^{\mp}(i) = a_{\mp} |\psi(i-1)|^2 + a_0 |\psi(i)|^2 + a_{\pm} |\psi(i+1)|^2 \quad (\text{A3.25})$$

Our 1-D approximation

$$\frac{1}{2} \int_{z_i - (\Delta x)}^{z_i + (\Delta x)} dx (\rho \tau_x - j_x^2) = \frac{1}{2} (\Delta x) (\rho^+ \tau_x^+ - j_x^{+2} + \rho^- \tau_x^- - j_x^{-2}) \quad (\text{A3.26})$$

becomes in 3-D

$$\int dz dy dx (\rho \tau_x - j_x^2) = (\Delta x)^3 R_x \quad (\text{A3.27})$$

where

$$R_{qq'x} = \frac{1}{2} \sum_{ijk} (\rho_{qx}^+(i,j,k) \tau_{q'x}^+(i,j,k) + \rho_{qx}^-(i,j,k) \tau_{q'x}^-(i,j,k) - j_{qx}^{+2}(i,j,k) j_{q'x}^+(i,j,k) - j_{qx}^{-2}(i,j,k) j_{q'x}^-(i,j,k)) \quad (\text{A3.28})$$

(We have included the  $x$  in  $\rho_x$  also since this determines the direction of the points  $\pm(\Delta x)$ .) We must also discretize the  $y$  and  $z$  components to form  $R_y$  and  $R_z$ . Then with

$$R = R_x + R_y + R_z \quad (\text{A3.29})$$

The net result is

$$H_{NL} = \left( \frac{t_1 + t_2}{4} \right) (R_{pn} + R_{np}) + \left( \frac{t_1 + 3t_2}{8} \right) (R_{pp} + R_{nn}) \quad (\text{A3.30})$$

We can simplify the expression for  $R$  considerably, since we used a linear combination of  $\rho(i,j,k)$  to make our  $\rho^{\mp}(i,j,k)$ , by rearranging the terms in the sum. In 1-D

$$\begin{aligned} \sum_i [\rho^+(i) \tau^+(i) + \rho^-(i) \tau^-(i)] &= \sum_i ([a_+ \rho(i-1) + a_0 \rho(i) + a_- \rho(i+1)] \tau^+(i) \\ &\quad + [a_- \rho(i-1) + a_0 \rho(i) + a_+ \rho(i+1)] \tau^-(i)) \\ &= \sum_i \rho(i) (a_+ \tau^+(i+1) + a_0 \tau^+(i) + a_- \tau^+(i-1) + a_- \tau^-(i+1) + a_0 \tau^-(i) + a_+ \tau^-(i-1)) \end{aligned} \quad (\text{A3.31})$$

In 3-D we rearrange the entire sum of  $\rho \tau$  terms

$$\frac{1}{2} \sum_{ijk} [\rho_x^+ \tau_x^+ + \rho_x^- \tau_x^- + \rho_y^+ \tau_y^+ + \rho_y^- \tau_y^- + \rho_z^+ \tau_z^+ + \rho_z^- \tau_z^-] = \sum_{ijk} \rho(i,j,k) \tau(i,j,k) \quad (\text{A3.32})$$

where

$$\tau(i, j, k) = \tau_x(i, j, k) + \tau_y(i, j, k) + \tau_z(i, j, k) \quad (\text{A3.33})$$

and

$$\begin{aligned} \tau_x(i, j, k) = & \frac{1}{2}(\alpha_- [\tau_x^-(i+1, j, k) + \tau_x^+(i-1, j, k)] \\ & + \alpha_0 [\tau_x^-(i, j, k) + \tau_x^+(i, j, k)] + \alpha_+ [\tau_x^+(i+1, j, k) + \tau_x^-(i-1, j, k)]) \end{aligned} \quad (\text{A3.34})$$

and  $\tau_y$  and  $\tau_z$  are similarly defined with the index  $j$  or  $k$ , respectively, varying  $\pm 1$ .

This means we only need two extra arrays  $\tau_q$  rather than  $\rho_q^{\mp}$  and  $\tau_q^{\mp}$  in all three directions. As we shall see later, this  $\tau_q$  is precisely what we need for the TDHF Hamiltonian. (Because  $\frac{\delta}{\delta \psi_{\lambda q}^*} \rho(i, j, k) = \psi_{\lambda q}(i, j, k)$ .)

#### IV. Coulomb and Yukawa Terms

The Coulomb and Yukawa energies are simply summed using the densities and the Coulomb and Yukawa potentials.

$$\begin{aligned} E_{Yqq} &= \sum_{ijk} \rho_q(i, j, k) U_{Yq}(i, j, k) (\Delta x)^3 \quad (\text{A3.35}) \\ H_Y &= \frac{V_L}{2} (E_{Ypp} + E_{Ynn}) + V_U E_{Ypn} \\ H_C &= \frac{1}{2} \sum_{ijk} \rho_p(i, j, k) U_{Cp}(i, j, k) (\Delta x)^3 \end{aligned}$$

These potentials,  $U$ , are calculated by the solution of discrete Poisson or Helmholtz problems with the conjugate gradient method as described in (FL 78). We also choose the boundary conditions zero for the short range Yukawa force resulting in a repulsion from the edges of the box which destroys energy conservation when the density approaches too near the edge. For the Coulomb boundary conditions, we use a multipole expansion including multipole moments of the mass and charge density through order 3. These are important to calculate anyway since they will be used to divide the density into two spherical fragments and calculate their mass and position at each time step. (See Appendix A7)

## Appendix A4: Finite Difference Form for the TDHF Equations in Space

### I. Introduction and Zero-Range Terms

The TDHF equations are partial differential equations in time and space. Since we need ordinary differential equations for numerical computations, we first need a spatial discretization of the equations, specifically for

$$h_q(i, j, k) = \frac{\delta}{\delta \psi_{\lambda q}^*(i, j, k)} H = h_{qZ} + h_{qK} + h_{qNL} + h_{qY} + h_{qC} \quad . \quad (A4.1)$$

Then we need to specify the time evolution algorithm.

We obtain our discretization by the variation of the discretized form of the energy functional with respect to the single-particle wavefunctions at the mesh points. Thus, our discretized equations will properly embody the conservation laws satisfied by the continuous equations, particularly energy conservation and the orthogonality of the single-particle wavefunctions. We first do the variations in 1-D and generalize to 3-D for which all directions are equivalent.

First, we calculate the zero-range piece of the TDHF Hamiltonian

$$h_{qZ} = \frac{\delta}{\delta \psi_{\lambda q}^*(i, j, k)} H_Z \quad (A4.2)$$

by varying the densities in Eq. (3.6)

$$\frac{\delta}{\delta \psi_{\lambda q}^*(i, j, k)} \left( \sum_{i'j'k'} \rho_q^2(i', j', k') \right) = 2\rho_q(i, j, k) \psi_{\lambda q}(i, j, k) \delta_{qq'} \quad (A4.3)$$

$$\frac{\delta}{\delta \psi_{\lambda q}^*(i, j, k)} \left( \sum_{i'j'k'} \rho_p(i', j', k') \rho_n(i', j', k') \right) = \rho_{q' \neq q}(i, j, k) \psi_{\lambda q}(i, j, k)$$

$$\frac{\delta}{\delta \psi_{\lambda q}^*(i, j, k)} \left( \sum_{i'j'k'} \rho(i', j', k') \rho_p(i', j', k') \rho_n(i', j', k') \right) = (\rho^2(i, j, k) - \rho_q^2(i, j, k)) \psi_{\lambda q}(i, j, k)$$

Therefore,

$$h_{qZ}(i, j, k) = \left[ \tilde{\chi}_0 \left[ (1 - \tilde{\chi}_0) \rho_q(i, j, k) + (2 + \tilde{\chi}_0) \rho_{q' \neq q}(i, j, k) \right] + \frac{\tilde{t}_9}{4} [\rho^2(i, j, k) - \rho_q^2(i, j, k)] \right] \psi_{\lambda q}(i, j, k) \quad (A4.4)$$

## II. Kinetic Energy Terms

Varying our expression for the kinetic energy (A3.7-9) gives a 5 point formula for the operator  $\nabla^2$  as in (FL 78).

$$\begin{aligned} \frac{\delta}{\delta\psi_k(i)} \sum_{i'} \frac{1}{2} [\tau^-(i') + \tau^+(i')] &= \frac{1}{2} \sum_{i'} [(b_-\delta_{i'-1} + b_0\delta_{i'} + b_+\delta_{i'+1})(b_-\psi_k(i'-1) + b_0\psi_k(i') + b_+\psi_k(i'+1)) \\ &\quad + (b_+\delta_{i'-1} + b_0\delta_{i'} + b_-\delta_{i'+1})(b_+\psi_k(i'-1) + b_0\psi_k(i') + b_-\psi_k(i'+1))] \\ &= \frac{1}{(\Delta x)^2} \left( \frac{1}{12}\psi_k(i-2) - \frac{4}{3}\psi_k(i-1) + \frac{5}{2}\psi_k(i) - \frac{4}{3}\psi_k(i+1) + \frac{1}{12}\psi_k(i+2) \right) \end{aligned} \quad (A4.5)$$

Thus, in 3-D

$$h_{qK}(i,j,k) = \frac{\hbar^2}{2m} \frac{1}{(\Delta x)^2} (K_{qx}(i,j,k) + K_{qy}(i,j,k) + K_{qz}(i,j,k)) \quad (A4.6)$$

where

$$\begin{aligned} K_{qx}(i,j,k) &= \frac{1}{12}\psi_{\lambda q}(i-2,j,k) - \frac{4}{3}\psi_{\lambda q}(i-1,j,k) \\ &\quad + \frac{5}{2}\psi_{\lambda q}(i,j,k) - \frac{4}{3}\psi_{\lambda q}(i+1,j,k) + \frac{1}{12}\psi_{\lambda q}(i+2,j,k) \end{aligned} \quad (A4.7)$$

and  $K_{qy}$  and  $K_{qz}$  are similarly defined with  $j$  or  $k$ , respectively, varying  $\pm 1$ .

## III. Nonlocal Terms

The nonlocal terms  $H_{NL}$ , Eq. (A3.27-34), are the new contribution. Since this discretization also involved only the points  $i, i \pm 1$  (like the kinetic energy), it also gives a 5 point formula in each direction. We begin with

$$\frac{\delta}{\delta\psi_k(i)} \sum_{i'} \rho(i') \tau(i') = \tau(i) \psi_k(i) + \sum_{i'} \rho(i') \frac{\delta}{\delta\psi_k(i)} \tau(i') \quad (A4.8)$$

From Eq. (A3.21), we get

$$\begin{aligned} \frac{\delta}{\delta\psi_k(i)} \tau(i') &= \frac{1}{2(\Delta x)^2} [\psi_k(i-2) \left( \frac{1}{36} (\delta_{i'+2} + 4\delta_{i'+1} + \delta_{i'}) \right) \\ &\quad + \psi_k(i-1) \left( \frac{1}{9} (\delta_{i'+2} - 13\delta_{i'+1} - 13\delta_{i'} + \delta_{i'-1}) \right) \\ &\quad + \psi_k(i) \left( \frac{1}{36} (-5\delta_{i'+2} + 44\delta_{i'+1} + 102\delta_{i'} + 44\delta_{i'-1} - 5\delta_{i'-2}) \right) \\ &\quad + \psi_k(i+1) \left( \frac{1}{9} (\delta_{i'+1} - 13\delta_{i'} - 13\delta_{i'-1} + \delta_{i'-2}) \right) + \psi_k(i+2) \left( \frac{1}{36} (\delta_{i'} + 4\delta_{i'-1} + \delta_{i'-2}) \right) \end{aligned} \quad (A4.9)$$

Therefore, the variation of the  $\rho\tau$  term gives

$$\frac{\delta}{\delta\psi_k^*(i)} \sum_{i'} \rho(i') \tau(i') = \quad (\text{A4.10})$$

$$\psi_k(i-2)A(i-1) + \psi_k(i-1)B(i) + \psi_k(i)C(i) + \psi_k(i+1)B(i+1) + \psi_k(i+2)A(i+1)$$

where

$$A(i) = \frac{1}{72(\Delta x)^2} (\rho(i-1) + 4\rho(i) + \rho(i+1)) \quad (\text{A4.11})$$

$$B(i) = \frac{1}{18(\Delta x)^2} (\rho(i-2) - 13\rho(i-1) - 13\rho(i) + \rho(i+1))$$

$$C(i) = \tau(i) + \frac{1}{72(\Delta x)^2} (-5\rho(i-2) + 44\rho(i-1) + 102\rho(i) + 44\rho(i+1) - 5\rho(i+2))$$

Now we must do the  $j^2$  term. From Eq. (A3.22), with reasoning like above, we get

$$\begin{aligned} \frac{\delta}{\delta\psi_k^*(i)} \frac{1}{2} \sum_{i'} (j^{+2}(i') + j^{-2}(i')) = & -i [\psi_k(i-2)D(i-1) + \psi_k(i-1)E(i) \\ & - \psi_k(i+1)E(i+1) - \psi_k(i+2)D(i+1)] \end{aligned} \quad (\text{A4.12})$$

where

$$D(i) = -\frac{1}{12(\Delta x)} [j^+(i) + j^-(i)] \quad (\text{A4.13})$$

$$E(i) = -\frac{1}{2(\Delta x)} [\gamma j^+(i) + \beta j^-(i) + \beta j^+(i-1) + \gamma j^-(i-1)]$$

and

$$\gamma = \left(-\frac{2}{3} + \frac{1}{\sqrt{3}}\right) \quad (\text{A4.14})$$

$$\beta = -\left(\frac{2}{3} + \frac{1}{\sqrt{3}}\right)$$

Thus, we see that the coefficients for the 5 points are complex functions of the densities and currents.

For the 3-D result, we need

$$\frac{\delta}{\delta\psi_{\lambda q}^*(i, j, k)} (R_{pp} + R_{nn}) \quad (\text{A4.15})$$

and

$$\frac{\delta}{\delta\psi_{\lambda q}^*(i, j, k)} (R_{pm} + R_{rp}) \quad (\text{A4.16})$$

The first, Eq. (A4.15), is straightforward since one term contributes

$\frac{\delta}{\delta\psi_{\lambda q}^*(i, j, k)} (\rho_q \tau_q - j_q^2)$  as previously discussed, and the other term is zero. We

can generalize the previous discussion to give

$$\begin{aligned} \frac{\delta}{\delta\psi_{\lambda q}^*}(R_{pp}+R_{nn}) &= \tau q_q(i,j,k) \\ &= \tau q_{qx}(i,j,k) + \tau q_{qy}(i,j,k) + \tau q_{qz}(i,j,k) \end{aligned} \quad (A4.17)$$

where

$$\begin{aligned} \tau q_{qx}(i,j,k) &= [A_{qx}(i-1,j,k) + iD_{qx}(i-1,j,k)]\psi_{\lambda q}(i-2,j,k) \\ &\quad + [B_{qx}(i,j,k) + iE_{qx}(i,j,k)]\psi_{\lambda q}(i-1,j,k) + C_{qx}(i,j,k)\psi_{\lambda q}(i,j,k) \\ &\quad + [B_{qx}(i+1,j,k) - iE_{qx}(i+1,j,k)]\psi_{\lambda q}(i+1,j,k) \\ &\quad + [A_{qx}(i+1,j,k) - iD_{qx}(i+1,j,k)]\psi_{\lambda q}(i+2,j,k) \end{aligned} \quad (A4.18)$$

The subscripts (x,y,z) in the coefficients give the index (i,j,k) respectively to vary and the component of  $\tau$  and  $j$  to use. For instance, using the definition of  $D(i)$  and  $A(i)$  from Eq. (A4.13 and 10),

$$\begin{aligned} D_{qx}(i,j,k) &= -\frac{1}{12}(\vec{j}_{qx}^+(i,j,k) + \vec{j}_{qx}^-(i,j,k)) \\ A_{qx}(i,j,k) &= \frac{1}{72(\Delta x)^2}(\rho_q(i-1,j,k) + 4\rho_q(i,j,k) + \rho_q(i+1,j,k)) \end{aligned} \quad (A4.19)$$

For the second term, Eq. (A4.16), we adopt the convention  $q' \neq q$

$$\frac{\delta}{\delta\psi_{\lambda q}^*}(R_{pn}+R_{np}) = \frac{\delta}{\delta\psi_{\lambda q}^*}(\rho_q\tau_{q'} + \rho_{q'}\tau_q - 2\vec{j}_q\vec{j}_{q'}) \quad (A4.20)$$

We can see that by adding the terms  $R_{qq'}$  and  $R_{q'q}$ , we have arrived at the same formula as for  $R_{qq}$  with one exception. The wavefunctions involved are precisely the same  $\psi_{\lambda q}$ , but the coefficients use  $q'$  rather than  $q$ . We call

$$\begin{aligned} \frac{\delta}{\delta\psi_{\lambda q}^*}(R_{pn}+R_{np}) &= \tau q'_q(i,j,k) \\ &= \tau q'_{qx}(i,j,k) + \tau q'_{qy}(i,j,k) + \tau q'_{qz}(i,j,k) \end{aligned} \quad (A4.21)$$

where

$$\begin{aligned} \tau q'_{qx}(i,j,k) &= [A_{q'z}(i-1,j,k) + iD_{q'z}(i-1,j,k)]\psi_{\lambda q}(i-2,j,k) \\ &\quad + [B_{q'z}(i,j,k) + iE_{q'z}(i,j,k)]\psi_{\lambda q}(i-1,j,k) + C_{q'z}(i,j,k)\psi_{\lambda q}(i,j,k) \\ &\quad + [B_{q'z}(i+1,j,k) - iE_{q'z}(i+1,j,k)]\psi_{\lambda q}(i+1,j,k) \\ &\quad + [A_{q'z}(i+1,j,k) - iD_{q'z}(i+1,j,k)]\psi_{\lambda q}(i+2,j,k) \end{aligned} \quad (A4.22)$$

Thus, the final result is

$$h_{qNL}(i,j,k) = \left(\frac{t_1+t_2}{4}\right)rq'_q(i,j,k) + \left(\frac{t_1+3t_2}{8}\right)rq_q(i,j,k) \quad \text{where } q' \neq q \quad (\text{A4.23})$$

We can see that since  $rq$  and  $rq'$  are linear in  $\rho, \tau, j$  we can evaluate  $h_{qNL}$  more easily by combining densities:

$$\left(\frac{t_1+t_2}{4}\right)\rho_{q'}(i,j,k) + \left(\frac{t_1+3t_2}{8}\right)\rho_q(i,j,k) = \tilde{\rho}_q(i,j,k) \quad (\text{A4.24})$$

and likewise for  $\tau$  and each component of  $j$ . We can use these densities in the formulas for the coefficients  $A, B, C, D$ , and  $E$  in the three directions to form  $\tilde{A}, \tilde{B}, \tilde{C}, \tilde{D}$ , and  $\tilde{E}$ , respectively, in the three directions. Applying these new coefficients to the formula for  $rq$  will give  $h_{qNL}$  directly while cutting the coefficients evaluated in half.

#### IV. Coulomb and Yukawa Terms

The variation for  $H_Y$  and  $H_C$  is straightforward as in previous work (FL 78). The discretized form of the potentials  $U(i,j,k)$  must be equivalent to a sum

$$U(i,j,k) = \sum_{i',j',k'} O(ii',jj',kk') \rho(i',j',k') \quad (\text{A4.25})$$

where  $O_Y$  is a discrete representation for  $\frac{\exp(-|\vec{r}-\vec{r}'|/\alpha)}{|\vec{r}-\vec{r}'|/\alpha}$  and  $O_C$  for  $\frac{e^2}{|\vec{r}-\vec{r}'|}$ .

Since the continuous functions  $O$  are symmetric in  $r$  and  $r'$ , the discrete representation must be also symmetric if we switch primed and unprimed.

Thus, from Eq. (A3.35) we get

$$\frac{\delta}{\delta\psi_{\lambda q}(i,j,k)} E_{Yq} = [U_{Yq'}(i,j,k)\delta_{qq'} + U_{Yq}(i,j,k)\delta_{qq'}] \psi_{\lambda q}(i,j,k) \quad (\text{A4.26})$$

We can see that these terms are also completely local. Therefore,

$$h_{Yq}(i,j,k) = [V_L U_{Yq}(i,j,k) + V_U U_{Yq+\tau q}(i,j,k)] \psi_{\lambda q}(i,j,k) \quad (\text{A4.27})$$

Similarly,

$$h_{Cqs}(i,j,k) = \frac{\delta}{\delta\psi_{\lambda q}(i,j,k)} H_C = U_{Cqs}(i,j,k) \psi_{\lambda q}(i,j,k) \delta_{qs} \quad (\text{A4.28})$$

## Appendix A5: Implementation of the Separable Approximation

### I. General Features

The main saving from using this approximation is, of course, that the wavefunctions which are evolved are only two dimensional. The discretized form of the separable ansatz is

$$\psi_{\lambda q}(i, j, \mathbf{k}, t) = \varphi_{\lambda q}(i, j, t) B_{\alpha}(k) \quad (\text{A5.1})$$

Evolving only the  $\varphi_{\lambda q}$  saves an order of magnitude in both storage and computing time. However, the entire problem is not two dimensional, and we need to keep many three dimensional quantities.

Using the separable ansatz, we can rewrite the particle, kinetic energy and current densities:

$$\rho_q(i, j, \mathbf{k}) = \sum_{\alpha} \rho_{q\alpha}(i, j) B_{\alpha}^2(k) \quad (\text{A5.2})$$

$$\tau_{qz}^{\mp}(i, j, \mathbf{k}) = \sum_{\alpha} \tau_{q\alpha z}^{\mp}(i, j) B_{\alpha}^2(k)$$

$$\tau_{qy}^{\mp}(i, j, \mathbf{k}) = \sum_{\alpha} \tau_{q\alpha y}^{\mp}(i, j) B_{\alpha}^2(k)$$

$$\tau_{qz}^{\mp}(i, j, \mathbf{k}) = \sum_{\alpha} \rho_{q\alpha}(i, j) D_{\alpha}^{\mp 2}(k)$$

$$j_{qz}^{\mp}(i, j, \mathbf{k}) = \sum_{\alpha} j_{q\alpha z}^{\mp}(i, j) B_{\alpha}^2(k)$$

$$j_{qy}^{\mp}(i, j, \mathbf{k}) = \sum_{\alpha} j_{q\alpha y} B_{\alpha}^2(k)$$

$$\text{and } j_{qz}^{\mp}(i, j, \mathbf{k}) = 0$$

The z current is zero since the  $|\varphi_{\lambda q}(i, j)|^2$  factors out and  $B_{\alpha}(k)$  are real. The new densities are:

$$\rho_{q\alpha}(i, j) = \sum_{\substack{\lambda \text{ with} \\ a(\lambda) = \alpha}} |\varphi_{\lambda q}(i, j)|^2 \quad (\text{A5.3})$$

$$\tau_{q\alpha z}^{\mp}(i, j) = \sum_{\substack{\lambda \text{ with} \\ a(\lambda) = \alpha}} |b_{\mp} \varphi_{\lambda q}(i-1, j) + b_0 \varphi_{\lambda q}(i, j) + b_{\pm} \varphi_{\lambda q}(i+1, j)|^2 \quad (\text{A5.4})$$

$$j_{q\alpha z}^{\mp}(i, j) = \sum_{\substack{\lambda \text{ with} \\ a(\lambda) = \alpha}} \text{Im} \left[ [a_{\mp} \varphi_{\lambda q}(i-1, j) + a_0 \varphi_{\lambda q}(i, j) + a_{\pm} \varphi_{\lambda q}(i+1, j)]^* \right. \\ \left. [b_{\mp} \varphi_{\lambda q}(i-1, j) + b_0 \varphi_{\lambda q}(i, j) + b_{\pm} \varphi_{\lambda q}(i+1, j)] \right] \quad (\text{A5.5})$$

with  $\tau_{q\alpha y}^{\mp}$  and  $j_{q\alpha y}^{\mp}$  the same except using  $j \pm 1$  instead of  $i \pm 1$  and

$$D_{\alpha}^{\mp}(k)=[b_{+}B_{\alpha}(k-1)+b_0B_{\alpha}(k)+b_{-}(k+1)]^2 \quad (\text{A5.6})$$

Some of the savings are very obvious. First,  $j_z^{\mp}$  is eliminated and, second,  $\tau_z^{\mp}$  becomes trivial since  $\rho_{q\alpha}(i,j)$  is already calculated and the  $D_{\alpha}^{\mp}(k)$  need be calculated only one time along with the basis functions  $B_{\alpha}(k)$ . The savings for the other densities are not as substantial since we need to store them separately for the different  $z$  quantum numbers,  $\alpha$ . This saves some storage since we use fewer numbers  $\alpha$  than points  $k$ , and saves more computing time since each density is summed only over wavefunctions with a particular  $z$  quantum number rather than over all wavefunctions. This fact also indicates that the most efficient grouping of wavefunctions is by the  $z$  quantum number.

The other quantities we need for the evaluation of the energy functional and TDHF Hamiltonian are the Yukawa and Coulomb potentials. These are calculated from the three-dimensional proton and neutron densities without any changes due to the separable ansatz, so we must still calculate these densities  $\rho_q(i,j,k)$ .

## II. Incorporation into the Energy Functional

Since we still calculate the proton and neutron densities, and the Coulomb and Yukawa potentials in three dimensions, the evaluation of the zero-range component,  $H_Z$ , and the Coulomb and Yukawa components,  $H_C$  and  $H_Y$ , is unaffected by the separable approximation.

$$H_Z = \sum_{ijk} \left[ \frac{\tilde{t}_0}{4} (1 - \tilde{\chi}_0) [\rho_p^2(i,j,k) + \rho_n^2(i,j,k)] + \tilde{t}_0 (1 + \frac{1}{2}\tilde{\chi}_0) \rho_p(i,j,k) \rho_n(i,j,k) \right. \\ \left. + \frac{t_3}{4} (\rho_p(i,j,k) + \rho_n(i,j,k)) \rho_p(i,j,k) \rho_n(i,j,k) \right] (\Delta x)^3 \quad (\text{A5.7})$$

$$H_C = \frac{1}{2} \sum_{ijk} \rho_p(i,j,k) U_C(i,j,k) (\Delta x)^3 \quad (\text{A5.8})$$

$$H_Y = \frac{V_L}{2} (E_{Ypp} + E_{Ynn}) + V_U E_{Ypn} \quad (\text{A5.9})$$

where

$$E_{Yqq} = \sum_{ijk} \rho_q(i,j,k) + U_{Yq}(i,j,k) (\Delta x)^3 \quad (\text{A5.10})$$

The kinetic energy term,  $H_K$ , is simplified. In the x direction,

$$\sum_{ijk} \tau_{qx}^{\mp}(i,j,k) = \sum_{\alpha} \sum_{ij} \tau_{q\alpha}^{\mp}(i,j) \frac{1}{(\Delta x)} \quad (A5.11)$$

since  $\sum_k B_{\alpha}^2(k)(\Delta x) = 1$ , and similarly for y. There is a slight savings because fewer orbitals  $\alpha$  are used than points k. In the z direction:

$$\sum_{ijk} \tau_{qz}^{\mp}(i,j,k) = N_{q\alpha} T_Z(\alpha) \quad (A5.12)$$

where

$$T_Z(\alpha) = (\Delta x) \sum_k \mathcal{H}_k [D_{\alpha}^{-2}(k) + D_{\alpha}^{+2}(k)] \quad (A5.13)$$

is the kinetic energy in the z direction for each basis state and

$$N_{q\alpha} = \sum_{ij} \rho_{q\alpha}(i,j) (\Delta x)^2 \quad (A5.14)$$

is the number of particles with isospin q and z quantum number  $\alpha$ . Now, the result is

$$H_K = \frac{\hbar^2}{2m} \sum_q \sum_{\alpha} \left\{ \frac{1}{2} \sum_{ij} [\tau_{q\alpha x}^{-} + \tau_{q\alpha x}^{+} + \tau_{q\alpha y}^{-} + \tau_{q\alpha y}^{+}] (\Delta x)^2 + N_{q\alpha} T_Z(\alpha) \right\} \quad (A5.15)$$

and the z component need be calculated only one time along with the basis functions.<sup>+</sup>

The nonlocal terms,  $H_{NL}$ , were given by Eqs. (A3.28-34). We look first at the  $\rho\tau$  terms and substitute the separable approximation. We can do the sums over k to form

$$BM(\alpha, \alpha') = \sum_k B_{\alpha}^2(k) B_{\alpha'}^2(k) (\Delta x) \quad (A5.16)$$

and

$$DM(\alpha, \alpha') = \sum_k D_{\alpha}(k) B_{\alpha'}^2(k) (\Delta x) \quad (A5.17)$$

where

<sup>+</sup> We don't actually calculate the total kinetic energy in this way, instead, we use the single particle energies  $\epsilon_{\lambda} = \langle \psi_{\lambda} | h | \psi_{\lambda} \rangle$ .  $ESPT = \sum_{\lambda} \epsilon_{\lambda}$  and  $ETOT = \langle \Psi | H | \Psi \rangle$ . Then  $ETOT = ESPT - EPOT - ET3$  where  $EPOT$  is the potential energy and  $ET3$  is the three-body term (triple counted in  $ESPT$ ). Therefore  $EKIN = ETOT - EPOT$ . The calculation of the  $\epsilon_{\lambda}$  is straightforward following the calculation of  $h\psi$  as discussed later in Appendix A6.

$$D_{\alpha}(k) = \alpha_{-}[D_{\alpha}^{-z}(k+1) + D_{\alpha}^{+z}(k-1)] + \alpha_0[D_{\alpha}^{-z}(k) + D_{\alpha}^{+z}(k)] \\ + \alpha_{+}[D_{\alpha}^{+z}(k+1) + D_{\alpha}^{-z}(k-1)] \quad (A5.18)$$

Then with

$$\tau_{q\alpha z}(i,j) = \alpha_{-}[\tau_{q\alpha z}^{-}(i+1,j) + \tau_{q\alpha z}^{+}(i-1,j)] \\ + \alpha_0[\tau_{q\alpha z}^{-}(i,j) + \tau_{q\alpha z}^{+}(i,j)] \\ + \alpha_{+}[\tau_{q\alpha z}^{+}(i+1,j) + \tau_{q\alpha z}^{-}(i-1,j)] \quad (A5.19)$$

and a similar expression for  $\tau_{q\alpha y}$ , we calculate

$$T_{q\alpha}(i,j) = \sum_{\alpha'} [\tau_{q\alpha z}(i,j) + \tau_{q\alpha y}(i,j)] BM(\alpha, \alpha') + \rho_{q\alpha}(i,j) DM(\alpha, \alpha') \quad (A5.20)$$

Once again, the z direction is only calculated once at the initial time. This quantity is stored since it will be useful for calculating  $h\psi$ . We can then write

$$\sum_{ijk} \rho_q(i,j,k) \tau_q(i,j,k) = \sum_{\alpha} \sum_{ij} \rho_{q\alpha}(i,j) T_{q\alpha}(i,j) (\Delta x)^2 \quad (A5.21)$$

We rewrite the j terms in a similar way, combining the functions of k and doing the sum over k. We form

$$J_{q\alpha}(i,j) = \sum_{\alpha'} j_{q\alpha'}(i,j) BM(\alpha, \alpha') \quad (A5.22)$$

and then

$$(\Delta x)^3 \sum_{ijk} j_q(i,j,k) j_{q'}(i,j,k) = (\Delta x)^2 \sum_{\alpha} \sum_{ij} j_{q\alpha}(i,j) J_{q'\alpha}(i,j) \quad (A5.23)$$

for each of the four currents (x or y) and (+ or -).

We store  $J_{q\alpha}(i,j)$  since it will be useful in calculating  $h\psi$ . However, we do not need  $j_{q\alpha}(i,j)$ , since we can do the sums needed to calculate the energy while constructing the  $J_{q\alpha}(i,j)$ . First, calculate the currents for each wavefunction,  $j_{\lambda q}$ . Therefore, for each wavefunction we can form the partial sums for each of the four currents

$$J_q^{\lambda}(i,j) = \sum_{\lambda'=1}^{\Lambda} j_{\lambda'q} BM(\alpha(\lambda), \alpha(\lambda')) \quad (A5.24)$$

We can write

$$E_{J_{qq}} = (\Delta x)^2 \sum_{\text{4 currents } ij} \sum_{\lambda} j_{\lambda q}(i,j) [j_{\lambda q}(i,j) BM(\alpha(\lambda), \alpha(\lambda)) + 2J_q^{\lambda-1}(i,j)] \quad (A5.25)$$

so that we can do the sum for  $E_{J_{qq}}$  without storing  $j_{\lambda q}(i,j)$ . For  $q' \neq q$  that is  $E_{pq}$ ,

the sum is simpler. Since we do all proton wavefunctions first, we have stored the full  $J_{p\alpha}(i,j)$ . We can then sum

$$E_{Jpn} = \sum_{\text{currents}} \sum_{ij} \sum_{\lambda} j_{\lambda n}(i,j) J_{p\alpha}(i,j) (\Delta x)^2 = E_{Jnp} \quad (\text{A5.26})$$

The total is then

$$\begin{aligned} H_{NL} = (\Delta x)^2 \sum_{ij} \sum_{\alpha} \left[ \left( \frac{t_1 + 3t_2}{8} \right) [\rho_{p\alpha}(i,j) T_{p\alpha}(i,j) + \rho_{n\alpha}(i,j) T_{n\alpha}(i,j)] \right. \\ \left. + \left( \frac{t_1 + t_2}{4} \right) [\rho_{n\alpha} T_{p\alpha}(i,j) + \rho_{p\alpha}(i,j) T_{n\alpha}(i,j)] \right] \\ - \left[ \left( \frac{t_1 + 3t_2}{8} \right) \frac{1}{2} (E_{Jpp} + E_{Jnn}) + \left( \frac{t_1 + t_2}{4} \right) \frac{1}{2} (E_{Jpn} + E_{Jnp}) \right] \end{aligned} \quad (\text{A5.27})$$

### III. Incorporation into the TDHF Hamiltonian

The discretized version of the TDHF equation is given in Appendix A4. The separable approximation gives:

$$i\hbar \frac{\partial}{\partial t} \varphi_{\lambda q}(i,j) = h'_{q\alpha}(i,j) \quad (\text{A5.28})$$

where

$$h'_{q\alpha}(i,j) = \sum_k B_{\alpha}(k) h_q(i,j,k) (\Delta x) \quad (\text{A5.29})$$

Notice that since the operator  $h'$  depends on  $\alpha$ , we have a second reason for grouping wavefunctions by their  $z$  quantum number.

The zero-range terms and the Coulomb and Yukawa potentials are very straightforward. First, these are all diagonal, that is

$$h(i,j,k) = f(i,j,k) \psi_{\lambda q}(i,j,k) \quad (\text{A5.30})$$

and, second, the function,  $f$ , is dependent on proton and neutron densities and Coulomb and Yukawa potentials, all of which are calculated in the full three dimensions, unaffected by the separable approximation. We, therefore, combine these elements

$$h_{qZ}(i,j,k) + h_{qY}(i,j,k) + h_{qC}(i,j,k) = f_q(i,j,k) \psi_{\lambda q}(i,j,k) \quad (\text{A5.31})$$

where

$$f_q(i,j,k) = \frac{1}{2}\tilde{\xi}_0(1-\tilde{\chi}_0)\rho_q(i,j,k) + \rho_{q' \neq q}(i,j,k) \quad (\text{A5.32})$$

$$[\tilde{\xi}_0(1+\frac{1}{2}\tilde{\chi}_0) + \frac{\xi_3}{4}(2\rho_q(i,j,k) + \rho_{q' \neq q}(i,j,k))] + V_L U_{Yq}(i,j,k) + V_Y U_{Yq' \neq q}(i,j,k) + U_{Qp}(i,j,k)\delta_{qp}$$

The effect of the separable approximation is to replace these  $h$  by

$$h'_{q\alpha}(i,j) = \sum_k B_\alpha^2(k) f_q(i,j,k) (\Delta x) \varphi_{\lambda q}(i,j) \quad (\text{A5.33})$$

resulting in a two-dimensional potential  $f'_{q\alpha}(i,j)$  for each set of wavefunctions with  $z$  quantum number  $\alpha$ .

The kinetic energy part  $h_{qK}$  gives a discretized approximation to the Laplacian,  $\nabla^2$ . Each direction involves off-diagonal elements in that direction only, so  $h_{qKx}(i,j,k)$  and  $h_{qKy}(i,j,k)$  are functions of  $i$  and  $j$  multiplied by  $B_\alpha(k)$ . This means the projections are trivial, since  $(\Delta x) \sum_k B_\alpha^2(k) = 1$ . We can write

$$h'_{qKx}(i,j) = \frac{\hbar^2}{2m} \frac{1}{(\Delta x)^2} \left[ \frac{1}{12} \varphi_{\lambda q}(i-2,j) - \frac{4}{3} \varphi_{\lambda q}(i-1,j) + \frac{5}{2} \varphi_{\lambda q}(i,j) - \frac{4}{3} \varphi_{\lambda q}(i+1,j) + \frac{1}{12} \varphi_{\lambda q}(i+2,j) \right] \quad (\text{A5.34})$$

and similarly for  $y$ . In the  $z$  direction,  $h'$  will be diagonal in  $i,j$ :

$$h'_{q\alpha Kz}(i,j) = \frac{\hbar^2}{2m} \frac{1}{(\Delta x)^2} \varphi_{\lambda q}(i,j) \sum_k B_\alpha(k) \left[ \frac{1}{12} B_\alpha(k-2) - \frac{4}{3} B_\alpha(k-1) + \frac{5}{2} B_\alpha(k) - \frac{4}{3} B_\alpha(k+1) + \frac{1}{12} B_\alpha(k+2) \right] (\Delta x) \quad (\text{A5.35})$$

and only  $h'_{q\alpha Kz}$  is dependent on the quantum number  $\alpha$ . Note: Although this would be quite easy to calculate, we don't actually use it. For the time evolution, we use an operator  $(h - \langle h \rangle)$  which would eliminate  $h'_{qKz}$ . For the single particle energies  $e_\lambda$ , we add a  $z$  kinetic energy to the  $\langle h \rangle$  above using the discretization for  $\int dz \left| \frac{dB_\alpha(z)}{dz} \right|^2$  as described earlier rather than the less accurate discretization of  $\int dz B_\alpha(z) \frac{d^2 B_\alpha(z)}{dz^2}$ . Therefore,

$$h'_{qK}(i,j) = h'_{qKx}(i,j) + h'_{qKy}(i,j) \quad (\text{A5.36})$$

independent of  $\alpha$ .

The new, nonlocal part,  $h_{qNL}$ , contributes non-constant off-diagonal pieces. For the separable approximation, in the x and y directions all the wavefunctions are  $\psi_{\lambda q}(i', j', k)$ , so we may form

$$A'_{qaz}(i, j) = \sum_k B_\alpha^2(k) \tilde{A}_{qz}(i, j, k) (\Delta x) \quad (A5.37)$$

and similarly form B', C', D' and E' in these two directions. In the z direction, all the wavefunctions involve  $\psi_{\lambda q}(i, j, k')$  so the terms are diagonal in the separable approximation. Of course since  $j_z = 0$ ,  $\tilde{D}_z = \tilde{E}_z = 0$ .

Looking first at the off-diagonal terms, for a particular  $\alpha$  we calculate

$$\tilde{P}_{q\alpha}(i, j) = (\Delta x) \sum_k B_\alpha^2(k) \tilde{\rho}_q(i, j, k) = \sum_{\alpha'} \tilde{\rho}_{q\alpha'} BM(\alpha, \alpha') \quad (A5.38)$$

and then calculate the needed coefficients:

$$A'_{qaz}(i, j) = \frac{1}{72(\Delta x)^2} [\tilde{P}_{q\alpha}(i-1, j) + 4\tilde{P}_{q\alpha}(i, j) + \tilde{P}_{q\alpha}(i+1, j)] \quad (A5.39)$$

and

$$B'_{qaz}(i, j) = \frac{1}{18(\Delta x)^2} [\tilde{P}_{q\alpha}(i-2, j) - 13\tilde{P}_{q\alpha}(i-1, j) - 13\tilde{P}_{q\alpha}(i, j) + \tilde{P}_{q\alpha}(i+1, j)] \quad (A5.40)$$

with similar equations for the y direction. To calculate D' and E', we need the analogous sum

$$J_{q\alpha}(i, j) = \sum_{\alpha'} j_{q\alpha'}(i, j) BM(\alpha, \alpha') \quad (A5.41)$$

which was mentioned in the last chapter and stored. Thus with

$$\tilde{J}_{q\alpha} = \left(\frac{t_1+t_2}{4}\right) J_{q' \neq q\alpha} + \left(\frac{t_1+3t_2}{8}\right) J_{q\alpha} \quad (A5.42)$$

we get

$$D'_{qaz}(i, j) = -\frac{1}{12(\Delta x)} [\tilde{J}_{qaz}^+(i, j) + \tilde{J}_{qaz}^-(i, j)] \quad (A5.43)$$

and

$$E'_{q\alpha z}(i,j) = -\frac{1}{2(\Delta x)} [\gamma \tilde{J}_{q\alpha z}^+(i,j) + \beta \tilde{J}_{q\alpha z}^-(i,j) + \beta \tilde{J}_{q\alpha z}^+(i-1,j) + \gamma \tilde{J}_{q\alpha z}^-(i-1,j)] \quad (A5.44)$$

The diagonal part is given by

$$G_{q\alpha}(i,j)\varphi_{\lambda q}(i,j) = [C'_{q\alpha z}(i,j) + C'_{q\alpha y}(i,j) + h'_{q\alpha NLz}(i,j)]\varphi_{\lambda q}(i,j) \quad (A5.45)$$

where

$$h'_{q\alpha NLz}(i,j) = (\Delta x) \sum_k B_\alpha^2(k) \tilde{t}_z(i,j,k) + \sum_{\alpha'} \tilde{\rho}_{q\alpha'}(i,j) PM(\alpha, \alpha') \quad (A5.46)$$

and

$$PM(\alpha, \alpha') = (\Delta x) \sum_k B_\alpha(k) \left\{ \frac{1}{72(\Delta x)^2} [B_\alpha \alpha'^2(k-2) + 4B_\alpha \alpha'^2(k-1) + B_\alpha \alpha'^2(k)] B_\alpha(k-2) + \frac{1}{18(\Delta x)^2} [B_\alpha \alpha'^2(k-2) - 13B_\alpha \alpha'^2(k-1) - 13B_\alpha \alpha'^2(k) + B_\alpha \alpha'^2(k+1)] B_\alpha(k-1) + \frac{1}{72(\Delta x)^2} [-5B_\alpha \alpha'^2(k-2) + 44B_\alpha \alpha'^2(k-1) + 102B_\alpha \alpha'^2(k) + 44B_\alpha \alpha'^2(k+1) - 5B_\alpha \alpha'^2(k+2)] B_\alpha(k) + \frac{1}{18(\Delta x)^2} [B_\alpha \alpha'^2(k-1) - 13B_\alpha \alpha'^2(k) - 13B_\alpha \alpha'^2(k+1) + B_\alpha \alpha'^2(k+2)] B_\alpha(k+1) + \frac{1}{72(\Delta x)^2} [B_\alpha \alpha'^2(k) + 4B_\alpha \alpha'^2(k+1) + B_\alpha \alpha'^2(k+2)] B_\alpha(k+2) \right\} \quad (A5.47)$$

This matrix  $PM$  need be calculated only once along with the basis  $B_\alpha$ . The first term can be combined with the  $\tau$  terms from  $C'_z$  and  $C'_y$  to give

$$\begin{aligned} \tilde{T}_{q\alpha}(i,j) &= (\Delta x) \sum_k B_\alpha^2(k) \tilde{t}(i,j,k) \\ &= \left(\frac{t_1+t_2}{4}\right) T_{q' \neq q\alpha}(i,j) + \left(\frac{t_1+t_2}{4}\right) T_{q\alpha}(i,j) \end{aligned} \quad (A5.48)$$

using the  $T_{q\alpha}$  as defined in the last section and stored. Thus, we can write the entire diagonal part

$$\begin{aligned}
 G_{q\alpha}(i,j) &= \tilde{T}_{q\alpha}(i,j) + \sum_{\alpha'} \tilde{\rho}_{q\alpha'}(i,j) PM(\alpha, \alpha') & (A5.49) \\
 &+ \frac{1}{72(\Delta x)^2} [-5\tilde{P}_{q\alpha}(i-2,j) + 44\tilde{P}_{q\alpha}(i-1,j) \\
 &+ 102\tilde{P}_{q\alpha}(i,j) + 44\tilde{P}_{q\alpha}(i+1,j) - 5\tilde{P}_{q\alpha}(i+2,j) \\
 &- 5\tilde{P}_{q\alpha}(i,j-2) + 44\tilde{P}_{q\alpha}(i,j-1) + 102\tilde{P}_{q\alpha}(i,j) + 44\tilde{P}_{q\alpha}(i,j+1) - 5\tilde{P}_{q\alpha}(i,j+2)]
 \end{aligned}$$

Then, the final result for the nonlocal term is

$$\begin{aligned}
 h'_{q\alpha NL}(i,j) &= G_{q\alpha}(i,j) \varphi_{\lambda q}(i,j) & (A5.50) \\
 &+ [A'_{q\alpha x}(i-1,j) + iD'_{q\alpha x}(i-1,j)] \varphi_{\lambda q}(i-2,j) + [A'_{q\alpha y}(i,j-1) + iD'_{q\alpha y}(i,j-1)] \varphi_{\lambda q}(i,j-2) \\
 &\quad + [B'_{q\alpha x}(i,j) + iE'_{q\alpha x}(i,j)] \varphi_{\lambda q}(i-1,j) + [B'_{q\alpha y}(i,j) + iE'_{q\alpha y}(i,j)] \varphi_{\lambda q}(i,j-1) \\
 &+ [B'_{q\alpha x}(i+1,j) - iE'_{q\alpha x}(i+1,j)] \varphi_{\lambda q}(i+1,j) + [B'_{q\alpha y}(i,j+1) - iE'_{q\alpha y}(i,j+1)] \varphi_{\lambda q}(i,j+1) \\
 &+ [A'_{q\alpha x}(i+1,j) - iD'_{q\alpha x}(i+1,j)] \varphi_{\lambda q}(i+2,j) + [A'_{q\alpha y}(i,j+1) - iD'_{q\alpha y}(i,j+1)] \varphi_{\lambda q}(i,j+2)
 \end{aligned}$$

and the total discrete representation of  $h\psi$  is

$$h'_{q\alpha}(i,j) = f'_{q\alpha}(i,j) \varphi_{\lambda q}(i,j) + h'_{qK}(i,j) + h'_{q\alpha NL}(i,j) \quad (A5.51)$$

(neglecting the  $\nabla_x^2$  operator).

## Appendix A6: Discretization of the TDHF Equations in Time

### I. Introduction and Statement of the Problem

The evolution of the TDHF wavefunctions,  $\psi_{\lambda q}$ , is given by

$$i\hbar \left( \frac{\partial}{\partial t} \right) \psi_{\lambda q} = h_q \psi_{\lambda q} \quad (\text{A6.1})$$

where  $\psi_{\lambda q} = \psi_{\lambda q}(x, y, z, t)$  in three-dimensional calculations (or  $\psi_{\lambda q}(x, y, t)$  in the separable approximation) and  $h$  is a hermitian operator,  $h = h(x, x', y, y', z, z', t)$  (or  $h(x, x', y, y', t)$  in the separable approximation). For the rest of this appendix, all dependence except time will be suppressed. This equation is formally solved by using time evolution operator,  $U_q$ , as

$$\psi_{\lambda q} = U_q(t, t_0) \psi_{\lambda q}(t_0) \quad (\text{A6.2})$$

where  $U_q$  is the unitary operator

$$U_q(t, t_0) = T \exp \left[ \left( \frac{-i}{\hbar} \right) \int_{t_0}^t dt' h_q(t') \right] \quad (\text{A6.3})$$

with  $T$  the time ordering operator. Discretization defines a time mesh  $t_m = (m)\Delta t$  where  $(m)$  is an integer and calculates  $\psi_{\lambda q}$  at each time step from

$$\psi_{\lambda q}(m+1) = U_q(m+1, m) \psi_{\lambda q}(m) \quad (\text{A6.4})$$

This discrete evolution operator can be written as

$$U_q(m+1, m) = \exp \left[ \left( \frac{-i}{\hbar} \right) \Delta t h_q(m+\frac{1}{2}) \right] \quad (\text{A6.5})$$

where  $h_q(m+\frac{1}{2})$  must represent the average effect of  $h(t')$  over the interval  $t$  to  $t+\Delta t$ . Thus, determination of the correct operator  $h_q(m+\frac{1}{2})$  accomplishes the discretization in time. An obvious possibility,  $h_q(m+\frac{1}{2}) = \frac{1}{2}(h_q(m) + h_q(m+1))$  is very close to the operator we use.

Part II of this appendix compares the Taylor expansions in  $\Delta t$  for exact and discrete solutions. This procedure determines an arbitrarily accurate approximation for  $h_q(m+\frac{1}{2})$  as a function of  $h_q$ ,  $\psi_{\lambda q}$ ,  $\psi_{\lambda q}^*$ , and functional derivatives of  $h_q$  with respect to  $\psi$  and  $\psi^*$ ; but, of course, the higher-order terms are very

cumbersome to calculate. Therefore, this expression for  $h_q(m+\frac{1}{2})$  is not used in the actual evolution code. Instead, it is used to estimate the error arising from other choices for  $h_q(m+\frac{1}{2})$ .

These other choices use the values of  $h$ ,  $\psi$ , and  $\psi^*$  at various discrete time steps, rather than derivatives or functional derivatives. We use a two point formula involving the time steps  $(m)$  and  $(m+1)$ . With only two points, this approximation can match only the first two terms in the exact expansion for  $h_q(m+\frac{1}{2})$ . This results in an error of order  $\Delta t^2$  for  $h_q(m+\frac{1}{2})$ ; or order  $\Delta t^3$  for  $U_q(m+1, m)$  (since the first order term is 1). There is an ambiguity in this two point formula since changing terms of order  $\Delta t^2$  or higher won't change the order of the error. This ambiguity is resolved by choosing the higher-order terms to conserve energy.

Part III of this appendix calculates the energy difference  $E(m+1)-E(m)$  and expresses it in terms of a single-particle operator  $O_q$  as

$$E(m+1)-E(m)=\sum_{\lambda q}[\psi_{\lambda q}^*(m+1)O_q\psi_{\lambda q}(m+1)-\psi_{\lambda q}^*(m)O_q\psi_{\lambda q}(m)] \quad (A6.6)$$

This means that

$$\Delta E=\sum_{\lambda q}\psi_{\lambda q}^*(m)[U_q^+O_qU_q-O_q]\psi_{\lambda q}(m) \quad (A6.7)$$

(where  $U$  is the evolution operator as before) and energy is conserved if  $[U_q, O_q]=0$  From Eq. (A6.4), choosing  $h_q(m+\frac{1}{2})=O_q$  conserves energy. Part III also checks that the operator  $h_q(m+\frac{1}{2})$  determined this way matches the expansion through order  $\Delta t$  as expected for the best two point formula. These calculations are based on those of (FL 7B).

A problem with choosing  $h_q(m+\frac{1}{2})$  to depend on quantities at time steps  $(m)$  and  $(m+1)$  is that the quantities at step  $(m+1)$  are not yet known (they depend on  $h_q(m+\frac{1}{2})$ ). Part IV of this appendix discusses the algorithm used to achieve this self-consistency and other details of the actual evolution code. This kind of

self-consistency is necessary because the simplest guess  $h_q(m+\frac{1}{2})=h_q(m)$  doesn't work. This operator would evolve  $\psi_{\lambda q}$  in a potential always lagging behind its proper position. This gradually slows motion and results in a continuous decrease in energy.

## II. Comparison of Taylor Expansions for the Exact and Discrete Solutions

The exact solution at  $t+\Delta t$  can be expanded as

$$\psi_{\lambda q}(t+\Delta t)=\psi_{\lambda q}(t)+\Delta t\left(\frac{\partial}{\partial t}\right)\psi_{\lambda q}+\frac{\Delta t^2}{2}\left(\frac{\partial}{\partial t}\right)^2\psi_{\lambda q}+\dots \quad (\text{A6.8})$$

where the exact solution obeys the TDHF equation and  $h=h(t)$  because  $h$  is a function of  $\psi_{\lambda q}(t)$ . The various derivatives of  $\psi_{\lambda q}$  can be written exactly in terms of derivatives of  $h$  as

$$\left(\frac{\partial}{\partial t}\right)\psi_{\lambda q}=\left(\frac{-i}{\hbar}\right)h_q\psi_{\lambda q} \quad (\text{A6.9})$$

$$\left(\frac{\partial}{\partial t}\right)^2\psi_{\lambda q}=\left[\left(\frac{-i}{\hbar}\right)^2h_q^2+\left(\frac{-i}{\hbar}\right)\left(\frac{\partial}{\partial t}\right)h_q\right]\psi_{\lambda q}$$

etc.

The time derivatives of  $h$  can be written exactly in terms of functional derivatives as

$$\left(\frac{\partial}{\partial t}\right)h_q=\sum_{\lambda q'}\left[\left(\frac{\delta}{\delta\psi_{\lambda q'}}\right)h_q\right]\left(\frac{\partial}{\partial t}\right)\psi_{\lambda q'}+\left[\frac{\delta}{\delta\psi_{\lambda q'}^*}\right]_{right}h_q\left(\frac{\partial}{\partial t}\right)\psi_{\lambda q'}^* \quad (\text{A6.10})$$

$$=\left(\frac{-i}{\hbar}\right)\sum_{\lambda q'}\left[\left(\frac{\delta}{\delta\psi_{\lambda q'}}\right)h_q\right]h_q\psi_{\lambda q'}-\left[\frac{\delta}{\delta\psi_{\lambda q'}^*}\right]h_q\psi_{\lambda q'}^*$$

$$\left(\frac{\partial}{\partial t}\right)^2h_q=\left(\frac{-i}{\hbar}\right)\sum_{\lambda q'}\left[\frac{\delta}{\delta\psi_{\lambda q'}}\left[\left(\frac{\partial}{\partial t}\right)h_q\right]h_q\psi_{\lambda q'}-\frac{\delta}{\delta\psi_{\lambda q'}^*}\left[\left(\frac{\partial}{\partial t}\right)h_q\right]h_q\psi_{\lambda q'}^*\right]$$

etc.

The discrete TDHF solution is given by

$$\psi_{\lambda q}(m+1)=\exp\left[\left(\frac{-i}{\hbar}\right)\Delta t h_q\left(m+\frac{1}{2}\right)\right]\psi_{\lambda q}(m) \quad (\text{A6.11})$$

In the expansion,  $h_q(m+\frac{1}{2})$  is time dependent, involving  $h$  at future times

$$h_q\left(m+\frac{1}{2}\right)=f_0+\Delta t f_1+\frac{\Delta t^2}{2}f_2+\dots \quad (\text{A6.12})$$

The net result is

$$\psi_{\lambda_q}(m+1) = \psi_{\lambda_q}(m) + \Delta t \left( \frac{-i}{\hbar} \right) f_0 \psi_{\lambda_q}(m) + \Delta t^2 \left[ \frac{1}{2} \left( \frac{-i}{\hbar} \right)^2 f_0^2 + \left( \frac{-i}{\hbar} \right) f_1 \right] \psi_{\lambda_q}(m) + \dots \quad (\text{A6.13})$$

Matching this to the exact solution determines the operators  $f_i$ ; and gives  $h_q(m+\frac{1}{2})$  accurate to any order. The first-order terms give

$$f_0 = h_q(t) \quad (\text{A6.14})$$

The second-order terms give

$$f_1 = \frac{1}{2} \left( \frac{\partial}{\partial t} \right) h_q |_t \quad (\text{A6.15})$$

The third-order terms give

$$f_2 = \frac{1}{3} \left( \frac{\partial}{\partial t} \right)^2 h_q - \frac{1}{6} \left( \frac{-i}{\hbar} \right) [h_q \left( \frac{\partial}{\partial t} \right) h_q - \left( \left( \frac{\partial}{\partial t} \right) h_q \right) h_q] \quad (\text{A6.16})$$

The fourth-order terms give

$$f_3 = \frac{1}{4} \left( \frac{\partial}{\partial t} \right)^3 h_q - \frac{1}{4} \left( \frac{-i}{\hbar} \right) [h_q \left( \frac{\partial}{\partial t} \right)^2 h_q - \left( \left( \frac{\partial}{\partial t} \right)^2 h_q \right) h_q] \quad (\text{A6.17})$$

etc.

So now given  $h_q$  and  $\psi_{\lambda_q}$ , we can compute the operator  $h_q(m+\frac{1}{2})$  and compute to any order  $\psi_{\lambda_q}(m+1)$ . However, we want to derive an approximate formula based on  $h_q(m)$  and  $h_q(m+1)$ . The easiest way is to look for conservation of energy.

### III. Derivation of the Discrete Evolution Operator from Energy Conservation

Defining

$$\delta \rho_q = \rho_q(m+1) - \rho_q(m), \quad \delta \tau_q = \tau_q(m+1) - \tau_q(m), \quad \delta \vec{j}_q = \vec{j}_q(m+1) - \vec{j}_q(m), \quad (\text{A6.18})$$

and taking  $E(m) = \langle H \rangle$  from Eq. (2.7) or (A2.29), the energy difference between two time steps can be written

(A6.19)

$$\begin{aligned}
 E(m+1)-E(m) = & \int dx \left[ \frac{\hbar^2}{2m} [\delta\tau_p + \delta\tau_n] + \frac{T_{0L}}{2} \{ \delta\rho_p [\rho_p(m+1) + \rho_p(m)] + \delta\rho_n [\rho_n(m+1) + \rho_n(m)] \} \right. \\
 & + \frac{T_{0Y}}{2} \{ \delta\rho_p [\rho_n(m+1) + \rho_n(m)] + \delta\rho_n [\rho_p(m+1) + \rho_p(m)] \} \\
 & + T_3 \{ \delta\rho_p [ \frac{2}{3}\rho_p(m+1)\rho_n(m+1) + \frac{1}{3}\rho_p(m+1)\rho_n(m) + \frac{1}{3}\rho_p(m)\rho_n(m+1) + \frac{2}{3}\rho_p(m)\rho_n(m) \\
 & \quad + \frac{1}{3}\rho_n^2(m+1) + \frac{1}{3}\rho_n(m+1)\rho_n(m) + \frac{1}{3}\rho_n^2(m) ] \\
 & + \delta\rho_n [ \frac{2}{3}\rho_p(m+1)\rho_n(m+1) + \frac{1}{3}\rho_p(m+1)\rho_n(m) + \frac{1}{3}\rho_p(m)\rho_n(m+1) + \frac{2}{3}\rho_p(m)\rho_n(m) \\
 & \quad + \frac{1}{3}\rho_p^2(m+1) + \frac{1}{3}\rho_p(m)\rho_p(m+1) + \frac{1}{3}\rho_p^2(m) ] \} \\
 & + \frac{C_L}{2} \{ \delta\rho_p [\tau_p(m+1) + \tau_p(m)] + \delta\tau_p [\rho_p(m+1) + \rho_p(m)] \\
 & \quad + \delta\rho_n [\tau_n(m+1) + \tau_n(m)] + \delta\tau_n [\rho_n(m+1) + \rho_n(m)] \\
 & \quad - \delta\vec{j}_p [\vec{j}_p(m+1) + \vec{j}_p(m)] \} \\
 & + \frac{c_Y}{2} \{ \delta\rho_p [\tau_n(m+1) + \tau_n(m)] + \delta\rho_n [\tau_p(m+1) + \tau_p(m)] \\
 & \quad + \delta\tau_p [\rho_n(m+1) + \rho_n(m)] + \delta\tau_n [\rho_p(m+1) + \rho_p(m)] \\
 & \quad - 2\delta\vec{j}_p [\vec{j}_n(m+1) + \vec{j}_n(m)] - 2\delta\vec{j}_n [\vec{j}_p(m+1) + \vec{j}_p(m)] \} \\
 & + \frac{V_L}{2} \{ \delta\rho_p [U_{Yp}(m+1) + U_{Yp}(m)] + \delta\rho_n [U_{Yn}(m+1) + U_{Yn}(m)] \} \\
 & + \frac{V_Y}{2} \{ \delta\rho_p [U_{Yn}(m+1) + U_{Yn}(m)] + \delta\rho_n [U_{Yp}(m+1) + U_{Yp}(m)] \} \\
 & \quad + \delta\rho_p \frac{1}{2} [U_C(m+1) + U_C(m)] \}
 \end{aligned}$$

We would like to write this difference in energy as

$$\psi_{\lambda q}^*(m+1) O_q \psi_{\lambda q}(m+1) - \psi_{\lambda q}^*(m) O_q \psi_{\lambda q}(m) \quad (A6.20)$$

to choose an evolution operator which conserves energy. Since

$\psi_{\lambda q}(m+1) = U_q \psi_{\lambda q}(m)$ , the energy difference can then be expressed as

$$\Delta E = \psi_{\lambda q}^*(m) (U_q^\dagger O_q U_q - O_q) \psi_{\lambda q}(m) \quad (A6.21)$$

Thus, for any  $U_q$  which commutes with  $O_q$  energy is conserved exactly. Since we

have  $U_q = \exp((\frac{-i}{\hbar}) \Delta t h_q(m+\frac{1}{2}))$ , choosing  $h_q(m+\frac{1}{2}) = O_q$  conserves energy.

$$\delta\rho_q = \sum_{\lambda} [ |\psi_{\lambda q}(m+1)|^2 - |\psi_{\lambda q}(m)|^2 ] \quad (A6.22)$$

Therefore,

$$O_q = 1 \quad (\text{A6.23})$$

Similarly, for  $\delta\rho_q F(\tau)$

$$O_q = F(\tau) \quad (\text{A6.24})$$

For  $\delta\tau_q$  and  $\delta\vec{j}_q$  the calculation requires integrating by parts as in Section 2.

Therefore,

$$\int d\tau \delta\tau_q(\tau) F(\tau) \text{ yields } O_q = -\vec{\nabla} \cdot F \vec{\nabla} \quad (\text{A6.25})$$

where  $\vec{\nabla}$  operates on everything to the right, and

$$\int d\tau \delta\vec{j}_q(\tau) F(\tau) \text{ yields } O_q = \frac{F \vec{\nabla} + \vec{\nabla} F}{2i} \quad (\text{A6.26})$$

Applying these Eqs. (A6.22-25), we rewrite the energy difference as

$$\Delta E = \int d\tau \sum_{\lambda q} [\psi_{\lambda q}^*(m+1) O_q \psi_{\lambda q}(m+1) - \psi_{\lambda q}^*(m) O_q \psi_{\lambda q}(m)] \quad (\text{A6.27})$$

where with the exception of the three-body  $T_3$  terms;

$$O_q = \frac{1}{2} [\tilde{h}_q(m+1) + \tilde{h}_q(m)] = \tilde{h}_q \quad (\text{A6.28})$$

with

$$\tilde{h}_q = h(\rho_q = \frac{1}{2}[\rho_q(m+1) + \rho_q(m)], \tau_q = \frac{1}{2}[\tau_q(m+1) + \tau_q(m)], \vec{j}_q = \frac{1}{2}[\vec{j}_q(m+1) + \vec{j}_q(m)]) \quad (\text{A6.29})$$

The three-body terms are

$$T_3 O_q^3 = T_3 \left[ \frac{1}{3} \rho_q^2(m+1) + \frac{1}{3} \rho_q'(m) \rho_q(m+1) + \frac{1}{3} \rho_q^2(m) \right. \\ \left. + \frac{2}{3} \rho_q(m+1) \rho_q'(m+1) + \frac{1}{3} \rho_q(m+1) \rho_q'(m) + \frac{1}{3} \rho_q(m) \rho_q'(m+1) + \frac{2}{3} \rho_q(m) \rho_q'(m) \right] \quad (\text{A6.30})$$

where  $q' \neq q$ . Since we will use  $\tilde{h}_q$ , that is a calculation of the discretized version of  $h$  for the average densities of the two time steps, we must calculate the correction  $\tilde{C}_q$ , due to three-body forces  $O_q = \tilde{h}_q + \tilde{C}_q$ .

$$\tilde{C}_q = T_3 [O_q^3 - (2\frac{1}{2}[\rho_q(m+1) + \rho_q(m)] \frac{1}{2}[\rho_q'(m+1) + \rho_q'(m)] + [\frac{1}{2}[\rho_q'(m+1) + \rho_q'(m)]]^2) \\ = \frac{T_3}{12} [(\delta\rho_q)^2 + 2\delta\rho_q \delta\rho_{q'}] \quad (\text{A6.31})$$

Thus, choosing  $h_q(m+\frac{1}{2}) = \tilde{h}_q + \tilde{C}_q$  conserves energy exactly, but how accurately does this operator approximate the TDHF evolution?

To check this, we write  $O_q$  as

$$O_q = h_q(m + \frac{1}{2}) = \frac{1}{2}[h_q(m+1) + h_q(m)] + C_q \quad (\text{A6.32})$$

with a different correction term, where again  $C_q$  only involves three-body terms,  $T_3$ .

$$C_q = -\frac{T_3}{6}[(\delta\rho_q)^2 + 2\delta\rho_q\delta\rho_{q'}] \quad (\text{A6.33})$$

Now we can expand

$$\delta\rho_q = \Delta t \frac{d\rho_q}{dt} + \dots \quad (\text{A6.34})$$

and

$$h_q(m+1) = h_q(m) + \Delta t \frac{dh_q}{dt} + \frac{\Delta t^2}{2} \frac{d^2h_q}{dt^2} + \dots \quad (\text{A6.35})$$

giving

$$O_q = h_q(m) + \Delta t \frac{1}{2} \frac{dh_q}{dt} + \Delta t^2 \left[ \frac{1}{4} \frac{d^2h_q}{dt^2} - \frac{T_3}{4} \left[ \left( \frac{d\rho_q}{dt} \right)^2 + 2 \frac{d\rho_q}{dt} \frac{d\rho_{q'}}{dt} \right] \right] \quad (\text{A6.36})$$

By comparing this expression with our previous expansion for  $h_q(m + \frac{1}{2})$ , Eqs. (A6.14-17), we see that terms through  $\Delta t$  match, meaning that  $\psi(t + dt)$  matches through terms of  $\Delta t^2$ . With or without the correction term  $C_q$  or  $\tilde{C}_q$ , the error is order  $\Delta t^3$ , but including the correction term conserves energy for this approximate TDHF evolution, thus providing us with a check on the numerical accuracy of the program.

#### IV. Evolution Algorithm

We must calculate  $\psi_{\lambda q}(m+1) = \exp\left[\left(\frac{-i}{\hbar}\right)\Delta t h_q(m + \frac{1}{2})\right]\psi_{\lambda q}(m)$  for each orbital, with the Hamiltonian for the average densities and a correction term, as discussed previously. There is a self-consistency problem because the operator  $h_q(m + \frac{1}{2})$  depends on the wavefunctions at the next time step ( $m+1$ ). A double-stepping procedure gives sufficiently accurate self-consistency (as measured by energy conservation). First, the wavefunctions  $\psi_{\lambda q}(m+1)$  are estimated using

$h_q(m+\frac{1}{2})=h_q(m)$ . Then, these estimates for  $\psi_{\lambda q}(m+1)$  are used to construct the  $h_q(m+\frac{1}{2})$  which performs the actual calculation of  $\psi_{\lambda q}(m+1)$ . Further iterations could be done if necessary. The exponential is expanded in a power series and the evolution operator is modified slightly to give better convergence. This modification consists of adding a phase  $\frac{i}{\hbar}\Delta t \langle h_q \rangle$ . This phase is physically irrelevant (since the particles are independent), but now the evolution operator becomes

$$U_q = \exp\left[\left(\frac{-i}{\hbar}\right)\Delta t (h_q - \langle h_q \rangle)\right] . \quad (\text{A6.37})$$

The exponent is now a "smaller" operator and the expansions of the exponential are more accurate.

The wavefunctions,  $\psi_{\lambda q}(m)$  are used to construct the densities  $\rho_q(m)$ ,  $\tau_q(m)$ , and  $\vec{j}_q(m)$ . These densities are stored and used to calculate the total energies  $H_C$ ,  $H_Y$ ,  $H_{NL}$  and  $H_Z = \text{ET0}$  and  $\text{ET3}$  at time step ( $m$ ) (as discussed in Appendices A3 and A5 part II) and to calculate the operators  $h_q(m)$  (as discussed in Appendices A4 and A5 part III). This Hamiltonian is used to calculate

$$\tilde{\psi}_{\lambda q}(m+1) = \left(\frac{-i}{\hbar}\right)\Delta t h_q(m) \psi_{\lambda q}(m) \quad (\text{A6.38})$$

and the single-particle energies

$$e_{\lambda q} = \langle h_q(m) \rangle = \frac{\hbar}{\Delta t} \langle \psi_{\lambda q}(m) | \tilde{\psi}_{\lambda q}(m+1) \rangle . \quad (\text{A6.39})$$

The exponential of the modified evolution operator can be expanded yielding

$$\psi_{\lambda q}(m+1) = \sum_k \frac{\left(\left(\frac{-i}{\hbar}\right)\Delta t [h_q(m) - \langle h_q(m) \rangle]\right)^k}{k!} \psi_{\lambda q}(m) \quad (\text{A6.40})$$

$$= \sum_k \psi_{\lambda q}^k(m+1) ,$$

where  $\psi_{\lambda q}^0(m+1) = 1 \times \psi_{\lambda q}(m)$ . Therefore, the quantities  $\tilde{\psi}_{\lambda q}(m+1)$  and  $\langle h_q(m) \rangle$  are used to calculate the first term,

$$\psi_{\lambda q}^1(m+1) = \tilde{\psi}_{\lambda q}(m+1) + \left(\frac{i}{\hbar}\right)\Delta t \langle h_q(m) \rangle \psi_{\lambda q}(m) . \quad (\text{A6.41})$$

The energies  $e_{\lambda q}$  are also used to calculate the total single-particle energy and total energy (as discussed in Appendix A5 part II). Higher-order terms in the expansion are calculated from the previous term by

$$\psi_{\lambda q}^k(m+1) = \left(\frac{-i}{\hbar}\right)\Delta t \frac{(h_q(m) - \langle h_q(m) \rangle)}{k} \psi_{\lambda q}^{k-1}(m+1) \quad (\text{A6.42})$$

and a running sum is kept

$$\psi_{\lambda q}(m+1) = \sum_{k=0}^k \psi_{\lambda q}^k(m+1) . \quad (\text{A6.43})$$

(This requires storage space for two wavefunctions - the most recent term, and the running sum.) For this first step, two terms are typically used in expansion of the exponential.

From the estimate of  $\psi_{\lambda q}(m+1)$ , we construct the average densities by returning to the same routine used for the densities in the first step, but not initializing the sums over the wavefunctions to zero. Instead, the final results are multiplied by one half. These  $\psi_{\lambda q}(m+1)$  are also used to calculate the correction term,  $\tilde{C}_q$ , from  $\frac{1}{2}\delta\rho_q = \tilde{p}_q - \rho_q(m)$  before storing the average densities where  $\rho_q(m)$  was previously stored. Now the same routines are used to calculate  $h_q(m+\frac{1}{2})$ , except for the addition of the correction term. However, calculation of the energies is skipped. The same evolution routine is used to calculate the new wavefunctions,

$$\psi_{\lambda q}(m+1) = \exp\left[\left(\frac{-i}{\hbar}\right)\Delta t (h_q(m+\frac{1}{2}) - \langle h_q(m+\frac{1}{2}) \rangle)\right] \psi_{\lambda q}(m) ; \quad (\text{A6.44})$$

but for the actual time step four or five terms are used in the expansion of the exponential. Also, the single-particle energies are unchanged; they are not set to  $\langle h_q(m+\frac{1}{2}) \rangle$  and the calculation of the total energies is skipped.

### **Appendix A7: Binary Partition of the Nuclear Density**

We choose a convenient reference frame centered at the total center of mass with axes parallel to the principle axes of inertia. These are easily found from the spatial distribution of nuclear matter. Due to the assumed reflection symmetry through the scattering plane, one axis OZ is perpendicular to the scattering plane. The remaining two axes in the scattering plane are denoted by OX and OY, OX being associated with the smallest moment of inertia (see Fig. 32a).

For symmetric systems such as  $^{16}\text{O} + ^{16}\text{O}$ , the analysis of the nuclear density is rather simple. The center of mass, O, is a center of inversion symmetry so that the Y,Z plane provides a natural division of the system. However, for asymmetric systems this is not an adequate procedure. As shown in Fig. 32, the total center of mass may be well within the heaviest fragment even when the two nuclei are physically separated and no longer interact through the short-range nuclear forces. Under such circumstances, it is desirable to divide the system into two pieces by a plane between the two fragments parallel to the Y,Z plane and in some sense as far as possible from each of them; for instance a plane through the dashed line in Fig. 32.

We present two systematic procedures to automatically define this dividing line. The first one was used in the O+Ca calculations (see Section 7) and in the first few Kr + La calculations (see Section 8). The second one has since been introduced into most of our Kr + La calculations. There are no significant differences between the two methods, which are only useful tools to analyze TDHF solutions. However, the second one is better suited to very asymmetric events found in many TDHF studies which result in scattering for angular momenta below the fusion window.

In both methods, we analyze the system in terms of two spheres with

uniform density, each centered on the X axis. These spheres are characterized by four parameters: the positions  $x_1$  and  $x_2$  of their centers along the X axis and their masses,  $A_1$  and  $A_2$ . Equivalently, their radii  $R_1$  and  $R_2$  are known if their density is given.

The spheres are constrained to have the same total mass, A, and center of mass position ( $=0$ ) as those of the actual system:

$$A_1 + A_2 = A \quad (A7.1)$$

$$A_1 x_1 + A_2 x_2 = 0 \quad (A7.2)$$

The two-sphere system must also reproduce the mean square extension along the X axis

$$A_1(x_1^2 + \frac{1}{5}R_1^2) + A_2(x_2^2 + \frac{1}{5}R_2^2) = \langle X^2 \rangle \quad (A7.3)$$

with

$$\langle X^2 \rangle = \int dX dY dZ \rho(X, Y, Z) X^2$$

Finally, the sum of the mean square extensions in the Y and Z directions must be reproduced

$$\frac{2}{5}A_1 R_1^2 + \frac{2}{5}A_2 R_2^2 = \langle Y^2 + Z^2 \rangle \quad (A7.4)$$

We now need only a relationship between R and A to solve these equations. In the first method, a uniform time-independent density is assumed for the two sphere, namely

$$R_{1,2} = \tau_0 A_{1,2}^{\frac{1}{3}} \quad (A7.5)$$

where  $\tau_0$  is time independent and is determined by the initial condition through Eq. (A7.4), where  $A_1$  and  $A_2$  are set to the masses of the colliding ions. Substitution of (A7.5) into (A7.4) and a combining of (A7.3) and (A7.4) then results in a set of four equations with four unknowns

$$A_1 + A_2 = A \quad (A7.6)$$

$$A_1^{\frac{5}{3}} + A_2^{\frac{5}{3}} = \frac{5}{2} \frac{\langle Y^2 + Z^2 \rangle}{\tau_0^2} \equiv P \quad (A7.7)$$

$$A_1 x_1 + A_2 x_2 = 0 \quad (\text{A7.6})$$

$$A_1 x_1^2 + A_2 x_2^2 = \frac{1}{2} \langle 2X^2 - Y^2 - Z^2 \rangle \equiv \frac{Q}{2} \quad (\text{A7.9})$$

Eqs. (A7.6) and (A7.7) are solved iteratively for  $A_1$  and  $A_2$  at each time step, with the initial guess being the values of  $A_1$  and  $A_2$  from the previous time step. For convergence, the smaller  $A$  is substituted into Eq. (A7.7) and the new value of the larger  $A$  is substituted into Eq. (A7.6). Eqs. (A7.8) and (A7.9) are then solved for  $x_1^2$  and  $x_2^2$  :

$$x_1^2 = \frac{A_2 Q}{A_1 2A} \quad \text{and} \quad x_2^2 = \frac{A_1 Q}{A_2 2A} \quad (\text{A7.10})$$

These solutions do not specify the signs of  $x_1$  and  $x_2$ . However, the two spheres must be on opposite sides of the total center of mass, i.e.  $x_1 x_2 < 0$ . To completely determine the signs, we require that the expectation value  $\langle X^3 \rangle$  has the same sign in both the actual and two-sphere systems.

Having defined these two spheres, we divide the system along a line equidistant from the surface of each of the spheres, as illustrated in Fig. 33, i.e. at  $x + (R_1 - R_2)/2$  where  $x = (x_1 + x_2)/2$ . (The location of this line is really the only quantity of interest in the procedure.) It should be noted that this procedure does not depend upon the orientation of the  $X$  axis, which is, of course, changing throughout the collision.

In solving Eqs. (A7.6) and (A7.7), difficulties may arise if the coefficient  $P$  is either too large or too small, since a solution is possible only for  $P$  between  $A^{\frac{5}{3}}$  and  $2\left(\frac{A}{2}\right)^{\frac{5}{3}}$ . Since the definition of the axes requires  $\langle Y^2 \rangle \leq \langle X^2 \rangle$  and  $\langle Z^2 \rangle$  is frozen by the separable approximation,  $P$  will be large when a fused system is formed with an almost oblate shape:  $\langle X^2 \rangle \approx \langle Y^2 \rangle$ . This will then result in a very asymmetric solution with one mass, say  $A_1$ , almost equal to  $A$ , and the other,  $A_2$ , unphysically small, with the sphere corresponding to  $A_2$  unphysically distant ( $\langle x_2^2 \rangle$  large).

To avoid this difficulty, whenever  $A_2$  (or  $A_1$ ) becomes smaller than a specified critical mass  $A_{\min}^+$ , a binary division is not attempted. Rather, the analysis is done as a single nucleus and the Coulomb boundary conditions are calculated assuming a single fused system. The maximum value of  $P$  for a binary division is then

$$P_{\max} = (A - A_{\min})^{\frac{5}{3}} + A_{\min}^{\frac{5}{3}} \quad (\text{A7.11})$$

The other extreme is when  $P$  is too small, as for a system which is highly elongated along the  $X$  axis. Whenever  $P$  becomes smaller than

$$P_{\min} = 2\left(\frac{A}{2}\right)^{\frac{5}{3}} \quad (\text{A7.12})$$

during the collision, we have arbitrarily chosen  $A_1$  and  $A_2$  to be

$$A_{1,2} = \frac{A}{2} \pm 1$$

The above prescription in which  $\tau_0$  is time independent, has proven to be adequate for scattering events of impact parameters larger than the maximum one for fusion. The accurate determination of an  $l$ -window for fusion does not require a refined division of the density, as we only need to know whether or not fusion is achieved. However, for scattering events at angular momentum smaller than  $l_c$ , the outgoing fragments are highly excited and deformed and  $\langle X^3 \rangle$  for the actual system is then quite different from its value for the two-sphere system defined above. The ansatz of time-independent uniform density for the spheres is then not appropriate for those events.

This defect is remedied in the second method, which we describe now. We shall use Eq. (A7.1) through (A7.5) but instead of having  $\tau_0$  time independent, we require that the actual  $\langle X^3 \rangle$  be reproduced by the two spheres. This furnishes a subsidiary condition which determines  $\tau_0$  as a function of time:

<sup>+</sup> Note that  $A_{\min}$  must be smaller than the lightest fragment to be emitted. Otherwise, when the fused system scissions with a light fragment mass smaller than  $A_{\min}$ , the analysis of the density would be done as if the system had remained fused.

$$A_1(x_1^3 + \frac{3}{5}R_1^2x_1) + A_2(x_2^3 + \frac{3}{5}R_2^2x_2) = \langle X^3 \rangle \quad (A7.13)$$

The system of Eqs. (A7.1) through (A7.5) (or equivalently (A7.5-9) together with Eq. (A7.13)) can then be stated implicitly. Eqs. (A7.6,8,9) are combined to give

$$A_{1,2} = \frac{A}{2} \left( 1 \pm \frac{1}{\sqrt{1 + Q/2Ax^2}} \right) \quad (A7.14)$$

and Eqs. (A7.13,14) give

$$x = \frac{\langle X^3 \rangle}{Q - \frac{6}{5} \frac{A_1 A_2}{A_1 - A_2} (R_1^2 - R_2^2)} \quad (A7.15)$$

$$\tau_0^2 = \frac{P'}{(A_1^{\frac{5}{3}} + A_2^{\frac{5}{3}})} \quad (A7.16)$$

i.e.  $P' = P\tau_0^2$  and Eq. (A7.5) is unchanged. Note that  $x$ ,  $R_1$  and  $R_2$  are the only quantities of interest. Having a first guess for the two masses  $A_1$  and  $A_2$ ,  $\tau_0$  is obtained from (A7.16), the two radii from (A7.17), and then  $x$  through (A7.15). This procedure is then iterated, the new masses being given by (A7.14). Although this algorithm may not be rigorously convergent for all values of  $Q$ ,  $P$ , and  $\langle X^3 \rangle$ , due to the physical nature of the problem these quantities are not strictly independent parameters and there is convergence in all practical situations. The convergence is rather slow but can be accelerated by averaging the  $x$ 's obtained before and after each iteration.

This alternate method offers three advantages over the previous one. First, there are no limiting cases; if the system fuses,  $x$  goes to zero, the masses  $A_1$  and  $A_2$  become close to each other ( $\approx \frac{A}{2}$ ) but Eq. (A7.15) is always soluble. Second,  $x$  is directly obtained, not  $|x_1|$  and  $|x_2|$ . Finally, less emphasis is put on the mean square extension perpendicular to the  $X$  axis and the asymmetry of the system is fully exploited. If the system is symmetric,  $\langle X^3 \rangle$  goes to zero, but the denominator in Eq. (A7.15) has a finite limit, so that  $x$  is zero, as it should be.

**Appendix B1: Expectation Values Needed for TDRPA**

We calculate the various expectation values used in the derivation of our time-dependent generalization of the RPA theory. The normalization condition required evaluating several expectation values.

$$\eta = \langle \varphi | \varphi \rangle + \langle \vec{c}^{\circ} \cdot \vec{A} \rangle + \langle \vec{c} \cdot \vec{A}^{\dagger} \rangle + \langle \vec{c}^{\circ} \cdot \vec{A} \vec{c} \cdot \vec{A}^{\dagger} \rangle + \frac{1}{2} [\langle (\vec{c}^{\circ} \cdot \vec{A})^2 \rangle + \langle (\vec{c} \cdot \vec{A}^{\dagger})^2 \rangle] \quad (\text{B1.1})$$

Since  $A^{\dagger}$  creates a particle-hole pair and  $A$  annihilates a particle-hole pair, all terms with unequal numbers of  $A^{\dagger}$  and  $A$  give zero. The only term left is

$$\begin{aligned} \langle \vec{c}^{\circ} \cdot \vec{A} \vec{c} \cdot \vec{A}^{\dagger} \rangle &= \sum_{php'h'} c_{ph}^{\circ} c_{p'h'} \langle A_{ph} A_{p'h'}^{\dagger} \rangle \\ &= \sum_{php'h'} c_{ph}^{\circ} c_{p'h'} \delta_{p'p} \delta_{h'h} = \vec{c}^{\circ} \cdot \vec{c} \end{aligned} \quad (\text{B1.2})$$

Therefore,

$$\eta = 1 + \vec{c}^{\circ} \cdot \vec{c} \quad (\text{B1.3})$$

Precisely the same reasoning is used in evaluating the  $\vec{c}^{\dagger}$  terms in the first step of  $\langle \Psi | i \frac{\partial}{\partial t} | \Psi \rangle$  which is to second order

$$\begin{aligned} &= -\frac{1}{2} \frac{d}{dt} (\vec{c}^{\circ} \cdot \vec{c}) + \langle \vec{c}^{\circ} \cdot \vec{A} \vec{c}^{\dagger} \cdot \vec{A}^{\dagger} \rangle + \langle \vec{c} \cdot \vec{A}^{\dagger} \rangle \\ &\quad + \frac{1}{2} \langle \vec{c}^{\dagger} \cdot \vec{A}^{\dagger} \vec{c} \cdot \vec{A}^{\dagger} + \vec{c} \cdot \vec{A}^{\dagger} \vec{c}^{\dagger} \cdot \vec{A}^{\dagger} \rangle \\ &= -\frac{1}{2} \frac{d}{dt} (\vec{c}^{\circ} \cdot \vec{c}) + \vec{c}^{\circ} \cdot \vec{c}^{\dagger} \end{aligned} \quad (\text{B1.4})$$

This same reasoning is used in the orthogonality condition  $\langle \frac{\partial}{\partial t} \Phi | \Psi \rangle = 0$ .

$$0 = \langle \Phi | \bar{h} (1 - \frac{1}{2} \vec{c}^{\circ} \cdot \vec{c} + \vec{c} \cdot \vec{A}^{\dagger} + \frac{1}{2} (\vec{c} \cdot \vec{A}^{\dagger})^2) | \Phi \rangle \quad (\text{B1.5})$$

Since

$$\bar{h} = \sum_{ph} [\bar{h}_{ph} a_p^{\dagger} a_h + \bar{h}_{hp} a_h^{\dagger} a_p] \quad (\text{B1.6})$$

can be written

$$\bar{h} = \vec{h} \cdot \vec{A}^{\dagger} + \vec{h}^{\circ} \cdot \vec{A} \quad (\text{B1.7})$$

the only term with equal numbers of  $A^{\dagger}$  and  $A$  is  $\langle \vec{h}^{\circ} \cdot \vec{A} \vec{c} \cdot \vec{A}^{\dagger} \rangle$ . Therefore,

$$0 = \vec{h}^{\circ} \cdot \vec{c} = \sum_{ph} h_{ph}^{\circ} c_{ph} \quad (\text{B1.8})$$

Now we need to calculate the expectation values used to get Eq. (3.24) in Part II. We first calculate the various expectation values for the full two-body Hamiltonian  $H$ . Then we are able to write down the expectation values for the evolution operator  $\bar{h}$  from the one-body terms in  $H$  if we simply remember that  $\bar{h}$  has only hole-particle and particle-hole components. Throughout these derivations  $i, j, k$ , and  $l$  label general states whereas  $p$  or  $h$  refer specifically to empty or occupied states of the TDHF solution. For the two-body  $H$  in Eq. (3.7).

$$\langle H \rangle = \sum_{ij} t_{ij} \langle a_i^\dagger a_j \rangle + \frac{1}{4} \sum_{ijkl} \tilde{V}_{ijkl} \langle a_i^\dagger a_j^\dagger a_i a_k \rangle . \quad (\text{B1.9})$$

Since

$$\langle a_i^\dagger a_j \rangle = \delta_{ij_{holes}} , \quad (\text{B1.10})$$

(meaning  $\delta_{ij}$  plus the condition that both states must be normally occupied, therefore labelled by  $h$ ) and

$$\langle a_i^\dagger a_j^\dagger a_i a_k \rangle = \delta_{j_{holes}} \delta_{ik_{holes}} - \delta_{jk_{holes}} \delta_{i_{holes}} , \quad (\text{B1.11})$$

we get

$$\langle H \rangle = \sum_h t_{hh} + \frac{1}{2} \sum_{hh'} \tilde{V}_{hh'hh'} . \quad (\text{B1.12})$$

The next expectation

$$\langle A_{ph} H \rangle = \sum_{ij} t_{ij} \langle a_h^\dagger a_p a_i^\dagger a_j \rangle + \frac{1}{4} \sum_{ijkl} \tilde{V}_{ijkl} \langle a_h^\dagger a_p a_i^\dagger a_j^\dagger a_i a_k \rangle . \quad (\text{B1.13})$$

Since

$$\langle a_h^\dagger a_p a_i^\dagger a_j \rangle = \delta_{pi} \delta_{hj} \quad (\text{B1.14})$$

and

$$(\text{B1.15})$$

$$\langle a_h^\dagger a_p a_i^\dagger a_j^\dagger a_i a_k \rangle = \delta_{pi} (\delta_{j_{holes}} \delta_{kh} - \delta_{jk_{holes}} \delta_{ih}) - \delta_{pj} (\delta_{i_{holes}} \delta_{kh} - \delta_{ik_{holes}} \delta_{ih}) ,$$

we get

$$\langle A_{ph} H \rangle = t_{ph} + \sum_{hh'} \tilde{V}_{ph'hh'} . \quad (\text{B1.16})$$

The next expectation value is

$$\langle A_{ph} H \vec{c} \cdot \vec{A}^+ \rangle = \sum_{p'h'} \langle A_{ph} H A_{p'h'}^+ \rangle \quad (B1.17)$$

The one-body terms are

$$\begin{aligned} \sum_{ij} t_{ij} \langle a_n^+ a_p a_i^+ a_j a_p^+ a_n \rangle &= \sum_{ij} t_{ij} [\delta_{ij} \delta_{ip'} \delta_{hh'} + \delta_{pp'} (\delta_{ijholes} \delta_{hh'} - \delta_{ih'} \delta_{jh})] \\ &= t_{pp'} \delta_{hh'} - t_{h'h} \delta_{pp'} + \delta_{pp'} \delta_{hh'} \sum_{h''} t_{h''h''} \end{aligned} \quad (B1.18)$$

Two-body terms are

$$\frac{1}{4} \sum_{ijkl} \tilde{V}_{ijkl} \langle a_n^+ a_p a_i^+ a_j^+ a_k a_p^+ a_n \rangle \quad (B1.19)$$

Using the symmetry properties of  $\tilde{V}$  to combine various terms such as  $\delta_{pi}$  and  $-\delta_{pj}$  gives a result

$$\tilde{V}_{ph'hp'} + \delta_{hh'} \sum_{h''} \tilde{V}_{ph''p'h''} - \delta_{pp'} \sum_{h''} \tilde{V}_{h''h''hh''} + \delta_{pp'} \delta_{hh'} \sum_{h''h'''} \tilde{V}_{h''h''h''h'''} \quad (B1.20)$$

Therefore, the net result is

$$\begin{aligned} \langle A_{ph} H \vec{c} \cdot \vec{A}^+ \rangle &= \sum_{p'h'} c_{p'h'} [t_{pp'} \delta_{hh'} - t_{h'h} \delta_{pp'} + \delta_{pp'} \delta_{hh'} \sum_{h''} t_{h''h''} \\ &+ \tilde{V}_{ph'hp'} + \delta_{hh'} \sum_{h''} \tilde{V}_{ph''p'h''} - \delta_{pp'} \sum_{h''} \tilde{V}_{h''h''hh''} + \delta_{pp'} \delta_{hh'} \sum_{h''h'''} \tilde{V}_{h''h''h''h'''}] \end{aligned} \quad (B1.21)$$

The next expectation value is

$$\langle A_{ph} \vec{c}^* \cdot \vec{A} H \rangle = \sum_{p'h'} c_{p'h'}^* \langle A_{ph} A_{p'h'} H \rangle \quad (B1.22)$$

The one-body terms give zero. Therefore,

$$\begin{aligned} \langle A_{ph} A_{p'h'} H \rangle &= \frac{1}{4} \sum_{ijkl} \tilde{V}_{ijkl} (-\delta_{pi} \delta_{pj} + \delta_{p'j} \delta_{p'i}) (\delta_{h'l} \delta_{hk} - \delta_{h'k} \delta_{hl}) \\ &= \tilde{V}_{pp'h'h'} \end{aligned} \quad (B1.23)$$

Therefore,

$$\langle A_{ph} \vec{c}^* \cdot \vec{A}^+ H \rangle = \sum_{p'h'} c_{p'h'}^* \tilde{V}_{pp'h'h'} \quad (B1.24)$$

Since  $\tilde{V}_{pp'h'h'} = \tilde{V}_{p'p'h'h}$ ,

$$\langle \vec{c}^* \cdot \vec{A} A_{ph} H \rangle = \langle A_{ph} \vec{c}^* \cdot \vec{A} H \rangle \quad (B1.25)$$

These expressions for expectation values of  $H$  can be simplified by using the equation

$$h_{ij} = t_{ij} + \sum_h \tilde{V}_{ihjh} \quad (B1.26)$$

$$\langle A_{ph} H \rangle = h_{ph} \quad . \quad (B1.27)$$

$$\langle A_{ph} H \vec{c} \cdot \vec{A}^+ \rangle = \sum_{p'h'} c_{p'h'} (\delta_{hh'} h_{pp'} - \delta_{pp'} h_{h'h} + \tilde{V}_{ph'hp'}) + c_{ph} \langle H \rangle \quad . \quad (B1.28)$$

Now we can write the expectation values for  $\bar{h}$ . From Eq. (B1.12),

$$\langle \bar{h} \rangle = \sum_h \bar{h}_{hh} = 0 \quad . \quad (B1.29)$$

From Eq. (B1.27),

$$\langle A_{ph} \bar{h} \rangle = \bar{h}_{ph} = h_{ph} \quad . \quad (B1.30)$$

From Eq. (B1.28),

$$\langle A_{ph} \bar{h} \vec{c} \cdot \vec{A}^+ \rangle = \sum_{p'h'} c_{p'h'} [\delta_{hh'} \bar{h}_{pp'} - \delta_{pp'} \bar{h}_{h'h}] + c_{ph} \langle \bar{h} \rangle = 0 \quad . \quad (B1.31)$$

From Eq. (B1.24),

$$\langle A_{ph} c \cdot \vec{A} \bar{h} \rangle = 0 \quad . \quad (B1.32)$$

The evolution equation is thus

$$\begin{aligned} i\dot{c}_{ph} = & \sum_{p'h'} c_{p'h'} (\delta_{hh'} h_{pp'} - \delta_{pp'} h_{h'h} + \tilde{V}_{ph'hp'}) \\ & + \sum_{p'h'} c_{p'h'} \tilde{V}_{pp'h'h} - \lambda h_{ph} \quad . \end{aligned} \quad (B1.33)$$

### Appendix B2: Invariance of the TDRPA Equations

We prove that an arbitrary unitary transformation among particle states or among hole states does not change the eigenvalues,  $\omega$ , of the time-dependent RPA equations. (Repeated indices are summed.)

$$i\dot{c}_{ph} = \bar{A}_{ph,p'h'} c_{p'h'} + \bar{B}_{ph,p'h'} c_{p'h'}^* \quad (\text{B2.1})$$

or

$$\omega \begin{bmatrix} X \\ Y \end{bmatrix} = \begin{bmatrix} \bar{A} & \bar{B} \\ -\bar{B}^* & -\bar{A}^* \end{bmatrix} \begin{bmatrix} X \\ Y \end{bmatrix} \quad (\text{B2.2})$$

where

$$c_{ph} = X_{ph} e^{-i\omega t} + Y_{ph}^* e^{+i\omega t} \quad (\text{B2.3})$$

$$\bar{A} = PAP \quad \bar{B} = PBB^*$$

$$A_{ph,p'h'} = \delta_{hh'} h_{pp'} - \delta_{pp'} h_{h'h} + \tilde{V}_{ph,h'p'}$$

$$B_{ph,p'h'} = \tilde{V}_{p'p'h}$$

$$\text{and} \quad P_{ph,p'h'} = \delta_{pp'} \delta_{hh'} - \frac{h_{ph} h_{p'h'}}{h_{p'h'} h_{p'h'}}$$

We transform either particle states

$$\varphi'_p = U_{pp'} \varphi_p \quad (\text{B2.4})$$

or hole states

$$\varphi'_h = U_{hh'} \varphi_h \quad (\text{B2.5})$$

with a unitary operator  $U^* U = 1 = U U^*$ . With  $\Phi = \det\{\varphi_h\}$  and  $\Psi = \det\{\chi_h\}$ , we get single-particle wavefunctions

$$\chi_h = \varphi_h + c_{hp} \varphi_p \quad (\text{B2.6})$$

Therefore,

$$c_{hp} = \langle \varphi_p | \chi_h \rangle \quad (\text{B2.7})$$

Since the proofs for the two transformations are so similar, only the second, (B2.5), will be shown. Under this transformation

$$c'_{hp} = \langle \varphi_p | \chi'_h \rangle = U_{hh'} c_{h'p} \quad (\text{B2.8})$$

and

$$h'_{ij} = U_{ij}^{\circ} h_{ij} U_{jj} \quad (\text{B2.9})$$

Therefore,

$$\begin{aligned} h'_{pp'} &= h_{pp'} & (\text{B2.10}) \\ h'_{hh} &= U_{hh}^{\circ} h_{hh} U_{hh}^{\circ-1} \\ h'_{ph} &= U_{hh} h_{ph} \\ h'_{hp} &= h_{hp} U_{hh}^{-1} \end{aligned}$$

Although the position of the U's is arbitrary, they have been chosen for later convenience.

The  $\delta$  functions can be trivially rewritten,

$$\delta'_{hh} = U_{hh}^{\circ} \delta_{hh} U_{hh}^{\circ-1} \quad (\text{B2.11})$$

The transformation of the potentials;

$$\tilde{V}'_{ph'hp'} = \langle ph' | V | hp' - p'h \rangle \quad (\text{B2.12})$$

gives

$$\tilde{V}'_{ph'hp'} = U_{hh}^{\circ} \tilde{V}_{ph''h''p'} U_{hh}^{\circ-1} \quad (\text{B2.13})$$

and of

$$\tilde{V}'_{pp'hh} = \langle pp' | V | hh' - h'h \rangle \quad (\text{B2.14})$$

gives

$$\tilde{V}'_{pp'hh} = U_{hh}^{\circ} \tilde{V}_{pp'h''h''} U_{hh}^{\circ-1} \quad (\text{B2.15})$$

Therefore, the matrix transformations give

$$\begin{aligned} A'_{ph'p'h'} &= U_{hh}^{\circ} A_{ph''p'h''} U_{hh}^{\circ-1} & (\text{B2.16}) \\ &= U_{hh}^{\circ} A_{ph''p'h''} U_{hh}^{\circ-1} \end{aligned}$$

and

$$B'_{ph'p'h'} = U_{hh}^{\circ} B_{ph''p'h''} U_{hh}^{\circ-1} \quad (\text{B2.17})$$

With

$$h'_{ph} h'_{hp} = U_{hh} h_{ph} h_{hp} U_{hh}^{-1} = h_{ph} h_{hp} \quad (\text{B2.18})$$

the projector transforms as

$$P'_{ph'p'h'} = U_{hh}^{\circ} P_{ph''p'h''} U_{hh}^{\circ-1} \quad (\text{B2.19})$$

We define

$$U = U_{hh'} \delta_{pp'} \quad (B2.20)$$

and rewrite these equations as

$$\begin{aligned} C' &= UC & (B2.21) \\ C^{*'} &= U^* C^* \\ A' &= UAU^{-1} \\ B' &= UBU^{*'} \\ P' &= UPU^{-1} \\ P^{*'} &= U^* P^* U^{*'} \end{aligned}$$

The only change in the proof for the first transformation, (B2.4) is that

$$U = U_{pp'}^* \delta_{hh'}$$

Therefore,

$$\bar{A}' = U\bar{A}U^{-1} \quad (B2.22)$$

and

$$\bar{B}' = U\bar{B}U^{*'} \quad (B2.23)$$

so the first equation, (B2.1), is invariant.

$$i\dot{C}' = \bar{A}'C' + \bar{B}'C^{*'} \quad (B2.24)$$

becomes

$$iU\dot{C} = U(\bar{A}C + \bar{B}C^*) \quad (B2.25)$$

The eigenvalue matrix in the new coordinate system is

$$\begin{pmatrix} \bar{A}' & \bar{B}' \\ -\bar{B}^{*'} & -\bar{A}^{*'} \end{pmatrix} = \begin{pmatrix} U & 0 \\ 0 & U^* \end{pmatrix} \begin{pmatrix} \bar{A} & \bar{B} \\ -\bar{B}^* & -\bar{A}^* \end{pmatrix} \begin{pmatrix} U^{-1} & 0 \\ 0 & U^{*'} \end{pmatrix} \quad (B2.26)$$

Since this is a similarity transformation the eigenvalues,  $\omega$ , are not changed.

### Appendix B3: Expectation Values for the SU(3) Model

In this appendix, we calculate the expectation values of several operators for a general TDHF state  $|\psi\rangle = \prod_n \alpha_{ni}^+ |0\rangle$ . The number operator for each level  $i$  is  $G_{ii} = \sum_n \alpha_{ni}^+ \alpha_{ni}$ . Remembering that  $\alpha^+ = A^{-1} a^+$ , we can transform  $G$  from the representation convenient for the levels, using  $a$ 's, to the representation convenient for our states, using  $\alpha$ 's. Thus

$$G_{ij} = \sum_{i'j'} A_{i'i} A_{j'j}^* \sum_n \alpha_{ni'}^+ \alpha_{nj'} \quad (\text{B3.1})$$

and

$$\begin{aligned} \langle G_{ii} \rangle &= \sum_{i'j'} A_{i'i} A_{i'j}^* \sum_n \delta_{i'j} \delta_{j'1} \\ &= N A_{i1} A_{i1}^* \end{aligned} \quad (\text{B3.2})$$

To calculate the various expectation values used in the TDRPA analysis, we need to rewrite  $H$  in the more convenient representation using  $\alpha$ 's. Thus,

$$H = \sum_{i'j'} \varepsilon_i A_{i'i} A_{i'j}^* K_{i'j} + \sum_{i'j'k'l} V_{ij} A_{j'i} A_{i'j}^* A_{jk} A_{i'l}^* K_{i'j} K_{k'l} \quad (\text{B3.3})$$

where  $K_{ij} \equiv \sum_{n'\sigma} \alpha_{ni'}^+ \alpha_{nj\sigma}$ . We could now calculate all the various expectation values.

However, by finding the correct substitutes for  $t_{ij}$  and  $\tilde{V}_{ijkl}$  we are able to substitute directly into our previous general formulas for these various values (Appendix B1). This method requires fewer calculations but we have, of course, checked that the results of the complete calculation agree with the shorter transcription derived in this appendix.

Thus,  $t_{ij} = \langle i | t | j \rangle = \langle 0 | \alpha_i t \alpha_j^+ | 0 \rangle$  now becomes

$$t_{kl} = \langle 0 | \alpha_{nk} t \alpha_{nl}^+ | 0 \rangle \quad (\text{B3.4})$$

for any particle  $n$  where  $k, l = 1, 2, 3$ .

$$\begin{aligned} t_{kl} &= \sum_{i'k'l'} \varepsilon_i A_{i'i} A_{i'l}^* \sum_n \langle 0 | \alpha_{nk} \alpha_{n'k}^+ \alpha_{n'l'} \alpha_{n'l}^+ | 0 \rangle \\ &= \sum_i \varepsilon_i A_{ik} A_{il}^* \end{aligned} \quad (\text{B3.5})$$

independent of the particle  $n$ .

The potential term  $\tilde{V}_{ijkl}$  becomes

$$\tilde{V}_{ijkl} = \langle 0 | \alpha_{n'j} \alpha_{ni} V \alpha_{nk}^+ \alpha_{n'l}^+ | 0 \rangle \quad (\text{B3.6})$$

(the particles  $n, n'$  are distinguishable). This expression is true for any  $n, n'$  but for  $n=n'$  the two consecutive creation or annihilation operators give zero. Therefore, the result is evaluated for  $n \neq n'$  and multiplied by  $(1-\delta_{nn'})$ . We have

$$\begin{aligned} \tilde{V}_{klmq} = & \sum_{ijkl'm'q'} V_{ij} A_{jk} A_{il}^* A_{jm'} A_{iq}^* \times \\ & \sum_{n2, n3} \langle 0 | \alpha_{n'l} \alpha_{nk}^+ \alpha_{n2k'}^+ \alpha_{n2l'} \alpha_{n3m'}^+ \alpha_{n3q'} \alpha_{nm}^+ \alpha_{n'q}^+ | 0 \rangle \end{aligned} \quad (\text{B3.7})$$

Using  $\alpha_{n3q'}$  to eliminate one of the creation operators to its right, using  $\alpha_{n2k'}$  to eliminate one of the annihilation operators to its left, performing the sum over  $n2$  and  $n3$ , and remembering that  $n' \neq n$  gives

$$\begin{aligned} \sum_{n2, n3} \langle 0 \rangle = & \delta_{q'm} [\delta_{kk'} \delta_{l'm'} \delta_{iq} + \delta_{lk'} \delta_{km'} \delta_{ql'}] \\ & + \delta_{qq'} [\delta_{kk'} \delta_{lm'} \delta_{m'l'} + \delta_{lk'} \delta_{l'm'} \delta_{km}]. \end{aligned} \quad (\text{B3.8})$$

The two terms above with  $\delta_{l'm'}$  do not contribute since

$$\sum_{l'm'} A_{il}^* A_{jm'} \delta_{l'm'} = \sum_{l'} A_{il}^* A_{jl'} = \delta_{ij} \quad (\text{B3.9})$$

and

$$V_{ij} \delta_{ij} = 0 \quad (\text{B3.10})$$

for all  $i, j$ . Thus, we are left with

$$\tilde{V}_{klmq} = \sum_{ij} V_{ij} A_{jk} A_{jl} A_{im}^* A_{iq}^* \times 2(1-\delta_{nn'}) \quad (\text{B3.11})$$

for any  $n, n'$ .

We substitute these values into our previous formulas. We also need  $\delta_{hh'}$ , which becomes  $\delta_{nn'}$ , and  $\delta_{pp'}$ , which becomes  $\delta_{nn'} \delta_{\sigma\sigma'}$ , for  $\sigma, \sigma'=2,3$ . Thus,  $W_{ij} = \sum_h \tilde{V}_{ihjh}$  becomes, for any  $n$ ,

$$\begin{aligned} W_{kl} = & \sum_n \tilde{V}_{kll1} = \sum_{ij} V_{ij} A_{jk} A_{il}^* A_{j1} A_{i1}^* \times 2 \sum_{n'} (1-\delta_{nn'}) \\ & = \sum_{ij} 2 V_{ij} (N-1) A_{jk} A_{il}^* A_{j1} A_{i1}^* \end{aligned} \quad (\text{B3.12})$$

and  $h_{kl}$  becomes

$$h_{kl} = \sum_i \varepsilon_i A_{ik} A_{il}^* + \sum_{ij} 2V_{ij} (N-1) A_{j1} A_{i1}^* A_{jk} A_{il}^* , \quad (\text{B3.13})$$

for any particle  $n$ . The elements  $h_{\sigma 1}$  are used in the TDHF equations; all  $h_{kl}$  are used in the TDRPA analysis.

With these substitutions, the energy  $\langle H \rangle$  becomes

$$\begin{aligned} \langle H \rangle &= \sum_n (t_{11} + \frac{1}{2} W_{11}) \\ &= N \left[ \sum_i \varepsilon_i A_{i1} A_{i1}^* + \sum_{ij} V_{ij} (N-1) (A_{j1})^2 (A_{i1}^*)^2 \right] . \end{aligned} \quad (\text{B3.14})$$

Substituting directly into the general TDRPA matrices, we get for  $A_{ph,p'h'}$  a new matrix

$$A_{n\sigma,n'\sigma'} = \delta_{nn'} h_{\sigma\sigma'} - \delta_{nn'} \delta_{\sigma\sigma'} h_{11} + \tilde{V}_{\sigma 11 \sigma'} (1 - \delta_{nn'}) , \quad (\text{B3.15})$$

and for  $B_{ph,p'h'}$  a new matrix

$$B_{n\sigma,n'\sigma'} = \tilde{V}_{\sigma\sigma' 11} (1 - \delta_{nn'}) . \quad (\text{B3.16})$$

We use these new matrices in our time-dependent RPA equations

$$i\dot{c}_{n\sigma} = \sum_{n'\sigma'} A_{n\sigma,n'\sigma'} c_{n'\sigma'} + \sum_{n'\sigma'} B_{n\sigma,n'\sigma'} c_{n'\sigma'}^* - \lambda h_{\sigma 1} . \quad (\text{B3.17})$$

### Appendix B4: Energy and Evolution Equation as Functions of the Four Rotation Angles

In this appendix we would like to rewrite some of the equations, which were written in terms of matrix elements of A, in terms of the four rotation angles  $\vartheta_1$ ,  $\vartheta_2$ ,  $\psi_1$ , and  $\psi_2$ . We choose for our Hamiltonian, equal level spacing ( $\varepsilon_1 = -\varepsilon$ ,  $\varepsilon_2 = 0$ ,  $\varepsilon_3 = \varepsilon$ ) and equal interaction strength ( $V_{ij} = \frac{V}{2}(1 - \delta_{ij})$ ). We choose for A

$$A = \begin{pmatrix} \cos\vartheta_1 & -\cos\vartheta_2 \sin\vartheta_1 e^{i\psi_1} & -\sin\vartheta_2 \sin\vartheta_1 e^{i\psi_2} \\ \cos\vartheta_2 \sin\vartheta_1 e^{-i\psi_1} & 1 + \cos^2\vartheta_2 (\cos\vartheta_1 - 1) & \sin\vartheta_2 \cos\vartheta_2 (\cos\vartheta_1 - 1) e^{-i(\psi_1 - \psi_2)} \\ \sin\vartheta_2 \sin\vartheta_1 e^{-i\psi_2} & \sin\vartheta_2 \cos\vartheta_2 (\cos\vartheta_1 - 1) e^{i(\psi_1 - \psi_2)} & 1 + \sin^2\vartheta_2 (\cos\vartheta_1 - 1) \end{pmatrix} \quad (B4.1)$$

The energy, from Appendix 3, is

$$\langle H \rangle = N \left[ \sum_i \varepsilon_i |A_{ki}|^2 + \sum_{ij} V_{ij} (N-1) (A_{j1})^2 (A_{ki}^*)^2 \right] \quad (B4.2)$$

Substituting the values of the matrix elements of A and  $\chi = \frac{V(N-1)}{\varepsilon}$  gives

$$\langle H \rangle = N\varepsilon (\sin^2\vartheta_2 \sin^2\vartheta_1 - \cos^2\vartheta_1 - \chi \sin^2\vartheta_1 [\cos^2\vartheta_1 (\cos^2\vartheta_2 \cos 2\psi_1 + \sin^2\vartheta_2 \cos 2\psi_2) + \cos^2\vartheta_2 \sin^2\vartheta_2 \sin^2\vartheta_1 \cos 2(\psi_1 - \psi_2)]) \quad (B4.3)$$

Next we must derive the equations of motion for the rotation angles from the two complex equations of motion for matrix elements of A. Because of the unitarity of A, Eq. (4. ) becomes

$$\sum_k i \dot{A}_{k1}^* A_{kj} = \sum_k \varepsilon_k A_{kj} A_{k1}^* + \sum_{kl} 2V_{kl} (N-1) (A_{k1}^*)^2 A_{l1} A_{lj} \quad (B4.4)$$

for  $j=2,3$ . First we evaluate the left-hand side for  $j=2$ ,

$$i \sum_k \dot{A}_{k1}^* A_{k2} = e^{i\psi_1} [i\vartheta_1 \cos\vartheta_2 - i\vartheta_2 \sin\vartheta_2 \sin\vartheta_1 - \psi_1 \cos\vartheta_2 \sin\vartheta_1 (1 + \cos^2\vartheta_2 (\cos\vartheta_1 - 1)) - \psi_2 \sin^2\vartheta_2 \cos\vartheta_2 \sin\vartheta_1 (\cos\vartheta_1 - 1)] \quad (B4.5)$$

Next we evaluate the left-hand side for  $j=3$ ,

$$i \sum_k \dot{A}_{k1} \dot{A}_{k3} = e^{i\psi_2} [i\dot{\vartheta}_1 \sin\vartheta_2 + i\dot{\vartheta}_2 \cos\vartheta_2 \sin\vartheta_1 \quad (\text{B4.6})$$

$$-\dot{\psi}_1 \cos^2\vartheta_2 \sin\vartheta_2 \sin\vartheta_1 (\cos\vartheta_1 - 1) - \dot{\psi}_2 \sin\vartheta_2 \sin\vartheta_1 (1 + \sin^2\vartheta_2 \sin\vartheta_1)]$$

Next we need to evaluate the right-hand side for  $j=2$ ,

$$\begin{aligned} h_{21} = & \varepsilon e^{i\psi_1} (\cos\vartheta_2 \sin\vartheta_1 [\sin^2\vartheta_2 (\cos\vartheta_1 - 1) + \cos\vartheta_1] - \chi \sin\vartheta_1 \cos\vartheta_2 \quad (\text{B4.7}) \\ & [\cos^2\vartheta_1 (1 + \cos^2\vartheta_2 (\cos\vartheta_1 - 1)) e^{-2i\psi_1} + \cos^2\vartheta_1 \sin^2\vartheta_2 (\cos\vartheta_1 - 1) e^{-2i\psi_2} \\ & - \cos^2\vartheta_2 \sin^2\vartheta_1 \cos\vartheta_1 e^{2i\psi_1} + \cos^2\vartheta_2 \sin^2\vartheta_2 \sin^2\vartheta_1 (\cos\vartheta_1 - 1) e^{2i(\psi_1 - \psi_2)} \\ & - \sin^2\vartheta_2 \sin^2\vartheta_1 \cos\vartheta_1 e^{2i\psi_2} + \sin^2\vartheta_2 \sin^2\vartheta_1 (1 + \cos^2\vartheta_2 (\cos\vartheta_1 - 1)) e^{-2i(\psi_1 - \psi_2)}] \end{aligned}$$

Next we need to evaluate the right-hand side for  $j=3$ ,

$$\begin{aligned} h_{31} = & \varepsilon e^{i\psi_2} \sin\vartheta_2 \sin\vartheta_1 (1 + \sin^2\vartheta_2 (\cos\vartheta_1 - 1) + \cos\vartheta_1 - \chi \quad (\text{B4.8}) \\ & [\cos^2\vartheta_2 \cos^2\vartheta_1 (\cos\vartheta_1 - 1) e^{-2i\psi_1} + \cos^2\vartheta_1 (1 + \sin^2\vartheta_2 (\cos\vartheta_1 - 1)) e^{-2i\psi_2} \\ & - \cos^2\vartheta_2 \sin^2\vartheta_1 \cos\vartheta_1 e^{2i\psi_1} + \cos^2\vartheta_2 \sin^2\vartheta_1 (1 + \sin^2\vartheta_2 (\cos\vartheta_1 - 1)) e^{2i(\psi_1 - \psi_2)} \\ & - \sin^2\vartheta_2 \sin^2\vartheta_1 \cos\vartheta_1 e^{2i\psi_2} + \cos^2\vartheta_2 \sin^2\vartheta_2 \sin^2\vartheta_1 (\cos\vartheta_1 - 1) e^{-2i(\psi_1 - \psi_2)}] \end{aligned}$$

If we divide by the common phase  $e^{i\psi_1}$  for the equation with  $j=2$  and by  $e^{i\psi_2}$  for the equation with  $j=3$ , the real and imaginary parts of the left-hand side are quite obvious. This results in four equations:

$$\dot{\vartheta}_1 \cos\vartheta_2 - \dot{\vartheta}_2 \sin\vartheta_2 \sin\vartheta_1 = \text{Im} \left( \frac{h_{21}}{e^{i\psi_1}} \right) \quad (\text{B4.9})$$

$$\dot{\vartheta}_1 \sin\vartheta_2 + \dot{\vartheta}_2 \cos\vartheta_2 \sin\vartheta_1 = \text{Im} \left( \frac{h_{31}}{e^{i\psi_2}} \right)$$

$$\begin{aligned} \dot{\psi}_1 \cos\vartheta_2 \sin\vartheta_1 (1 + \cos^2\vartheta_2 (\cos\vartheta_1 - 1)) + \dot{\psi}_2 \sin^2\vartheta_2 \cos\vartheta_2 \sin\vartheta_1 (\cos\vartheta_1 - 1) \\ = -\text{Re} \left( \frac{h_{21}}{e^{i\psi_1}} \right) \end{aligned}$$

$$\begin{aligned} \dot{\psi}_1 \cos^2\vartheta_2 \sin\vartheta_2 \sin\vartheta_1 (\cos\vartheta_1 - 1) + \dot{\psi}_2 \sin\vartheta_2 \sin\vartheta_1 (1 + \sin^2\vartheta_2 (\cos\vartheta_1 - 1)) \\ = -\text{Re} \left( \frac{h_{31}}{e^{i\psi_2}} \right) \end{aligned}$$

We can solve the first two equations for  $\dot{\vartheta}_1$  by multiplying the first by  $\cos\vartheta_2$ , the second by  $\sin\vartheta_2$ , and adding.

$$\dot{\vartheta}_1 = \cos\vartheta_2 \text{Im} \left( \frac{h_{21}}{e^{i\psi_1}} \right) + \sin\vartheta_2 \text{Im} \left( \frac{h_{31}}{e^{i\psi_2}} \right) \quad (\text{B4.10})$$

Similarly,

$$\dot{\vartheta}_2 = \frac{1}{\sin\vartheta_2} \left[ -\sin\vartheta_2 \text{Im} \left( \frac{h_{21}}{e^{i\psi_1}} \right) + \cos\vartheta_2 \text{Im} \left( \frac{h_{31}}{e^{i\psi_2}} \right) \right] \quad (\text{B4.11})$$

The second equation, (B4.11), looks like it might give trouble for  $\vartheta_1=0$ . However, both imaginary parts of  $h$  contain  $\sin\vartheta_1$  also. The first equation, (B4.10) gives

$$\dot{\vartheta}_1 = \varepsilon \chi \sin\vartheta_1 \cos\vartheta_1 (\sin 2\psi_1 \cos^2\vartheta_2 + \sin 2\psi_2 \sin^2\vartheta_2) \quad (\text{B4.12})$$

The second equation, Eq. (B4.11), gives

$$\dot{\vartheta}_2 = \varepsilon \chi \cos\vartheta_2 \sin\vartheta_2 (\sin 2\psi_1 (-\cos^2\vartheta_1) + \sin 2\psi_2 \cos^2\vartheta_1 + \sin 2(\psi_1 - \psi_2) (-\sin^2\vartheta_1)) \quad (\text{B4.13})$$

Now having solved the first two equations for  $\vartheta_1$  and  $\vartheta_2$ , we must solve the last two equations for  $\psi_1$  and  $\psi_2$ . We can simplify some of the mathematics by noticing a common factor  $\cos\vartheta_2 \sin\vartheta_1$  in the third equation and  $\sin\vartheta_2 \sin\vartheta_1$  in the fourth equation. After dividing by these factors, the determinant of the coefficients is  $\cos\vartheta_1$ .

Once again, these expressions look like they might cause trouble if  $\cos\vartheta_1=0$  but the numerators also contain a  $\cos\vartheta_1$ . For  $\dot{\psi}_1$  we get

$$\dot{\psi}_1 = -\varepsilon (1 + \chi [\cos 2\psi_1 (-\cos^2\vartheta_1 + \cos^2\vartheta_2 \sin^2\vartheta_1) + \cos 2\psi_2 (\sin^2\vartheta_2 \sin^2\vartheta_1) + \cos 2(\psi_1 - \psi_2) (-\sin^2\vartheta_2 \sin^2\vartheta_1)]) \quad (\text{B4.14})$$

For  $\dot{\psi}_2$  we get

$$\dot{\psi}_2 = -\varepsilon (2 + \chi [\cos 2\psi_1 \cos^2\vartheta_2 \sin^2\vartheta_1 + \cos 2\psi_2 (-\cos^2\vartheta_1 + \sin^2\vartheta_2 \sin^2\vartheta_1) + \cos 2(\psi_1 - \psi_2) (-\cos^2\vartheta_2 \sin^2\vartheta_1)]) \quad (\text{B4.15})$$

REFERENCES

- (AD 68) J.R. Adam, N.R. Lindblad, and C.D. Hendricks, *J. Appl. Phys.* 39, 5173 (1968)
- (BEI 75) M. Beiner, H. Flocard, Nguyen Van Giai, and P. Quentin, *Nucl. Phys.* A238, 29 (1975)
- (BER 75) G.F. Bertsch and S.F. Tsai, *Phys. Reports* 18, 125 (1975)
- (BO 76a) P. Bonche, S. Koonin, and J.W. Negele, *Phys. Rev.* C13, 1226 (1976)
- (BO 76b) P. Bonche, *J. de Physique* 37 Colloque C5, 213 (1976)
- (BO 78) P. Bonche, B. Grammaticos, and S.E. Koonin, *Phys. Rev.* C17, 1700 (1978)
- (BO 79) P. Bonche, K.T.R. Davies, B. Flanders, H. Flocard, B. Grammaticos, S.E. Koonin, S.J. Krieger, and M.S. Weiss, *Phys. Rev.* C20, 641 (1979)
- (BR 60) D.A. Bromley, J.A. Kuchner, and E. Almquist, *Phys. Rev. Lett.* 4, 365 (1960)
- (BR 78) R.A. Broglia, C.H. Dasso, G. Pollarolo, and A. Winther, *Phys. Rev. Lett.* 40, 707 (1978)
- (DAS 79) C.H. Dasso, T. Døssing, and H.C. Pauli, *Z. Phys.* A289, 395 (1979)
- (DAV 74) K.T.R. Davies, R.J. McCarthy, J.W. Negele, and P.U. Sauer, *Phys. Rev.* C10, 2607 (1974)
- (DAV 78a) K.T.R. Davies, V. Maruhn-Rezwani, S.E. Koonin, and J.W. Negele, *Phys. Rev. Lett.* 41, 632 (1978)
- (DAV 78b) K.T.R. Davies, H.T. Feldmeier, H. Flocard, and M.S. Weiss, *Phys. Rev.* C18, 2631 (1978)
- (DAV 79) K.T.R. Davies, K.R. Sandhya Devi, and M.R. Strayer, *Phys. Rev.* C20, 1372 (1979)
- (DAV 80) K.T.R. Davies, K.R. Sandhya Devi, and M.R. Strayer, *Phys. Rev. Lett.* 44, 23 (1980)
- (DAV 81) K.T.R. Davies and S.E. Koonin, *Phys. Rev.* C23, 2042 (1981)
- (DE 78a) K.R. Sandhya Devi and M.R. Strayer, *J. Phys.* G4, L97 (1978)

- (DE 78b) K.R. Sandhya Devi and M.R. Strayer, *Phys. Lett.* 77B, 135 (1978)
- (DI 30) P.A.M. Dirac, *Proc. Cam. Phil. Soc.* 26, 376 (1930)
- (DY 80) P. Dyer, M.P. Webb, R.J. Puigh, R. Vandenbosch, T.D. Thomas, and M.S. Zisman, *Phys. Rev.* C22, 1509 (1980)
- (EN 75) Y.M. Engel, D.M. Brink, K. Goeke, S.J. Krieger, and D. Vautherin, *Nucl. Phys.* A249, 215 (1975)
- (FL 78) H. Flocard, S.E. Koonin, and M.S. Weiss, *Phys. Rev.* C17, 1682 (1978)
- (GA 75) B. Gatty, D. Guerreau, M. Lefort, X. Tarrago, J. Galin, B. Cauvin, J. Girard, and H. Nifenecker, *Nucl. Phys.* A253, 511 (1975)
- (GA 76) J. Galin, B. Gatty, D. Guerreau, M. Lefort, X. Tarrago, R. Babinet, B. Cauvin, J. Girard, and H. Nifenecker, *Nucl. Phys.* A278, 347 (1976)
- (GO 50) H. Goldstein, *Classical Mechanics*, (Addison-Wesley, Cambridge, 1950), p. 83
- (HOL 74) G. Holzworth and T. Yukawa, *Nucl. Phys.* A219, 125 (1974)
- (HOO 77) P. Hoodboy and J.W. Negele, *Nucl. Phys.* A288, 23 (1977)
- (HU 76) J.R. Huizenga, J.R. Birkelund, W.U. Schröder, K.L. Wolf, and V.E. Viola, *Phys. Rev. Lett.* 37, 885 (1976)
- (KE 76) A.K. Kerman and S.E. Koonin, *Ann. Phys.* 100, 332 (1976)
- (KO 76) S. Koonin, *Phys. Lett.* 61B, 227 (1976)
- (KO 77) S.E. Koonin, K.T.R. Davies, V. Maruhn-Rezwani, H. Feldmeier, S.J. Krieger, and J.W. Negele, *Phys. Rev.* C15, 1359 (1977)
- (KO 78) S.E. Koonin, B. Flanders, H. Flocard, and M.S. Weiss, *Phys. Lett.* 77B, 13 (1978)
- (KO 79a) S.E. Koonin, *Marmal Aid Preprint 5* (1979)
- (KO 79b) S.E. Koonin, *Marmal Aid Preprint 6* (1979)
- (KRA 77) V. Kratz, H. Ahrens, W. Bögl, W. Bröchle, G. Franz, M. Schadel, I. Warnecke, G. Wirth, G. Klein and M. Weiss, *Phys. Rev. Lett.* 39, 984 (1977)
- (KRI 77) S.J. Krieger, *Nucl. Phys.* A276, 12 (1977)

- (KRI 78) S.J. Krieger and K.T.R. Davies, Phys. Rev. C18, 2567 (1978)
- (LE 73) M. Lefort, C. Ngô, J. Péter, and B. Tamain, Nucl. Phys. A216, 166 (1973)
- (LE 78) M. Lefort and C. Ngô, Ann. Phys. Series 15 V.3, 5 (1978)
- (LI 70) S.Y. Li, A. Klein, and R.M. Dreizler, J. Math Phys. 11, 975 (1970)
- (LIP 65) H.J. Lipkin, N. Meshkov, and A.J. Glick, Nucl. Phys. 62, 188 (1965)
- (MA 70) J. Mathews and R.L. Walker, Mathematical Methods of Physics, Second Edition, (Benjamin, New York, 1970), p. 107
- (NA 79) J.B. Natowitz, G. Doukellis, B. Kolb, G. Rosner, and Th. Walcher, Nukleonika 24, 443 (1979)
- (NE 70) J.W. Negele, Phys. Rev. C1, 1260 (1970)
- (NE 72) J.W. Negele and D. Vautherin, Phys. Rev. C5, 1472 (1972)
- (NE 78) J.W. Negele, S.E. Koonin, P. Möller, J.R. Nix, and A.J. Sierk, Phys. Rev. C17, 1098 (1978)
- (NO 76) W. Nörenberg and H.A. Weidenmüller, Introduction to the Theory of Heavy-Ion Collisions, Lecture Notes in Physics, 51, (Springer-Verlag, Heidelberg, 1976)
- (PI 66) D. Pines and P. Nozières, The Theory of Quantum Liquids Vol. 1, (Benjamin, N.Y. 1966), Chapter 1
- (SC 77) W.U. Schröder, J.R. Birkelund, J.R. Huizenga, K.L. Wolf, and V.E. Viola, Jr., Phys. Rev. C16, 623 (1977)
- (SI 76) K. Siwek-Wilczynski and J. Wilczynski, Nucl. Phys. A264, 115 (1976)
- (SK 56) T.H.R. Skyrme, Phil. Mag. 1, 1043 (1956)
- (TA 75) B. Tamain, C. Ngô, J. Péter, and F. Hanappe, Nucl. Phys. A252, 187 (1975)
- (TH 61) D.J. Thouless, Nucl. Phys. 21, 225 (1961)
- (TI 74) C. Titin-Schnaider and P. Quentin, Phys. Lett. 49B, 397 (1974)
- (TS 74) C.F. Tsang, Physica Scripta 10A, 90 (1974)
- (VAN 78) R. Vandenbosch, M.P. Webb, P. Dyer, R.J. Puigh, R. Weisfield, T.D. Thomas, and M.S. Zisman, Phys. Rev. C17, 1672 (1978)

- (VAU 72) D. Vautherin and D.M. Brink, Phys. Rev. C5, 626 (1972)
- (VI 79) S.E. Vigdor, D.G. Kovar, P. Sperr, J. Mahoney, A. Menchaca -  
Rocha, C. Olmer, and M.S. Zisman, Phys. Rev. C20, 2147 (1979)
- (WI 73) J. Wilczynski, Phys. Lett. 47B, 484 (1973)

FIGURE CAPTIONS

- Figure 1. Schematic possibilities for the double differential cross section of heavy-ion reactions. Shaded areas indicate peaks. Fig. 1a shows fusion-fission; whereas Fig. 1b shows deep-inelastic reactions.
- Figure 2. Schematic classical analysis of heavy-ion scattering; each initial angular momentum leads to a definite energy and scattering angle. These can be plotted as a trajectory for comparison with experiment as in Fig. 2a; or plotted separately as in Figs. 2b and 2c to determine various macroscopic parameters, such as the interaction time as in Fig. 2d.
- Figure 3. Rms. radius of the Kr + La system as a function of time for four initial angular momenta. These show both scattering and fusion events, along with one ambiguous event.
- Figure 4. Comparison of our calculated trajectory of energy vs. scattering angle for Kr + La with the axially symmetric calculation and the experimental contours of the double differential cross section.
- Figure 5. Energy, scattering angle and interaction times as functions of the initial angular momentum for Kr + La.  $E_i$  denotes the initial bombarding energy.

Figure 6. Charge and mass transfers, charge and mass widths, and charge to mass ratio as functions of the initial angular momentum. Charge to mass ratios of the original Kr nucleus and the total system are also shown.

Figure 7. Schematic illustration of (a) stable and (b) unstable TDHF solutions.

Figure 8. Contours of the potential energy surface in the SU(3) model for  $\chi = 0.5$ .

Figure 9. Energy surface for  $\chi = 2.5$

Figure 10. Energy surface for  $\chi = 5$

Figure 11. Energy surface for  $\chi = 10$

Figure 12. Energy surface for  $\chi = 20$

Figure 13. Energy surface for  $\chi = 100$

Figure 14. Oscillations of the TDHF solution near the minimum of the SU(3) model with  $\chi = 10$  and the periods derived from an RPA analysis.

Figure 15. TDHF path and TDRPA frequencies for a stable path, in valley, with  $\chi = 100$ . Position is shown at time steps  $dt = 0.01$ .

Figure 16. TDHF path and TDRPA frequencies for an unstable path, across ridges, with  $\chi = 100$ .  $dt = 0.01$ .

Figure 17. TDHF path and TDRPA frequencies for an intermediate path with  $\chi = 100$ .  $dt = 0.01$ .

Figure 18. TDHF path and TDRPA frequencies for a stable path, in a valley, with  $\chi = 5$ .  $dt = 0.1$ .

Figure 19. Comparison of the HF and exact ground state energies.

Figure 20. Deviation of the exact ground states from independent particle states,  $\text{Tr}(\rho - \rho^A)$ .

Figure 21. Comparisons of the positions of the HF and exact ground states.

Figure 22. Comparisons of stable and unstable TDHF paths with exact paths for  $\chi = 5$ .

Figure 23. Comparison of TDHF and exact oscillations near the minimum for  $\chi = 5$ .

Figure 24. Comparison of TDHF and exact oscillations near the minimum for  $\chi = 10$ .

Figure 25. Comparison of TDHF and exact oscillations near the minimum for  $\chi = 20$ .

Figure 26. Comparison of TDHF and exact oscillations near the minimum for  $\chi = 100$ .

Figure 27. Deviation of the exact solutions from independent particle states for the paths in Figure 26.

Figure 28. Comparison of the TDHF and exact positions,  $\theta_1$ , for an unstable path with  $\chi = 100$ .

Figure 29. Comparison of the TDHF and exact positions,  $\theta_2$ , for an unstable path with  $\chi = 100$ .

Figure 30. Comparison of an unstable TDHF path with exact paths for  $\chi = 100$ .

Figure 31. Deviation of the exact solutions from independent particle states for the paths in Figures 28 - 30.

Figure 32. Slicing of the densities (projected onto the scattering plane) for separated and unseparated fragments.

Figure 33. Equivalent two-sphere systems for the densities in Figure 32.

Energy - Mass Correlations in Heavy-Ion Scattering

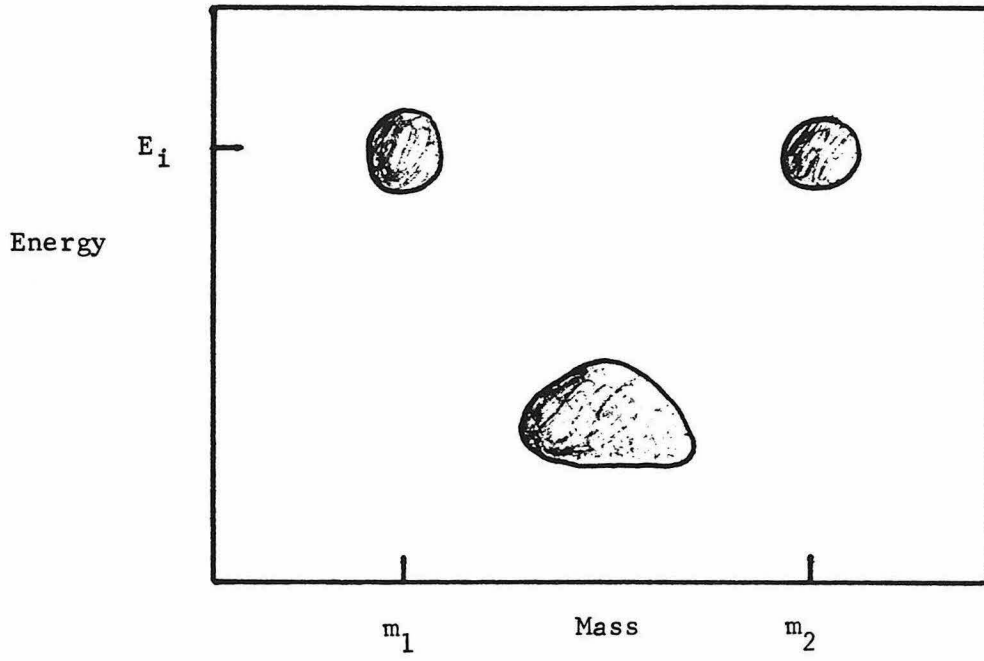


Figure 1a

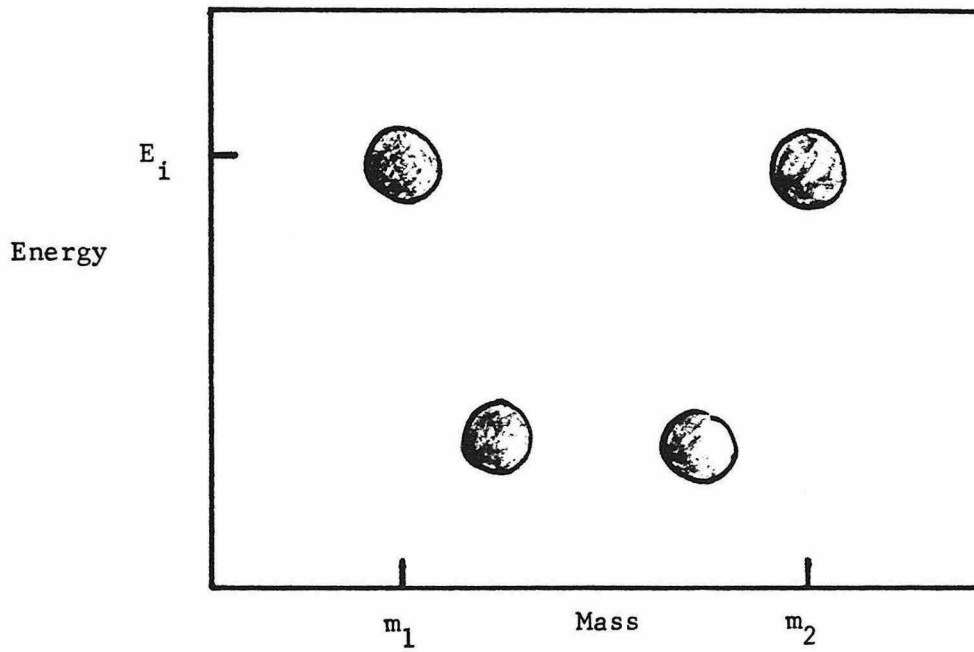


Figure 1b

Classical Analysis of Heavy-Ion Scattering

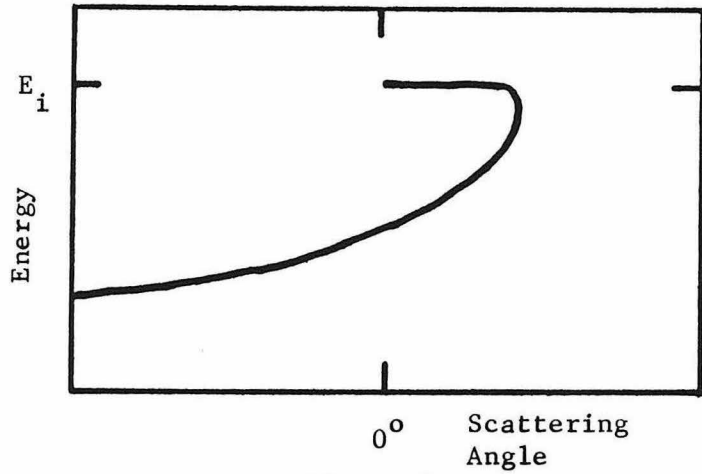


Figure 2a

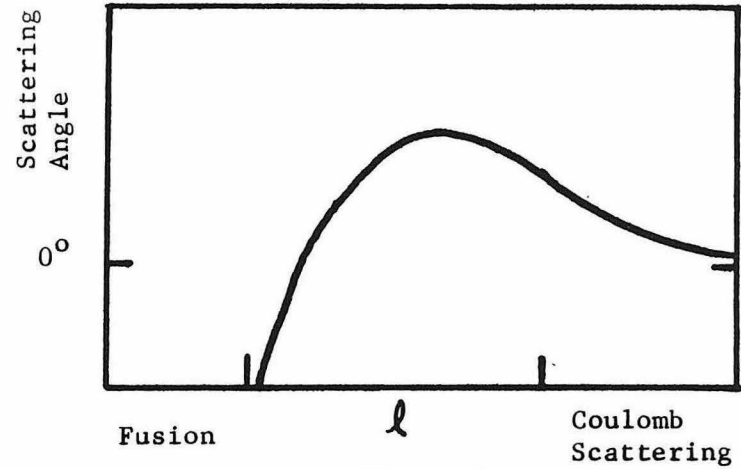


Figure 2c

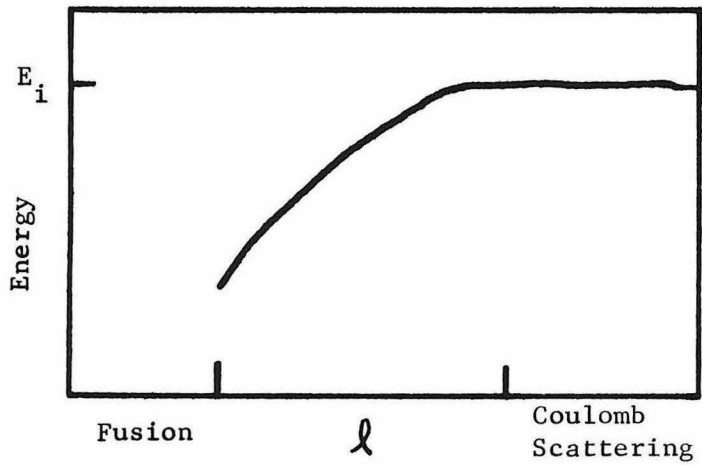


Figure 2b

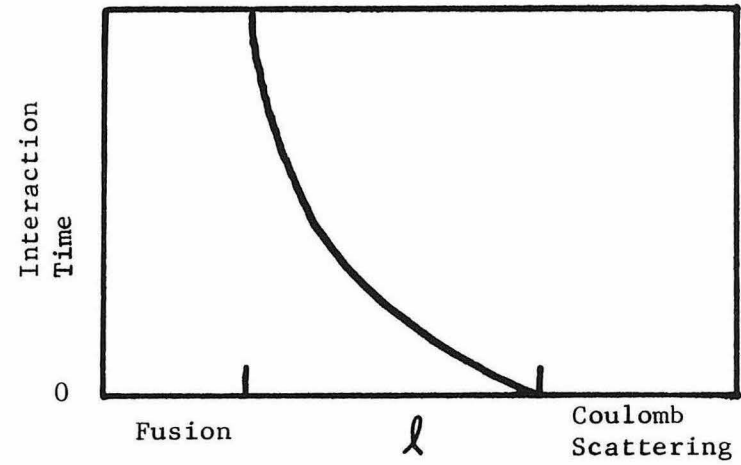


Figure 2d

TDHF Results for  $^{86}\text{Kr} + ^{139}\text{La}$

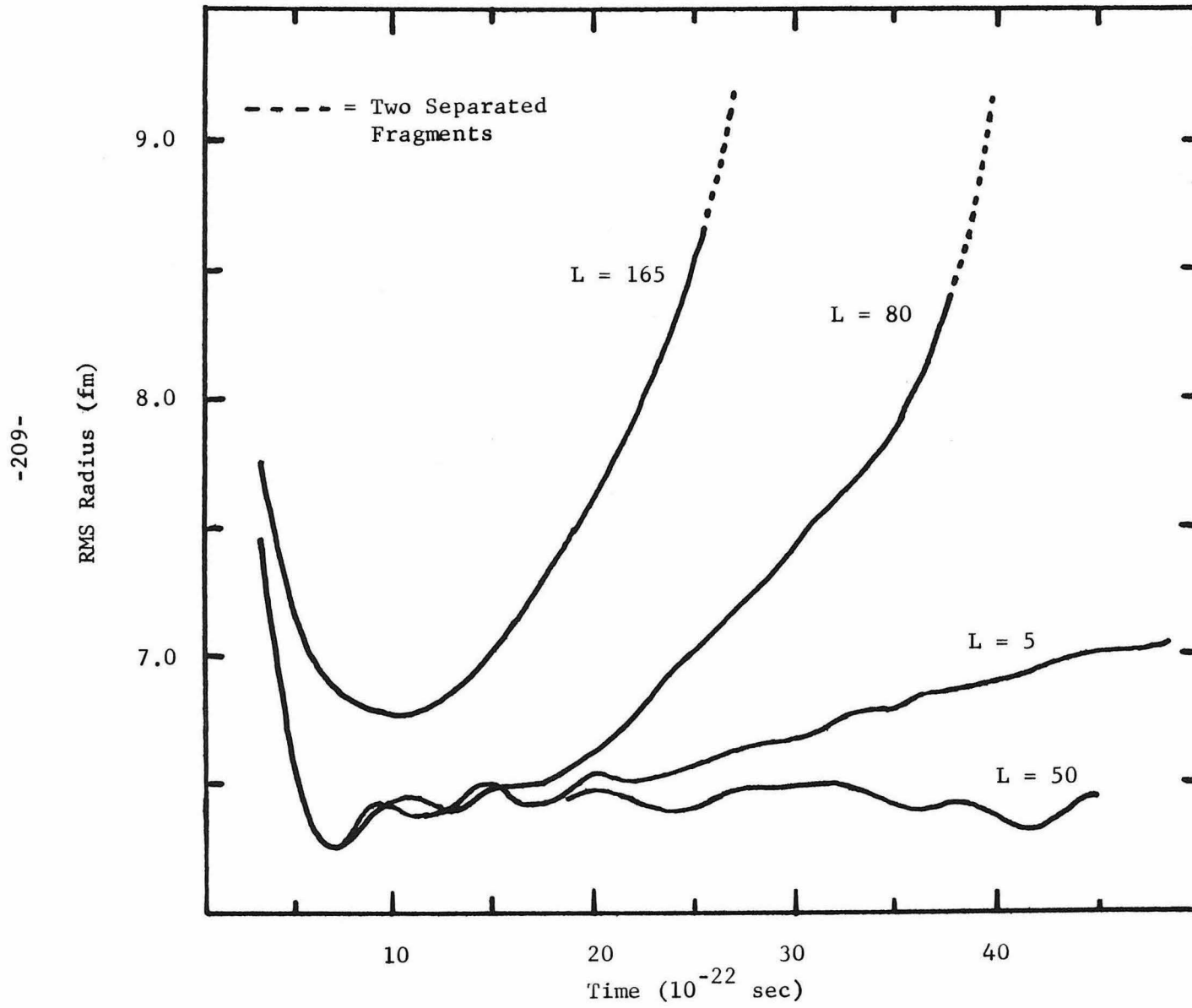


Figure 3

Comparison of TDHF Results with the Experimental Double Differential Cross Section

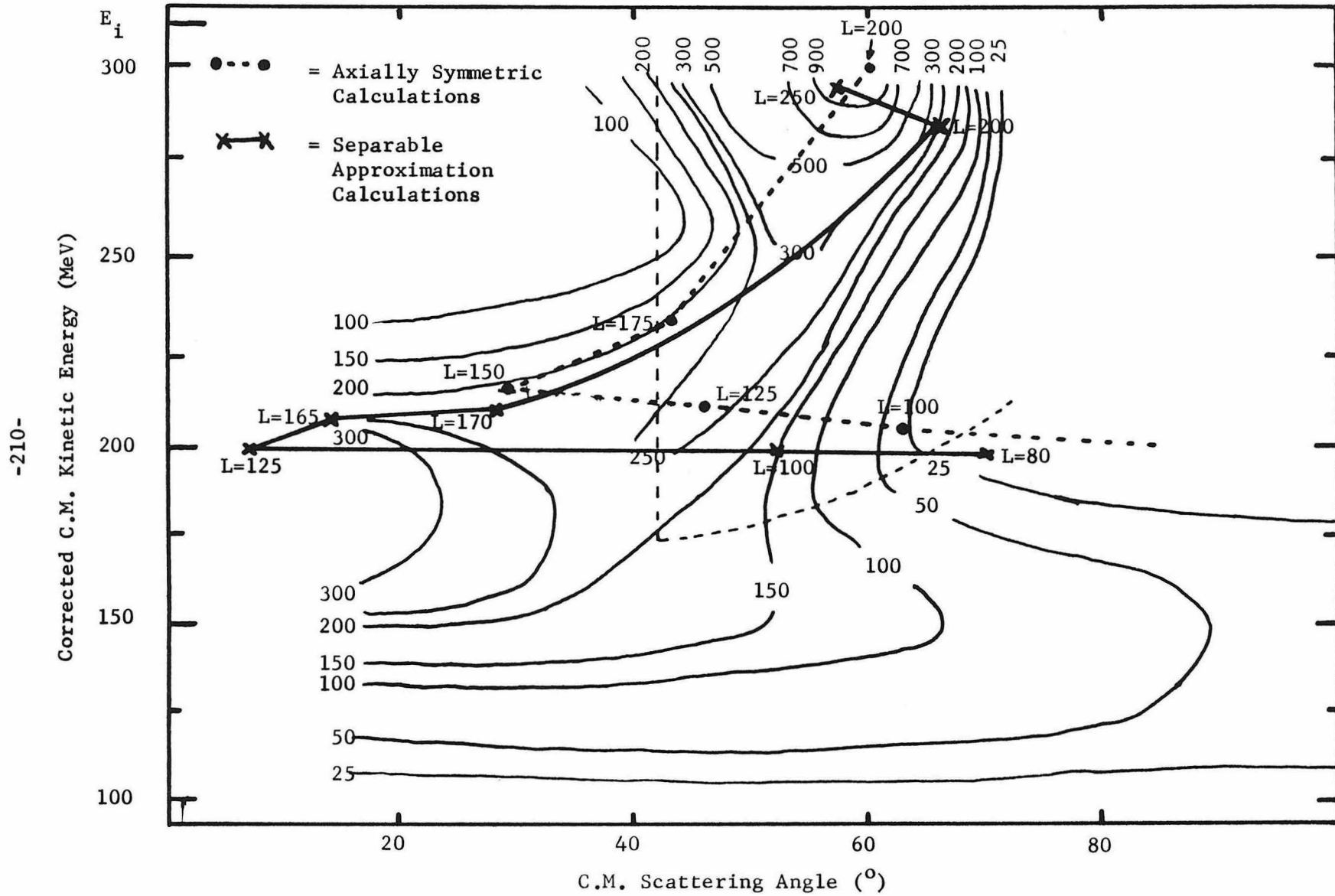
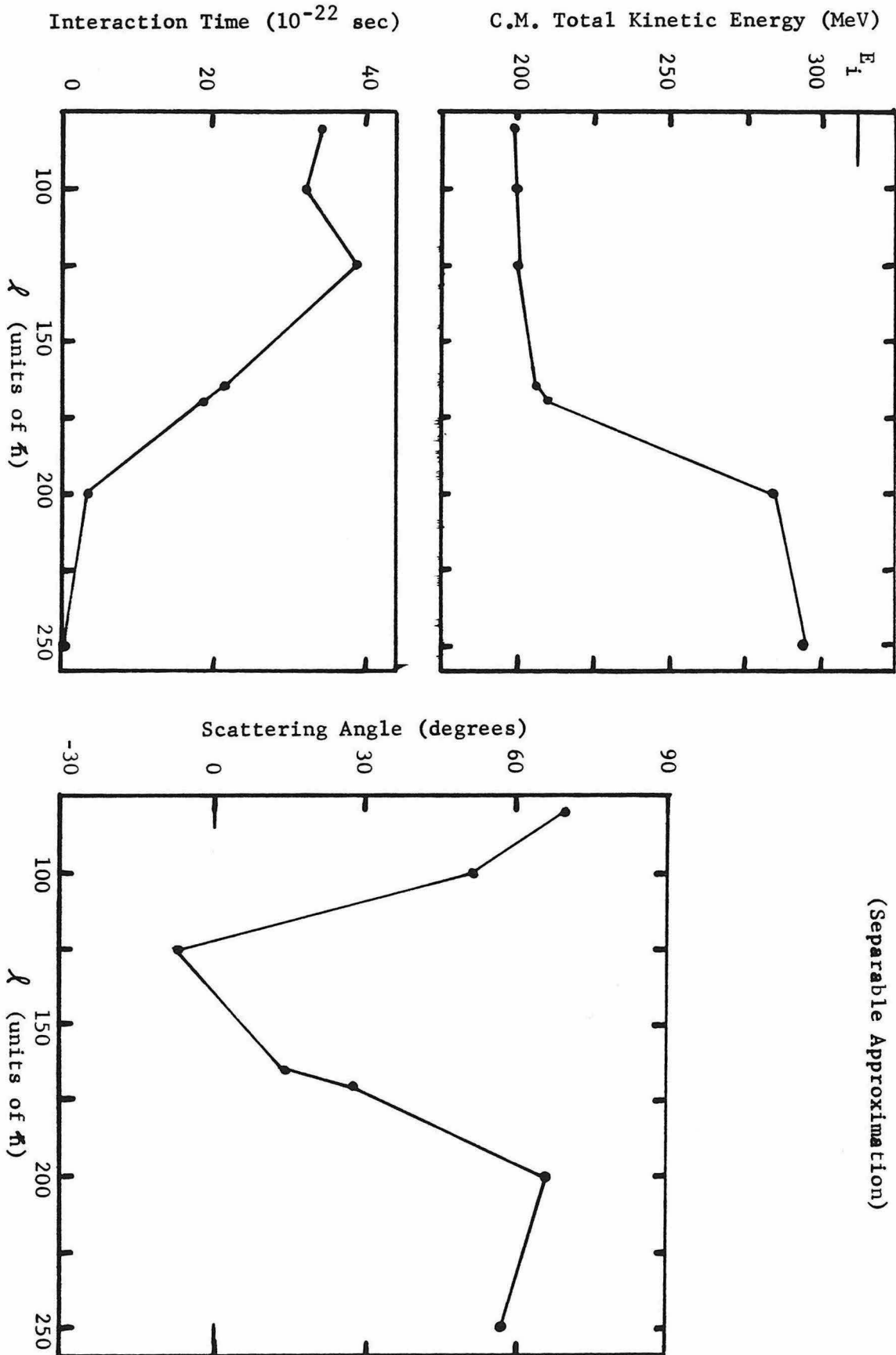
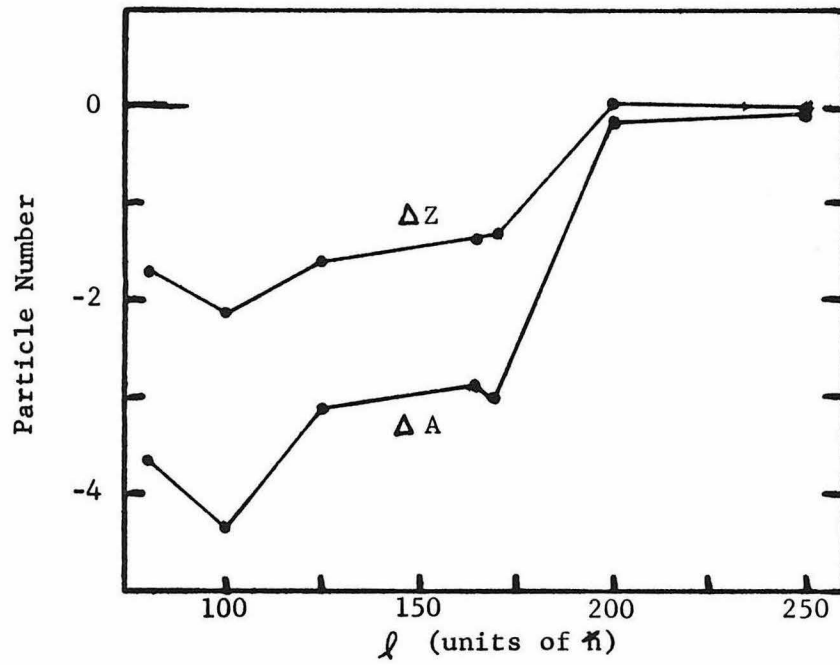
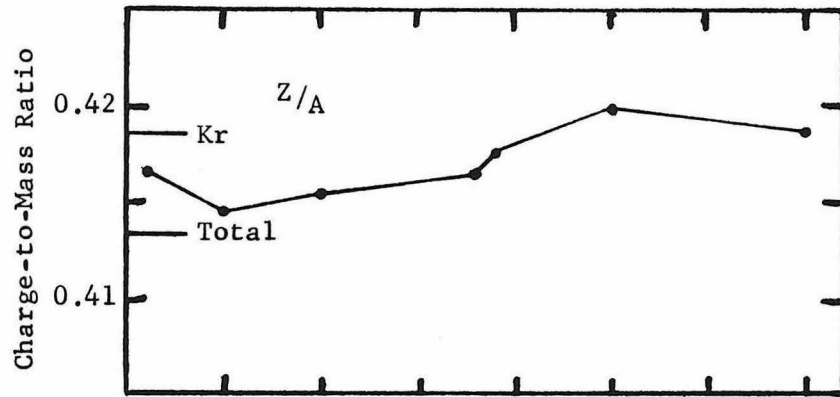


Figure 4



TDHF Results for  $^{86}\text{Kr} + ^{139}\text{La}$   
(Separable Approximation)

Figure 5



TDHF Results for  $^{86}\text{Kr} + ^{139}\text{La}$   
(Separable Approximation)

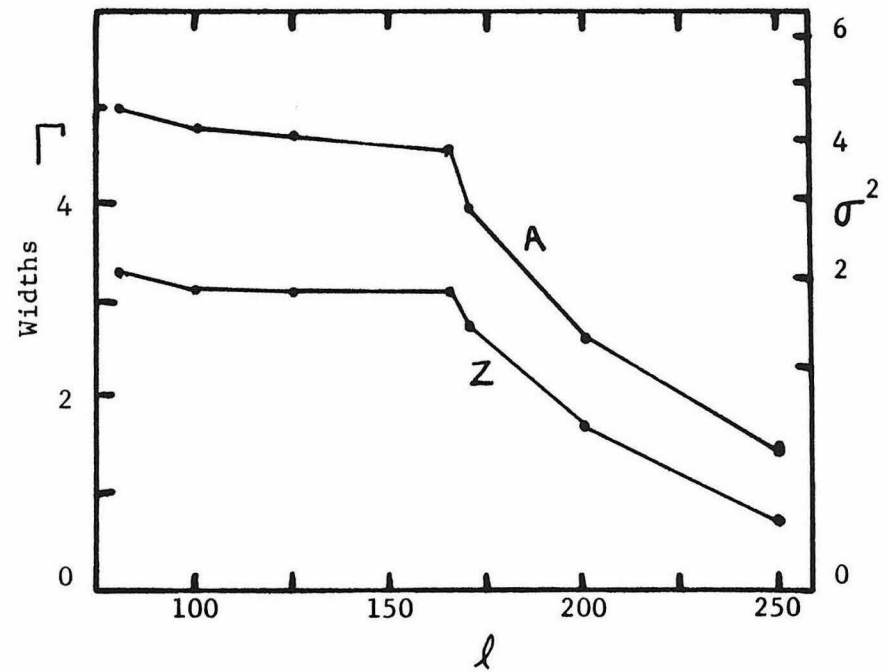
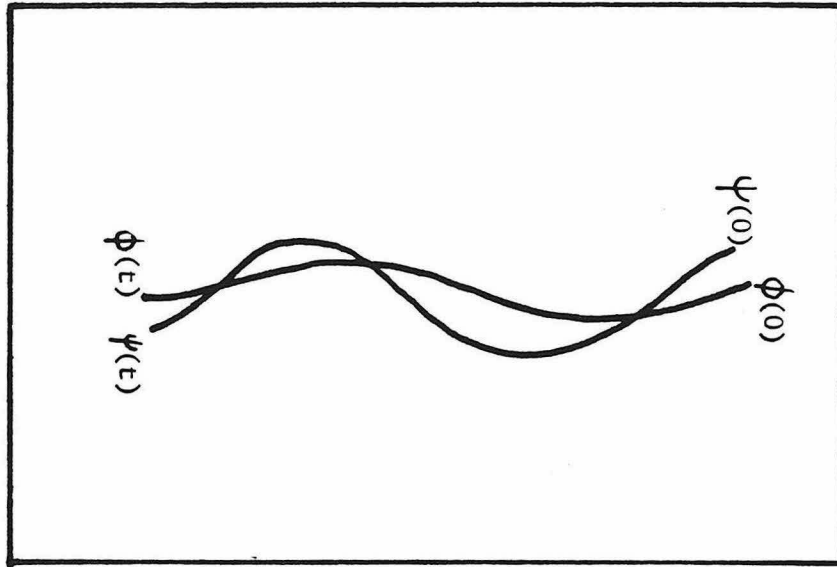
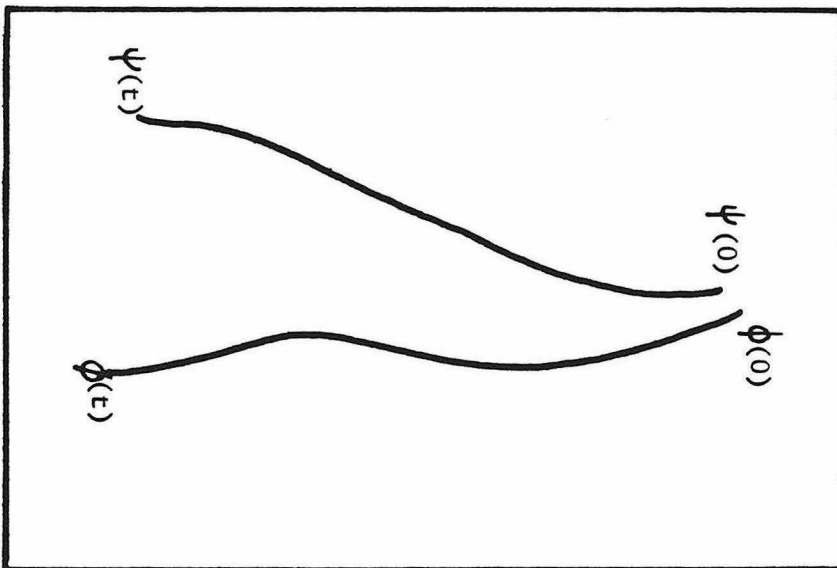


Figure 6



Stable

Figure 7a



Unstable

Figure 7b

Contours  $H/N\epsilon$   $\chi = 0.5$

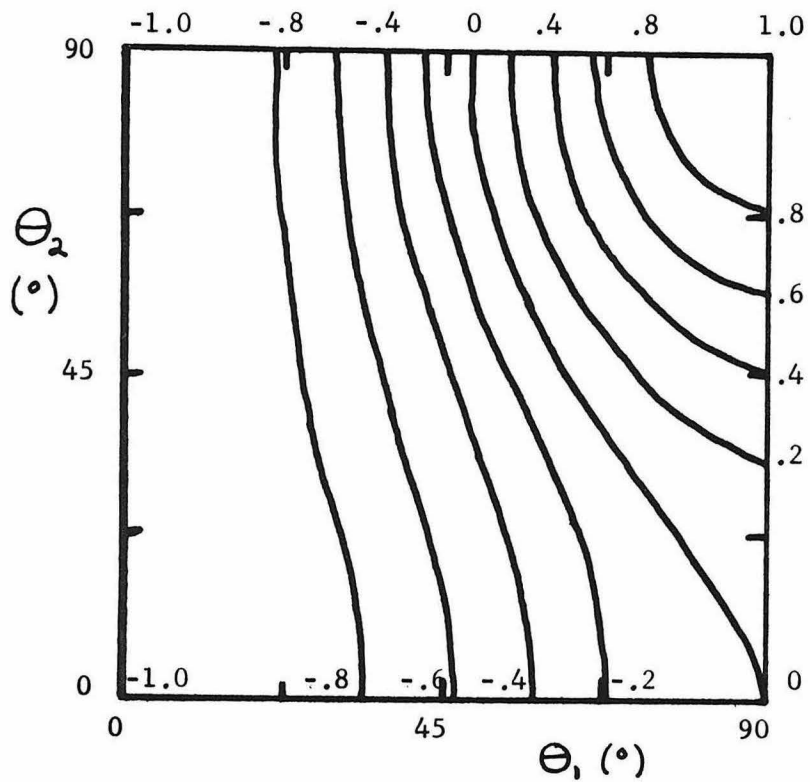


Figure 8

$\chi = 2.5$

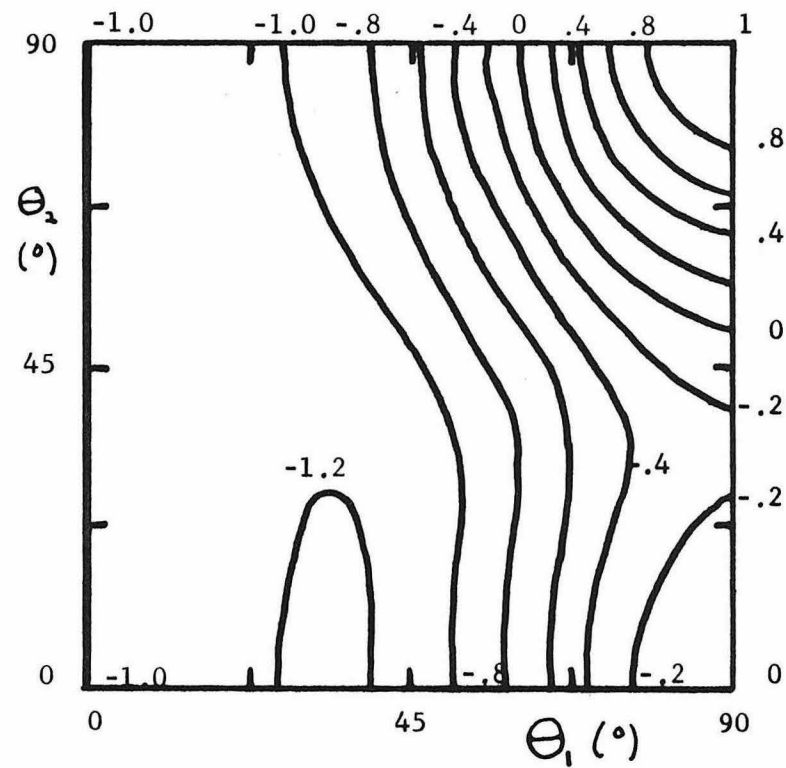


Figure 9

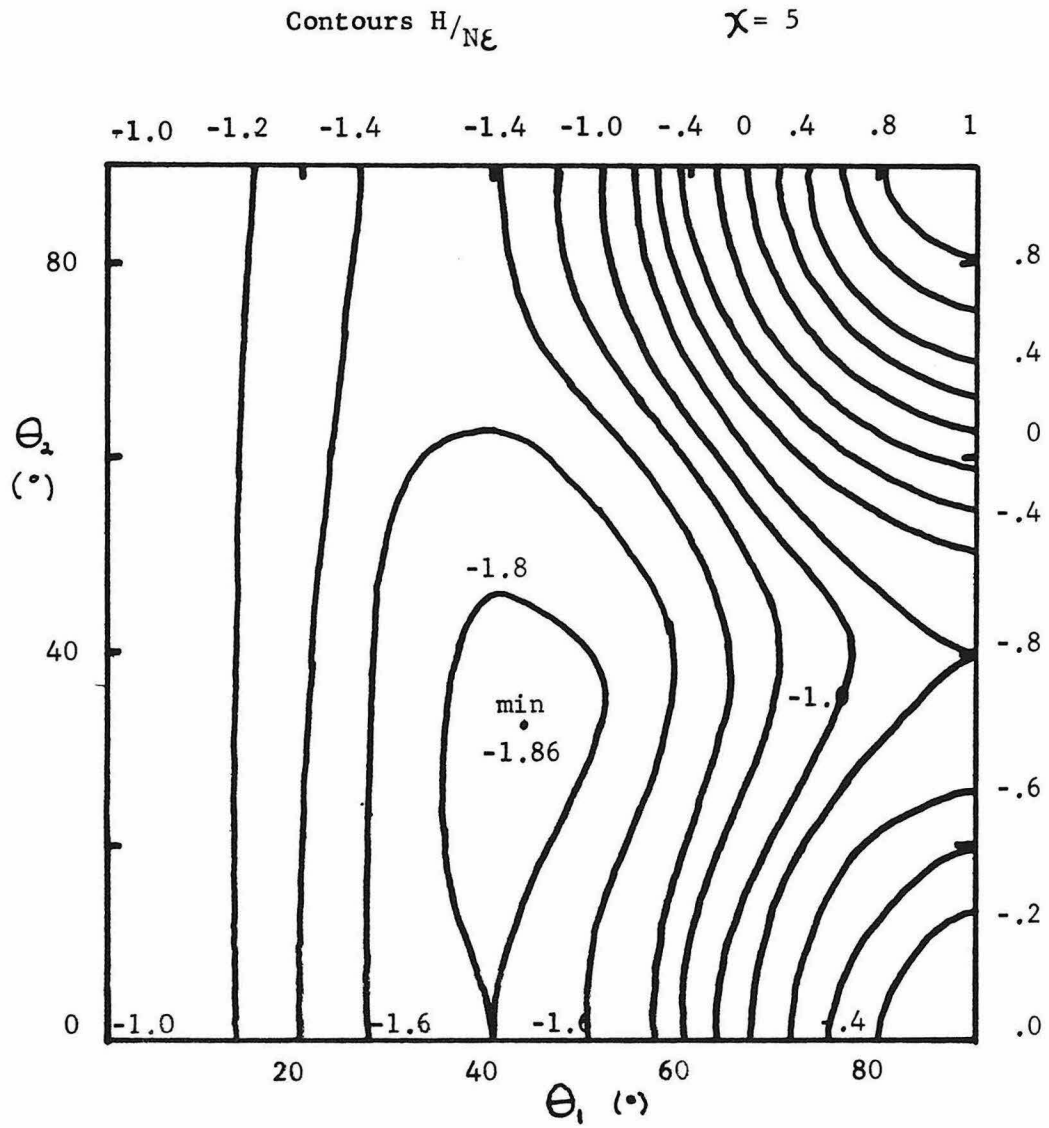


Figure 10

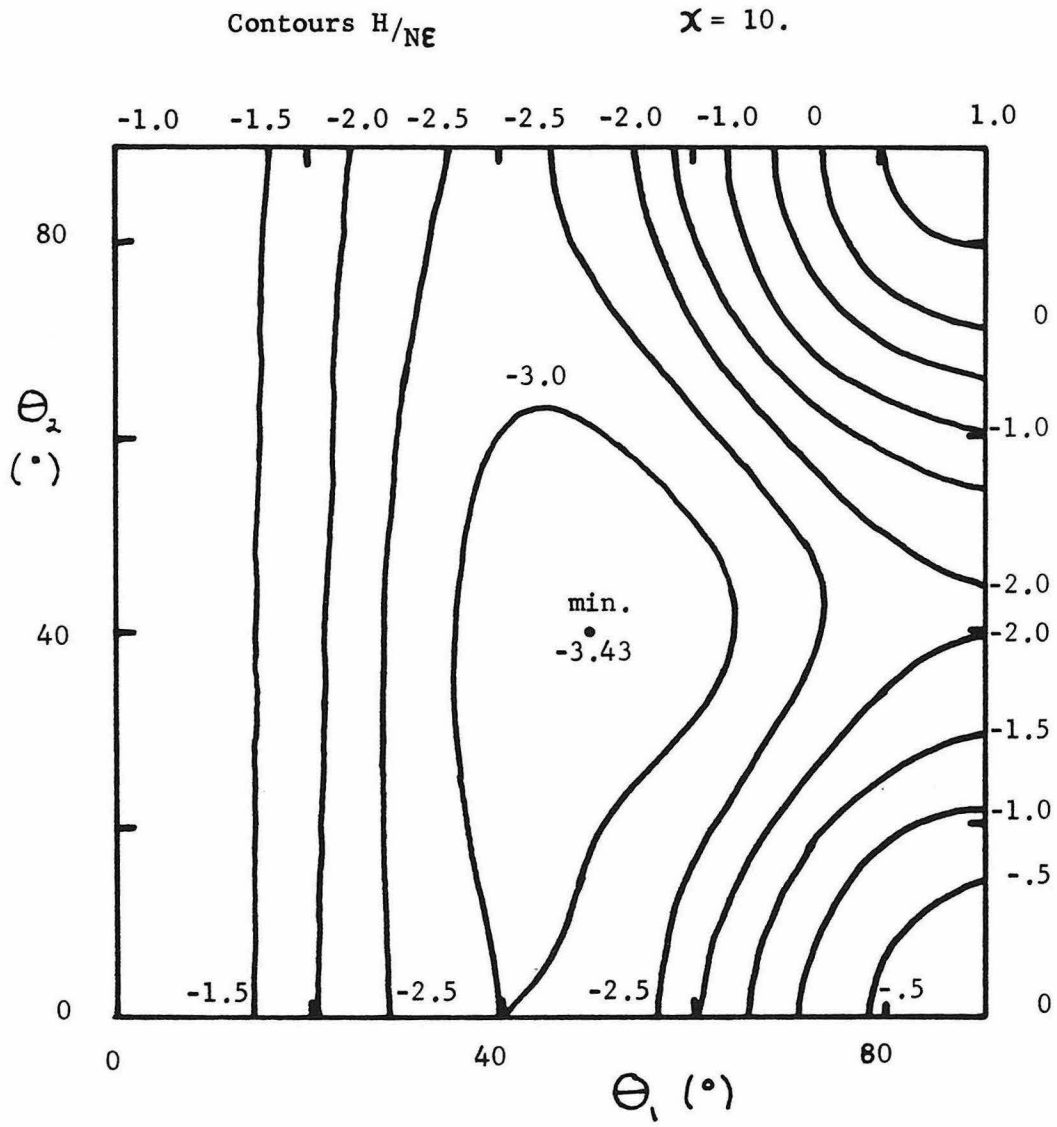


Figure 11

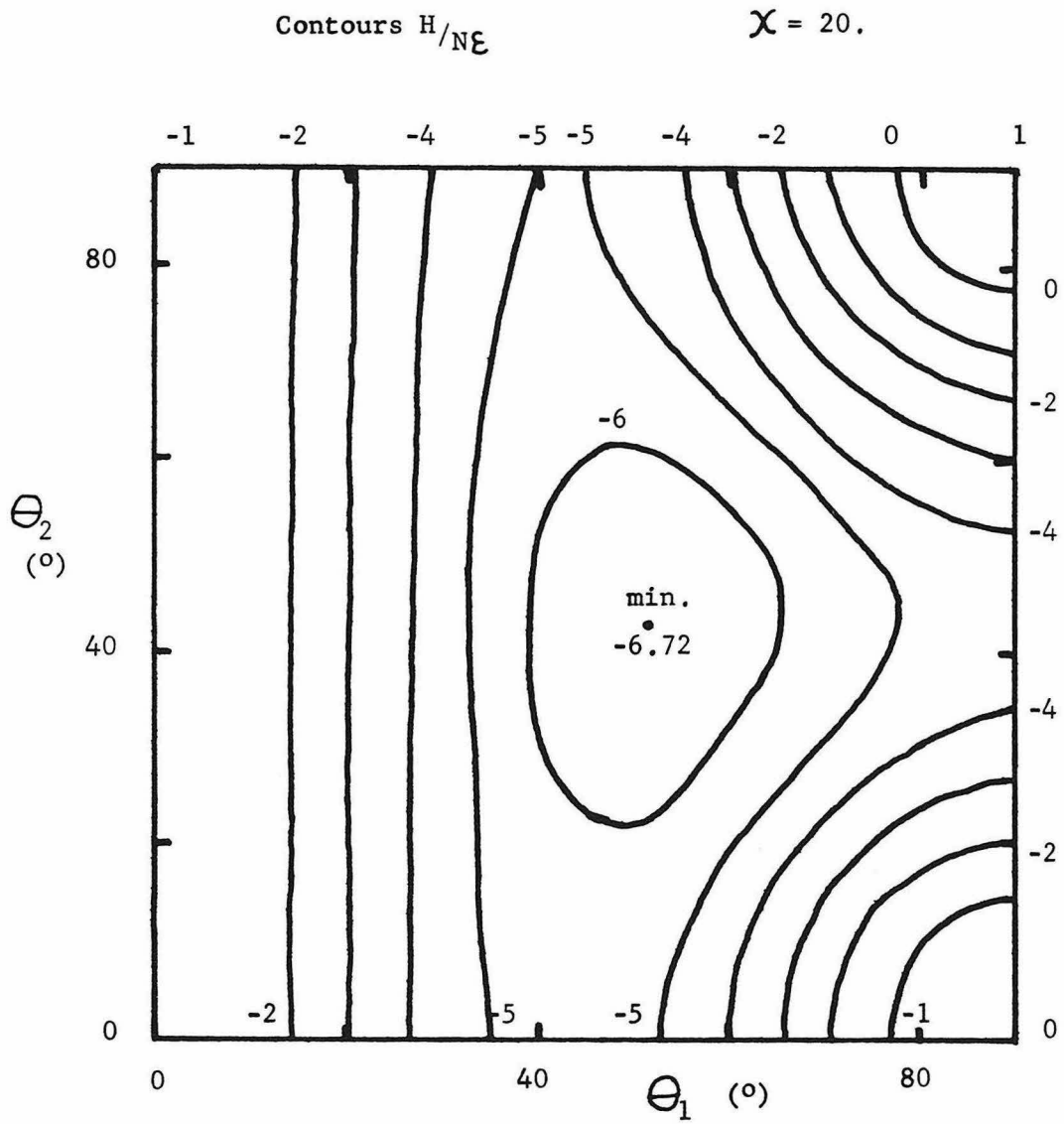


Figure 12

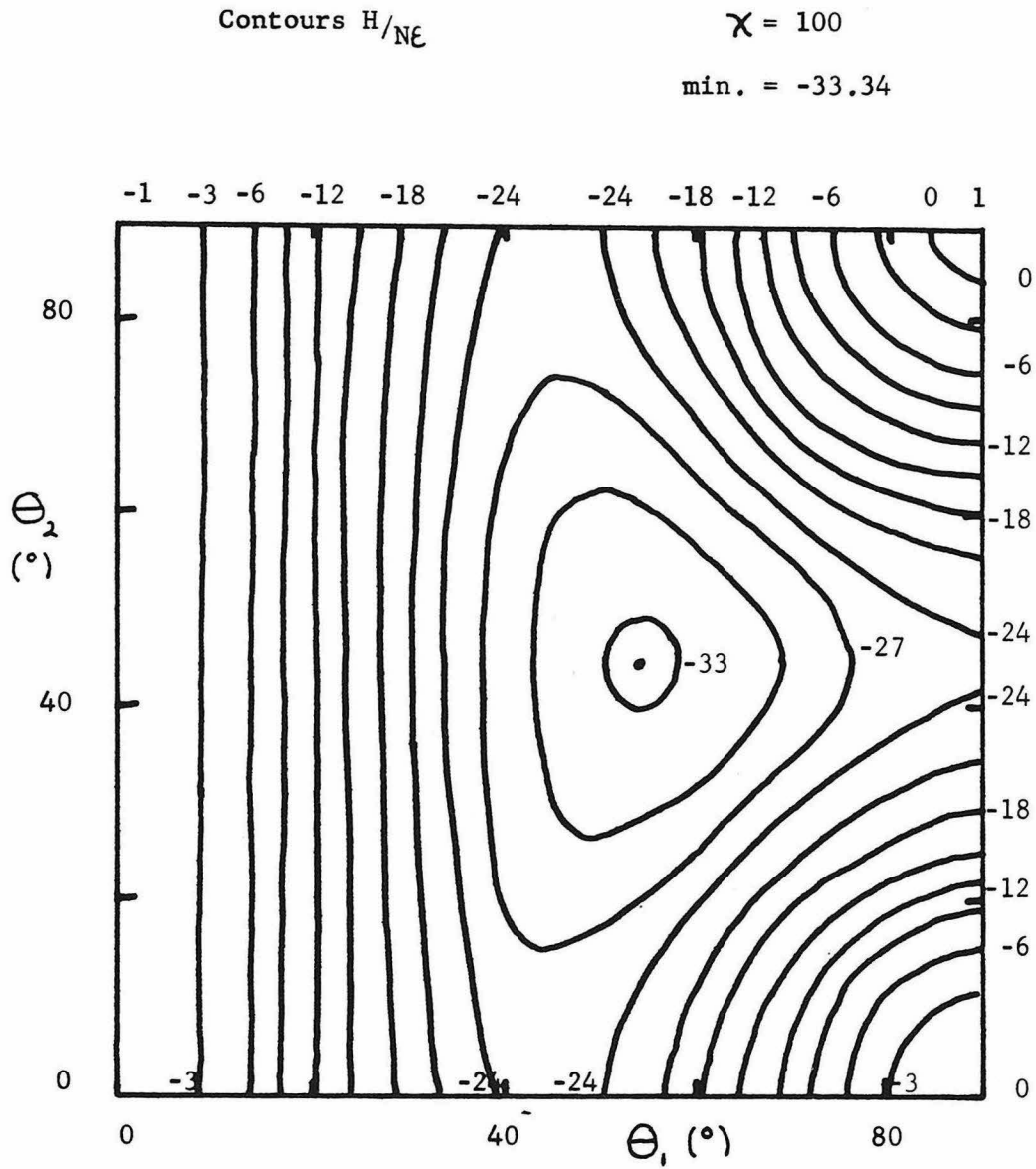


Figure 13

TDHF Positions and RPA Periods

$$\chi = 10$$

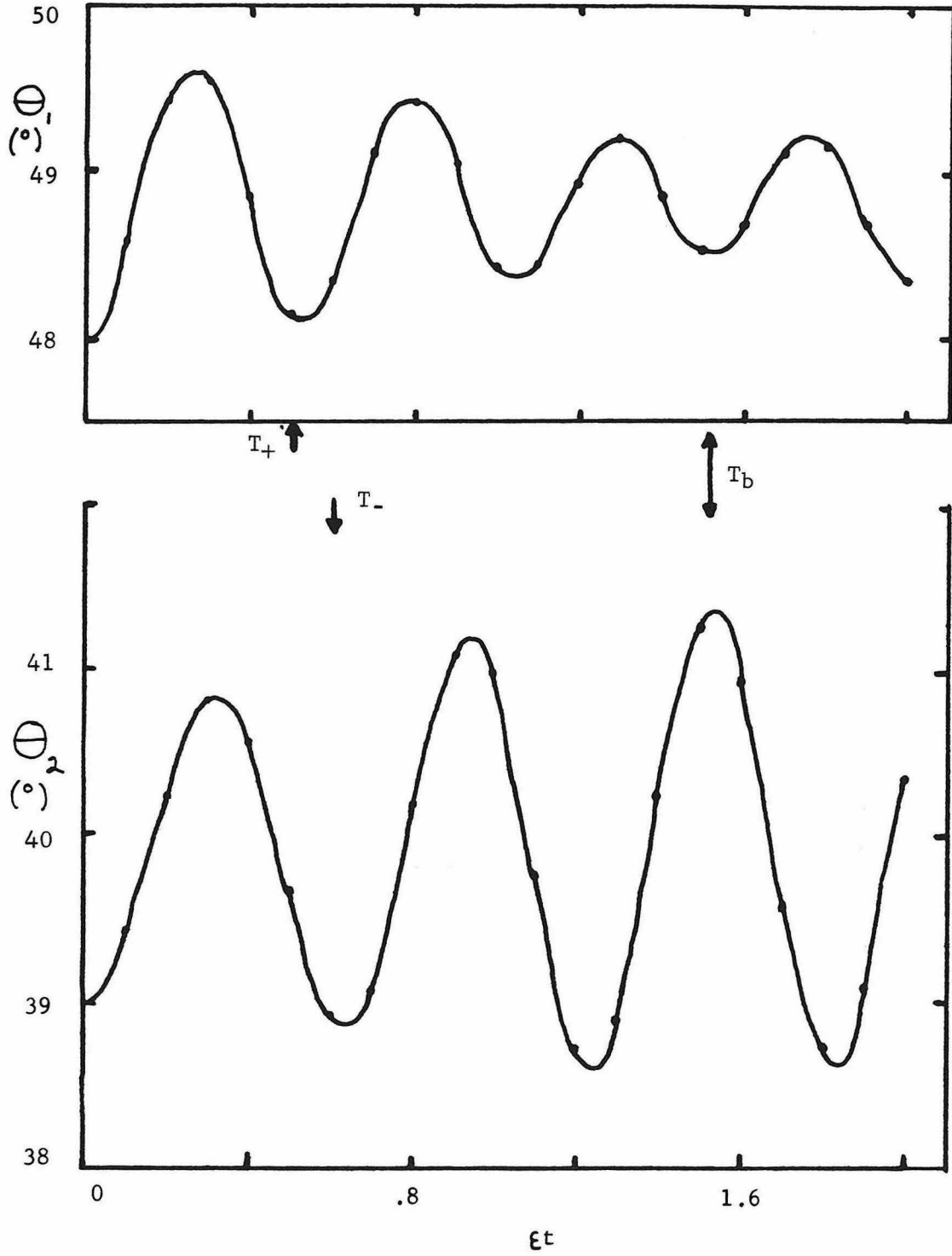


Figure 14

TDHF Path with TDRPA Frequencies  $(\omega/\epsilon)^2 (10^4)$

$\chi = 100$

$dt = .01$

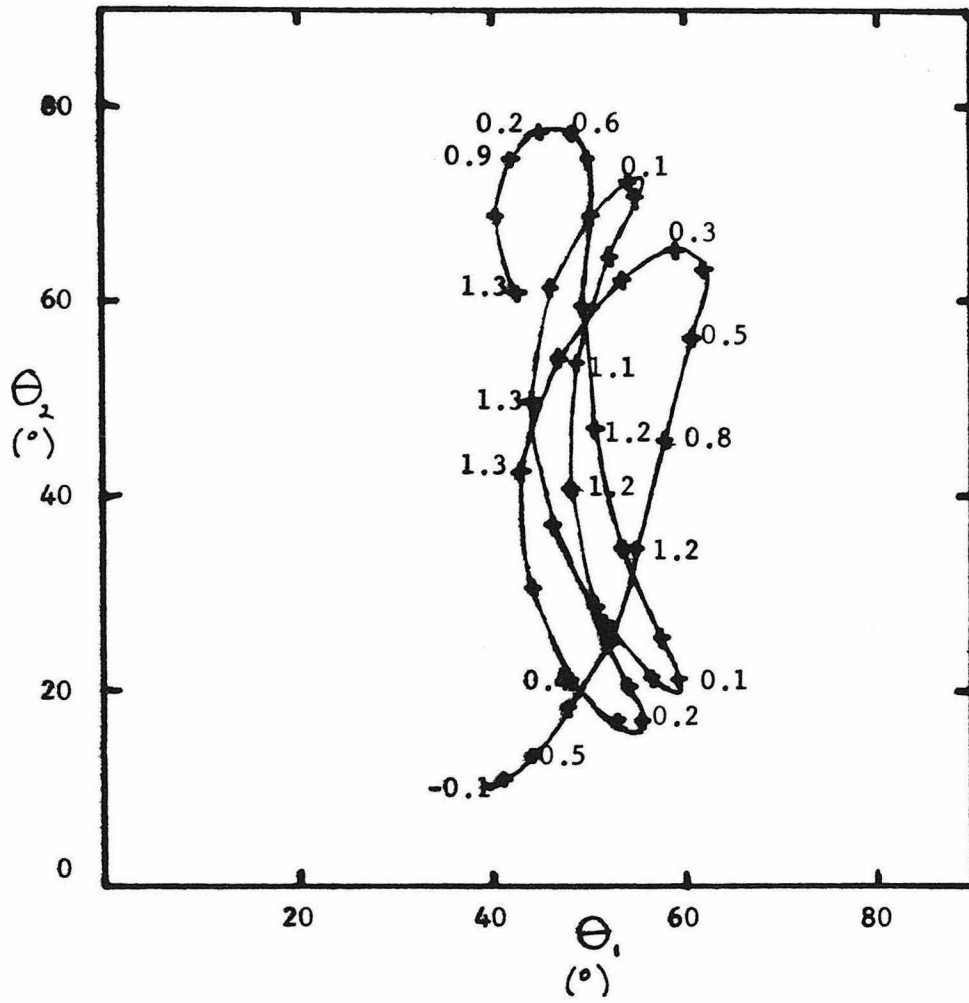


Figure 15

TDHF Path with TDRPA Frequencies  $(\omega/\varepsilon)^2 (10^4)$

$\chi = 100$

$dt = .01$

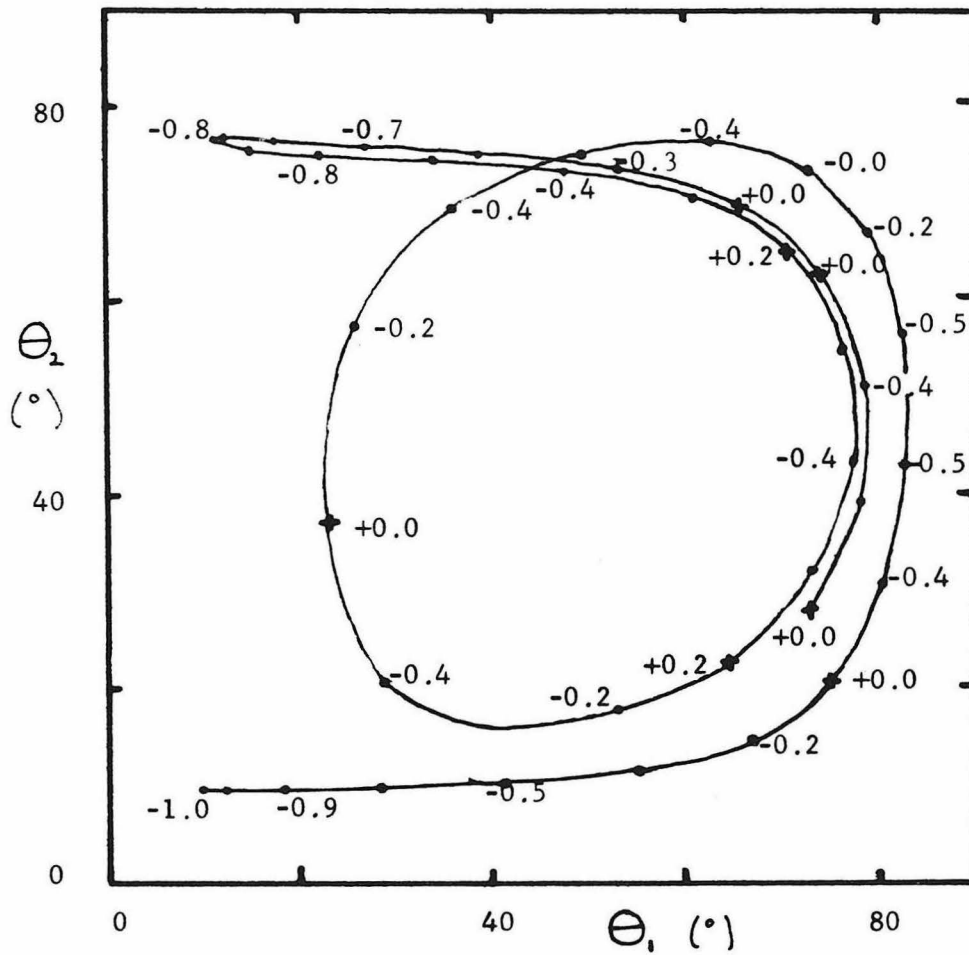


Figure 16

TDHF Path with TDRPA Frequencies  $(\omega/\epsilon)^2 (10^4)$

$\chi = 100$

$dt = .01$

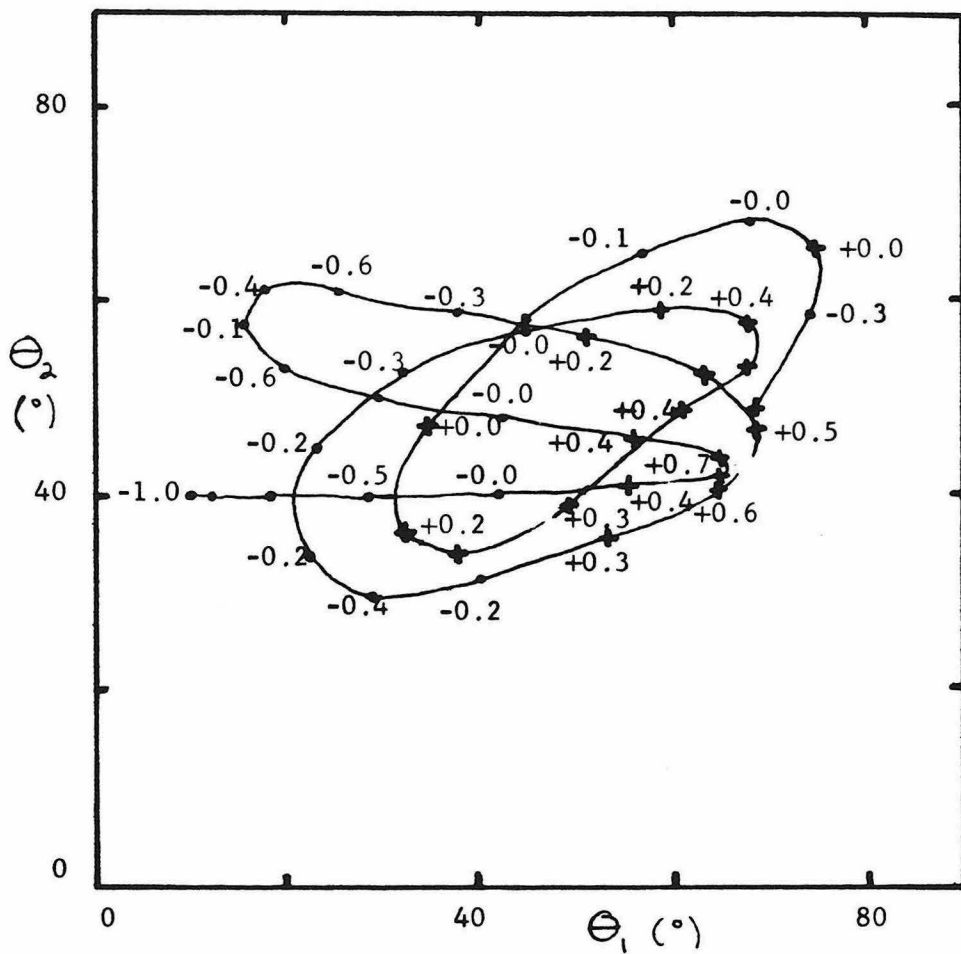


Figure 17

TDHF Path with TDRPA Frequencies  $(\omega/\epsilon)^2$

$\chi = 5$

$dt = .1$

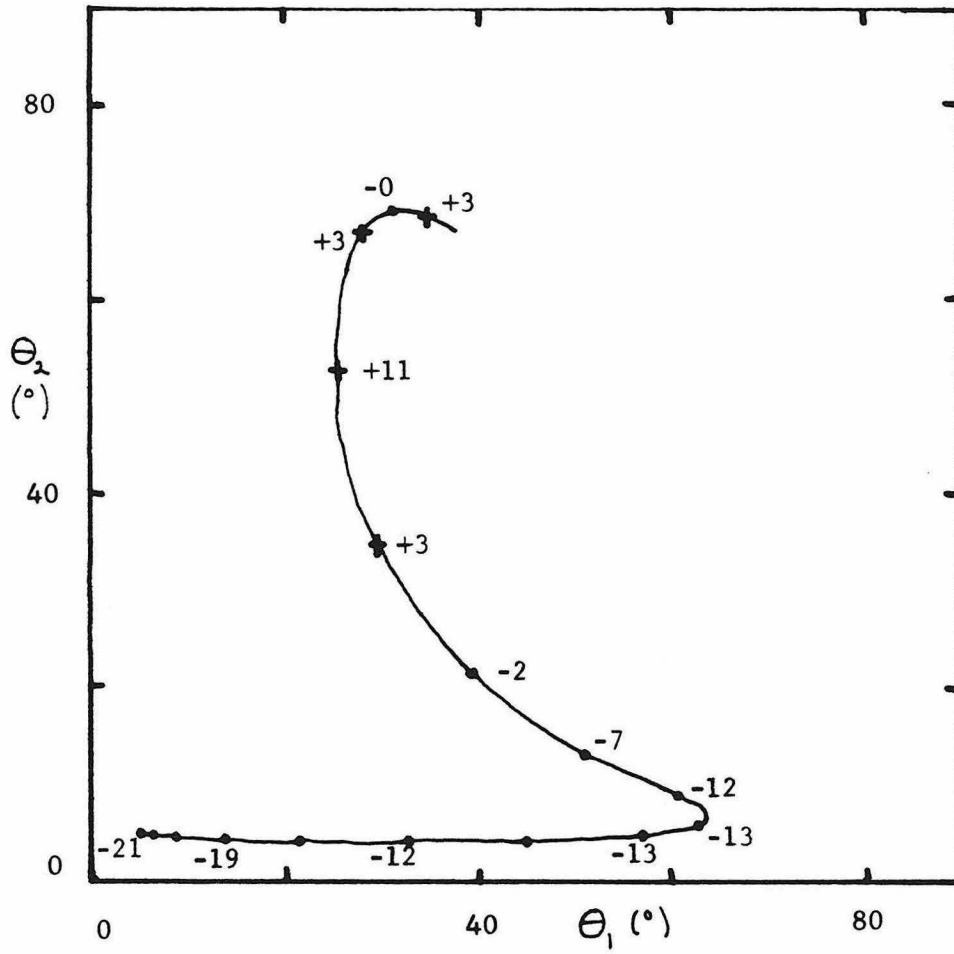


Figure 18

# Comparison of Ground State Energies

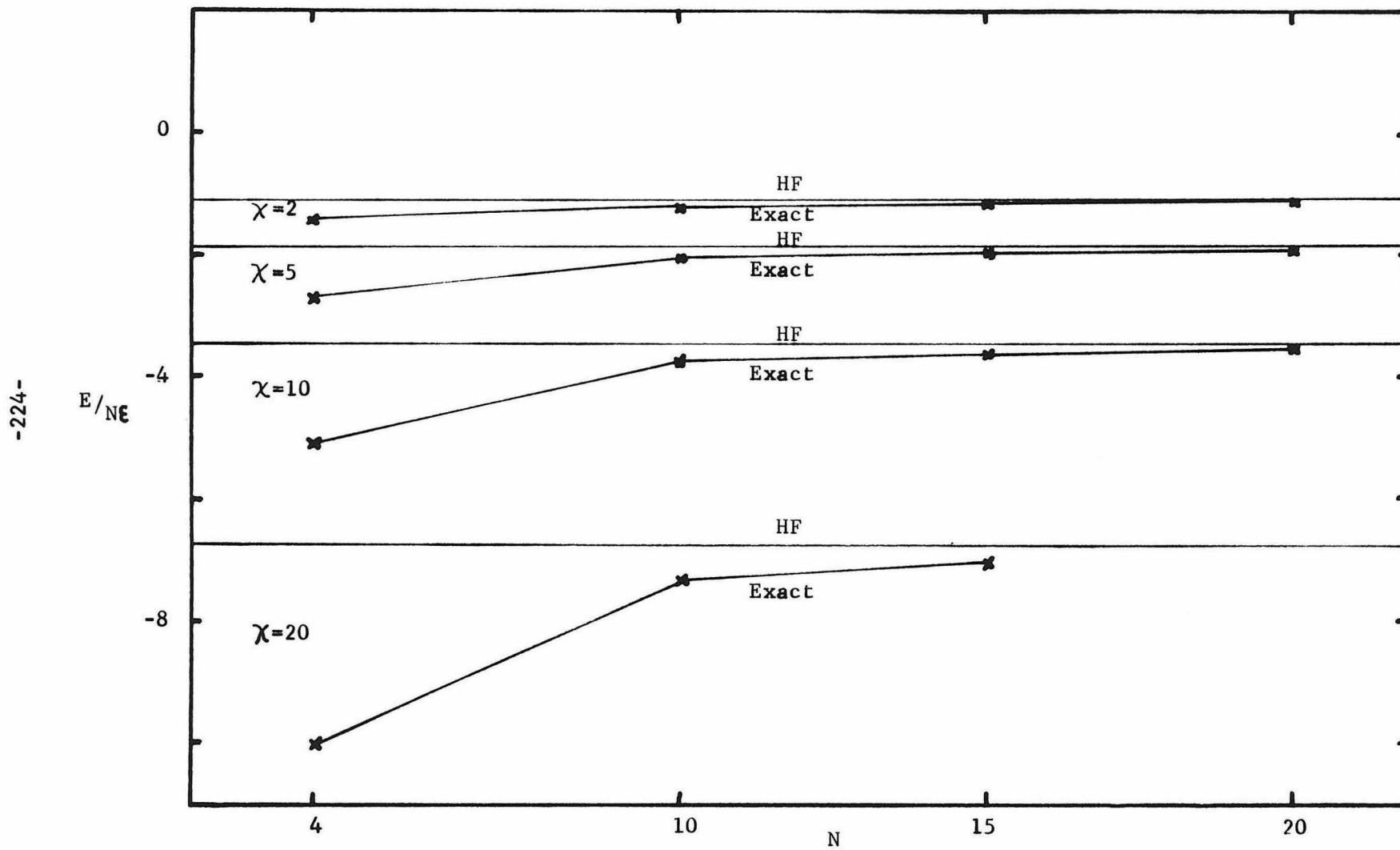


Figure 19

Deviation of Exact Ground States from  
Independent Particle States

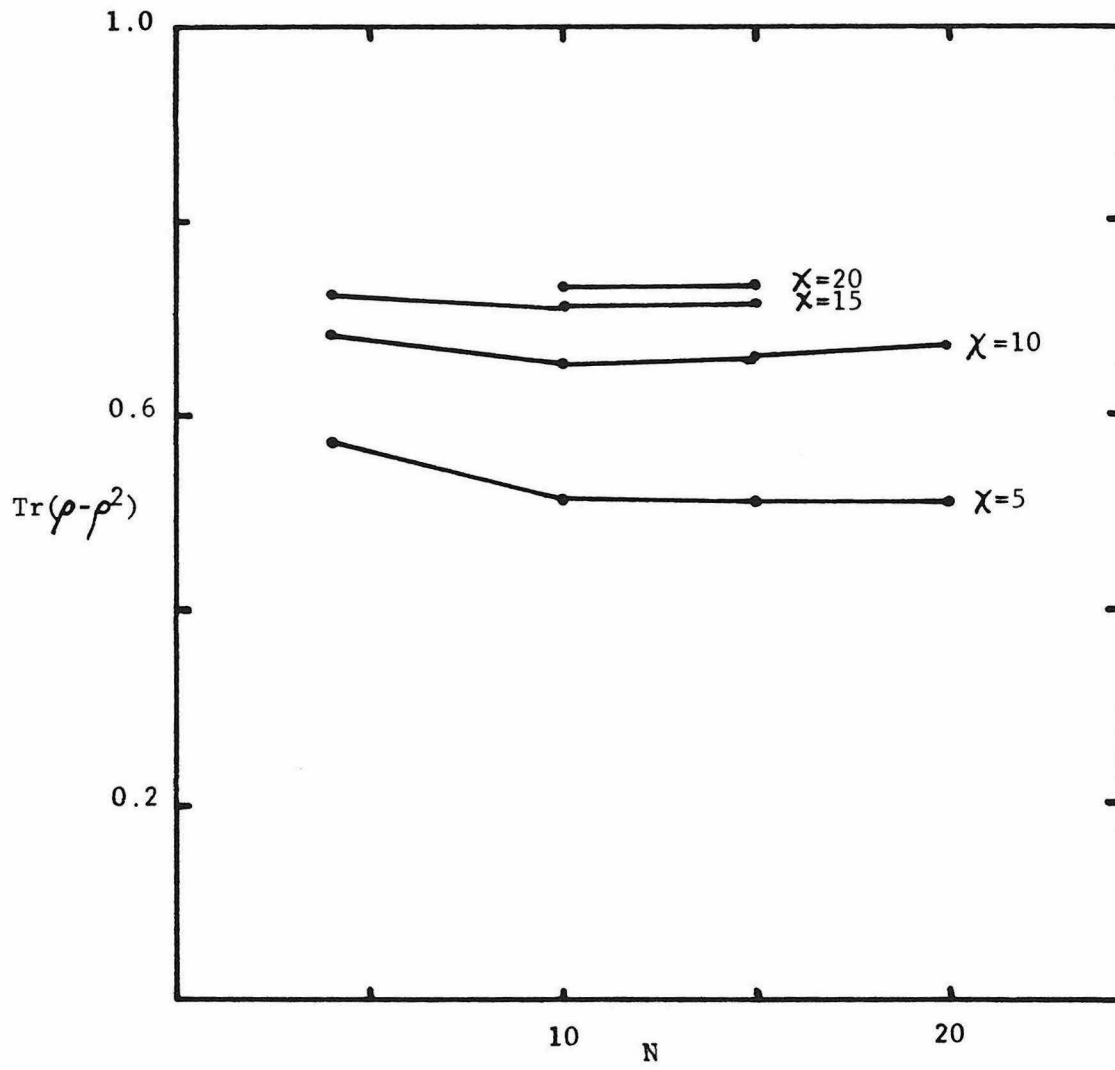


Figure 20

Position of Ground States

✕ HF Solution      ● Numbers Label N for Exact Solution

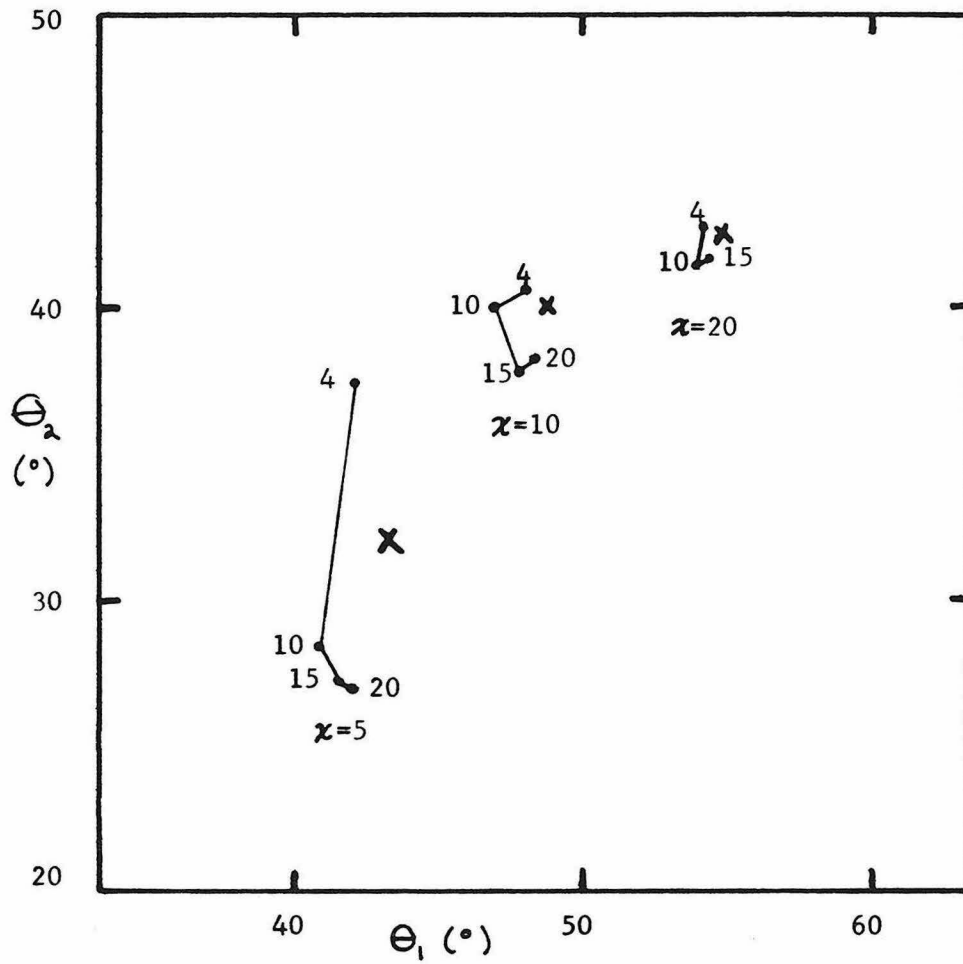


Figure 21

Comparison of Two TDHF Paths with Exact Paths

$$\chi = 5$$

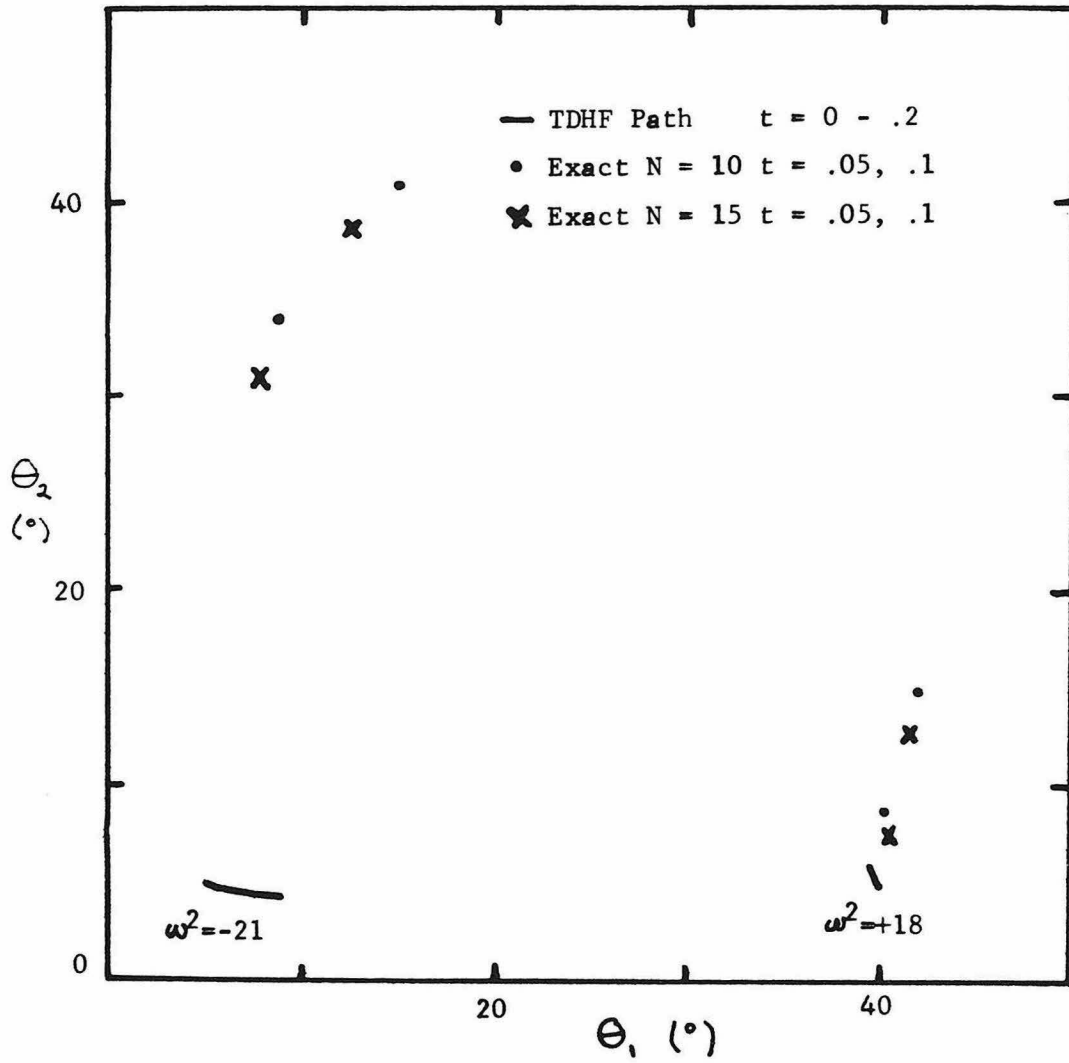


Figure 22

Comparison of TDHF and Exact Positions

$$\chi = 5$$

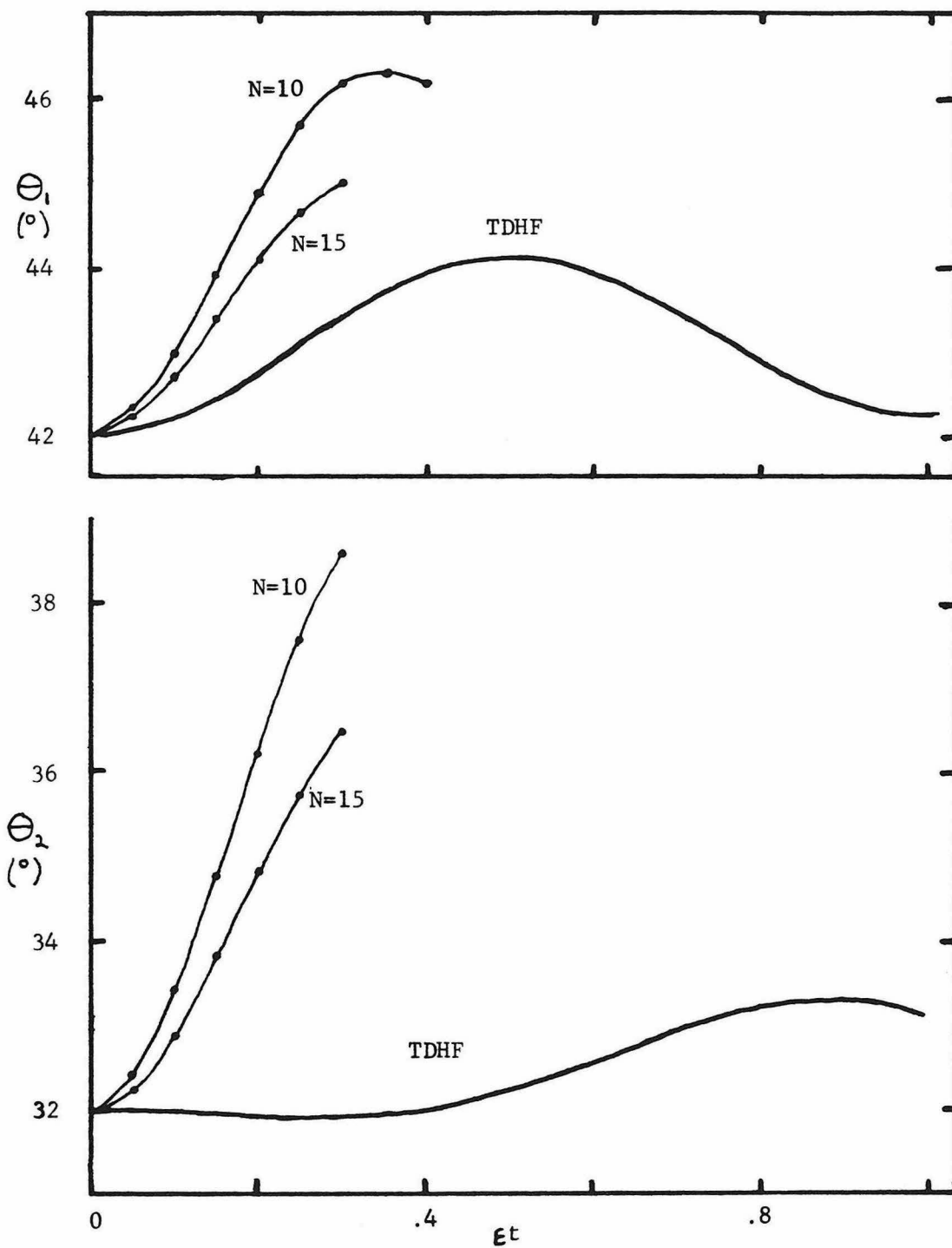


Figure 23

Comparison of TDHF and Exact Positions

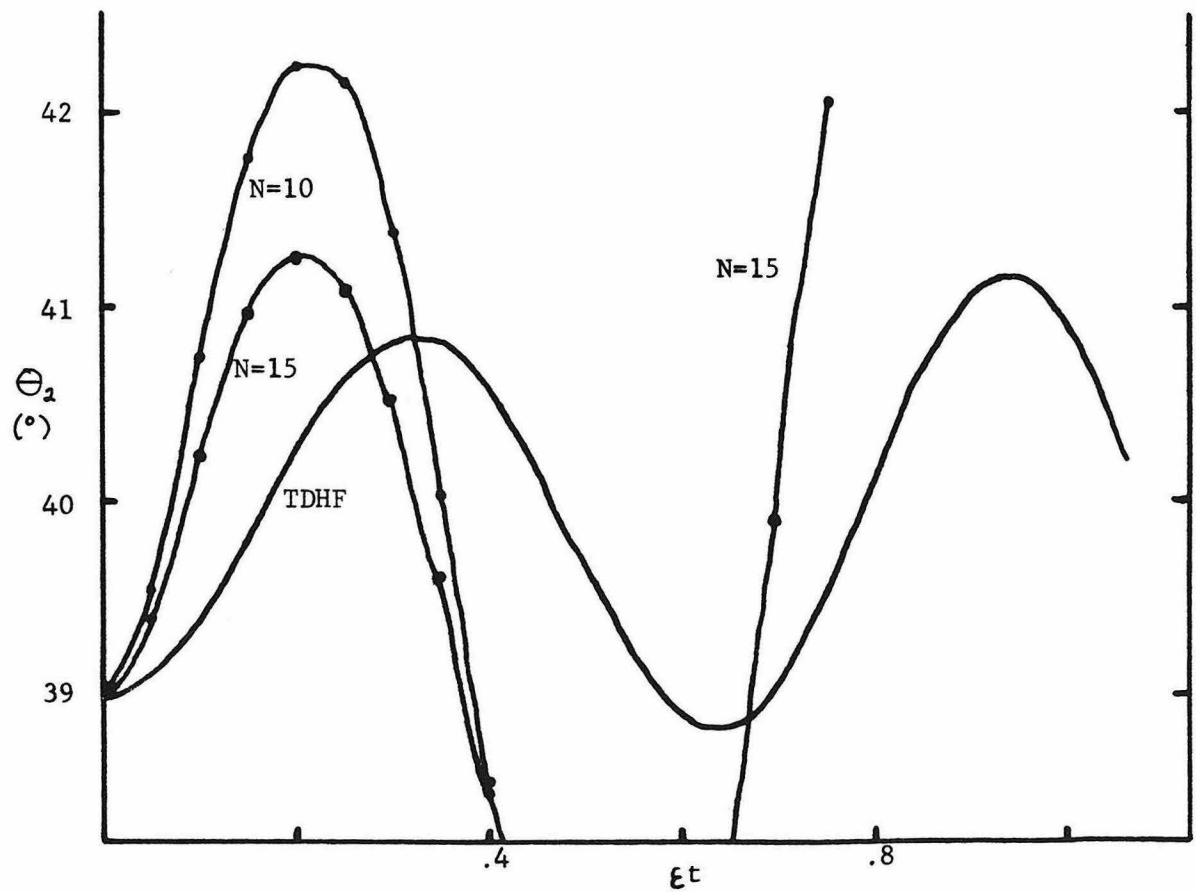
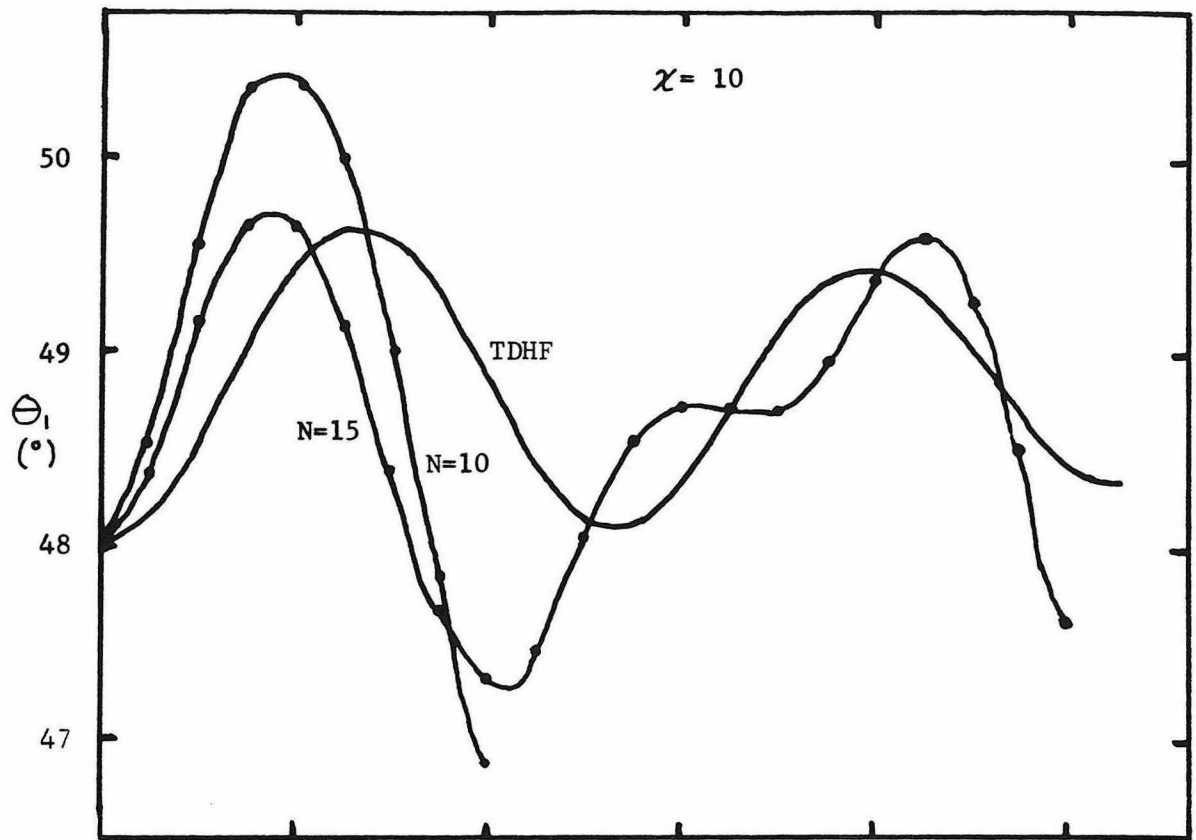


Figure 24

Comparison of TDHF and Exact Positions

$\lambda = 20$

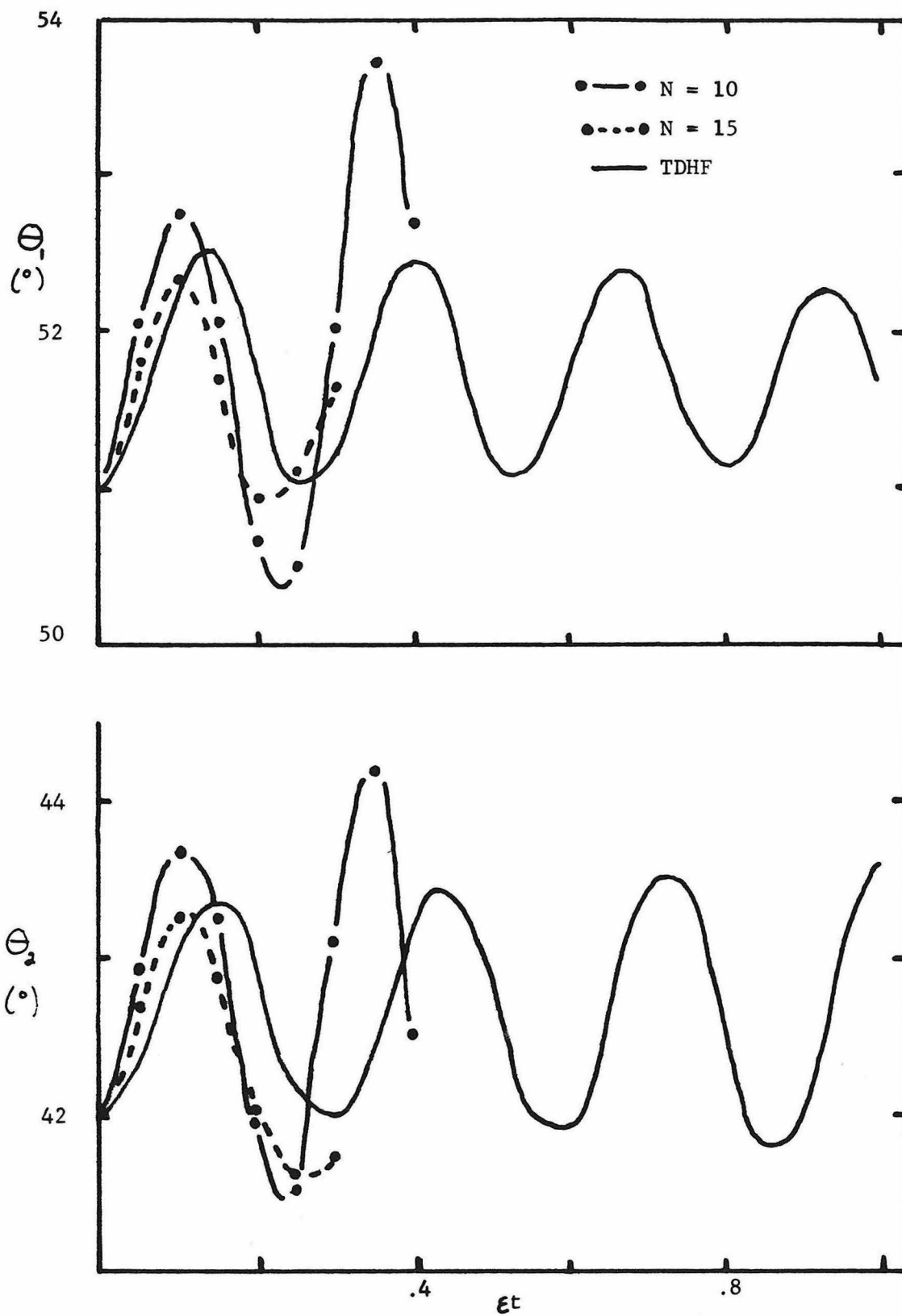


Figure 25

Comparison of TDHF and Exact Positions

$\chi = 100$

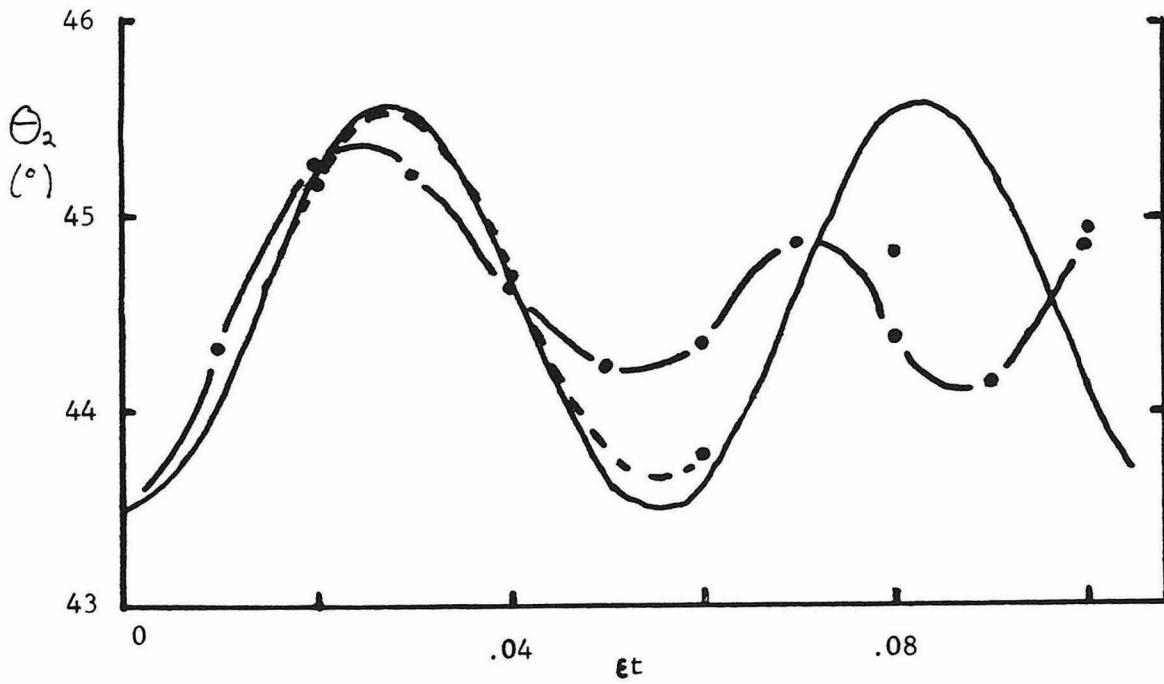
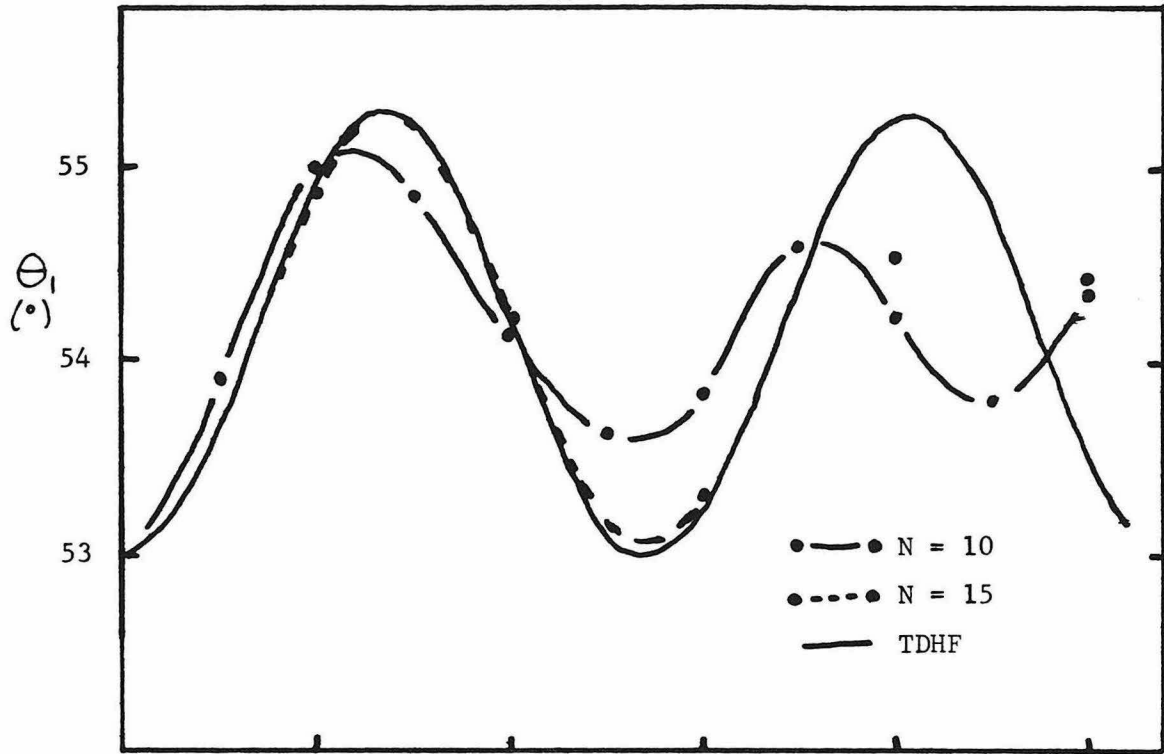


Figure 26

Deviation from Independent Particle States  
of the Exact Paths in Figure 26

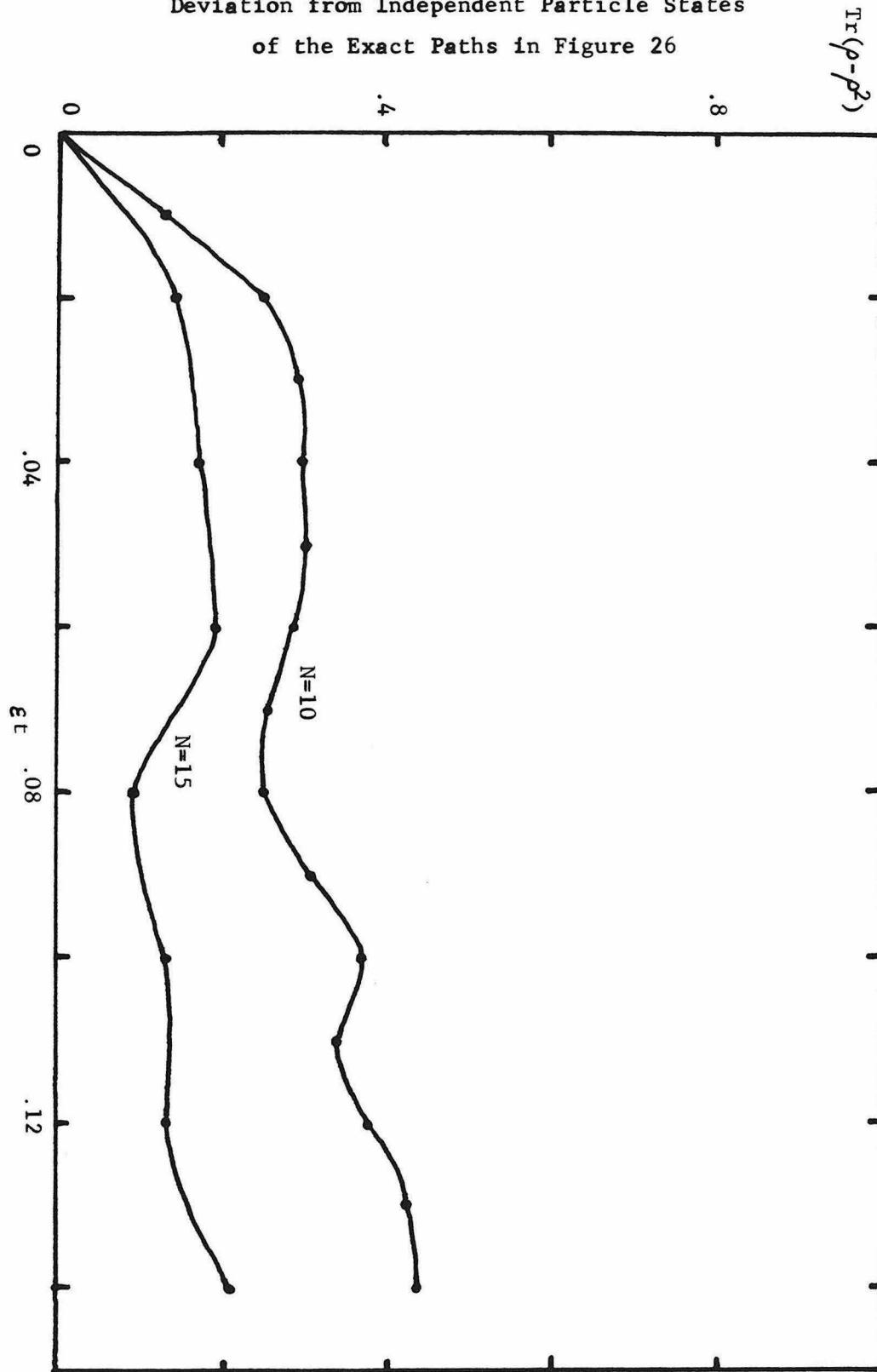


Figure 27

Comparison of TDHF and Exact Positions

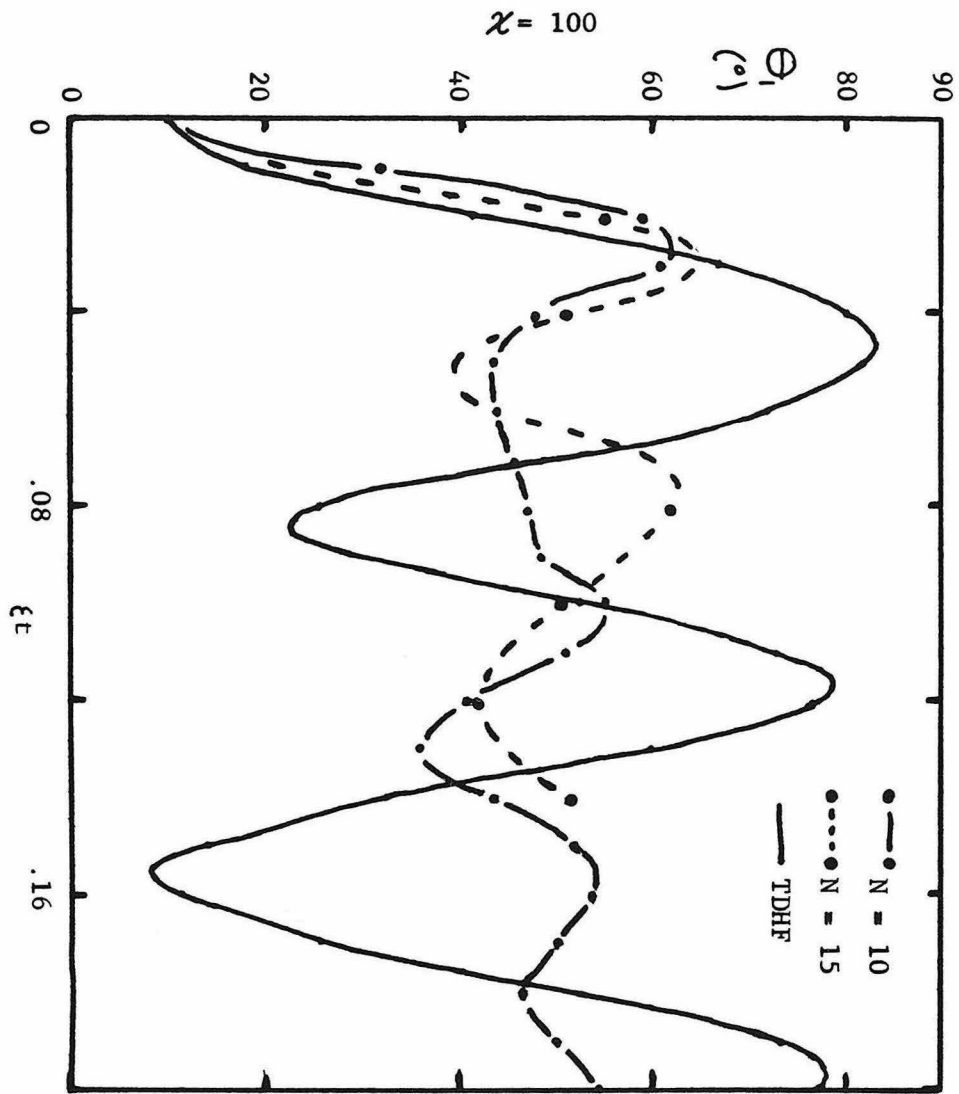


Figure 28

Comparison of TDHF and Exact Positions

$\chi = 100$

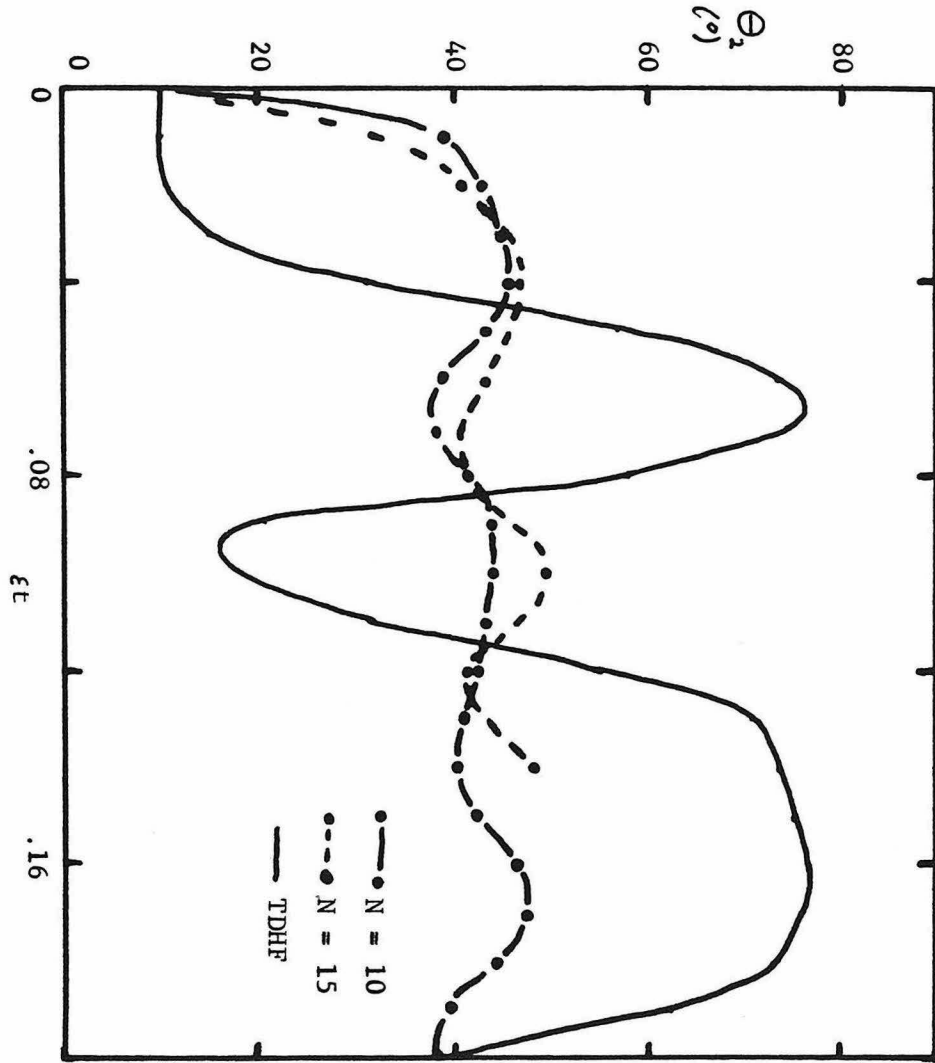


Figure 29

Comparison of TDHF and Exact Paths

$\chi = 100$

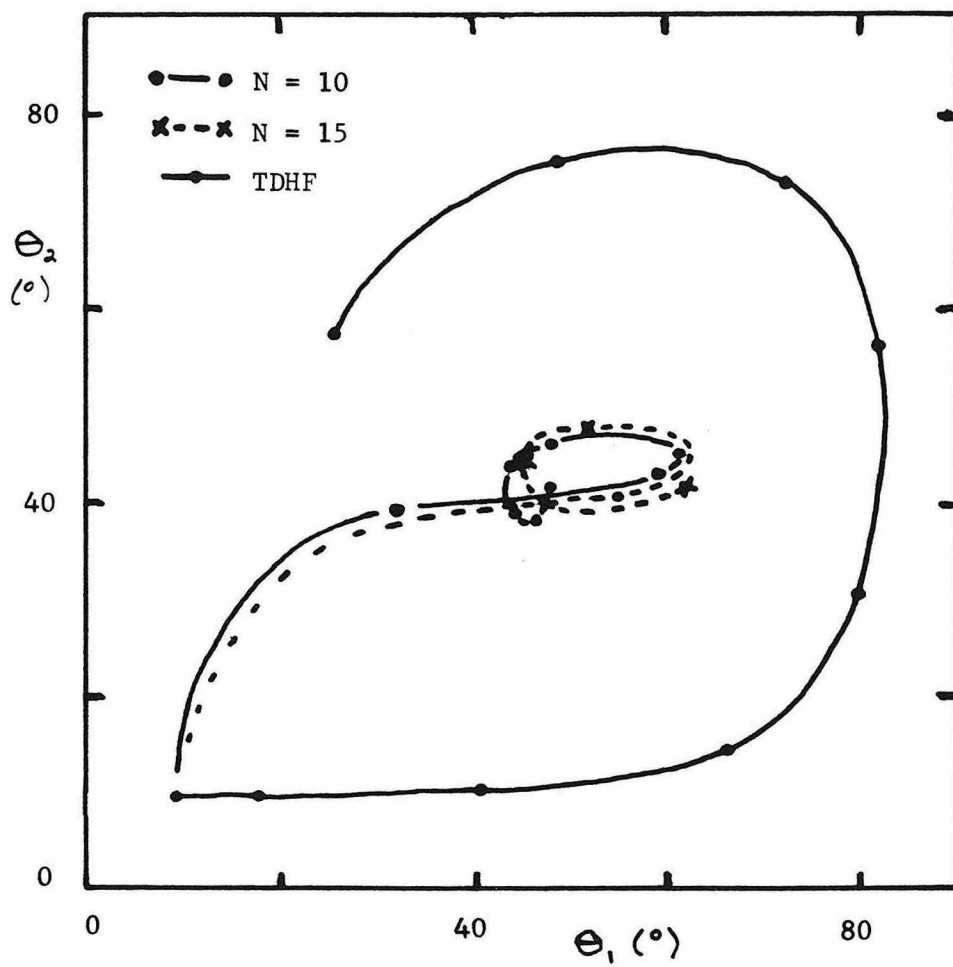


Figure 30

Deviation from Independent Particle States  
of the Exact Paths in Figure 30

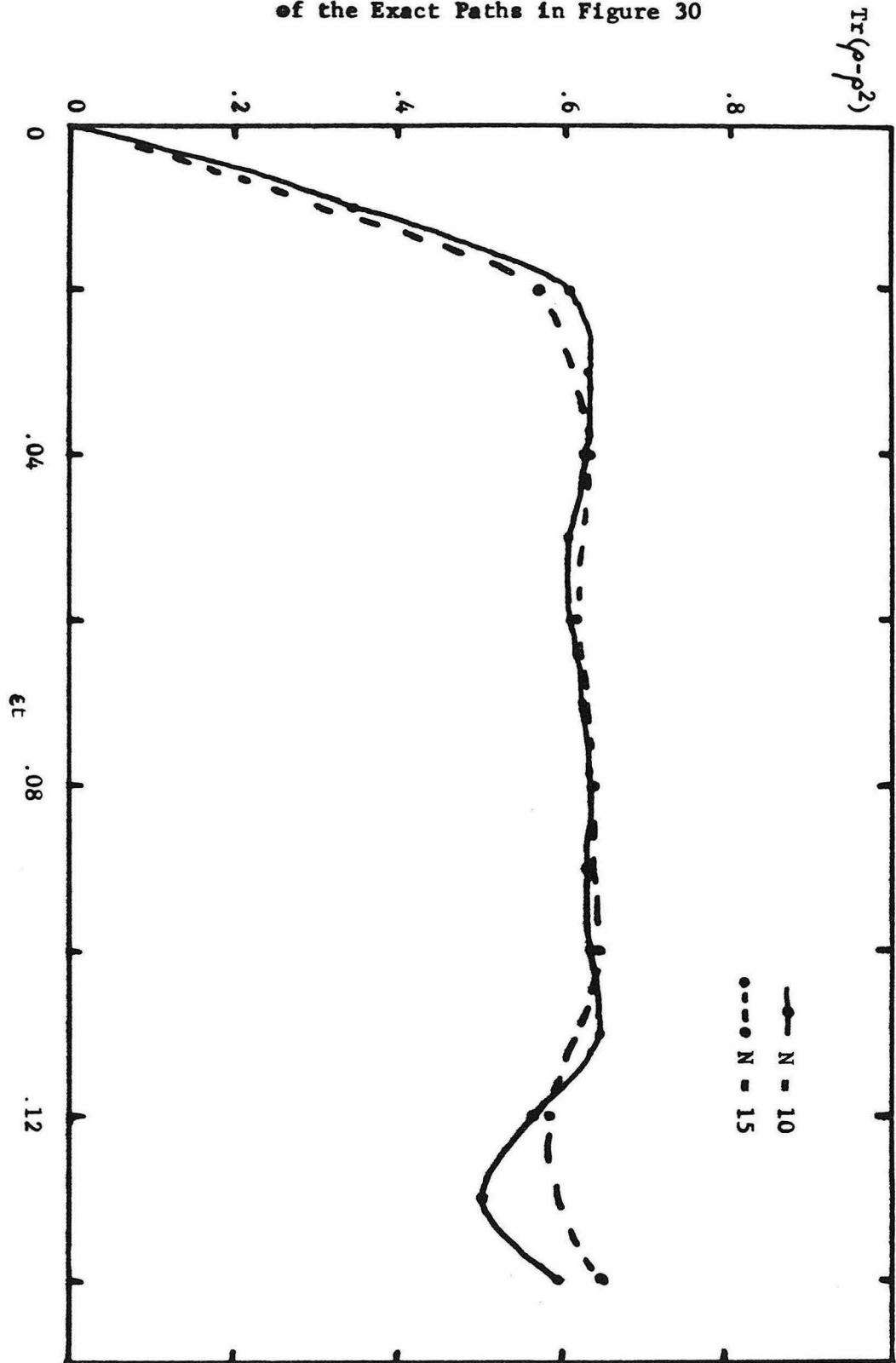


Figure 31

Slicing of the Density

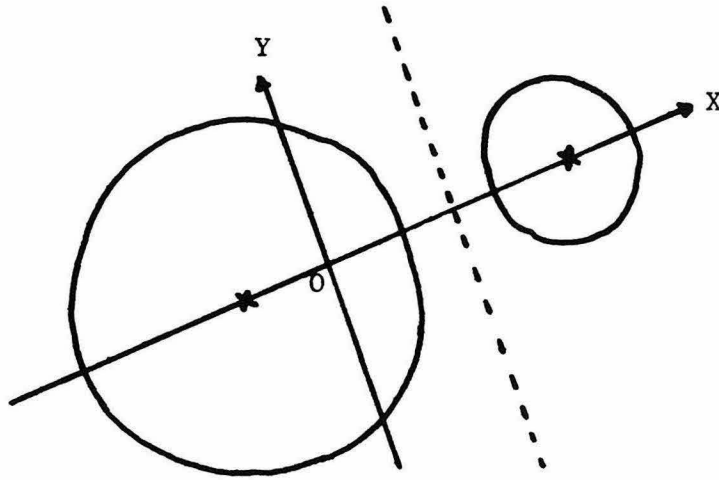


Figure 32a

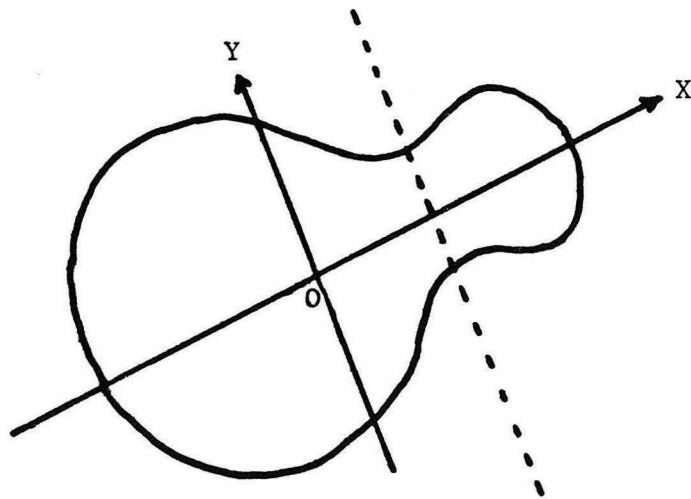


Figure 32b

Equivalent Two-Sphere System

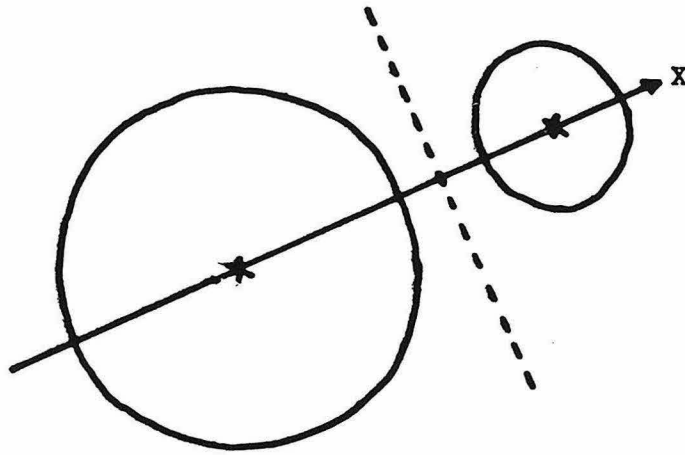


Figure 33a

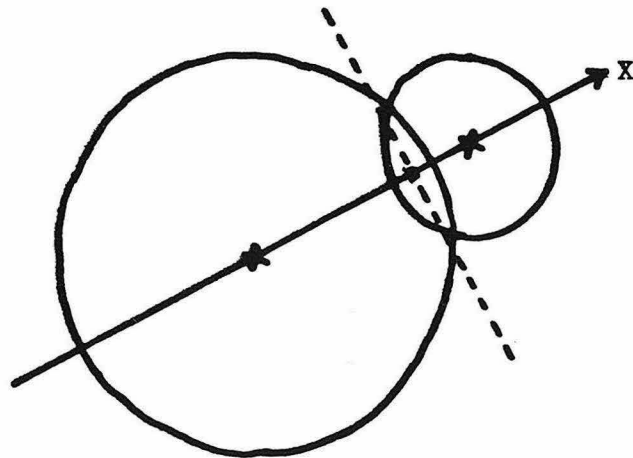


Figure 33b